

**Reconstruction of the Phanerozoic tectono-thermal history  
of central and southern Madagascar, based on fission track  
thermochronology**

Dissertation zur Erlangung des Doktorgrades der  
Naturwissenschaften am Fachbereich Geowissenschaften  
der Universität Bremen

Vorgelegt von  
Benjamin Emmel  
Bremen, 2004

Tag des Kolloquiums: 25.05.2004

Gutachter: P.D. Dr. J. Jacobs  
Prof. Dr. J. Kuss

Prüfer: Prof. Dr. R. Henrich  
Dr. A. Klügel

*„man auf hohen Bergen häufig Muscheln und Austernschalen sieht, die bisweilen in Felsen eingebettet sind. Diese Felsen bildeten einstmals den Erdboden, und die Schalentiere und Austern lebten im Wasser. Späterhin wurde alles umgestülpt. Dinge vom Boden kamen nach oben, und das Weiche wurde hart. Sorgfältiges Nachdenken über diese Tatsachen wird zu weitreichenden Schlüssen führen“*

*Chu Hsi (1131-120)*

# Contents

<b>Summary</b>	1
<b>Zusammenfassung</b>	3
<b>Chapter 1</b> Introduction	
1. The working area, why Madagascar?	6
2. The method, why fission track thermochronology?	7
3. Scope of this thesis	8
4. Outline of this thesis	9
References	
<b>Chapter 2</b> Divergent continental margins	
1. Introduction	14
2. Mechanisms of rift initiation	15
2.1 Passive rifting	15
2.2 Active rifting	16
3. Intracontinental rifts	17
4. Basins controlled by wrench tectonics	18
5. Successful rifted continental margins: passive margins	19
References	
<b>Chapter 3</b> Post collisional (<500 Ma) tectono-thermal evolution of central Madagascar: a combined structural and fission track study	
Abstract	24
1. Introduction	25
2. Geological framework and tectonic evolution of Madagascar	27
2.1 The basement of central Madagascar	27
2.2 Separation of Madagascar	30
3. Structural analysis	31
3.1 Ductile structures	31
3.2 Brittle structures and magmatic dykes	33
4. Fission track analysis	34
4.1 Titanite and apatite FT preparation, dating and modelling procedure	36
4.2 Results and interpretation of titanite FT data	36
4.3 Results and interpretation of apatite FT data	39
4.4 Calculated cooling and denudation rates from FT data	41
5. Discussion	48
6. Conclusions	53
References	

**Chapter 4** Titanite and apatite fission track analyses on basement rocks of central-southern Madagascar: constraints on exhumation and denudation rates along the eastern rift shoulder of the Morondava basin

Abstract	60
1. Introduction	61
2. Geological framework of Madagascar	62
3. Previous fission track analyses in Madagascar	67
4. Method	68
5. Results	69
5.1 Samples northeast of the Bongolava/Ranotsara and Zazafotsy shear zones	69
5.2 Samples from/around the Bongolava/Ranotsara and Zazafotsy shear zones	69
5.3 Samples south of the Bongolava/Ranotsara shear zone	72
6. Interpretation of titanite and apatite FT data	72
7. Discussion	77
8. Conclusions	84
References	

**Chapter 5** Thermal history of the southern Morondava basin (south-west Madagascar) and a Late Permian – Jurassic provenance record: constraints from detrital fission track and palaeo-current data

Abstract	94
1. Introduction	95
2. Geology and tectonic evolution of south-west Madagascar	95
2.1. Karoo Supergroup	97
2.2 Jurassic	99
2.3 Post Jurassic	100
3. Material and Methods	100
4. Geochronological data from potential Gondwana sources	102
4.1 East Africa	102
4.1.1 Kenya	102
4.1.2 Tanzania, Malawi and Mozambique	102
4.2 South-west India and Sri Lanka	103
4.3 East Antarctica	103
4.4 Madagascar	104
5. Tracking the provenance	106
6. Results and interpretation	109
6.1 Sakoa Group	109
6.2 Sakamena Group	111
6.3 Jurassic strata	112
7. Discussion	113
7.1 Sedimentological indications; basement development	113
7.2 Thermal history of the Sakoa Group, southern Morondava basin	116
7.3 Provenance analysis applying FT data	116
7.3.1 Late Permian to Early Triassic provenance	116
7.3.2 Jurassic provenance	118
7.3.3. Detrital fission track age clusters	119
7.4 Sedimentary and tectonic model for the Late Carboniferous to the Late Jurassic	121
8. Conclusion	123
References	

<b>Chapter 6</b>	Post collisional tectono-thermal evolution of Madagascar in a global tectonic setting	
1. Introduction		132
2. Thermal stage		134
3. Wrench stage		137
4. Rift stage		138
5. Passive margin stage		138
6. Comparison with the Mesozoic East African rift systems		140
6.1 Related geochronological data from East Africa		142
References		

**Appendix**    Equations, parameters and statistics

A 1 Sampling and preparation		148
A 2 Technical equipment, software, track counting and measurement		149
A 3 Zeta calibration		149
A 4 Fission track age calculation and statistics		150
A 5 Analytical data of samples used to construct age distribution maps (Chapter five, Fig. 5.3b)		153
A 6 Modelled cooling paths of samples used to construct a map, which shows the times of rapid cooling (Chapter five, Fig. 5.3c)		153
A 7 General abbreviations		157
References		

<b>Acknowledgements</b>		159
-------------------------	--	-----

<b>Erklärung</b>		160
------------------	--	-----

## Summary

Titanite and apatite fission track (FT) thermochronology on 127 basement and 18 sedimentary rock samples from central and southern Madagascar record a complex cooling and denudation history since the Early Palaeozoic.

New constraints were placed about:

- the tectono-thermal evolution of central and southern Madagascar after the collision of East and West Gondwana (~700-500 Ma)
- the reactivation of Late Neoproterozoic/Early Cambrian ductile high strain zones
- the basement denudation dynamics during two phases
  - the Late Palaeozoic to Early Mesozoic intracontinental Karoo rift evolution
  - the Late Jurassic transform margin formation between East Africa and Madagascar
- the Late Permian to Jurassic provenance of the Morondava basin
- the thermal history of the southern Morondava basin
- the tectono-thermal influence of the Marion hot spot on the eastern basement during the Late Cretaceous break-up of Madagascar and India

Titanite fission track analyses on 27 basement samples gave ages ranging between  $483\pm 33$  Ma and  $266\pm 13$  Ma. Apatite FT ages from 123 basement samples vary between  $460\pm 21$  Ma and  $79\pm 5$  Ma. Additionally, 18 samples from Late Carboniferous to Early Jurassic sedimentary rock samples from the southern Morondava basin gave apatite FT ages ranging between  $462\pm 28$  Ma and  $184\pm 13$  Ma.

Calculated cooling rates based on titanite and apatite FT-data indicate a phase of thermal activity in the centre of the island during the ~420-360 Ma episode. It is related to the emplacement of pegmatite fields during the Silurian.

Pre-dating the initial opening of Madagascar's western basins during the Late Carboniferous/Early Permian, reactivation of ductile shear zones occurred. Reactivation along N-S trending high strain zones, bounding the eastern Morondava basin, was coupled with enhanced denudation with amounts of up to ~10 km crustal section. Apatite FT data suggest reactivation along the NW-SE trending Bongolava-Ranotsara shear zone during the same time.

In southern Madagascar pull apart basins were opened along N-S trending faults during the Late Carboniferous, and in the Early Permian a graben system evolved along the Bongolava-Ranotsara shear zone. This two directional graben system is related to a compressive

intraplate stress regime, which governed the Late Carboniferous to Late Permian rift development.

Modelled time-temperature paths of basement samples indicate that the subsequent Mesozoic rift evolution was accompanied with an eastward migration of areas of fast cooling (related to enhanced denudation). This observation supports the assumption, based on sedimentological evidences, that the source rock distances for the Morondava basin-fill increased during Mesozoic times.

Detrital apatite FT data derived from the outcropping Sakoa Group indicate, that after the Late Carboniferous/Early Permian deposition they were covered with sediments of up to ~2-4 km thickness. Mainly during the Jurassic a second exhumation to the surface occurred.

The final separation of Madagascar and East Africa during the Early Jurassic had only minor geomorphic impact in Madagascar. The transform margin evolution influenced only samples located close to the Davie transform fault, where basement regions and also former basin regions were exhumed. Detrital FT ages combined with palaeo current data of Jurassic samples from the southern Morondava basin indicate erosion of sediments belonging to the Karoo Supergroup and re-deposition in the Late Jurassic strata, northwest of the source.

The influence of the Marion hot spot during the Late Cretaceous initial break-up of Madagascar and India is controversially discussed. Combined Titanite FT and structural data argue for a minor tectono-thermal influence of the Marion hot spot during the Madagascar-India separation. However, apatite FT ages and modelled cooling paths indicate that the break-up during the Cretaceous was associated with a denudation amount of ~4 km crustal section along a narrow stripe parallel to the present eastern continental margin.

## Zusammenfassung

Die Ergebnisse der Titanit- und Apatit-Spaltspurthermochronologie an 127 Grundgebirgsproben und 18 Sedimentproben aus Zentral- und Süd-Madagaskar zeugen von einer komplexen Abkühlungs- und Denudationsgeschichte des Arbeitsgebietes seit dem frühen Paläozoikum.

Anhand der erhobenen Daten wurden neue Erkenntnisse gewonnen über:

- die thermo-tektonische Entwicklung Zentral- und Süd-Madagaskars nach der Kollision von Ost- und West- Gondwana (~700-500 Ma)
- die Reaktivierung spät neoproterozoischer / früh kambrischer duktiler Scherzonen
- die Dynamik der Grundgebirgsdenudation während zweier Phasen
  - der spät paläozoischen bis früh mesozoischen intrakontinentalen Karoo Riftphase
  - der spät jurassischen Anlage eines Transformrands zwischen Ost-Afrika und Madagaskar
- die spät permischen bis jurassischen Liefergebiete des Morondava Beckens
- die thermische Geschichte des südlichen Morondava Beckens
- den thermo-tektonischen Einfluss des *Marion hot spots* auf das östliche Grundgebirge während der spätkretazischen Trennung Madagaskars von Indien

Titanit-Spaltspuruntersuchungen an 27 Grundgebirgsproben ergaben Alter zwischen  $483 \pm 33$  Ma und  $266 \pm 13$  Ma. Die Apatit-Spaltspuralter von 123 Grundgebirgsproben reichen von  $460 \pm 21$  Ma bis  $79 \pm 5$  Ma. Weiterhin wurden 18 Proben von spät karbonischen bis spät jurassischen Sedimenten des südlichen Morondava Beckens datiert, welche Apatit-Spaltspuralter zwischen  $462 \pm 28$  Ma und  $184 \pm 13$  Ma ergaben.

Mittels Titanit- und Apatit-Spaltspurdaten aus dem Grundgebirge Zentral-Madagaskars wurden Abkühlungsraten kalkuliert, welche eine Phase thermischer Aktivität von ~420 Ma bis ~360 Ma belegen. Diese kann hauptsächlich mit der Entwicklung eines Pegmatitsystems während des Silurs in Zusammenhang gebracht werden.

Vor der initialen Öffnung des Morondava Beckens im späten Karbon kam es zur Reaktivierung entlang neoproterozoischer bis kambrischer duktiler Scherzonen. Entlang N-S verlaufender Scherzonen am östlichen Rand des Morondava Beckens kam es zu einer Denudation von max. ~10 km mächtigem Krustenmaterials. Apatit-Spaltspurdaten belegen eine zeitgleiche thermische Reaktivierung entlang der NW-SE streichenden Bongolava-Ranotsara Scherzone (BRSZ).

In Südwest-Madagaskar öffneten sich im späten Karbon entlang N-S streichender Störungen *Pull-Apart* Becken. Im Bereich der BRSZ entwickelte sich im frühen Perm ein Grabensystem. Die Entstehung zweier „Grabensysteme“ ist mit einem kompressiven regionalen Spannungsfeld während des späten Karbons bis zum späten Perm verbunden.

Modellierte Zeit-Temperatur Pfade der Proben des Grundgebirges belegen eine Ostmigration von Gebieten schneller Abkühlung (verursacht durch erhöhte Denudation) während der mesozoischen Riftentwicklung. Dies stützt die auf sedimentologische Daten basierende These, dass während des Mesozoikums die Liefergebietsentfernung der Sedimente des Morondava Beckens zunahm.

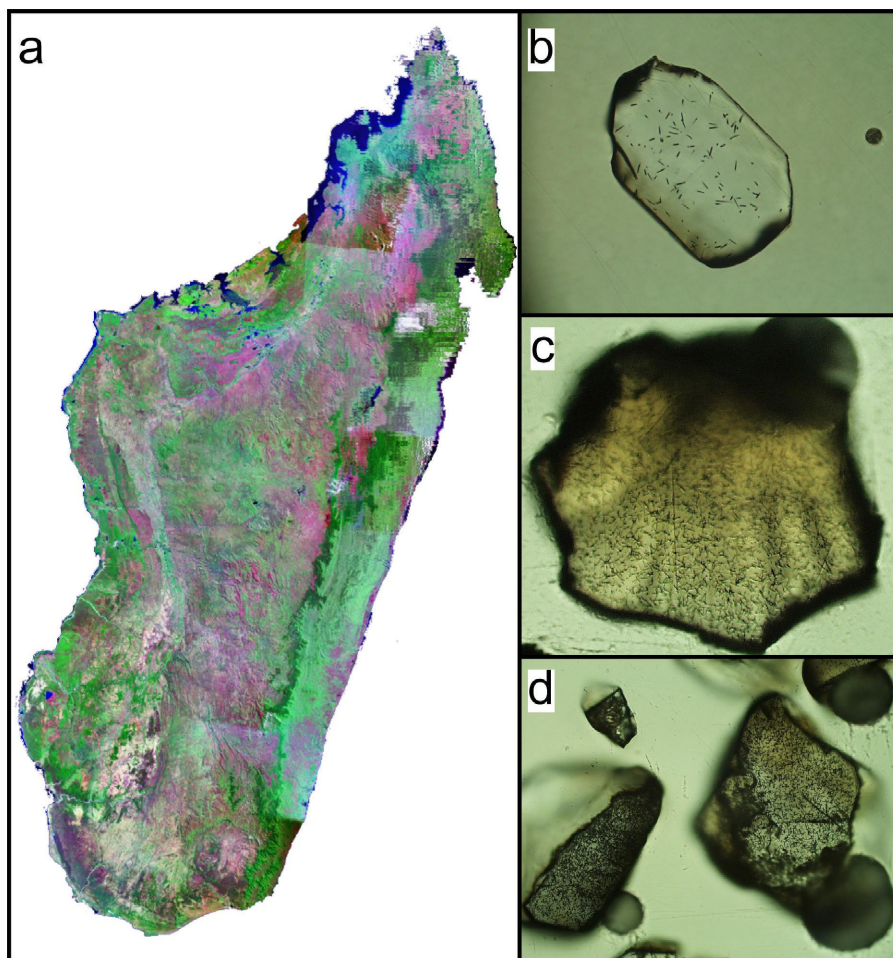
Anhand detritischer Apatit-Spaltspurdaten der aufgeschlossenen Sakoa Gruppe konnte nachgewiesen werden, dass diese Gesteine nach der Ablagerung im Permo-Karbon bereits in der Trias von einer ~2-4 km mächtigen Sedimentdecke überlagert waren. Eine zweite Exhumierung an die Oberfläche erfolgte hauptsächlich während des Juras.

Die spät jurassische Trennung von Madagaskar und Ost-Afrika und die damit assoziierte Entwicklung eines Transformrandes hatte einen geringen Einfluss auf die geomorphologische Entwicklung der Insel. Eine jurassische Exhumierung von Grundgebirgsgebieten als auch früherer Beckenregionen wurde im SW der Insel, nahe des *Davie transform fault* belegt. Detritische Spaltspuralter und Paläo-Strömungsrichtungsanalysen innerhalb jurassischer Sedimente des südlichen Morondava Beckens weisen darauf hin, dass während des frühen Juras Sedimente älterer Abfolgen (Karoo Supergruppe) erodiert wurden und nordwestlich in die jurassischen Einheiten umgelagert wurden.

In der späten Kreide kam es zur Trennung von Madagaskar und Indien. In diesem Kontext wird der Einfluss des *Marion hot spots* kontrovers diskutiert. Titanit-Spaltspuralter kombiniert mit strukturgeologischen Daten des östlichen Grundgebirges geben neue Hinweise für einen untergeordneten thermo-tektonischen Einfluss des *Marion hot spots*. Apatit-Spaltspurdaten belegen eine kretazische Denudation von ~4 km Krustenmaterials entlang eines schmalen Abschnitts parallel zum östlichen Kontinentalrand Madagaskars.

## Chapter 1

### Introduction



The title page of this chapter shows representative examples for the used methods.

- a) A Landsat 7 TM (RGB: 742) satellite image mosaic of Madagascar.
- b) An apatite grain of a basement sample (BE 014).
- c) A titanite grain of a basement sample (BE 038).
- d) Detrital apatite grains of sample BE 178.

The microphotographs of the apatite and titanite grains were taken after preparation for FT dating. The spontaneous fission tracks are visible due to chemical etching. Note all images are without a scale.

## 1. The working area, why Madagascar?

Madagascar is the world's fourth largest island, consisting of an ~580.000 km<sup>2</sup> area, located within the Indian Ocean, ~500 km east of the continental margin of Mozambique. Since the first geological mapping, under the leadership of Henry Besairie in the 1950s - 1960s (Besairie, 1953, 1961, 1964, 1967), the geology of Madagascar was of scientific and commercial interest.

At the first glance, the geology of the island seems to be simple – a Precambrian basement, three Phanerozoic sedimentary basins stretching along the western coast, and widespread volcanic rocks appear (Chapter four, Fig. 4.2).

New geological concepts and an integrated isotopic age data set show that most parts of the outcropping basement can be interpreted as the root of an ancient collisional orogen (e.g. Kröner et al., 1996, 2000; Collins et al., 2001; Meert, 2003). During the amalgamation of East and West Gondwana (~700-500 Ma) the East African-Antarctic Orogen developed, whereby the crust of Madagascar was partly reworked. After the continental collision Madagascar had a central position within the Gondwana supercontinent.

The sedimentary basins of Madagascar document the continental separation of Madagascar during the break-up of Gondwana and since the mapping of Henry Besairie the general lithology of the sedimentary rocks was known. The complex continental separation of Madagascar was investigated using combined approaches of sedimentology, palaeontology, and biostratigraphy (Hankel et al., 1994; Luger et al., 1994; Wescott and Diggins, 1997, 1998; Piqué et al., 1999). First signs of tectonic instabilities are recorded in Late Carboniferous sedimentary rocks of the southern Morondava basin. But as recently as the Late Cretaceous, after the subsequent secession from East Africa, Antarctica, and India, Madagascar had an isolated position within the Indian Ocean.

Today, Madagascar is completely fringed by passive margins, which evolved over a period of ~200 Ma and document different stages of the protracted Gondwana break-up. Therefore, the geology of Madagascar offers an incomparable opportunity to review key concepts regarding the development of continental margins related to the break-up of a supercontinent in a natural onshore laboratory.

## 2. The method, why fission track thermochronology?

Hitherto, the continental separation of Madagascar during the Gondwana break-up and the associated tectonics were mainly observed on sedimentary rocks of the island basins (Hankel et al., 1994; Montenat et al., 1996; Wescott and Diggens, 1997, 1998; Piqué, 1999). Rift processes and passive margin development are associated with different rift flank kinematics, and in many cases these rift flanks are linked to basement units. Two thirds of Madagascar are composed of basement rocks, which mostly represent the eastern rift shoulder of the three western sedimentary basins and the western rift shoulder of the eastern continental margin. Therefore, the basement rocks of Madagascar essentially recorded the subsequent continental separation of the island during the fragmentation of Gondwana. Using age determinations, that are sensitive to different temperatures and therefore different crustal levels, a reconstruction of the structural history during the continental separation of the island is possible.

The majority of published geochronological data from Madagascar (summary in Meert, 2003) is obtained from isotopic age determinations sensitive for high temperatures (>300 °C). These geochronological ages record in most cases the amalgamation of Gondwana (e.g. Martelat et al. 2000, de Wit et al., 2001), and the post-collisional orogen collapse (Collins et al., 2000). Nevertheless, some published basement zircon and apatite FT data from Madagascar with Palaeozoic and Mesozoic ages (Seward et al., 1998, 1999, 2000) show that the low temperature FT thermochronology is sensitive enough to record the continental separation of Madagascar in the basement rocks.

In this project, the low-temperature sensitive titanite and apatite FT thermochronological methods (310-60 °C) were chosen. Combined titanite and apatite FT data give the opportunity to reconstruct the exhumation and denudation history of the upper ~10 km of the crust. Especially, apatite fission track thermochronology (110-60 °C) is suitable to document the long-term landscape evolution and to model the thermal history below 110° C of different crustal and sedimentary sections. Combined with titanite FT thermochronology (310-265 °C; Coyle and Wagner, 1998) and stratigraphic ages of sedimentary rocks, a detailed cooling history of basement and sedimentary units can be obtained.

### 3. Scope of this thesis

The main purpose of this thesis is to reconstruct the exhumation and denudation history of central and southern Madagascar within the Late Palaeozoic to Mesozoic Gondwana stress fields using low temperature sensitive thermochronological methods. Using an interpreted thermochronological data set the influence of the different extensional phases during the continental separation of Madagascar on the vertical basement kinematics should be constraint.

The reactivation of pre-existing structures is discussed as a main cause or, at least, as the result of the intracontinental rift initiation (e.g. Ziegler et al., 1993). The separation of East Africa and Madagascar during the initial break-up of Gondwana is discussed in context with the reactivation of Late Neoproterozoic/Early Cambrian ductile structures dissecting the basement of Madagascar (e.g. Piqué, 1999). Dating and determining of vertical motions of different basement blocks, which are separated by ductile high strain zones, give in combination with structural observations new constraints about the timing and magnitude of possible tectonic reactivation of these ductile structures (Chapter three and four).

The development of the Morondava basin from an intracontinental rift to a passive margin is another focus of this thesis. The sedimentation and the basin configuration are closely connected with the denudation dynamics of the rift shoulder and/or the hinterland. Based on the basement exhumation and denudation history of central and southern Madagascar, and the detrital FT data of sedimentary rocks, a thermal history and a provenance record for the southern Morondava basin is proposed (Chapter three to five).

A general discussed feature of rift development is the involvement of mantle plumes during the initial continental separation (Chapter two). Late Cretaceous mafic igneous rocks from the eastern coast of Madagascar are related to the Marion hot spot. It has been suggested that this hot spot initiated the Madagascar-India break-up (Storey et al., 1995). Combined structural and thermochronological data provide important information about the effects of the mantle plume on the basement. Furthermore they give new information concerning the role of the hot spot during the continental separation of Madagascar and India (Chapter three).

#### 4. Outline of this thesis

This thesis is divided into six chapters. Chapter two gives a brief overview about the development and different stages of divergent continental margins. In chapter three to five three submitted publications present the main results of this project. These publications originated over a period of two years and therefore reflect different levels of knowledge. Reconstruction of the thermal history of the southern Morondava basin was improved by a growing data-set during the time. Consequently, the most reliable models are presented in chapter five. In chapter six a summary of the results is given and the basic findings were incorporated into a plate tectonic and rift development scheme for Madagascar.

Fission track thermochronology is a well-established dating method since the 1980s and a large number of publications about the FT methodology are available. Main parameters, equations of the age determination, and statistics are given in the appendix and in the three publications. For further reading concerning the FT thermochronological principles I refer to basic literature (e.g. Huford and Green, 1982; Gleadow, 1984; Wagner and van den Haute, 1989; Gallagher et al., 1998).

#### References:

- Besairie, H., 1953. 1:100.000 geological map series of Madagascar. *Sévice Géologique de Madagascar*, Antananarivo.
- Besairie, H., 1961. Carte Tectonique de Madagascar 1:3000000. *Sévice Géologique de Madagascar*, Antananarivo.
- Besairie, H., 1964. Madagascar carte géologique, 1:1.000.000. *Sévice Géologique de Madagascar*, Antananarivo.
- Besairie, H., 1967. The Precambrian of Madagascar. *The Precambrian* vol. 3, London, 1967, 133-142.
- Collins, A.S., Razakamanana, T., Windley, B.F., 2000. Neoproterozoic extensional detachment in central Madagascar; implications for the collapse of the East African Orogen. *Geological Magazine*, 137, 39-51.
- Collins, A.S., Windley, B., Kröner, A., Fitzsimons, I., 2001. The Tectonic Architecture of Central Madagascar: Implications on the Evolution of the East African Orogeny. *Gondwana Research* 4, 152-153.
- Coyle, D.A., Wagner, G.A., 1998. Positioning the titanite fission-track partial annealing zone. *Cemical Geology*, 149, 117-125.

- de Wit, M.J., Bowring, S.A., Ashwal, L.D., Randrianasolo, L.G., Morel, V.P.I., Rambeloson, R.A., 2001. Age and tectonic evolution of Neoproterozoic ductile shear zones in southwestern Madagascar, with implications for Gondwana studies. *Tectonics*, 20, 1-45.
- Gallagher, K., Brown, R., Johnson, C., 1998. Fission track analysis and its applications to geological problems. *Annu. Rev. Earth Planet. Sci.*, 26, 519-572.
- Gleadow, A.J.W., 1984. Fission track dating methods II - A manual of principles and techniques, Workshop on fission track analysis; principles and applications. James Cook University, Townsville, p. 35.
- Hankel, O., 1994. Early Permian to Middle Jurassic rifting and sedimentation in East Africa and Madagascar. *Geologische Rundschau*, 83, 703-710.
- Hurford, A.J., Green, P.F., 1982. A users guide to fission track dating calibration. *Earth and Planetary Science Letters*, 59, 343-354
- Kröner, A., Braun, I., Jaeckel, P., 1996. Zircon geochronology of anatectic melts and residues from a high grade pelitic assemblage at Ihosy, southern Madagascar: evidence for Pan-African granulite metamorphism. *Geological Magazine*, 133, 311-323.
- Kröner, A., Hegner, E., Collins, A.S., Windley, B.F., Brewer, T.S., Razakamanana, T., Pidgeon, R.T., 2000. Age and magmatic history of the Antananarivo Block, central Madagascar, as derived from zircon geochronology and Nd isotopic systematics. *American Journal of Science*, 300, 251-288.
- Luger, P., Gröschke, M., Bussmann, M., Dina, A., Mette, W., Uhlmann, A., Kallenbach, H., 1994. Comparison of the Jurassic and Cretaceous sedimentary cycles of Somalia and Madagascar: implications for the Gondwana breakup. *Geologische Rundschau*, 83, 711-727.
- Martelat, J.E., Lardeaux, J.M., Nicollet, C., Rakotondrazafy, R., 2000. Strain pattern and late Precambrian deformation history in southern Madagascar. *Precambrian Research*, 102, 1-20.
- Meert, J., 2003. A synopsis of events related to the assembly of eastern Gondwana. *Tectonophysics*, 262, 1-40.
- Montenat, C., Ramahavory, L., Croisile, M., 1996. Tectonic and sedimentary evolution of the western Madagascan margin during the Jurassic in the Morondava Basin, Madagascar. *Bull. Centres Rech. Explor.-Prod. Elf Aquitaine*, 20, 323-340.
- Piqué, A., 1999. The geological evolution of Madagascar: An introduction. *Journal of African Earth Sciences*, 28, 919-930.

- Piqué, A., Laville, E., Bignot, G., Rabarimanana, M., Thouin, C., 1999 a. The initiation and development of the Morondava Basin [Madagascar] from the Late Carboniferous to the middle Jurassic: Sedimentary, palaeontological and structural data. *Journal of African Earth Sciences*, 28, 931-948.
- Seward, D., Grujic, D., Schreurs, G., 1998. Exhumation history of the East Madagascar continental margin; inferences from apatite fission-track analysis. *Journal of African Earth Sciences*, 27, 176-178.
- Seward, D., Grujic, D., Schreurs, G., 1999. Exhumation history of Southern Madagascar as revealed by Zircon and Apatite Fission-Track Thermochronology. *Gondwana Research*, 2, 353-354.
- Seward, D., Grujic, D., Schreurs, G., 2000. Post Pan-African Events in Madagascar: Inferences from Apatite Fission-Track Analysis, 9th International Conference on Fission Track Dating and Thermochronology. Geological Society of Australia Abstract series, Lorne, Australia, 58, 289.
- Storey, M., Mahoney, J.J., Saunders, A.D., Duncan, R.A., Kelley, S.P., Coffin, M.F. 1995. Timing of hot spot-related volcanism and the breakup of Madagascar and India. *Science*, 267, 852-855.
- Wagner, G.A., Van den Haute, P., 1992. *Fission-Track Dating*. Ferdinand Enke Verlag, Stuttgart, 285 pp.
- Wescott, W., Diggins, J.N., 1997. Depositional history and stratigraphical evolution of the Sakoa Group (Lower Karoo Supergroup) in the southern Morondava Basin, Madagascar. *Journal of African Earth Sciences*, 24, 581-601.
- Wescott, W., Diggins, J.N., 1998. Depositional history and stratigraphical evolution of the Sakamena Group (Middle Karoo Supergroup) in the southern Morondava Basin, Madagascar. *Journal of African Earth Sciences*, 27, 467-479.
- Ziegler, P.A., 1993. Plate-moving mechanism: their relative importance. *Journal of the Geological Society, London*, 150, 927-940.



## Chapter 2

### Divergent continental margins



Photograph of the basement/basin boundary at Miandrivazo. The mountains in the background are composed of basement rocks and represent the Late Palaeozoic/Early Mesozoic eastern margin of the Morondava basin. The plain in the foreground is composed of Karoo related sedimentary rocks.

## 1. Introduction

Divergent tectonics can lead to the dispersal of continental crust and the subsequent new generation of oceanic crust (Fig. 2.1). Extensional basins cover large areas of the globe and contain important energy resources. High elevated rift shoulders and passive continental margins are impressive continental landscapes, which are related to divergent tectonic processes.

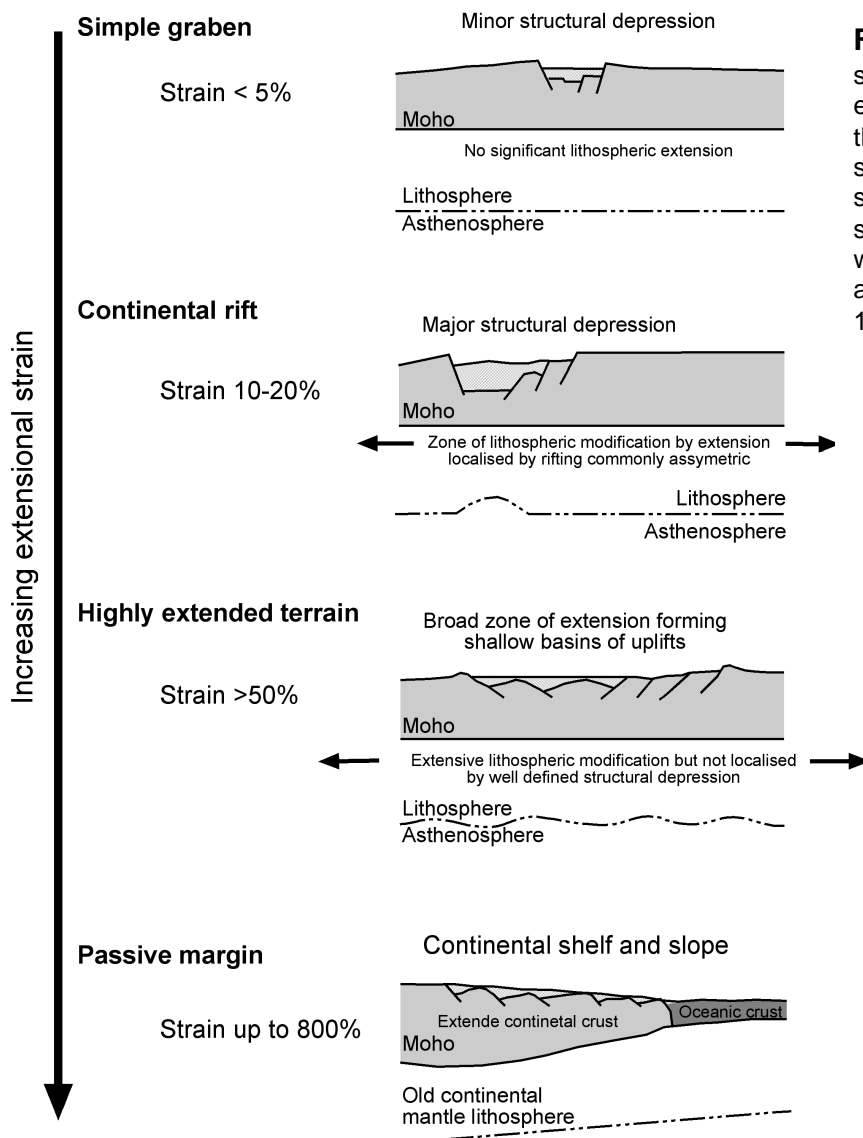


**Fig. 2.1:** Sketch of the main styles of continental extension, as a function of the increasing extensional strain, from the initial graben stage to the passive margin stage. Note: the figure is without a scale (compiled after Olsen and Morgan, 1995).

Madagascar as an ancient interior part of Gondwana is an ideal place to reconstruct the dispersal of a supercontinent in a microcontinental environment. After the final amalgamation of Gondwana (~700-500 Ma) divergent tectonics influenced Madagascar and the ancient adjacent continental fragments (mainly parts of East Africa, India, Sri Lanka and Antarctica),

although until Late Jurassic times Gondwana was influenced by a compressional stress regime along its continental margins. During the continental separation of Madagascar and the ancient adjacent continental fragments different landscapes linked to different extensional dynamics evolved around the island. Today, Madagascar is encircled by passive continental margins, and provides a unique natural microcontinental onshore laboratory for studying extensional tectonism associated with the subsequent break-up of a supercontinent.

## 2. Mechanisms of rift initiation

Which tectonic features and related forces drive and control the evolution of a rift system? Three-dimensional local and regional premises have to be taken into account. The style of rifting depends on a number of factors, including age, temperature and thickness of the lithosphere, composition and texture of the continental crust, the far-field plate tectonic kinematics and the existence and size of mantle plumes (Zeyen et al., 1997). Rifts can evolve in different tectonic regimes with prevailing compressional, extensional, wrench or even neutral tectonics. It should be noted that the stress regime governing the rift development might change in time, and in many cases different plate interactions control the subsequent rift evolution.

Stretching of continental lithosphere has been considered to develop in response to a regional stress field (passive rifting) or due to thermal upwelling of the asthenosphere (active rifting) (e.g. Sengör and Burke, 1978). Here, the terms "active" or "passive" describe the role of the asthenosphere during the initial separation of continental crust (Fig. 2.2). Certainly, field observations and different "geological tools" can give evidences for an active or passive rift initiation, but in most cases both features of these idealised end members are common along rifted margins. New concepts show, that many rifts start with an initial passive phase which is followed by a more active stage (e.g. Huisman et al., 2001; Ziegler and Cloetingh, 2003), but nevertheless some rifts only have a passive stage.

### 2.1 Passive rifting

The passive rift initiation is characterised by extensional stresses caused by an external regional stress field (Fig. 2.2a). The driving forces are plate boundary interactions driven by mantle convection and the associated plate tectonic forces, including slab pull, slab roll-back, ridge push, and collisional resistance (i.e. Ziegler, 1993; Ziegler and Cloetingh, 2003).

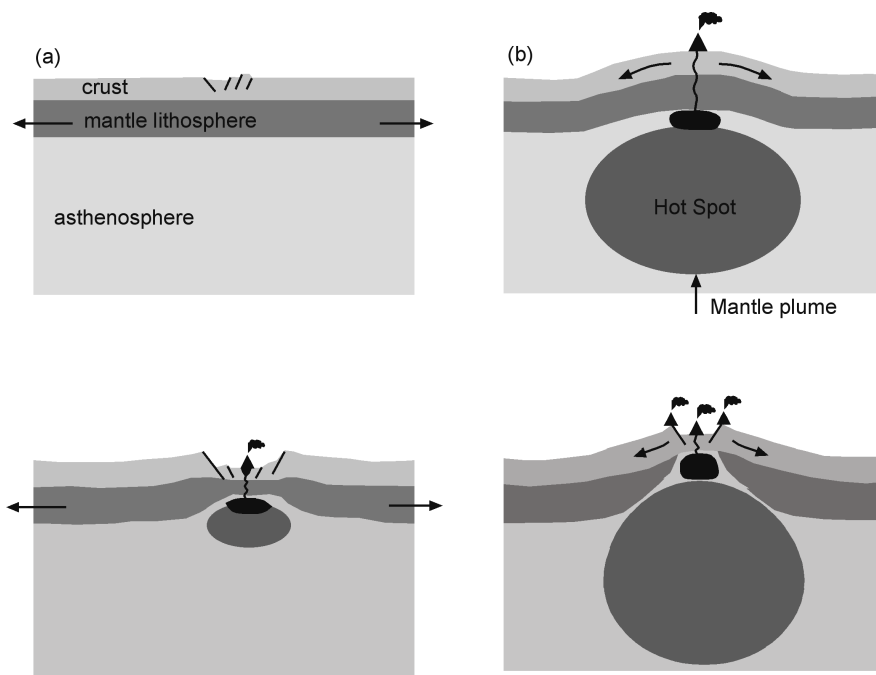


**Fig. 2.2:** The schematic diagram shows the differences between passive (a) and active (b) rift initiation.

a) Extension is driven by the far field stress regime. When the rift process is well developed magmatic underplating and volcanism can occur.

b) The emplacement of a hot spot in the sublithospheric mantle can be the primary cause for extension. Rifting is associated with voluminous basaltic flows (after Bott, 1995).

The process of lithospheric extension is mainly influenced by the strain rate, the initial conditions (thermal profiles and crustal thickness) and mechanical instabilities. Possibly, stress can be transmitted over a large distance through an e.g. rigid cratonic block and can act on weaker parts of a plate (e.g. Ziegler et al., 1995; Nyblade and Brazier, 2002). The distance from the active plate boundary to the weak zones doesn't influence rift activation (Janssen et al., 1995). The current far field stress regime has a main effect on the style of rifting. Under far field compression, rifts will open only a small amount, whereas under far-field extension continental break-up can be successful (Zeyen et al., 1997).

## 2.2 Active rifting

Active rifting is associated with mantle-lithosphere thermal interactions during the initial rift stages e.g., break-up is related to mantle plume (hot spot) activities (Fig. 2.2b). It is believed, that mantle plumes are generated at the core mantle boundary from where they rise diapirically through the lower mantle until they reach a density equilibrium with the surrounding material (Larson, 1991; Storey et al., 1992). All areas with major density and viscosity changes (660 km and 410 km discontinuities, and the base of the lithosphere) may stop their rise. When the ascension of the plume is stopped the plume head spreads out laterally and acts as a major heat source. The plume can trigger partial melting of the upper mantle and upwelling of a secondary plume system. Partial melts spread out on the base of

the lithosphere and magma can rise through the lithosphere and extrude as flood basalts (Smith and Lewis, 1999; Ziegler and Cloetingh, 2003). Plume related flood basalt provinces can have a radius of 1000 to 2000 km (e.g. Ziegler, 1988), and are characterised by the extrusion of large volumes of basalt in a relatively short time (Nikishin et al., 2002). Isostatic crustal doming over upwelling asthenosphere or an ascending mantle plume can cause lithospheric thinning and cracking of the crust. Depending on the temperature and density of the mantle material, dynamic uplift ranging from 1000 m to 2000 m accompanies the hot spot activities (White and McKenzie, 1989).

The active rifting model can explain some main observations along rift systems:

- the progression from uplift to volcanism to extension (Sengör and Burke, 1978)
- the development of rifts in zones in apparent compression
- the association of narrow rifts with long-wavelength topographic swells and flood basalt provinces (i.e. the East African rift system).

Main geological features observed along active passive margins are large volumes of volcanic rocks, basement stripping, and early uplift affecting areas hundreds of kilometres beyond the rift zone.

A further “active” approach to explain extensional features is the delamination model (Bird, 1979; Kay and Mahlburg Kay, 1993). This model is based on deep lithospheric-asthenospheric interactions. Parts of over-thickened crust can break away during or after e.g. the extensional collapse of an orogen. Gravity driven detachment of parts of the lower lithosphere seems to explain a late or post orogenic heat pulse, which is coupled with emplacement of extensive granitic plutons (Meissner and Mooney, 1998). Furthermore, the delamination model can explain a seamless transition from an orogenic phase to occurrence of mainly extensional features, like rapid regional uplift, lithospheric thinning and increased magma production. However, the observational basis is indirect and observational opportunities are limited (Kay and Mahlburg Kay, 1993).

### **3. Intracontinental rifts**

The first occurring landforms of intracontinental divergent movements are continental rifts. A rift is a major linear graben, a half graben or a complex graben system consisting of a complex of faults expanding laterally for many hundreds of kilometres (Park and Jaroszewski, 1994). These fault-bounded valleys can range in width from ~30 km to 70 km and in length from 10 to thousands of kilometres. Zones of crustal weakness like pre-existing shear zones often control the location of rift initiation. High strain zones are characterised by high material anisotropies compared to undeformed basement rocks. Mechanical load along

a shear zone can cause structural reactivation associated with several mechanisms such as vertical or lateral offsets, fluid pressure build-up, and shear heating. The weak zones remain susceptible to later tectonic reactivation regardless of their age, and play a role in the localisation and distribution of crustal strain (Hansen and Nielsen, 2003; Ziegler and Cloetingh, 2003).

Rifts can be separated according to their width. Examples for narrow rifts are the East African rift system, the Rio Grande rift, the Baikal rift, the northern Red Sea and the European Cenozoic rift system. These rifts are characterised by intense normal faulting, large lateral gradients in crustal thickness and topography, and low rates of extension (e.g. East African rift system <0.5 cm/yr). Within the rift zone the continental crust is thinned and heat flow is elevated. Along the rift shoulders the crust is relatively thick and heat flow is less. Examples for wide rifts are the Basin and Range Province and the Aegean Sea. Wide rifts are characterised by the abundance of a large number of separated basins over regions up to 1000 km wide. These areas are influenced by a non-uniform distributed high extensional strain ranging between ~10 % and ~400 % (Fig. 2.1). The Basin and Range Province is part of a broad topographically high region (1-2 km above sea level) with a high elevation in the centre and depressions on the eastern and western flanks. Structural, geophysical and topographic evidences indicate that the Basin and Range Province is probably much as twice of its original width, which underwent extension rates of 1-5 cm/yr. The area is characterised by a high heat flow.

#### **4. Basins controlled by wrench tectonics**

The combination of strike-slip motions during extension or compression is known as transtension and transpression, respectively. Transtension or transpression can lead to the evolution of a pull apart basin. Pull apart basins progressively grow in the same direction as the faults movements. In relation to their width, strike-slip related basins tend to be smaller, more elongate and deeper compared to basins formed by thermal subsidence or flexural loading. Some basins are as deep as wide (Sylvester, 1988). Strike-slip basins subside very rapidly because subsidence is localised along steep faults, and displacement along the faults is accompanied by lateral heat loss. This then allows thermally driven subsidence. Lithospheric thickness remains stable because the crust can compensate all subsidence and uplift along strike-slip related basins. The most prominent example is the Dead Sea. Along a ~1000 km long sinistral transform fault two major pull apart basins (gulf of Aqaba and the Dead Sea itself) developed.

## 5. Successful rifted continental margins: passive margins

The final stage of an intracontinental rift evolution is the passive continental margin (Fig. 2.1). The main characteristic of a passive continental margin is the development of oceanic crust by seafloor spreading. The sedimentary sequences along passive continental margins begin with rift related primarily continental siliciclastic units overlain by marine successions. Subsidence along passive continental margins results from thinning of continental crust by progressive creep of the ductile lower crust towards the sub-oceanic upper mantle and the contribution of increasing sedimentary loading.

The Red Sea is the classic example for a young ocean basin that developed a short time after the initial stage of intracontinental rifting. A number of classic examples for continental passive margins with a different structural development evolved around the Atlantic and Indian Ocean.

### References:

- Bird, P., 1979. Continental delamination and the Colorado Plateau. *J. Geophys. Res.*, 84, 7561-7571.
- Hansen, D.L., Nielsen, S.B., 2003. Why rifts invert in compression. *Tectonophysics*, 373: 5-24.
- Huismans, R.S., Podlachikov, Y.Y., Cloetingh, A., 2001. The transition from passive to active rifting: relative importance of asthenospheric doming and passive extension of the lithosphere. *J. Geophys. Res.*, 106, 11271-11291.
- Kay, R.W., Mahlburg Kay, S., 1993. Delamination and delamination magmatism. *Tectonophysics*, 219, 177-189.
- Larson, R.L., 1991. Latest pulse of Earth: evidence for a mid-Cretaceous superplume. *Geology*, 19, 547-550.
- Meissner, R., Mooney, W., 1998. Weakness of the lower continental crust: a condition for delamination, uplift, and escape. *Tectonophysics*, 296, 47-60.
- Nikishin, A.M., Ziegler, P.A., Abbott, D., Brunet, M.-F., Cloetingh, S., 2002. Permo-Triassic magmatism and rifting in Eurasia: implications for mantle plumes and mantle dynamics. *Tectonophysics*, 351, 3-39.
- Nyblade, A.A., Brazier, R.A., 2002. Precambrian lithospheric controls on the development of the East African rift system. *Geology*, 30, 755-758.

- Olsen, K.H., Morgan, P., 1995. Introduction: progress in understanding continental rifts. In: K.H. Olsen (Ed.), *Continental Rifts: Evolution, Structure, Tectonics*. *Developments in Geotectonics*, 25, 3-26.
- Sengör, A.M.C., Burke, K., 1978. Relative timing of rifting and volcanism on earth and its tectonic implications. *Geophysical Research Letters*, 5, 419-421.
- Smith, A.D., Lewis, C., 1999. The planet beyond the plume hypothesis. *Earth-Science Reviews*, 48, 135-182.
- Storey, B.C., Alabaster, T., Hole, M.J., Pankhurst, R.J., Wever, H.E., 1992. Role of Subduction-plate boundary forces during the initial stage of Gondwana break-up: evidence from the proto-Pacific margin of Antarctica. *Magmatism and the Causes of Continental Break-Up*. Spec. Publ. 68. *Up. Geol. Soc.*, London, 149-163 pp.
- Sylvester, A.G., 1988. Strike-slip faults. *Bull. geol. Soc. Am.*, 81, 1666-1703.
- White, R., McKenzie, D.P., 1989. Magmatism at rift zones: the generation of volcanic continental margins and flood basalts. *Journal of Geophysical Research*, 94, 7685-7729.
- Zeyen, H., Volker, F., Wehrle, V., Fuchs, K., Sobolev, S.V., Altherr, R., 1997. Styles of continental rifting: crust-mantle detachment and mantle plumes. *Tectonophysics*, 278, 329-352.
- Ziegler, P.A., 1988 Evolution of the Arctic-North Atlantic and the western Tethys. *Am. Assoc. Pet. Geol., Mem.*, 43, 198 p.
- Ziegler, P.A., 1993. Plate-moving mechanism: their relative importance. *Journal of the Geological Society, London*, 150, 927-940.
- Ziegler, P.A., Cloetingh, S., van Wees, J.-D., 1995. Dynamics of intra-plate compressional deformation: the Alpine foreland and other examples. *Tectonophysics*, 252, 7-59.
- Ziegler, P.A., Cloetingh, S., 2003. Dynamic processes controlling evolution of rifted basins. *Earth-Science Reviews*, in press.

### **For further reading:**

- Burbank, D.W., Anderson, R.S., 2001. *Tectonic Geomorphology*. Blackwell Science, Abingdon, 274 p.
- Corti, G., Bonini, M., Conticelli, S., Innocenti, F., Manetti, P., Sokoutis, D., 2003. Analogue modelling of continental extension: a review focused on the relations between the patterns of deformation and the presence of magma. *Earth-Science Reviews*, 63, 169-247.

Kearey, P., Vine, F.J., 1990. Global Tectonics. Blackwell Scientific Publications, Oxford, 302 p.

Moore, E.M., Twiss, R.J., 1995. Tectonics. W.H. Freeman and Company, New York, 415 p.

Summerfield, M.A., 1991. Global Geomorphology. An introduction to the study of landforms. Addison Wesley Longman Limited, Essex, 537 p.



## Chapter 3

### **Post collisional (<500 Ma) tectono-thermal evolution of central Madagascar: a combined structural and fission track study**

Emmel, B.<sup>a</sup>; Jacobs, J.<sup>a</sup>; Graser, G.<sup>a</sup>; Kastowski, M.<sup>a</sup> and Razakamanana, T.<sup>b</sup>

*Tectonophysics, submitted*

<sup>a</sup> Fachbereich Geowissenschaften, Universität Bremen, Postfach 330440, 28334 Bremen, Germany

<sup>b</sup> Département des Sciences de la Terre, Université de Toliara, Madagascar

## Abstract

Three fission track (FT) sections running from the western margin of the basement to the eastern continental margin of central Madagascar give titanite FT ages ranging between  $483\pm 33$  Ma and  $266\pm 13$  Ma and apatite FT ages varying between  $403\pm 33$  Ma and  $79\pm 5$  Ma. Calculated cooling rates from combined titanite and apatite FT data range between  $12.5$  °C $\text{Ma}^{-1}$  and  $0.4$  °C $\text{Ma}^{-1}$  and provide evidences for two episodes of accelerated cooling in the working area. The first phase, recorded between the Itremo region and the Angavo shear zone (AGSZ) at  $\sim 420$ - $330$  Ma reached cooling rates up to  $12.5$  °C $\text{Ma}^{-1}$ . The second cooling phase is documented at the present western basement/basin contact during the  $\sim 370$ - $260$  Ma period with cooling rates up to  $10$  °C $\text{Ma}^{-1}$ . The older cooling event is most probably related to temporally occurring phases of advective heating and fluid circulation during the Silurian until the Early Carboniferous. In contrast, cooling along the present western basement/basin contact is related to high denudation pre-dating and synchronous with deposition of the Karoo Supergroup in the Morondava basin. FT data suggest a brittle reactivation along Cambrian ductile high-strain zones predating the opening of the Karoo rift basins. Apatite FT ages from samples located between the western basement margin and the AGSZ were affected by the intracontinental Karoo rifting between Madagascar and East Africa, lasting from the Early Permian to the Early Jurassic. Additionally, the current distribution of brittle structures in this area was set up during this time. The Late Jurassic opening of the Somali and Mozambique basins had only a limited influence on the denudation dynamics in the study area. Nevertheless, structural data document the active tectonics during this time.

Along the eastern coast, the Cretaceous Madagascar-India break-up affects the apatite FT system of samples within a  $\sim 60$  km wide stripe along the eastern coastline. Here, apatite FT data and modelled T-t (time-temperature) paths indicate a Cretaceous cooling. Cooling was associated with a denudation amount of  $\sim 4$  km crustal section. Around and east of the AGSZ the orientation of brittle structures and thermally nearly unaffected Devonian basement titanite FT ages argue for a limited tectono-thermal impact of the Marion hot spot during the Madagascar-India break-up.

**Keywords:** Gondwana, Madagascar, fission track, thermochronology, structural geology, remote sensing

## 1. Introduction

After the final amalgamation of Gondwana during the Late Neoproterozoic/Early Cambrian Madagascar had a central position within Gondwana at the eastern margin of the East African-Antarctic Orogen (EAAO) (e.g. Stern, 1994; Shackleton, 1996; Collins and Windley, 2002; Fig. 3.1). The basement of Madagascar is composed of various lithospheric domains with different ages and tectonic histories (Fig. 3.2; e.g. Windley et al., 1994; Collins et al., 2000, 2003; Nédélec et al., 2000; Meert et al., 2002). In central Madagascar, the main tectonic fabric of the basement, including major ductile shear zones dissecting the different basement blocks, developed late tectonically during the Early Cambrian (Collins et al., 2000, 2003; Nédélec et al., 2000; Meert et al., 2002).

Ductile high strain zones or shear zones are characterised by a high material anisotropy compared to undeformed basement rocks. Mechanical load along pre-existing zones of weakness can cause reactivation (Hansen and Nielsen, 2003). Phanerozoic crustal extension between East Africa and Madagascar initiated large sedimentary basins that stretch along the western coast of Madagascar (Fig. 3.2; Besairie, 1972). It is believed that the main brittle structures of Madagascar are related to reactivation of major ductile high-strain zones during the extensional deformation (Tab. 3.1). In southwest Madagascar the eastern margin of the Morondava basin is bounded by the Edjeda and Ampanihy shear zones (Fig. 3.2). Some authors (e.g. Pili et al., 1997, Piqué et al., 1999) assume that reactivation along these structures initiated the opening of the Morondava basin at the end of the Carboniferous.

In the southern Morondava basin (Fig. 3.2) the record of the Gondwana fragmentation starts with Late Carboniferous (Wescott and Diggins, 1997) or Early Permian (Hankel, 1994) deposited sediments, dated by palynomorph assemblages. However, a few examples from East Africa show that structures related to the intracontinental Gondwana rifting developed probably ~100 Ma before the first deposition of rift related sediments (Sherlock and Hetzel, 2001; Hagen et al., 2001). Additionally, FT data from southern Madagascar indicate enhanced denudation along the western margin of the basement during the Carboniferous, pre-dating the deposition in the southern Morondava basin (Emmel et al., in press). Consequently, if sedimentary rocks were deposited during the Late Carboniferous/Early Permian, some former tectonic events must have created the required topography.

Late Cretaceous mafic igneous rocks are known from the eastern and western coasts of Madagascar, from a volcanic complex in the southern part of the island, and from numerous dykes that truncates the basement (Fig. 3.2; Storey et al., 1995). The basalts are thought to be related to the Marion hot spot (Storey et al., 1995) and it is believed, that the Late Cretaceous Madagascar-India break-up and the associated opening of the Mascarene basin

(~90-85 Ma) has been triggered by the Marion hot spot. It is still controversially discussed if hot spots can initiate the break-up of a continent or if hot spots are just a concomitant phenomenon during lithospheric thinning (e.g. Storey et al., 1995; Hawkesworth et al. 2000; Ziegler and Cloetingh, 2003).

Up to now, a limited number of low temperature geochronological data exists from Madagascar (e.g. Seward et al., 1998, 1999, 2000). In this study, structural data obtained by field observation and by remote sensing were combined with thermochronological data. We intended to localize and size the structural impact of temporal and regional different tectonic processes. Possible reactivation along Early Cambrian basement high-strain zones should be dated, and the degree of basement denudation associated with the Late Carboniferous to Late Jurassic rift and drift phases between East Africa and Madagascar should be quantified. Additionally, we intended to constrain the tectono-thermal influence of the Marion hot spot during the Madagascar-India break-up. Data for the thermal evolution of the different basement units are derived from combined titanite and apatite FT data. This combined approach resolves the temperature range between ~310 and 60 °C and can monitor episodes of different phases of uplift, exhumation, denudation and sedimentation in the upper ~10 km of the crust.

Strike of structures	Related structures	Kinematics/Timing	Author
NW-SE	BRSZ (Bongolava-Ranotsra shear zone)	separation of Madagascar and Africa, development of the Majunga and Morondava basins	Fournou and Roussel, 1994
NNE-SSW	shape of the east coast	separation of India and Madagascar	
N-S	alignment of magmatic rocks	magmatic reactivation	
NNE-SSW	Neogene graben		
NNE-SSW	eastern margin of the island	separation of India and Madagascar, development of the Lac Alaotra and Ankay grabens	Bertil and Regnault, 1998
NW-SE	BRSZ, northern limit of the Morondava basin	opening of the Somali basin	
W-E		recent N-S extension	
NW-SE	limit of the Ambatomena basin	synsedimentary activity during the deposition of the Sakoa and Sakamena Group	Piqué et al., 1999
N-S	E margin of the Isalo Group	recent	
NNW-SSE and NW-SE	E margin of the Morondava basin	Late Carboniferous - Early Jurassic reactivation of BRSZ, Ampanihy SZ	
N-S and NNE-SSW		Karoo rifting, Upper Cretaceous volcanics	Lardeaux et al., 1999
NW-SE	Davie transform fault	Karoo rifting, dextral wrench component, Upper Cretaceous volcanics	
W-E		reactivation during the Tertiary and the Quaternary	

**Tab. 3.1:** Summary of available structural data and related tectonic interpretations from Madagascar.

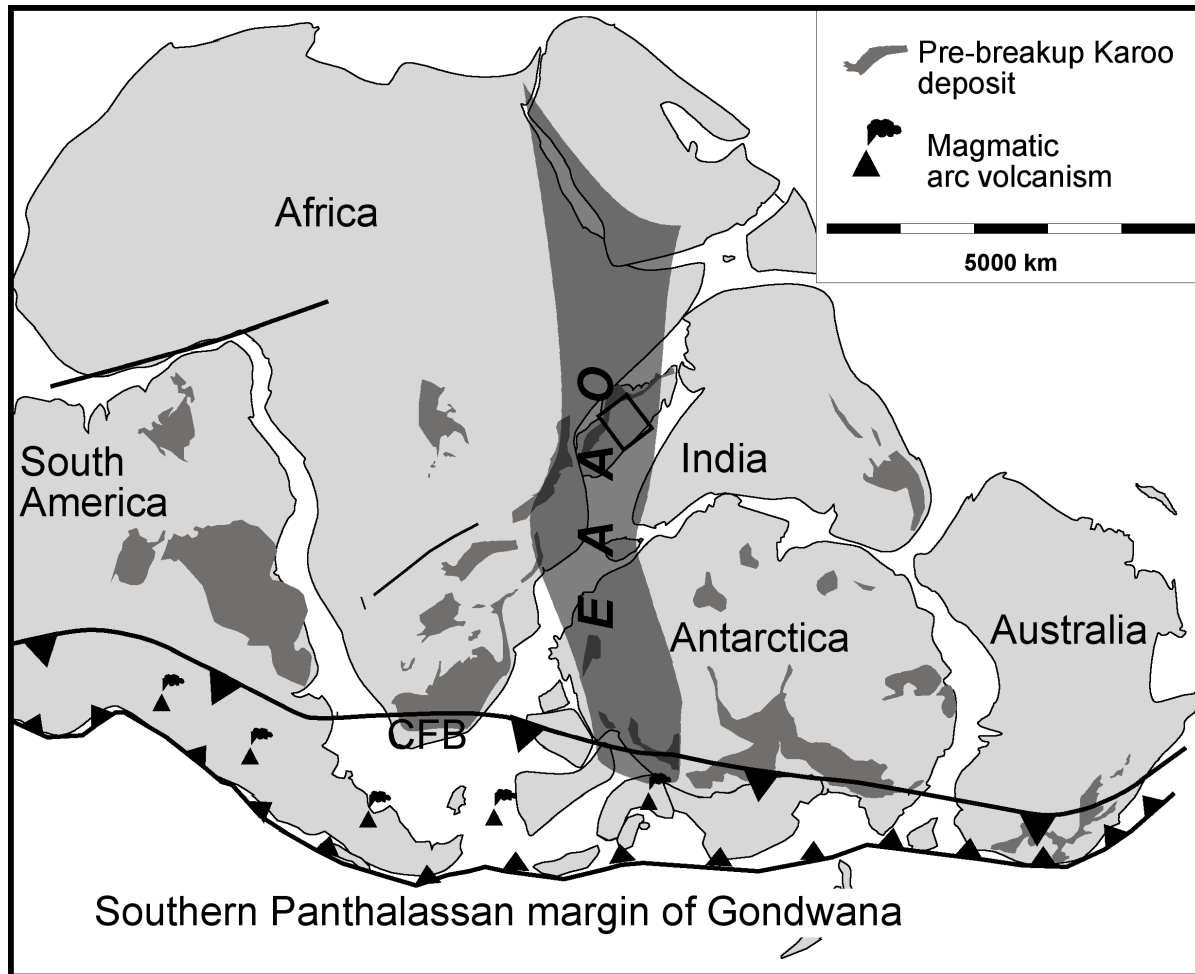


**Fig. 3.1:** Location of the study area in a pre drift reconstruction of Gondwana from Palaeozoic to Mesozoic times (modified after Stollhofen (1999), compiled from de Wit et al. (1988) and de Wit and Ransome (1992)). EAAO: East African-Antarctic Orogen, CFB: Cape Fold Belt.

## 2. Geological framework and tectonic evolution of Madagascar

### 2.1 The basement of central Madagascar

The eastern two thirds of Madagascar are mainly composed of Archean to Late Proterozoic basement rocks (Windley et al., 1994; Tucker et al., 1999; Collins and Windley, 2002). Most parts of the island were reworked and metamorphosed to high amphibolite-granulite facies grade during the Neoproterozoic/Early Cambrian collision of East and West Gondwana (Kröner et al., 2000).

Based on lithotectonic and isotopic evidences the central and northern part of the island is subdivided into five tectonic units (Collins et al., 2000; Fig. 3.2). These are: The Antongil block (after Hottin, 1976) which consists of amphibolite- and greenschist-facies metapelites that "rim" a meta-granite terrain. The Antananarivo block is the dominant unit north of the BRSZ. It is mainly composed of Late Archean granitoids, interlayered with Late Proterozoic granites, syenites and gabbros (Tucker et al., 1999; Kröner et al., 2000). The Tsaratanana unit contains three north-south striking greenstone belts made up of metabasic and pelitic gneisses, interlayered with chromites and intruded by gabbros and granites. In the far north of Madagascar, the Bemarivo orogenic belt is composed of paragneisses, orthogneisses, granites, quartzites and schists (Buchwaldt and Tucker, 2001; Collins et al., 2001). Predominant metasedimentary rocks of the Itremo Group (Cox et al., 1995, 1998) form the Itremo sheet in the central part of the island (Collins et al., 2000).

Meert et al. (2001) and Fernandez et al. (2003) describe the late and post metamorphic thermal evolution of central Madagascar. Meert et al. (2001) yielded a U-Pb zircon age of  $532\pm 5$  Ma from the post tectonic Carion granite in central Madagascar. The post collisional cooling history to below 500 °C is constrained by a hornblende  $^{40}\text{Ar}/^{39}\text{Ar}$  age of  $513\pm 3$  Ma. Biotite ( $479\pm 1$  Ma) and modelled K-feldspar ages indicate cooling from 350°C at 465 Ma to 100 °C by 410 Ma. Fernandez et al. (2003) dated samples from the Itremo region. Th-U-Pb electron microprobe and  $^{39}\text{Ar}/^{40}\text{Ar}$  dating give evidences for monazite growth events at ~565-540 Ma, ~500 Ma and ~430 Ma. They suggest that the ~565-540 Ma event is related to the latest metamorphism in this region and the ~500 Ma and ~430 Ma events are thought to have resulted from fluid circulation during the emplacement of pegmatite fields.

Several high-strain zones dissect the basement of central Madagascar. The AGSZ (Figs. 3.2 and 3.3) runs parallel to the eastern coast and has an estimated length of ~700 km and a width of ~40 km (Meert et al., 2002). The Virgation Zone (VZ) is located NW of Antananarivo (Fig. 3.3). Its trace and length is not well constraint. Both shear zone are influenced by thermal overprinting during the Early Cambrian (Meert et al., 2002).

The extensional Betsileo shear zone (BetSZ, Fig. 3.3) separates the predominantly metasedimentary rocks of the Itremo sheet (Fig. 3.2; Cox et al., 1995, 1998) from Late Archean to Late Proterozoic rocks (Tucker et al., 1999; Kröner et al., 2000) of the Antananarivo block. It is interpreted as a part of a major N-S trending extensional detachment, which is associated with post-orogenic collapse of the East African Orogen (Collins et al., 2000).

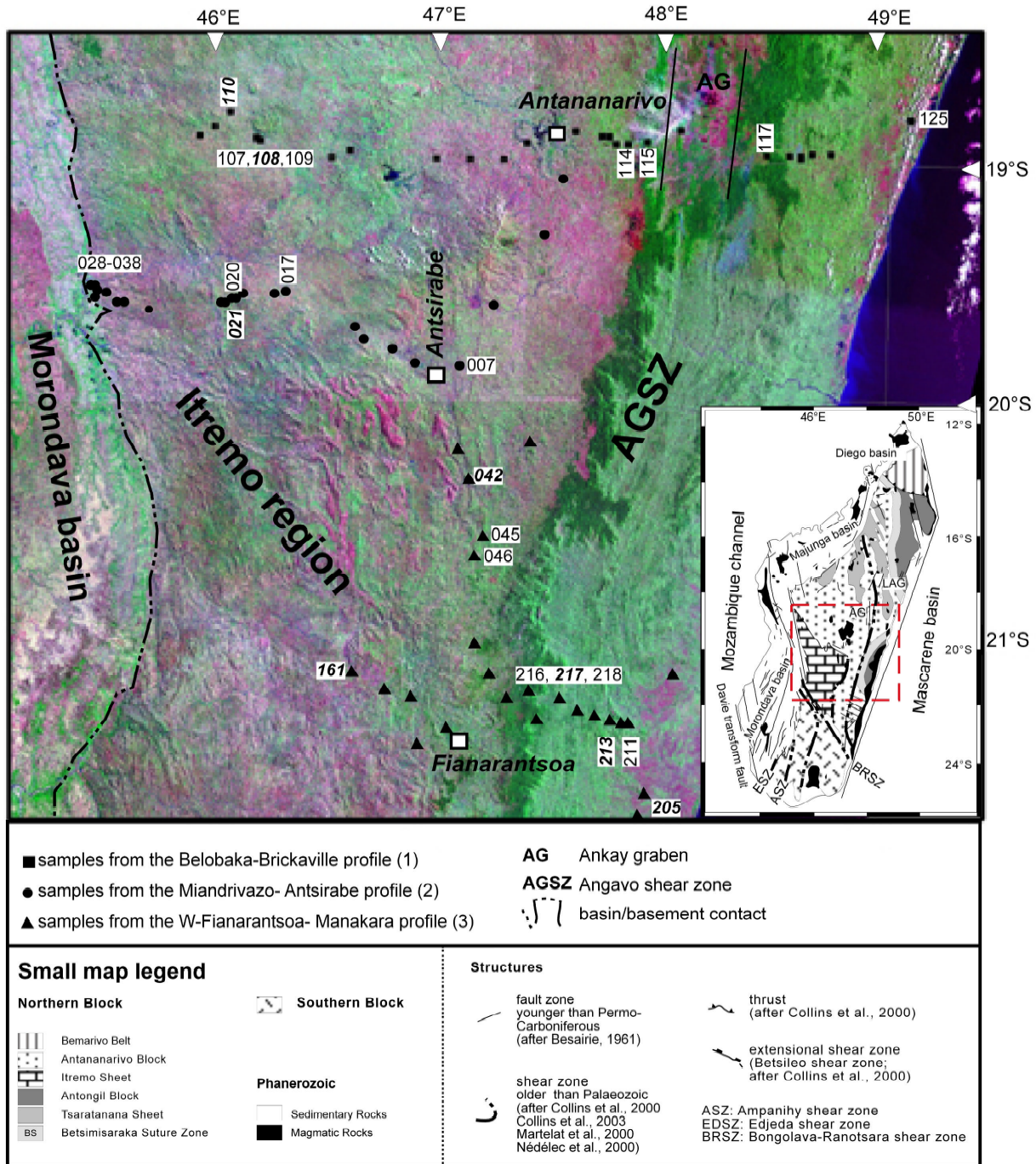


**Fig. 3.2:** Landsat 7 TM (RGB: 742; UTM Zone 38 south; WGS 84) satellite image of central Madagascar with superimposed sample locations. Discussed samples are given with numbers. Inlay: generalised geological and structural map of Madagascar, modified after Besairie, (1961, 1973), Collins et al. (2000, 2001), Martelat et al. (2000) and Nédélec et al. (2000). Abbreviations: AG: Ankay graben; AGSZ: Angavo shear zone; LAG: Lac Alaotra graben

## 2.2 Separation of Madagascar

Crustal extension between eastern (Madagascar, India, Antarctica and Australia) and western Gondwana (Africa, Arabia and South America) commenced along former Pan-African ductile high strain zones at the end of the Carboniferous (Piqué et al., 1999). The intracratonic rift basin evolution is recorded in the sedimentary rocks of the Karoo Supergroup (Upper Carboniferous-Middle Jurassic), which is divided in Madagascar into the Sakoa, Sakamena and the Isalo groups (Besairie, 1972).

The oldest sedimentary rocks of Madagascar belong to the Late Carboniferous to Late Permian Sakoa Group, the basal deposits of the Karoo Supergroup. The Sakoa succession is restricted to several local pull-apart basins, which evolved along N-S trending strike-slip faults. The development of the pull-apart basins is related to an N-S orientated intraplate compressive stress regime during the Late Carboniferous to the Late Permian (Schandelmeier et al., in press). Structural data obtained from the Sakamena and Isalo groups indicate a gradually development from a transtensional to a pure tensional stress regime. The tectonic reorganisation during the Permo-Triassic had a significant influence on the depositional system. The basin extended and a half-graben system developed as a result of an increasing orthogonal extensional strain (Schandelmeier et al., in press).

From the Middle Jurassic a passive margin formed along the northwestern coast of Madagascar, whereas a transform margin evolved along the southwest coast. The Davie transform fault southwest of Madagascar governed the translation between East Africa and Madagascar.

The Late Cretaceous Madagascar-India break-up was associated with Marion hot spot related volcanism (Storey et al., 1995), as indicated by voluminous volcanic rocks along the eastern coast of Madagascar (Figs. 3.2 and 3.3). It is uncertain whether the hot spot triggered the opening of the Mascarene basin (~90 Ma) or whether it was concomitantly coupled with transform movements along fracture zones (e.g. Storey et al., 1995; Chand and Subrahmanyam, 2003).

After a period of tectonic quiescence, crustal extension restarted in Miocene times. Some authors (e.g. Malod et al., 1991; Rasamimanana, 1996) suggest that extensional tectonism continued during Oligocene and Quaternary times as indicated by various volcanic rocks (Figs. 3.2 and 3.3) and recent seismic activities in central Madagascar. Thereafter the N-S striking Ankey graben was formed in the eastern part of the island (Fig. 3.2) in response to extensional tectonics. It is assumed that pre-existing basement structures were reactivated during this time (Piqué et al., 1999).

### 3. Structural analysis

The brittle structures of the basement were recorded in all visited outcrops and were compared with those recorded in the sedimentary rocks of the Morondava basin (Fig. 3.3), in order to investigate the different temporal structural evolution of the Gondwana break-up in the study area. Since the infrastructure is poorly developed and accessible outcrop locations are rare, field data were complemented by structural data obtained from satellite image interpretation. A set of Landsat 5 and 7 satellite images, covering most parts of central Madagascar, was used to identify the major ductile and brittle structures. After image processing (georeferenciation, image enhancement), selected regions were analysed. Interpretation of Landsat TM images was carried out using different 3-band composites (RGB compositions: 742, 741, 321 and 753). Lineament mapping was proceeded by visual inspection. Only obvious brittle structures (faults with clear linear anomalies, clear secant relation with ductile structures, relatively long structures >500 m) were mapped. Rose plots of brittle structures gained from remote sensing investigations are given with weighting the individual lengths of the structures (Fig. 3.3).

#### 3.1 Ductile structures

Using Landsat TM satellite images three main litho-structural trends are observed within the metamorphic basement of central Madagascar. These are, the structures related to the metasedimentary rocks of the Itremo region in the southwestern working area, a central area around Antananarivo, and the AGSZ in the eastern part of the island (Fig. 3.3). The main ductile lineaments in the western working area trend ~NW-SE and east of the Antananarivo-Antsirabe- Fianarantsoa axis ~N-S (Fig. 3.3).

Parts of the AGSZ, as the dominant ductile structure in the working area, can be traced for ~340 km along strike and ~60-80 km in width. A total length of ~85 km and a width of ~3-10 km for the VZ was estimated from Landsat TM satellite images. Using Landsat TM satellite images the ~N-S trending BetSZ is difficult to identify, because of its small width.

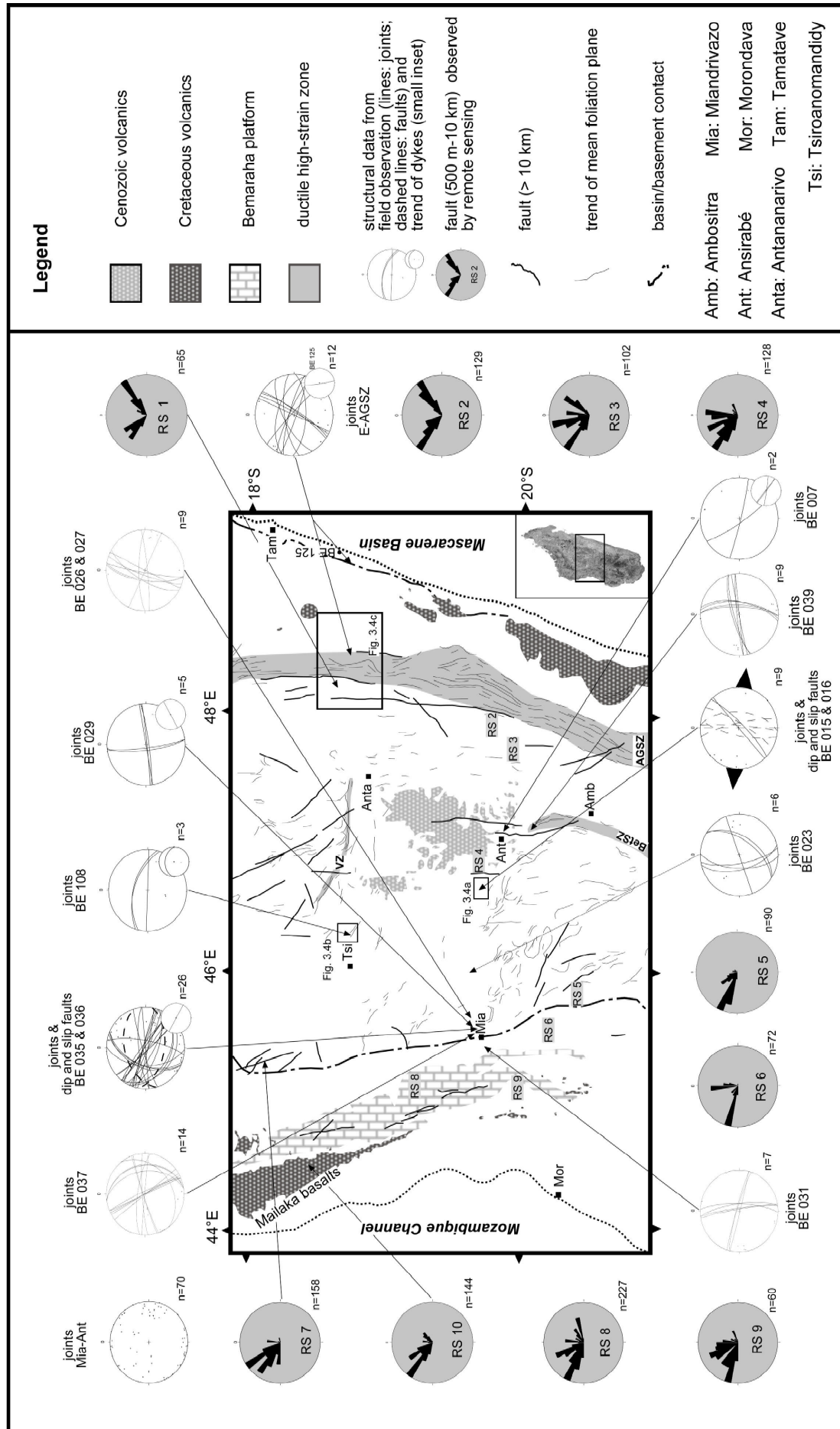


**Fig. 3.3:** Ductile structures and main lineaments >10 km derived from Landsat TM 5 and 7 image interpretation. Structural data based on fieldwork and examination of six Landsat 5 and 7 satellite images are given as stereoplots; white stereoplots: structural data from fieldwork; white subordinate stereoplots: magmatic dykes; grey stereoplots: structural data based on Landsat 5 and 7 satellite image interpretation. AGSZ: Angavo shear zone; BetsZ: Betsileo shear zone; VZ: Virgation zone

### 3.2 Brittle structures and magmatic dykes

Large brittle lineaments (>10 km in length) were documented using satellite images. These lineaments occur within the metamorphic basement and the Jurassic Bemaraha carbonate platform. The prominent brittle structures observed in the basement partly follow the foliation trend (Fig. 3.3). In the western and northern working area they mainly strike ~NW-SE. East of the Antananarivo- Antsirabe- Fianarantsoa axis the main lineaments strike ~N-S and follow again Early Cambrian ductile structures. Sets of ~NNW-SSE trending lineaments occur in the Middle Jurassic Bemaraha platform (Fig. 3.3).

Brittle structures obtained from field observations were compared with nearly 1200 small-scale lineaments (500 m to 10 km in length), which were mapped and measured using Landsat TM satellite images. Results of structural investigations are given as stereoplots (Fig. 3.3).

Many parts of central Madagascar show no brittle deformation. Only certain zones show brittle structures with inconsistent strike. Two main trends could be separated.

a) The brittle structures between the present basement/basin contact and the western limit of the AGSZ show a very complex distribution pattern. The main component along the western margin of the basement are ~NW-SE trending lineaments (Fig. 3.3: RS 5, RS 7, BE 035 and 036, BE 037). Subordinate occur ~N-S striking structures (Fig. 3.3: BE 037) and ~E-W trending joints (Fig. 3.3: BE 035 and 036, BE 037) which can be traced also further east (Fig. 3.3: RS 4, BE 039).

b) Around the AGSZ occur well defined ~NW-SE and ~NE-SW striking brittle structures (Fig. 3.3: RS 1, RS 2 and joints E-AGSZ). It is likely that these fabrics are related to the Cretaceous Madagascar-India break-up.

Brittle structures of five representative areas of sedimentary rocks within the northern Morondava basin were evaluated. These areas belong to the Late Permian-Early Triassic Sakamena Group (BE 031), the Middle-Late Triassic Isalo Group (RS 6), the Middle Jurassic Bemaraha platform (RS 8 and RS 9) and to the Late Cretaceous Mailaka basalts (RS 10). The dominant strike trend of brittle structures in all sedimentary units is ~NW-SE to ~WNW-ESE. Subordinate, ~N-S (Sakamena Group and Isalo Group) and ~NE-SW (Bemaraha platform and Mailaka basalts, RS 8, RS9 and RS 10) trending structures were observed.

Cretaceous and Tertiary magmatic dykes mapped in central Madagascar seem to follow pathways provided by brittle structures (Fig. 3.3: BE 005, BE 007, BE 035 and 036, BE 108). Thus, these structures must be older or of the same age than the emplacement of the mafic dykes. One dyke from the eastern coast seems to follow the ~N-S striking ductile lineaments, deviating from the main brittle deformation direction (Fig. 3.3: see BE 125 and normal faults E-AGSZ).

#### 4. Fission track analysis

Samples for the thermochronological studies were taken from three east-west traverses across central Madagascar (Fig. 3.2). Below, they are presented from the north to the south.

##### a) Belobaka to Brickaville

Twenty-seven basement rocks were sampled along an E-W section running from the central highland, east of the Morondava basin margin (45°54'E) towards the eastern coast of Madagascar (49°04'E). At three localities (BE 107-109) Cretaceous magmatic veins cross cut the metamorphic rocks (Fig. 3.4). The section crosses the Neogene Ankay graben east of Antananarivo, which is thought to be related to Cenozoic E-W extensional tectonics (Bertil and Regnault, 1998).

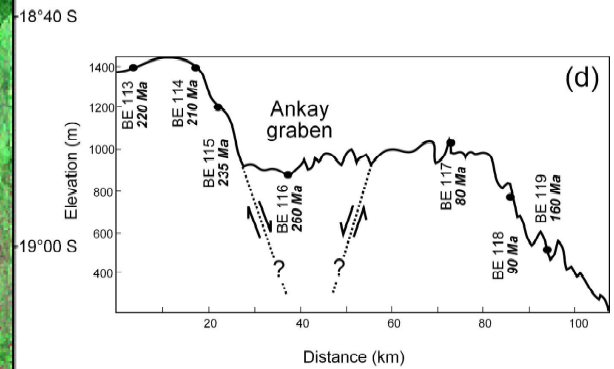
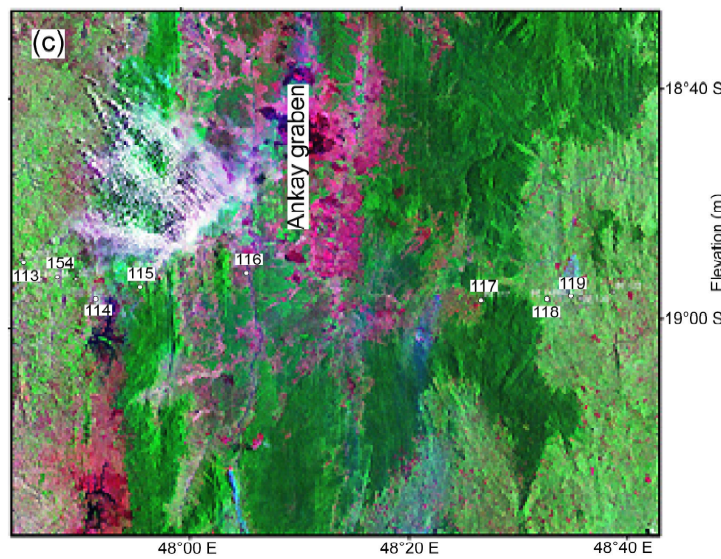
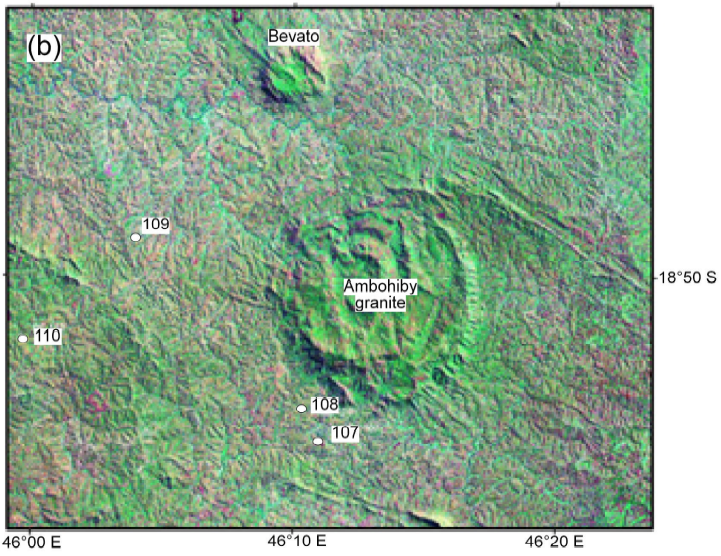
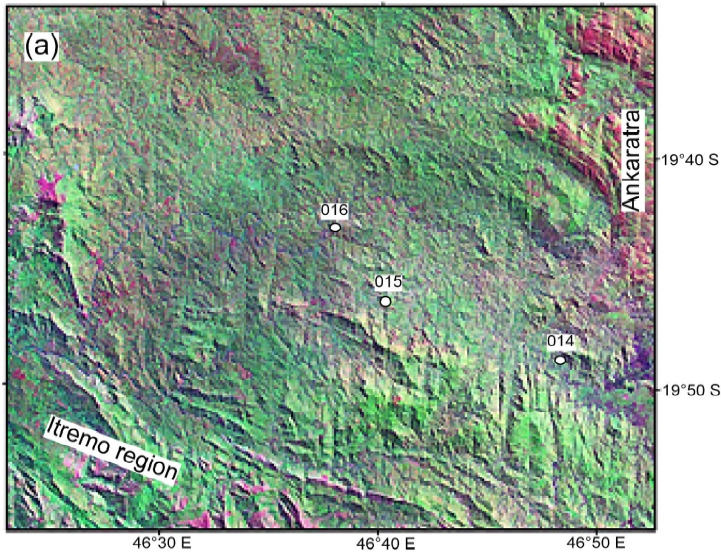
##### b) Miandrivazo to Antsirabe

The section (twenty-five basement rock samples) runs from the present basin/basement contact at Miandrivazo (45°27'E) towards east of Antsirabe (47°25'E), into the central highland. Near Antsirabe, samples were taken from basement units in the direct vicinity of the voluminous Ankaratra volcanic rocks (Figs. 3.2 and 3.3). Southeast of the profile the Antananarivo Block is overlain by metasedimentary rocks of the Itremo massive.

##### c) West of Fianarantsoa to Manakara

Twenty-two basement samples were taken from a traverse running from west of Fianarantsoa (46°38'E) towards Manakara (48°05'E). This is the southernmost section, which we investigated, in central Madagascar. Approximately 140 km south of Fianarantsoa the NW-SE running BRSZ is the border between the northern/central and the southern basement block (Fig. 3.2).

**Fig. 3.4** (next page): Landsat 7 TM satellite images (RGB: 742, UTM WGS 84, zone 38) of three selected areas and photographs of related outcrops. a) NS striking structures in a region east of Antsirabe. The apatite FT data of samples BE 014, 016 and 017 (~35 km NW of location BE 016, not on the map) suggests a Karoo-aged graben whereby BE 016 is located within the graben and BE 014 and BE 017 are at the eastern and western graben shoulders. Also the observed brittle structures (see photos BE 015a, b argue for a graben resulted from E-W extensional movements (see Fig. 3.3). Photograph BE 015 a: Cataclastic fault within the metamorphic basement; photograph BE 015 b: mesoscopic graben structure. b) The Ambohiby granite is surrounded by Cretaceous magmatic dykes, which are not apparent on satellite images. In the outcrops a number of ~10-20 cm wide mafic dykes, striking through the granitic basement, were observed (photo BE 108). Apatite FT data from the samples located around the Ambohiby granite are affected by the emplacement of the mafic dykes. c) Sampled profile across the Ankay graben. One sample (BE 116) with an apatite FT age of ~260 Ma is located within the graben. The youngest apatite FT age is ~80 Ma from a sample (BE 117) at the eastern graben shoulder. d) Vertical profile along 19 °S from 47.8° E to 48.6° E across the Ankay graben with sample locations and apatite FT ages.



#### 4.1 Titanite and apatite FT preparation, dating and modelling procedure

Titanite FT analysis documents the cooling of a sample to below 310-265 °C (Coyle and Wagner, 1998). Apatite FT analysis is an established technique to identify vertical movements of crustal units in the very low temperature range between ~110 and 60 °C.

Titanites and apatites were separated using conventional crushing, sieving, magnetic and heavy liquid separation techniques. Titanites were etched individually for 17-22 min in a mixture of HF, HNO<sub>3</sub>, HCl and H<sub>2</sub>O (1:2:3:6). Apatites were etched for 50 sec. in 5 % HNO<sub>3</sub> (23 °C) to reveal spontaneous tracks (e.g. Wagner and van den Haute, 1992). Samples were irradiated in channel 7 and 8 of the Thetis reactor at the Institute for Nuclear Sciences Gent (Belgium), using a total thermal neutron flux of  $1 \times 10^{16}$  ncm<sup>-2</sup> (apatite) and  $0.6 \times 10^{16}$  ncm<sup>-2</sup> (titanite). Detectors were etched for 15 min in 40 % HF (23 °C) to reveal induced tracks. Titanite and apatite FT ages were measured using the external detector method (Gleadow, 1981). Titanite and apatite ages are presented as central ages with 1 sigma error.

Apatite FT data, including single grain apatite FT ages, track lengths and standard deviations, were used to model specific hypothetical temperature-time (T-t) paths. An inverse modelling procedure applying the program "MONTE TRAX" (Gallagher, 1995) was carried out using the Laslett annealing model for Durango apatite (Laslett et al., 1987). The modelling was performed with a "genetic algorithm" (Gallagher and Sambridge, 1994), in which the best fitting model of the recent modelled generation is used as a basis for the next modelling step. Twenty generations were modelled with 100 individual T-t histories being tested per generation.

#### 4.2 Results and interpretation of titanite FT data

Twenty-two titanite FT ages vary between  $483 \pm 33$  Ma and  $266 \pm 13$  Ma (Tab. 3.2). Titanite FT ages are younger than the assumed crystallisation or metamorphic ages of the samples, indicating that the study area underwent a protracted thermal history since the last ductile deformation at ~550 Ma (Meert et al., 2002). Oldest titanite FT ages range between ~480-400 Ma. They occur in the centre of the island and indicate cooling to below ~300 °C after the last metamorphic event. Towards the east and west titanite FT ages decrease to ~340 Ma with youngest ages of ~270 Ma in the vicinity of the Ambohiby granite (Figs. 3.4b and 3.5e).

The single grain ages show a broad distribution ranging from ~800 Ma to ~200 Ma indicating that a few samples most probably reflect simple cooling ages whilst others show the effects of significant post emplacement and/or post metamorphic thermal events. Single grain ages can be grouped into four age groups related to main geological periods. These are the Pan-

African (>500 Ma), Palaeozoic (500-300 Ma), Karoo (300-200 Ma) and break-up (<200 Ma) related single grain ages (Fig. 3.6).

Samples from the central and the eastern part of the working area have Pan-African, Palaeozoic and Karoo titanite single grain age components, whereby the Palaeozoic age group is always dominant. The Pan-African related titanite single grain ages occur most frequently in the centre of the study area. The Karoo type component is common in the vicinity of the western basement margin with a maximum at ~46.3 °E (Fig. 3.6a). Remarkably, only one sample from the eastern coast has one grain with a break-up related titanite FT age.

The  $\chi^2$ -values of the samples vary between 0 % and 97 % (Tab. 3.2). Eight samples failed the  $\chi^2$ -test indicating a complex cooling history. Sample BE 108 located near the Ambohiby granite (Fig. 3.4b) has the youngest titanite FT age of  $266 \pm 13$  Ma. The relatively low  $\chi^2$ -value and the single grain age distribution of the sample argue for a later thermal overprint and partial annealing, potentially during the emplacement of Cretaceous magmatic dykes observed in the sampled outcrop (Fig. 3.4, BE 108). Sample BE 046 from the eastern margin of the Itremo group has a mixed titanite FT age of  $483 \pm 33$  Ma. Thermal effects of a postulated ~500 Ma fluid circulation event around the Itremo region (Fernandez et al., 2003) most likely caused partial annealing of the titanites. Sample BE 205 ( $\chi^2 = 0$  %) located ~20 km west of the eastern coastline has a titanite FT age of  $340 \pm 22$  Ma and a broad spread in single grain ages from ~500 Ma to ~200 Ma. The titanite FT data indicates that the sample was most probably slightly partially annealed by the Madagascar-India break-up related magmatism with temperatures not exceeding ~300 °C.

The titanite FT ages show a moderate positive correlation with elevation (Fig. 3.7d). Above 600 m elevation the distribution is wide gritted (~500-250 Ma) and below 600 m elevation (samples from the eastern continental margin and the western margin of the basement) a narrow age distribution (~400-340 Ma) is given (Fig. 3.7d). This argues for a nearly simultaneous thermal evolution between 310 °C and 260 °C for the samples from the western palaeo margin and the eastern continental margin.

The titanite FT ages plotted against the E-Longitude (Fig. 5e) show a complex age distribution from the western margin of the basement towards the eastern continental margin of the island. The westernmost samples, located near the present basement/basin contact are ~340 Ma old. After a break at ~46 °E the ages increase from ~250 Ma to ~450 Ma towards the centre of the island with oldest ages along the eastern margin of the Itremo Group. A set of six samples east of ~47.5 °E defines this trend. The samples located east of the AGSZ are significantly younger (~340 Ma) than samples from the central area. Their age distribution pattern is similar to those from the western palaeo margin (Fig. 3.5e).

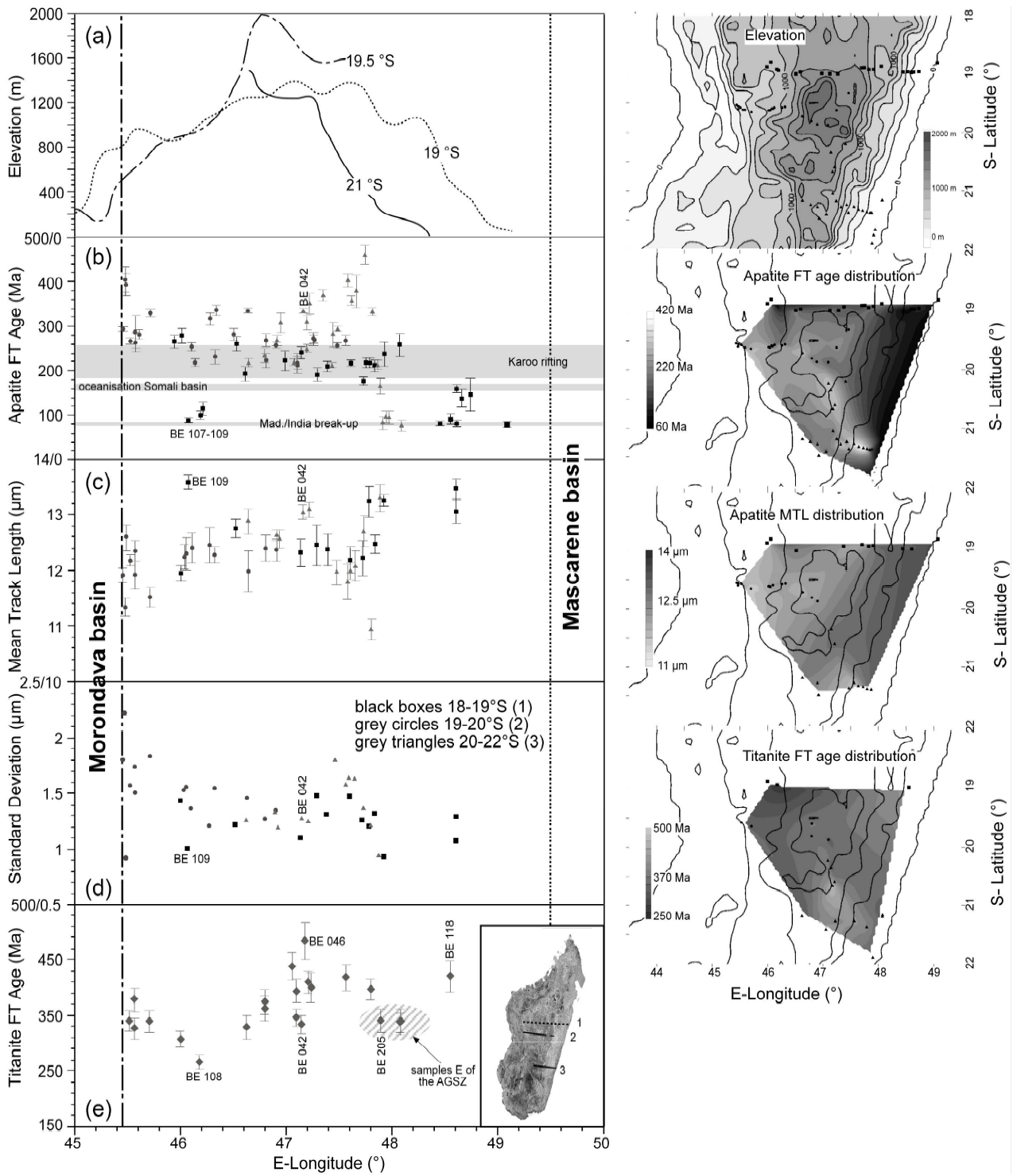


**Fig. 3.5:** FT data plotted against the E-Longitude.

- a) Topography of the sampled sections based on ETOPO 5 data-set
- b) Apatite FT ages
- c) Apatite mean track length
- d) Apatite standard deviation
- e) Titanite FT ages.

Errors are given at the one sigma interval. On the right side: elevation model and distribution maps of the FT parameter in central Madagascar.

### 4.3 Results and interpretation of apatite FT data

Forty-seven apatite FT ages vary between  $460 \pm 21$  Ma and  $77 \pm 9$  Ma. The mean track lengths (MTL) range from  $13.69 \pm 0.11$   $\mu\text{m}$  to  $11.34 \pm 0.52$   $\mu\text{m}$ . The standard deviations vary between  $2.22$   $\mu\text{m}$  and  $0.92$   $\mu\text{m}$  (Tab. 3.2). Twenty-one samples failed the  $\chi^2$ -test indicating a complex single grain age distribution and a protracted cooling path. Like the titanite single grain ages the apatite individual grain ages were divided into a Palaeozoic, Karoo and break-up related age group (see above). In general, the apatite single grain age distribution (Fig. 3.6b) shows two different regional patterns. The samples from the Mesozoic palaeo-western margin and from the central part show dominantly Palaeozoic and Karoo single grain age components. In contrast, the samples from the eastern coast (east of  $\sim 48^\circ\text{E}$ ) are characterised by break-up related single grain ages (Fig. 3.6b). This is a significant difference to the titanite single grain age distribution where samples from the western palaeo margin and from the eastern continental margin have nearly the same grain age distribution (compare Fig. 3.6a, b).

In general, the apatite FT ages show a complex distribution from the palaeo-western margin towards the eastern-coast (Fig. 3.5b). Along cross sections 1 and 2 (Fig. 3.2, grey circles and black boxes), from west to east apatite FT ages decrease from  $\sim 330$  Ma to  $\sim 100$  Ma. The apatite FT ages from the Fianarantsoa-Manakara profile increase from the west to the AGSZ from  $\sim 220$  Ma to  $\sim 380$  Ma. A break in the age trend to Cretaceous apatite FT ages ( $\sim 90$  Ma) occurs east of the AGSZ. The relationship between the MTL and the E-Longitude shows a general increase in MTL from  $\sim 11.5$   $\mu\text{m}$  to  $\sim 13.4$   $\mu\text{m}$  towards the eastern coast (Fig. 3.5c). Remarkable is the break in the trend at  $\sim 47^\circ 50' \text{E}$ . Here the samples from the southernmost profile have significantly shorter MTL ( $\sim 12$   $\mu\text{m}$ ) compared to samples immediately to the E and W ( $12.2$ - $13.4$   $\mu\text{m}$ ). Standard deviation of the MTL starting at  $\sim 1.5$ - $2.5$   $\mu\text{m}$  exhibit a decreasing trend towards the eastern coast to values less than  $1.5$   $\mu\text{m}$ . A significant exception for this general trend is found in four samples in the region around  $47^\circ 50' \text{E}$  where standard deviations  $> 1.5$   $\mu\text{m}$  were observed.

The samples from the Belobaka-Brickaville traverse show an increase of apatite FT age with elevation. The MTL decrease with elevation (Fig. 3.7a). A totally different trend is displayed by the samples from the Miandrivazo-Antsirabe profile. Figure 3.7b shows decreasing apatite FT ages with increasing elevation. Two samples in direct contact to the Sakamena Group have apatite FT ages of  $\sim 400$  Ma. All other samples show a broad scatter in apatite FT ages ranging from  $\sim 370$  Ma to  $\sim 240$  Ma.

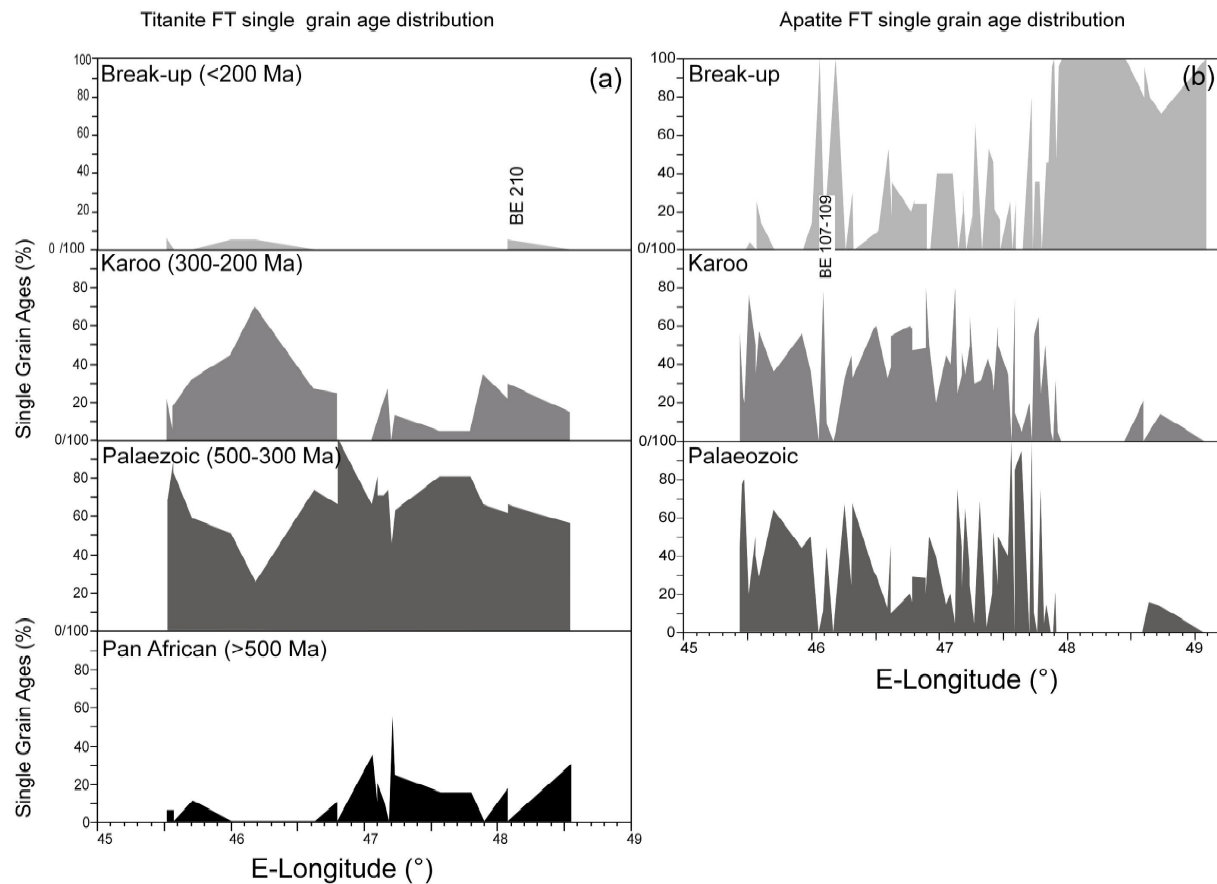


**Fig. 3.6:** Titanite and apatite single grain age components in percent plotted vs. the E- Longitude. The single grain ages of all dated samples were separated into specific age groups and were plotted against the eastern sample positions. The single grain age distribution between two sample locations is estimated by a linear regression.

The MTL tend to increase with elevation (Fig. 3.7b). The apatite FT age vs. elevation plot of the Fianarantsoa-Manakara section (Fig. 3.7c) shows a complex distribution pattern. In this profile the oldest apatite FT ages were observed at the eastern escarpment within the AGSZ. The youngest samples are from elevations <300 m. The samples from the eastern margin of the escarpment (600-300 m) show an increase in apatite FT ages with elevations. In contrast, the samples from elevation >800 m have a scattering age distribution. The MTL's decrease with decreasing elevation, with the exception of sample BE 211 ( $13.30 \pm 0.20 \mu\text{m}$ ). From the "Cretaceous" apatite FT ages no MTL information are available.

The relationship between the elevation and apatite FT age distribution from the three profiles is affected from the section positions with regard to the distance from the palaeo western continental margin. Different denudation/sedimentation cycles after Late Permian times affected the FT pattern of the three sections.

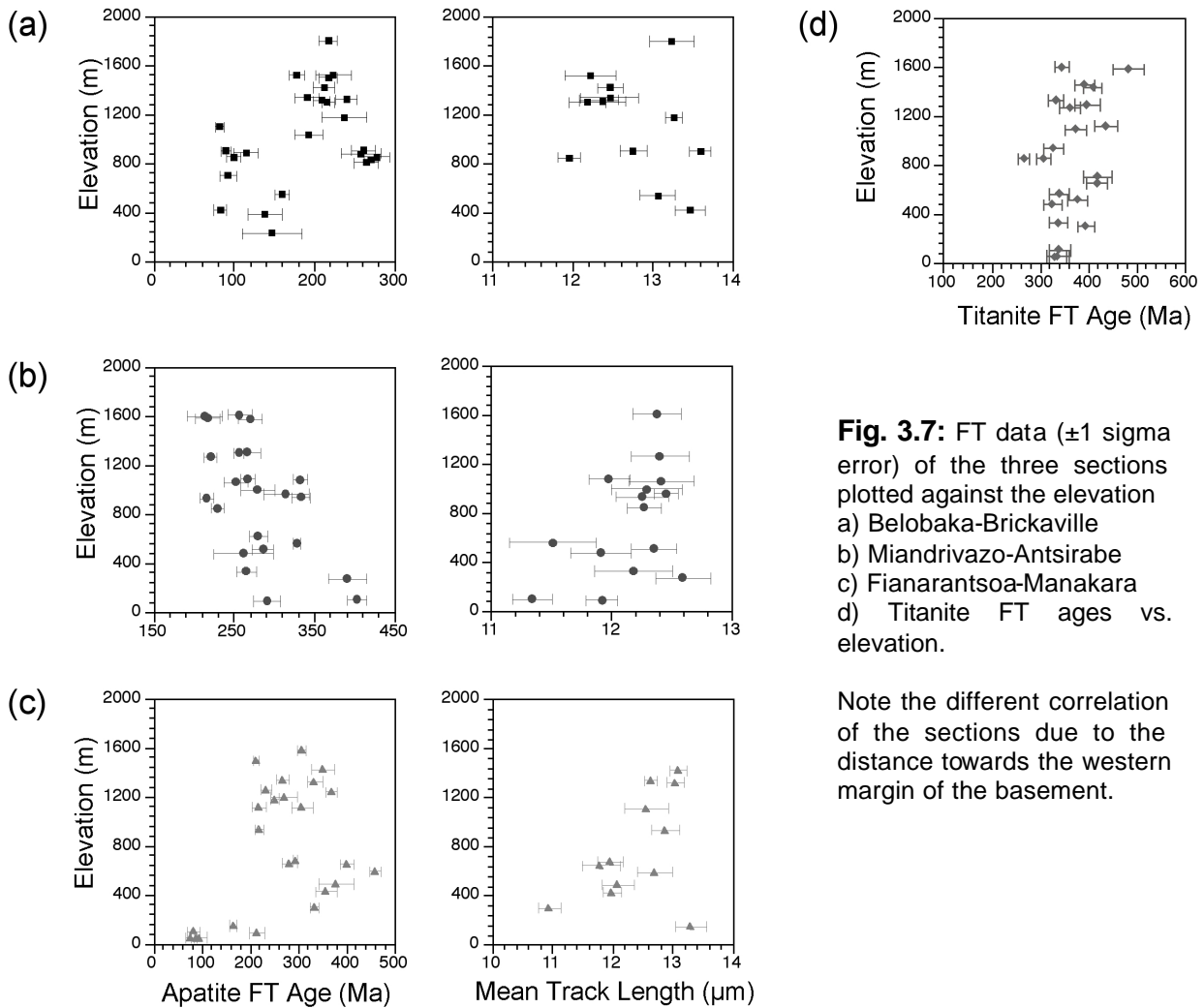


**Fig. 3.7:** FT data ( $\pm 1$  sigma error) of the three sections plotted against the elevation  
 a) Belobaka-Brickaville  
 b) Miandrivazo-Antsirabe  
 c) Fianarantsoa-Manakara  
 d) Titanite FT ages vs. elevation.

Note the different correlation of the sections due to the distance towards the western margin of the basement.

Samples BE 107-109 with apatite FT ages between  $\sim 90$  Ma and  $\sim 115$  Ma are located  $\sim 85$  km east of the palaeo-western margin (Fig. 3.2). The single grain ages are break-up related in contrast to the surrounding samples (Fig. 3.6b). Mafic magmatic dykes were observed close to the sampled outcrops (Fig. 3.4, BE 108). These are most probably associated with Late Cretaceous break-up related volcanism that especially affected the eastern coast and the sedimentary basins (Figs. 3.2 and 3.3).

#### 4.4 Calculated cooling and denudation rates from FT data

70 % of the titanite FT data from central Madagascar range between  $\sim 400$ - $310$  Ma. The broad single grain age distribution and the low  $\chi^2$ -values suggest that most ages are not simple cooling ages related to the last metamorphic event. For the calculation of exhumation and denudation rates we generally assumed a geothermal gradient of  $30$   $^{\circ}\text{Ckm}^{-1}$ .

Cooling rates for the ~500-100 Ma time span were calculated (calculation see Fig. 3.8b) using 19 combined titanite and apatite FT samples. Additionally, two samples linking biotite  $^{40}\text{Ar}/^{39}\text{Ar}$  ages (Meert et al., 2002) and apatite FT ages were taken into account. The calculated cooling rates range between  $12.5\text{ }^{\circ}\text{C/Ma}^{-1}$  and  $0.4\text{ }^{\circ}\text{C/Ma}^{-1}$ . The cooling rates decrease from the western palaeo margin with maximum rates of  $10\text{ }^{\circ}\text{C/Ma}$  towards the E-coast with maximum cooling rates of  $0.55\text{ }^{\circ}\text{C/Ma}$ . Some samples east of the Itremo region don't follow this trend (Fig. 3.8a).

We suggest that two periods of fast cooling affected the working area (Fig. 3.8c). Samples from the southernmost profile located east of the Itremo region and within the AGSZ are influenced by a ~420-330 Ma event, which itself most probably is caused by fluid circulation due to the emplacement of pegmatite fields in central Madagascar (Fernandez et al., 2003). Suggesting an average minimum cooling rate of  $1.9\text{ }^{\circ}\text{C/Ma}$  (calculated from samples BE 045, BE 213 and BE 217) ~5.5 km of crustal section was exhumed during this time. Samples located near the present basin/basement contact are influenced by a ~370-260 Ma phase of accelerated cooling (Fig. 3.8c). This event is pre- and synchronous with the deposition of the Karoo Supergroup within the northern Morondava basin. We suggest that it is related to fast denudation along the palaeo western margin. With an average minimum cooling rate of  $2.2\text{ }^{\circ}\text{C/Ma}^{-1}$  (calculated from samples BE 026, BE 037, BE 038 and BE 110) a minimum amount of ~8 km denudation for the ~370-260 Ma episode was estimated. Such estimates can vary between adjacent areas, as shown by the combined titanite FT data and modelled apatite FT data of sample BE 038 (Fig. 3.9). Using this data denudation of ~8 km during the shorter ~330-305 Ma period was calculated.

Sample BE 042 (from a highly strained granite located within the BetSZ) is characterised by nearly identical titanite ( $333\pm 16\text{ Ma}$ ) and apatite FT ( $334\pm 16\text{ Ma}$ ) ages, relatively long apatite MTL and highest maximum cooling rates of  $12.5\text{ }^{\circ}\text{C/Ma}$  (Fig. 3.8a). Most probably temporary hot fluids ascending along faults heated the rocks to  $>310\text{ }^{\circ}\text{C}$ , resulting in identical titanite and apatite FT ages. It is suggested, that these data indicate advective heating in the BetSZ at ~330 Ma.

T-t histories for 16 apatite FT samples were modelled. Based on these cooling paths amounts of denudation were calculated for several time spans. The modelled cooling paths of two samples from the AGSZ (BE 216 and BE 218) show a Silurian-Devonian cooling step (Fig. 3.9). These results are in good agreement with fast cooling derived from combined titanite and apatite FT analyses in this region (BE 217 and BE 213). Even though calculated cooling rates from combined analyses of titanite and apatite FT ages and from combined titanite FT ages and modelled cooling parameters do not fit exactly.

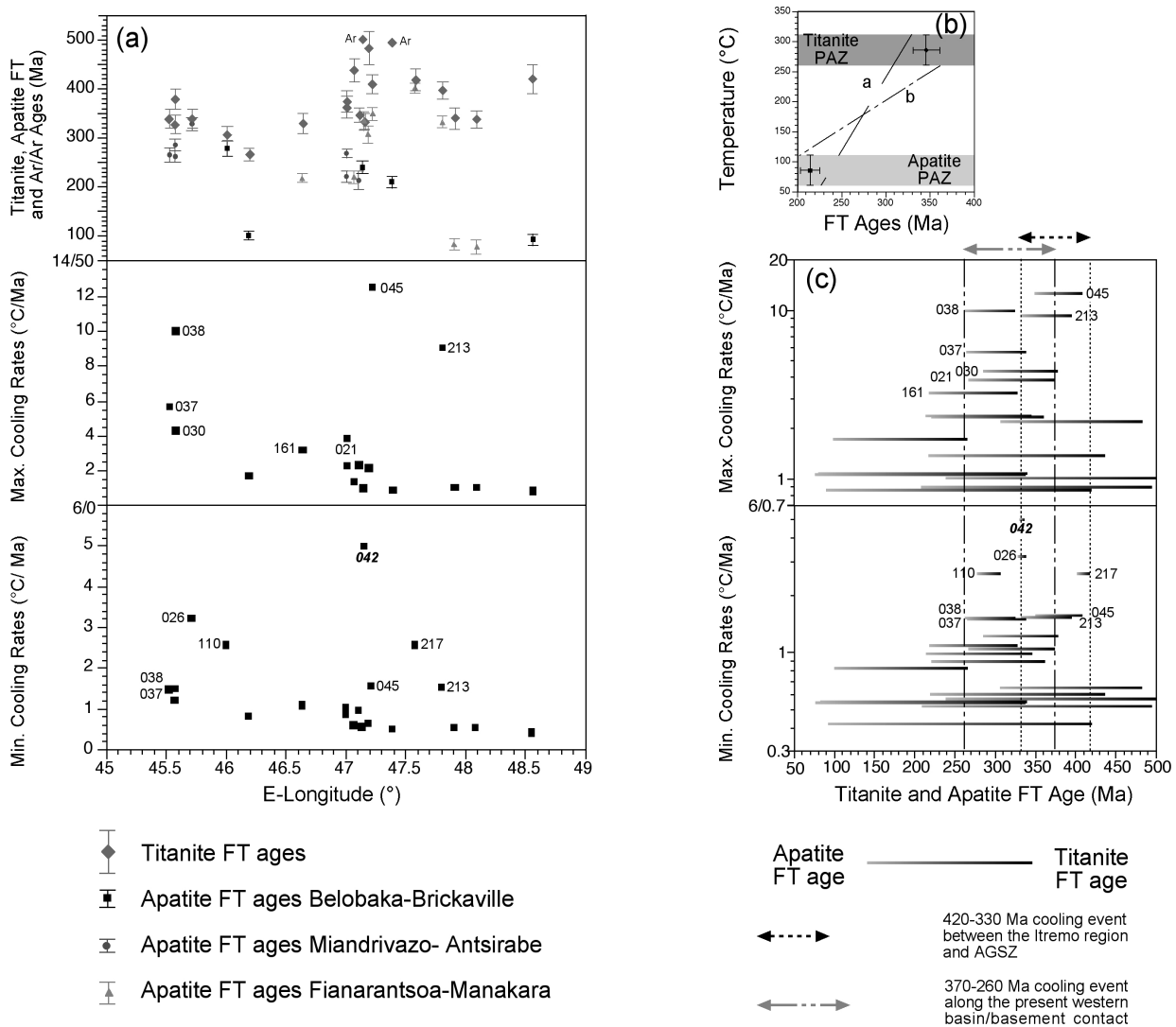


**Fig. 3.8:** Maximum and minimum cooling rates calculated from combined titanite and apatite FT data. a) Cooling rates plotted against the E-Longitude b) Titanite FT ages and apatite FT ages plotted against the temperature. In different greys the partial annealing zones for the two dating methods. Example for the calculation of cooling rates. Maximum cooling rates were calculated using slope a and minimum cooling rates using slope b. c) Titanite FT and apatite FT ages plotted against the maximum and minimum cooling rates to give time constraints of the cooling events. Numbers of discussed samples are given.

A Mesozoic denudation history can be constrained from modelled cooling paths of four samples (BE 017, BE 020, BE 114, BE 115). Sample BE 017 and BE 020 are located ~80 km and sample BE 114 and BE 115 ~250 km east of the present basin/basement contact. T-t paths (Fig. 3.9) show a ~300-250 Ma (BE 017, BE 020) and a ~270-230 Ma (BE 114 and BE 115) cooling step. The cooling paths of the samples argue for crossing the apatite partial annealing zone (PAZ: 110-60 °C) during these two time intervals. Thus, for these parts of the island an amount of ~2-4 km of denuded crustal section during these time periods can be assumed.

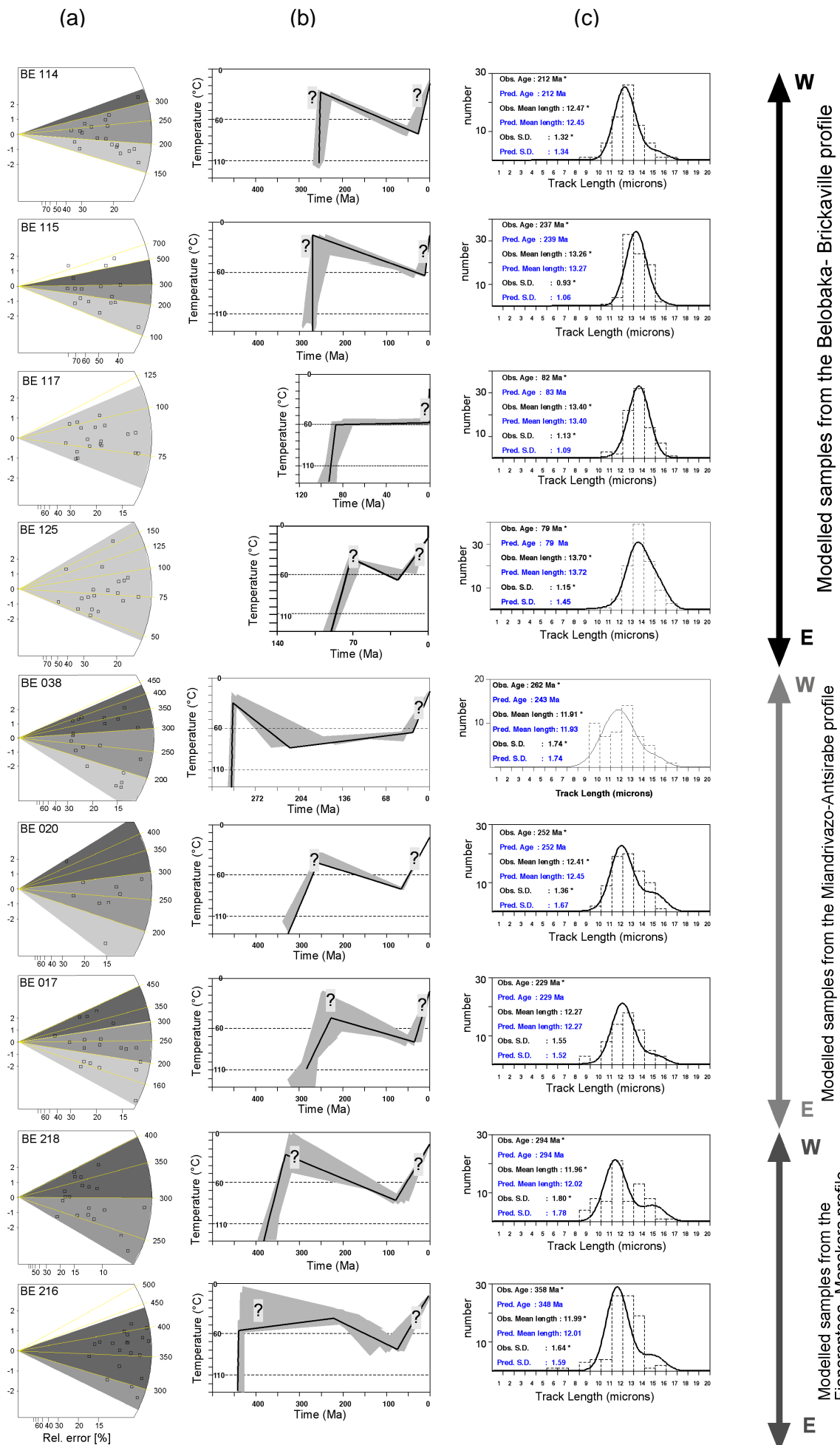
The modelled samples from the eastern coast show a Late Cretaceous cooling step. For sample BE 117 and BE 125 denudation of >3.5 km crustal section can be assumed. These samples are located ~60 km and ~10 km inland from the eastern coast of Madagascar. The modelled samples from the southernmost profile are located ~70-85 km inland (BE 216 and BE 218). The apatite FT ages are  $358\pm 14$  Ma and  $294\pm 14$  Ma. The models show a Late Cretaceous cooling step but the amounts of denudation are significantly lower (~2 km) compared to calculated denudation amounts of the northern samples. In the southernmost profile Cretaceous FT ages were observed, but no T-t modelling was conducted as only an insufficient number of confined tracks could be measured. Most of the modelled T-t paths of samples from western and central Madagascar show an Eocene final cooling (Fig. 3.9). Probably this event is only an artefact of the model program. However, the modelled last cooling steps pre-date the emplacement of the Ankaratra lava series (~28-3 Ma; Piqué et al., 1999). Modelled cooling paths of 11 samples argue for denudation of ~1.5-2.5 km since Eocene times in the centre of the island.

**Fig. 3.9** (next page): Modelling results of selected samples

a) Radial plots: Sample number is given on the left side of the plot. Note the variations in FT age between individual grains. The different greys mark the single grain age components (for explanations see text)

b) T-t path: the cooling histories were modelled using the program MONTE TRAX (Gallagher, 1995). The black line represents the thermal history that fits best the observed data; shaded areas are possible cooling histories.

c) Length histogram: The measured mean confined track lengths are shown as histograms. The curve displays the modelled track length distribution for the "best fit" (black line in b). Fitting parameters on the left side. Abbreviations: Obs.: Observed, Pred: predicted, SD: standard deviation.



Sample Nr.	E-Long.	Elev.	Grains	(N <sub>s</sub> )	(N <sub>i</sub> )	(N <sub>a</sub> )	P(c <sup>2</sup> )	FT Age ± 1 s	U-cont.	MTL ± 1s SD[μm] Nr. of ms. tracks
Rock Type	S-Lat.	[m]	Mineral	r <sub>s</sub> [x10 <sup>5</sup> cm <sup>-2</sup> ]	r <sub>i</sub> [x10 <sup>5</sup> cm <sup>-2</sup> ]	r <sub>a</sub> [x10 <sup>5</sup> cm <sup>-2</sup> ]	[%]	[Ma]	[ppm]	
BE 001 migmatite	47°33' 19°05'	1300	20 apatite	199 3.358	181 3.055	7400 14.83	47	266 ± 28	3	-
BE 003 migmatic gneiss	47°28' 19°19'	1300	20 apatite	1104 7.568	1043 7.149	7400 14.81	63	256 ± 13	7	-
BE 005 augen gneiss	47°15' 19°37'	1575	18 apatite	456 5.98	407 5.337	7400 14.78	47	270 ± 20	6	-
BE 007B pegmatite	47°06' 19°53'	1600	20 titanite	2968 79.24	1188 31.718	15914 22.977	23	<b>346 ± 15</b>	55	
BE 008 granite	47°06' 19°53'	1580	20 apatite	586 7.423	652 8.259	7400 14.72	23	217 ± 14	8	-
BE 011 augengneiss	47°25' 20°12'	1500	20 apatite	978 11.924	1054 12.851	7400 14.69	39	223 ± 12	13	-
BE 013 granitic gneiss	46°54' 19°52'	1610	25 apatite	905 8.451	990 9.245	7318 15.922	2	257 ± 16	8	12.37 ± 0.23 1.34 (34)
BE 014 granitic gneiss	46°48' 19°49'	1265	31 apatite	1428 10.949	1600 12.268	7318 15.153	7	221 ± 10	12	12.4 ± 0.13 1.27 (100)
BE 016 granitic gneiss	46°38' 19°43'	1080	24 apatite	1633 14.734	1378 12.433	7318 15.880	0	332 ± 31	11	11.98 ± 0.24 1.46 (36)
BE 017 granitic gneiss	46°19' 19°34'	845	20 apatite	1156 10.624	1370 12.59	7318 15.84	0	229 ± 18	11	12.27 ± 0.2 1.55 (63)
BE 018 granite	46°16' 19°35'	960	21 apatite	1307 11.146	1066 9.091	7318 15.79	10	315 ± 16	8	12.45 ± 0.18 1.21 (43)
BE 019 rhyolite	46°08' 19°35'	930	11 apatite	321 9.522	386 11.451	7318 15.024	0	216 ± 36	10	-
BE 020 metagranite	46°06' 19°36'	1060	9 apatite	778 33.337	788 33.765	7318 15.623	2	252 ± 20	30	12.41 ± 0.16 1.36 (75)
BE 021 granitic gneiss	46°06' 19°36'	1085	17 apatite	1058 29.144	1076 29.639	7318 15.709	1	252 ± 17	26	-
BE 022 granitic gneiss	46°03' 19°37'	995	22 apatite	1330 139.883	490 51.536	15914 22.881	73	<b>374 ± 22</b>	82	12.29 ± 0.47 1.56 (11)
BE 023 gneiss	46°02' 19°37'	935	21 apatite	2841 15.327	2289 12.349	7318 15.58	3	315 ± 14	11	12.25 ± 0.18 1.53 (71)
BE 026 orthogneiss	45°43' 19°39'	560	25 apatite	2124 22.942	1635 17.66	7318 15.538	3	328 ± 17	16	11.51 ± 0.22 1.84 (70)
BE 028 granitic gneiss	45°36' 19°37'	620	19 titanite	2058 71.191	847 29.3	15914 22.894	2	<b>339 ± 20</b>	40	-
BE 030 granitic gneiss	45°34' 19°37'	510	7 apatite	226 15.793	196 13.697	7318 14.896	38	280 ± 28	16	-
BE 033 b gabbro	45°27' 19°33'	90	20 apatite	1642 20.476	1474 18.381	7318 15.751	13	286 ± 13	17	12.35 ± 0.23 1.5 (44)
BE 034 granite	45°28' 19°37'	100	17 titanite	3087 104.7	1111 37.681	15914 22.817	1	<b>378 ± 21</b>	62	11.92 ± 0.24 1.8 (24)
BE 036 anorthosite	45°29' 19°34'	270	18 titanite	1196 17.639	1010 14.896	7318 15.11	50	291 ± 15	15	11.34 ± 0.52 2.22 (18)
BE 037 granite	45°31' 19°35'	330	13 apatite	462 10.762	287 6.685	7318 15.495	26	403 ± 33	6	11.51 ± 0.15 0.92 (36)
BE 038 granitic gneiss	45°34' 19°37'	475	10 apatite	419 10.338	261 6.44	7318 15.067	70	391 ± 33	6	12.59 ± 0.15 1.57 (90)
BE 041 granite	45°31' 19°35'	330	25 apatite	2609 30.285	2469 28.66	7318 15.367	31	265 ± 11	27	12.18 ± 0.17 1.57 (90)
BE 042A diorite	45°34' 19°37'	475	18 titanite	1415 45.195	574 18.333	15914 22.785	23	<b>339 ± 19</b>	31	-
BE 045 granod. gneiss	45°34' 19°37'	475	20 apatite	1367 21.831	1348 21.527	7318 15.452	0	262 ± 20	21	11.91 ± 0.24 1.74 (52)
BE 046 granitic gneiss	47°06' 20°14'	1450	11 titanite	1339 125.605	565 53	15914 22.754	94	<b>326 ± 19</b>	84	-
BE 047A granitic gneiss	47°06' 20°14'	1450	20 apatite	849 10.364	603 7.361	7400 15.353	3	353 ± 27	7	-
BE 048 granod. gneiss	47°09' 20°21'	1325	20 titanite	1885 58.241	656 20.269	15914 22.722	17	<b>393 ± 21</b>	32	-
BE 049 migmatite	47°09' 20°21'	1325	20 apatite	1550 16.385	1153 12.188	7400 15.324	6	334 ± 16	11	13.04 ± 0.25 1.27 (26)
BE 049 migmatite	47°13' 20°36'	1425	20 titanite	2054 106.935	845 43.992	15914 22.69	23	<b>333 ± 16</b>	70	-
BE 049 migmatite	47°13' 20°36'	1425	20 apatite	1214 13.099	863 9.312	7400 15.295	54	350 ± 19	10	13.09 ± 0.19 1.25 (41)
BE 046 granitic gneiss	47°11' 20°41'	1580	20 titanite	2446 76.482	813 25.421	15914 22.658	52	<b>409 ± 20</b>	42	-
BE 048 granod. gneiss	47°11' 21°03'	1185	20 apatite	456 4.079	375 3.354	7400 15.266	3	307 ± 29	3	-
BE 049 migmatite	47°15' 21°11'	1200	20 titanite	2902 82.334	815 23.123	15914 22.626	0	<b>483 ± 33</b>	39	-
BE 049 migmatite	47°11' 21°03'	1185	13 apatite	324 6.329	322 6.29	7400 15.237	38	250 ± 21	6	-
BE 049 migmatite	47°15' 21°11'	1200	20 apatite	536 5.771	491 5.287	7400 15.208	91	271 ± 19	5	-
BE 049 migmatite	47°14' 21°17'	1290	21 titanite	2027 57.509	688 19.52	15914 22.594	1	<b>399 ± 27</b>	33	-

Sample Nr.	E-Long.	Elev.	Grains	(N <sub>s</sub> )	(N <sub>i</sub> )	(N <sub>a</sub> )	P(c <sup>2</sup> )	FT Age ± 1 s	U-cont.	MTL ± 1s SD[μm] Nr. of ms. tracks
Rock Type	S-Lat.	[m]	Mineral	r <sub>s</sub> [x10 <sup>5</sup> cm <sup>-2</sup> ]	r <sub>i</sub> [x10 <sup>5</sup> cm <sup>-2</sup> ]	r <sub>a</sub> [x10 <sup>5</sup> cm <sup>-2</sup> ]	[%]	[Ma]	[ppm]	
BE 100	47°22'	1310	30	981	1135	7318	25	209 ± 11	11	12.37 ± 0.29 *
diorite	18°56'		apatite	7.931	9.175	14.725				1.31 (20)
BE 101	47°17'	1335	20	402	535	7089	84	191 ± 15 *	13	12.46 ± 0.36 *
dioritic gneiss	19°00'		apatite	10.153	13.511	14.71				1.48 (17)
BE 103	47°08'	1320	20	1296	1373	7089	86	240 ± 13 *	19	12.32 ± 0.25 *
granod. gneiss	19°00'		apatite	20.533	21.753	14.74				1.10 (20)
BE 104	46°59'	1520	20	221	253	7089	22	223 ± 22 *	4	-
migmatic gneiss	19°00'		apatite	3.568	4.084	14.77				
BE 105	46°36'	1035	15	271	342	7318	78	193 ± 17	3	-
augen gneiss	18°58'		apatite	3.818	4.819	14.811				
BE 106	46°31'	905	20	1255	1226	7089	35	261 ± 15 *	25	12.75 ± 0.17 *
amphibolite	19°00'		apatite	27.597	26.959	14.81				1.22 (50)
BE 107	46°12'	885	21	149	345	7089	3	115 ± 15 *	4	-
leuco granite	18°56'		apatite	15.480	35.850	14.84				
			16	210	545	7089	90	100 ± 9 *	6	-
BE 108	46°11'	850	apatite	2.337	6.064	14.87				
amphibolite	18°55'		20	1982	1022	15914	7	<b>266 ± 13</b>		
			titanite	60.167	31.024	22.567				
BE 109	46°04'	900	18	630	1809	7089	26	90 ± 6 *	30	13.59 ± 0.13
migmatic gneiss	18°49'		apatite	10.486	35.763	14.90				1.01 (58)
			25	2292	1995	7318	0	278 ± 16	28	11.95 ± 0.14
BE 110	46°00'	850	apatite	31.82	27.697	14.85				1.44 (100)
tonalitic gneiss	18°52'		20	1941	855	15914	44	<b>307 ± 15</b>	56	
			titanite	77.434	34.109	22.345				
BE 111	45°54'	805	18	919	912	7569	21	265 ± 15	18	-
augen gneiss	18°56'		apatite	19.853	19.701	16.133				
BE 112	47°43'	1520	20	2297	3129	7318	1	178 ± 9	25	12.22 ± 0.32 *
amphibolite	18°54'		apatite	20.048	27.309	14.768				1.26 (16)
BE 113	47°45'	1500	20	1131	1346	7089	29	217 ± 12 *	23	-
migmatic gneiss	18°54'		apatite	20.497	24.393	14.97				
BE 114	47°50'	1420	20	805	984	7089	35	212 ± 13 *	18	12.47 ± 0.16
porphyric granite	18°56'		apatite	14.435	17.645	15.00				1.32 (69)
BE 115	47°55'	1175	19	152	166	7089	16	237 ± 28 *	4	13.26 ± 0.10
amphibolite	18°54'		apatite	3.997	4.365	15.03				0.93 (83)
BE 116	48°04'	880	16	290	284	7643	48	258 ± 24	3	-
granitic gneiss	18°52'		apatite	2.66	2.605	14.62				
BE 117	48°27'	1100	19	690	2207	7089	98	82 ± 5 *	55	13.40 ± 0.13
augen gneiss	18°58'		apatite	18.625	59.572	15.06				1.13 (81)
			23	96	276	7089	44	92 ± 11 *	4	-
BE 118	48°33'	700	apatite	1.282	3.686	15.10				
augen gneiss	18°58'		20	1714	546	15914	3	<b>420 ± 29</b>	19	
			titanite	36.496	11.626	22.403				
BE 119	48°36'	545	24	1177	1927	7089	10	160 ± 9 *	13	13.06 ± 0.22
amphibolite	18°58'		apatite	8.696	14.237	15.13				1.29 (33)
BE 120	48°36'	420	22	163	523	7089	64	82 ± 8 *	12	13.46 ± 0.19
granod. gneiss	18°59'		apatite	4.046	12.983	15.16				1.07 (30)
BE 122	48°39'	385	19	71	136	7089	64	138 ± 21 *	2	-
granod. gneiss	18°58'		apatite	1.006	1.927	15.19				
BE 123	48°44'	230	14	25	45	7089	93	147 ± 37 *	1	-
amphibolite	18°58'		apatite	0.635	1.142	15.23				
BE 125	49°05'	305	19	468	1577	7089	6	79 ± 5 *	25	13.69 ± 0.11
granitic gneiss	18°49'		apatite	8.377	28.228	15.26				1.15 (100)
BE 151	47°37'	1300	20	2844	3393	7.400	43	216 ± 8	60	12.18 ± 0.23
porphyric granite	18°54'		apatite	56.838	68	15.756				1.47 (42)
BE 154	47°48'	1800	20	958	1135	7400	35	217 ± 12	13	13.23 ± 0.27
porphyric granite	18°56'		apatite	11.518	13.647	15.727				1.20 (20)
			20	449	528	7400	53	219 ± 15	32	-
BE 155	47°04'	1115	apatite	5.896	6.933	15.699				
granitic gneiss	21°25'		20	1941	596	15914	55	<b>437 ± 24</b>	30	
			titanite	57.909	17.782	22.371				
BE 157	46°56'	1114	20	1768	1462	7400	38	308 ± 14	49	12.56 ± 0.17
granitic migmatite	21°19'		apatite	29.407	24.318	15.67				1.19 (46)
BE 158	46°54'	1340	20	1843	1756	7400	22	268 ± 12	28	12.63 ± 0.28
granite	21°17'		apatite	34.146	32.534	15.641				1.33 (23)
BE 159	46°48'	1260	15	448	488	7400	18	234 ± 17	11	-
granite	21°15'		apatite	10.459	11.393	15.612				
			20	2660	3068	7400	0	218 ± 11	32	12.88 ± 0.15
BE 161	46°38'	935	apatite	29.093	33.556	15.583				1.26 (73)
augen gneiss	21°12'		11	1070	436	15914	92	<b>328 ± 21</b>	52	
			titanite	72.345	29.479	22.136				
			20	705	2236	7617	48	83 ± 4	11	-
BE 205	47°55'	100	apatite	3.766	11.946	15.927				
granitic gneiss	21°54'		20	2938	1158	15914	0	<b>340 ± 22</b>	45	
			titanite	68.284	26.914	21.849				
BE 206	47°56'	50	20	594	1655	7617	1	96 ± 7	14	-
quartzite	21°46'		apatite	5.264	14.666	15.91				
BE 207	47°57'	55	11	499	1391	7617	19	94 ± 6	22	-
granitic gneiss	21°41'		apatite	9.362	26.096	15.894				
			20	103	352	7617	100	77 ± 9	2	-
BE 209	48°05'	50	apatite	0.571	1.951	15.878				
biotite gneiss	21°10'		18	1830	715	15914	9	<b>337 ± 18</b>	37	
			titanite	50.677	19.8	21.792				

Sample Nr.	E-Long.	Elev.	Grains	(N <sub>s</sub> )	(N <sub>i</sub> )	(N <sub>d</sub> )	P( $\chi^2$ )	FT Age $\pm 1\sigma$	U-cont.	MTL $\pm 1\sigma$ SD[ $\mu\text{m}$ ] Nr. of ms. tracks
Rock Type	S-Lat.	[m]	Mineral	$r_s[\times 10^5 \text{cm}^{-2}]$	$r_i[\times 10^5 \text{cm}^{-2}]$	$r_d[\times 10^5 \text{cm}^{-2}]$	[%]	[Ma]	[ppm]	
BE 210	48°04'	55	19	846	330	15914	97	<b>337 <math>\pm</math> 23</b>	23	
biotite gneiss	21°08'		titanite	33.494	13.065	21.735				
BE 211	47°53'	150	20	2586	4005	7617	1	165 $\pm$ 8	26	13.30 $\pm$ 0.20
granitic gneiss	21°23'		apatite	18.532	28.7	15.83				0.94 (22)
BE 212	47°51'	90	20	1215	1441	7617	0	214 $\pm$ 17	11	-
granod. gneiss	21°23'		apatite	9.201	10.912	15.814				
BE 213	47°48'	300	20	1836	1442	7617	2	332 $\pm$ 19	10	10.94 $\pm$ 0.28
hornbl. gneiss	21°22'		apatite	13.23	10.391	15.798				1.21 (19)
			20	2990	984	15914	31	<b>396 <math>\pm</math> 18</b>	51	
			titanite	92.109	30.313	21.677				
BE 214	47°44'	595	20	2147	1183	7617	60	460 $\pm$ 21	12	12.7 $\pm$ 0.2
biotite gneiss	21°21'		apatite	24.326	13.403	15.782				1.37 (45)
BE 215	47°39'	490	20	2282	1534	7617	16	379 $\pm$ 17	23	12.08 $\pm$ 0.33
granitic migmatite	21°20'		apatite	37.36	25.114	15.766				1.63 (25)
BE 216	47°36'	430	20	3939	2806	7617	35	358 $\pm$ 14	13	11.99 $\pm$ 0.18
granitic migmatite	21°18'		apatite	20.61	14.682	15.749				1.64 (87)
			20	1475	932	7617	39	402 $\pm$ 21	7	11.80 $\pm$ 0.30
BE 217	47°34'	650	apatite	12.103	7.647	15.733				1.58 (27)
granite	21°17'		20	2880	897	15914	4	<b>418 <math>\pm</math> 23</b>	32	
			titanite	58.003	18.065	21.62				
BE 218	47°28'	680	20	3301	2932	7617	0	294 $\pm$ 14	17	11.96 $\pm$ 0.21
migmatite	21°16'		apatite	21.74	19.31	15.717				1.8 (70)
BE 219	47°26'	660	19	393	357	7617	34	282 $\pm$ 22	2	-
granite	21°15'		apatite	2.649	2.406	15.701				
BE 221	47°20'	1240	19	438	301	7617	16	369 $\pm$ 30	3	-
granitic migmatite	21°17'		apatite	4.616	3.172	15.669				

**Tab. 3.2:** FT results from basement rocks of central Madagascar. Ages calculated using dosimeter glasses: IRMM-540 (apatite) with  $\zeta_{\text{IRMM-540}}=333\pm 9$  (Emmel); samples with stars calculated with  $\zeta_{\text{IRMM-540}}=355\pm 13$  (Graser) and MTL measured from Graser; titanite FT ages are calculated using  $\zeta_{\text{CN2}}=124\pm 3.25$  (Emmel). FT ages are reported as pooled ages if  $\chi^2 > 5\%$ , otherwise the central age is given. Elev.: Elevation,  $\rho_s$ ,  $\rho_i$ ,  $\rho_d$ ,  $N_s$ ,  $N_i$ ,  $N_d$ : density and number of counted spontaneous, induced and dosimeter glass tracks, U-cont. = Uranium content,  $P(\chi^2)$ : Chi-square probability.

## 5. Discussion

Since Late Neoproterozoic/Early Cambrian times Madagascar had a central position within Gondwana and was far away from any potential subduction zones (Fig. 3.1). Nevertheless, Madagascar remains tectonically active after the cessation of collision related tectonism along the EAAO. Extensional tectonics started probably during the last stage of the East African-Antarctic Orogeny (since  $\sim 550$  Ma), as indicated by structural evidences along the BetSZ (Collins et al., 2000). Emplacement of pegmatite fields in central Madagascar affected the thermal evolution from  $\sim 500$ -430 Ma (Fernandez et al., 2003). We suggest that the  $\sim 420$ -330 Ma cooling event between the Itremo region and the AGSZ is related to the repeated occurrence of fluid circulation. The titanite FT age of one dated pegmatite (BE 007 B) located east of the Itremo region is  $346\pm 15$  Ma indicating cooling to below  $\sim 300$  °C. To which extend exhumation of  $\sim 5.5$  km was affected or associated with these fluid circulation during this time is unexplained at this stage.

Evidences for fault reactivation at  $\sim 330$  Ma were observed in the same area. Identical titanite and apatite FT ages from sample BE 042 located within the BetSZ argue for reactivation of the shear zone accompanied by advective heating at  $\sim 330$  Ma. Samples located east of the

AGSZ have relatively consistent titanite FT ages of ~340 Ma. They are younger than most apatite FT ages from the AGSZ, possibly indicating tectonic activities along the eastern margin of the AGSZ during this time. Furthermore, at the ~370-260 Ma period cooling up to  $10\text{ }^{\circ}\text{C}\text{Ma}^{-1}$  occurred along the present basin/basement contact, probably connected to reactivation of Late Neoproterozoic/Early Cambrian ductile structures. These tectono-thermal activities coincide temporally with reactivation along the Bongolava-Ranotsara and Ejeda shear zones, predating the initial opening of the Karoo basins (Emmel et al., in press). We suggest that during this time a change in the tectonic regime has affected central Madagascar. Structural data from the Late Carboniferous to Early Permian Sakoa Group (southern Morondava basin) suggest that ~N-S orientated compressive tectonics influenced Madagascar during the deposition of the sediments (Schandelmeier et al., in press). During this time the structural framework of the later rift related basins of Madagascar developed. Not only Madagascar was effected by vertical movements during this period. In general, the Carboniferous was a time of mountain building along much of the Palaeo-Pacific margin (e.g. Veevers and Powell, 1994; Visser and Praekelt, 1996). A number of authors resume that parts of Gondwana (especially large parts of Australia and India) were characterised by large-scale uplift that may have caused the Permo-Carboniferous glaciation (Veevers and Powell, 1994; Visser and Praekelt, 1996; Wescott and Diggens, 1997, 1998). This uplift is supposed to be related to subduction along the Palaeo-Pacific Ocean and/or the Palaeo-Tethys Ocean and a reorientation of the stress regime within Gondwana.

Crustal extension between East Africa and Madagascar started at the end of the Carboniferous. Even if we cannot date reactivation along the western basement margin directly, we suggest that scattering apatite FT ages and the observed non uniform brittle structures (Fig. 3.3) are related to the extensional stress regime during the main Karoo rift phase. Apatite FT data support the assumption that formation of local graben and horsts led to vertical offsets of the basement in the kilometre-scale. These structures are not restricted to the western margin of the basement. Apatite FT and structural data imply that ~120 km east of the western basement margin (east of Antsirabe) a Karoo-aged graben evolved (Fig. 3.4a). The apatite FT age of the hanging wall is ~330 Ma and the ages of the footwall block are ~220-230 Ma. Structural data show ~N-S trending structures implying ~W-E directed extension (Fig. 3.3, BE 015 and BE 016; Fig. 3.4, BE 015 a and BE 015 b).

Modelled apatite FT data show that the areas with highest denudation for the 270-230 Ma period are ~250 km east of the basin/basement contact at the western margin of the AGSZ (Figs. 3.2 and 3.9). This indicates that during the Late Palaeozoic-Early Mesozoic intracontinental rift phase, areas exposed to highest denudation probably migrated from the palaeo western margin of the basement inland. Therefore, areas which cooled rapidly during

the initial opening of the Karoo rift system could be buried thereafter with a sedimentary cover of up to 2.5 km (Fig. 3.9, model BE 038).

General observation along continental margins show that during the initial rifting phase extensive crustal warming caused by lateral heat flow occurs (McKenzie, 1978). This led to expansion and uplift along the continental margin during the early stages of rifting. In the later stages, flexure of the continental margin in response to offshore sediment loading becomes important. As the margin becomes more rigid a flexure bulge migrates inland (Summerfield, 1985). Wijk and Cloetingh (2002) describe basin migration, which is caused by very slow lithospheric extension, as given for the palaeo western margin of Madagascar. They concluded that lithospheric stretching with low velocities doesn't lead to continental break-up but rather to a two-sided migration of the maximum extension locus. In the case of Madagascar, such a mechanism could lead to westward basin subsidence migration which is observed within the Morondava basin (e.g. Piqué, 1999) and to the postulated eastward migration of highest degrees of denudation due to isostatic response over slightly stretched lithosphere.

Apatite FT data document that since Early Jurassic to Late Cretaceous times only minor denudation affected the basement of central Madagascar. Although at this time the opening of the Somali basin initiated the southwest drift of Madagascar with respect to East Africa and brittle deformation within the Jurassic Bemaraha platform and along the western basement margin suggest tectonic activities. Furthermore, apatite FT data from the southwestern margin of the island close to the Davie fracture zone argue for a denudation of ~3.5 km crustal section during this time (Emmel et al., in press). Either the distance from the samples of central Madagascar to the "Jurassic" western margin is too large or at this time the former Morondava basin had a greater eastern extension and therefore the samples were located in the region of basin subsidence. Alternatively, during this period the drift was associated with relatively low amounts of exhumation probably caused by the change to a transform margin that did not influence the apatite FT data significantly.

Tectonic activities in central Madagascar especially along the eastern coast restarted at ~90 Ma. At this time, the eastern continental margin of Madagascar was influenced by the Madagascar-India break-up. Structural data suggest that the break-up was associated with a reorganisation of brittle structures along the eastern coast following the main trend directions of faults of the Mascarene basin (Figs. 3.3 and 3.10). Also brittle structures along the western margin of the basement and apatite FT ages of ~100 Ma around the Ambohiby granite (Fig. 3.4b) indicate tectonic/magmatic activities during the Cretaceous most probably associated with the emplacement of the Mailaka basalts inside the northern Morondava basin (Figs. 3.2 and 3.3). The influence of the Marion hot spot seems to be restricted to temperatures <300 °C, as titanite FT data from the eastern coast basement are not significantly affected by

partial annealing (Tab. 3.2; BE 118, 205, 209, 210). Furthermore, the brittle structures from the eastern coast show two distinctive trend directions (Figs. 3.3 and 3.10). If hot spot activities led to a doming in the east and a westward dipping of Madagascar as suggested by Storey et al. (1995) a non-orientated pattern of brittle structures and higher denudation affecting larger areas of the island would have been expected. Thus, we interpret a passive role of the Marion hot spot during the break-up of India and Madagascar with emplacement of magma as a consequence of the strike slip related opening of the Mascarene basin along the Vishnu fracture zone (Norton and Sclater, 1979).

A suggested Cenozoic E-W or N-S extension of the island (Bertil and Regnault, 1998) did not influence the FT data. Also, our remote sensing data suggest that the post-Cretaceous sedimentary rocks of the northern Morondava basin are tectonically nearly unaffected. The N-S striking Ankay graben is supposed to be related to this Cenozoic extensional event (Bertil and Regnault, 1998). However, our apatite FT data suggest that the graben shoulders were not eroded significantly after the Cretaceous Madagascar-India break-up (Fig. 3.4c). One sample within the Ankay graben has an apatite FT age of ~260 Ma. The samples from the western flank range between ~235 and ~210 Ma and three samples from the eastern graben shoulder increase eastward from ~80 Ma to ~160 Ma (Fig. 3.4c). One modelled cooling path of sample BE 117 implies a Late Cretaceous cooling (Fig. 3.9). Cretaceous break-up related structures could be observed also along the southwestern margin of India. Subrahmanyam et al. (1995) describes NNW-SSE running rift related ridge complexes following pre-existing trends in the basement, which could be an equivalent to the Ankay graben.

De Wit (2003) suggests a young uplift in central Madagascar indicated from seismic and the Neogene-Quaternary volcanic activities. Also geomorphic indicators like the elevation of the Ankaratra massive (~1000 m above the surrounding highlands) should argue for a rise in elevation over the past 10-15 Ma. Our modelled apatite FT data give evidences for the Cenozoic thermal activity (Fig. 3.9) which possible led to a rise of the isotherms and/or up-doming of central Madagascar most probably before the emplacement of the Ankaratra volcanics (~28-3 Ma).

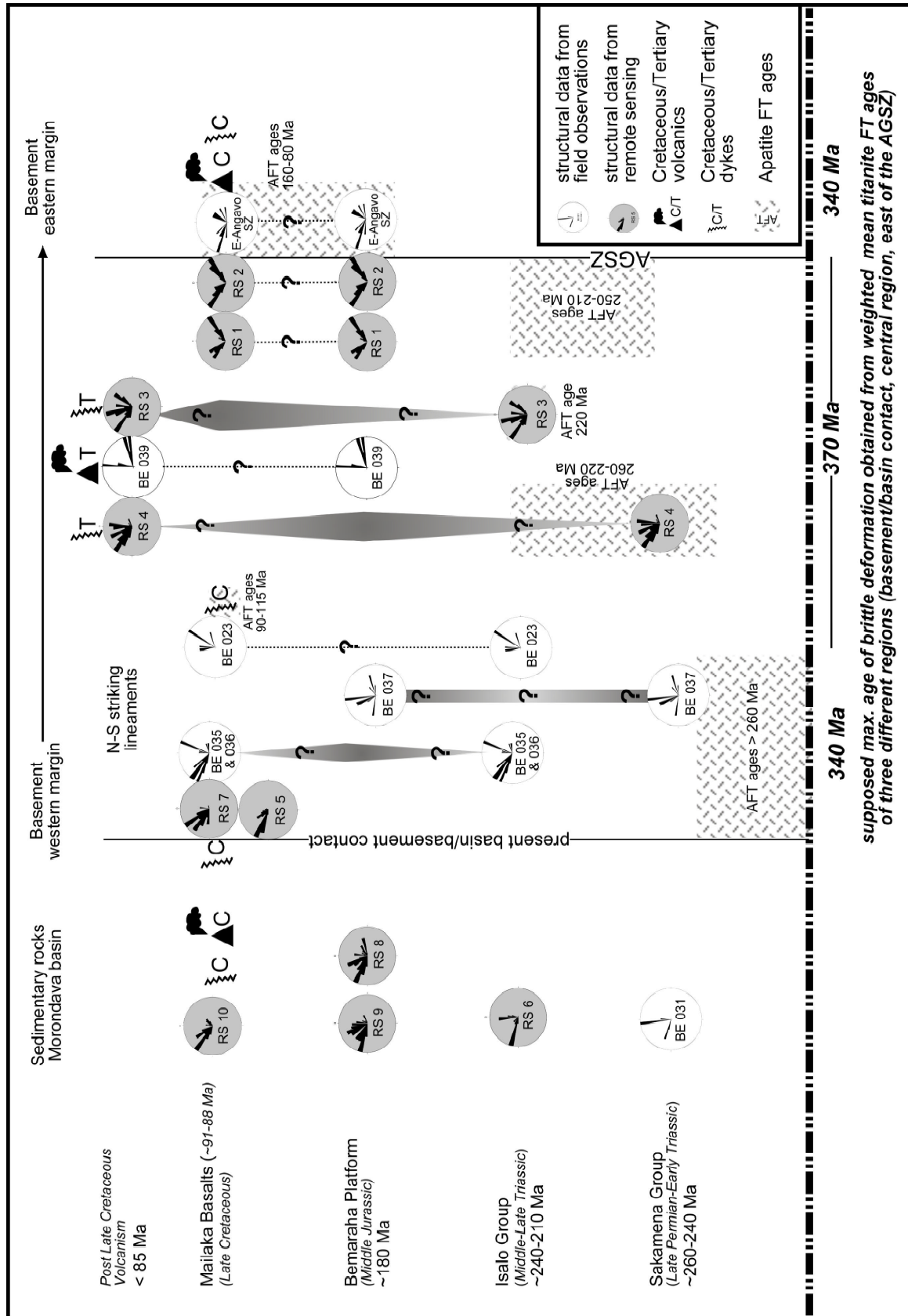


**Fig. 3.10:** Chronology of representative brittle structures in central Madagascar. All structural data are given as roseplots for a better correlation of remote sensing and field data. Broaden greyish lines indicate the supposed maximum brittle deformation phase.

## 6. Conclusions

This study shows in particular the advantages to deal with combined thermochronological methods with different closure temperatures to constraint: cooling rates, to calculate denudation rates and to date reactivation of faults and shear zones. The FT data from central Madagascar indicate two phases of accelerated cooling, which had the greatest effect on the low geothermal evolution of the island. The data give new time constraints about the reactivation along pre-existing basement structures prior to the opening of the Morondava basin. The Late Permian-Middle Jurassic Karoo rift episode affected the apatite FT data and brittle deformation style nearly of the whole working area. In contrast, the transform margin evolution since Late Jurassic times had no effects on the exhumation dynamics of the study area. Along the eastern continental margin of Madagascar, Cretaceous apatite FT ages and defined NW-SE and NE-SW trending brittle structures are related to the Late Cretaceous Madagascar-India break-up. Titanite FT and structural data imply a restricted thermal and tectonic influence of the Marion hot spot. We suggest that N-S trending structures associated with Cenozoic extension are older than previously assumed and are most likely connected to the Madagascar-India break-up.

## References:

- Bertil, D., Regnault, J.M., 1998. Seismotectonics of Madagascar. *Tectonophysics* 294, 57-74.
- Besairie, H., 1961. Carte Tectonique de Madagascar 1:3000000. *Sérvise Géologique de Madagascar*, Antananarivo.
- Besairie, H., 1972. Géologie de Madagascar I: Les terrains sédimentaires. *Annales Géologique Madagascar*, 35, 463pp.
- Besairie, H., 1973. Carte géologique à 1:2000000 de Madagascar. *Service Géologique de Madagascar*, Antananarivo.
- Buchwaldt, R., Tucker, R.D., 2001. P-T-Time constraints on the metamorphic rocks of north Madagascar and their relevance on the assembly of Gondwanaland. *Geological Society of America Abstracts with Programs* 33, A436.
- Chand, S., Subrahmanyam, C., 2003. Rifting between India and Madagascar-mechanism and isostasy. *Earth and Planetary Science Letters* 210, 317-332.
- Clark, D.N., Ramanampisoa, L., 2002. Hydrocarbon Potential of Madagascar. PESGB-HGS: First Annual International Symposium-Abstracts and Program, Kingston University 1, 26-27.

- Collins, A.S., Razakamanana, T., Windley, B.F., 2000. Neoproterozoic extensional detachment in central Madagascar; implications for the collapse of the East African Orogen. *Geological Magazine* 137, 39-51.
- Collins, A.S., Windley, B., Kröner, A., Fitzsimons, I., 2001. The Tectonic Architecture of Central Madagascar: Implications on the Evolution of the East African Orogeny. *Gondwana Research* 4, 152-153.
- Collins, A.S., Windley, B.F., 2002. The Tectonic Evolution of Central and Northern Madagascar and Its Place in the Final Assembly of Gondwana. *Journal of Geology* 110, 325-339.
- Collins, A.S., Fitzsimons, I.C.W., Hulscher, B., Razakamanana, T., 2003. Structure of the eastern margin of the East African Orogen in central Madagascar. *Precambrian Research* 123, 111-133.
- Cox, R., Armstrong, R.A., Ashwal, L.D., de Wit, M.J., 1995. Sedimentology, tectonics and geochronology of Proterozoic shelf sediments of the Itremo Group, central Madagascar; implications for the assembly of East Gondwana. In: Anonymous (Editor), Geological Society of America, 1995 annual meeting. Abstracts with Programs - Geological Society of America. Geological Society of America (GSA), Boulder, CO, United States, pp. 161.
- Cox, R., Armstrong, R. A., Ashwald, L., 1998. Sedimentology, geochronology and provenance of the Proterozoic Itremo Group, central Madagascar, and implications for pre-Gondwana palaeogeography. *Journal of Geological Society, London* 155, 1009-1024.
- Coyle, D.A., Wagner, G.A., 1998. Positioning the titanite fission-track partial annealing zone. *Chemical Geology* 149, 117-125.
- Daly, M., Chorowicz, J., Fairhead, J., 1989. Rift basin evolution in Africa: the influence of reactivated shear zones. *Inversion Tectonics* 44. Geological Society London, Special Publication, 309-334.
- Delvaux, D., 2001. Tectonic and palaeostress evolution of the Tanganyika-Rukwa-Malawi rift segment, East Africa Rift System. In: P.A. Ziegler, A.H.F. Robertson, S. Crasquin-Soleau (eds) *Peri-Tethys Memoir 6: Peri-Tethyan Rift/Wrench Basins and Passive Margins*. *Mèm. Mus. natn. Hist. nat.*, 186, 545-566.
- De Wit, M.J., Jeffery, M., Bergh, H. and Nicolaysen, L., 1988. Geological map of sectors of Gondwana reconstructed to their positions 150 Ma, scale 1:10.000.000. American Association Petroleum Geologists.
- De Wit, M.J. and Ransome, I.G.D., 1992. Regional inversion tectonics along the southern margin of Gondwana. *Inversion tectonics of the Cape Fold Belt, Karoo and*

- Cretaceous basins of southern Africa. de Wit, M.J., Ransome, I.G.D, (Editors) Rotterdam (Balkema), 15-21.
- De Wit, M. J., 2003. Madagascar: Heads It's a Continent, Tails t's an Island. *Annu. Rev. Earth Planet. Sci.* 31, 213-248.
- Emmel, B., Jacobs, J., Razakamanana, T., 2003. Titanite and apatite fission track analyses on basement rocks of central-southern Madagascar: constraints on exhumation and denudation rates along the eastern rift shoulder of the Morondava basin. *Journal of African Earth Sciences*, in press.
- Fernandez, A., Schreurs, G., Villa, I.M., Huber, S., Rakotondrazafy, M., 2003. Age Constraints on the tectonic of the Itremo region in Central Madagascar. *Precambrian Research* 123, 87-110.
- Fournou, J.P., Roussel, J., 1994. Imaging of the Moho depth in Madagascar through the inversion of gravity data: geodynamic implications. *Terra Nova* 6, 512-519.
- Gallagher, K., Sambridge, M., 1994. Genetic algorithms: a powerful method for large scale non-linear optimisation problems. *Comput. Geosci.* 20, 1229-1236.
- Gallagher, K., 1995. Evolving temperature histories from apatite fission-track data. *Earth and Planetary Science Letters* 136, 421-435.
- Gleadow, A.J.W., 1981. Fission-track dating methods: what are the real alternatives? *Nuclear Tracks* 5, 3-14.
- Hagen, E., Kelley, S.P., Dypvik, H., Nilsen, O., Kjølhamar, B., 2001. Direct dating of authigenic K-feldspar overgrowths from the Kilombero Rift of Tanzania. *Journal of Geological Society, London*, 158: 801-807.
- Hankel, O., 1994. Early Permian to Middle Jurassic rifting and sedimentation in East Africa and Madagascar. *Geologische Rundschau* 83, 703-710.
- Hansen, D.L., Nielsen, S.B., 2003. Why rifts invert in compression. *Tectonophysics*, 373: 5-24.
- Hawkesworth, C.J., Gallagher, K., Kirstein, L., Mantovani, M.S.M., Peate, D.W., Turner, S.P., 2000. Tectonic controls on magmatism associated with continental break-up: an example from the Paraná-Etendeka Province. *Earth and Planetary Science Letters*, 179, 335-349.
- Holdsworth, R.E., Butler, C.A., Roberts, A.M. 1997 The recognition of reactivation during continental deformation. *Journal of the Geological Society*, 154, 73-78.
- Hottin, G., 1976. Presentation et essai d'interprétation du Précambrien de Madagascar. *Bull. Bur. Rech. Geol. Min.* 4, 117-153.

- Kröner, A., Hegner, E., Collins, A.S., Windley, B.F., Brewer, T.S., Razakamanana, T., Pidgeon, R.T., 2000. Age and magmatic history of the Antananarivo Block, central Madagascar, as derived from zircon geochronology and Nd isotopic systematics. *American Journal of Science* 300, 251-288.
- Lardeaux, J.M., Martelat, J.E., Nicollet, C., Pili, E., Rakotondrazafy, R., Cardon, H., 1999. Metamorphism and tectonics in Southern Madagascar: an Overview. *Gondwana Research* 2, 355-362.
- Laslett, G.M., Green, P.F., Duddy, I.R., Gleadow, A.J.W., 1987. Thermal annealing of fission tracks in apatite 2. A Quantitative Analysis. *Chemical Geology (Isotope Geoscience Section)* 65, 1-13.
- Malod, J.-A., Mougnot, D., Raillard, S., Maillard, A., 1991. Nouvelles contraintes sur la cinématique de Madagascar: les structures de la chaîne Davie. *Comptes rendus de l'Académie des Sciences de Paris, Séries II* 312, 1639-1646.
- Martelat, J.E., Lardeaux, J.M., Nicollet, C., Rakotondrazafy, R., 2000. Strain pattern and late Precambrian deformation history in southern Madagascar. *Precambrian Research* 102, 1-20.
- McKenzie, D., 1978. Some remarks on the development of sedimentary basins. *Earth and Planetary Sciences Letters* 40, 25-32.
- Meert, J.G., Hall, C., Nédélec, A., Razanatseheno, M.O.M., 2001. Cooling of a Late-Syn Orogenic Pluton: Evidence from Laser Kfeldspar Modelling of the Carion Granite, Madagascar. *Gondwana Research* 4, 541-550.
- Meert, J.G., Nédélec, A., Hall, C., 2002. The stratoid granites of central Madagascar: paleomagnetism and further age constraints on neoproterozoic deformation. *Precambrian Research* 120, 101-129.
- Meert, J. G. 2003. A synopsis of Events Related to the Assembly of Eastern Gondwana. *Tectonophysics*, 262, 1-40.
- Nédélec, A., Ralison, B., Bouchez, J. L., Grégoire, V., 2000. Structure and metamorphism of the granitic basement around Antananarivo: A key to the Pan-African history of central Madagascar and its Gondwana connections. *Tectonics* 19, 997-1020.
- Norton, I.O., Sclater, J.G., 1979. A model for the evolution of the Indian Ocean and the breakup of Gondwanaland. *Journal Geophysic Research* 84, 6803-6830.
- Piqué, A., 1999. The geological evolution of Madagascar: An introduction. *Journal of African Earth Sciences* 28, 919-930.
- Piqué, A., Laville, E., Bignot, G., Rabarimanana, M., Thouin, C., 1999. The initiation and development of the Morondava Basin [Madagascar] from the Late Carboniferous to the middle Jurassic: Sedimentary, palaeontological and structural data. *Journal of African Earth Sciences* 28, 931-948.

- Pili, E., Ricard, Y., Lardeaux, J.-M., Sheppard, S.M.F., 1997. Lithospheric shear zones and mantle-crust connections. *Tectonophysics* 280, 15-29.
- Rasamimanana, G., Bardintzeff, J.M., Chorowicz, J., Chotin, P., Thouin, C., 1996. Montagne d'Ambre (Madagascar); relations volcanisme-tectonique. In: Anonymous (Editor), (16<sup>eme</sup>) reunion des sciences de la terre; Dynamique et economie Dynamique et economie de la Terre. Reunion Annuelle des Sciences de la Terre. Societe Geologique de France, Paris, France, pp. 80.
- Schandelmeier, H., Bremer, F., Holl, H.-G., 2003. Kinematic of the Morondava rift Basin of SW Madagascar - from shear zone controlled wrench tectonics to normal extension. *Journal of African Earth Sciences*, in press.
- Scotese, C.R., Boucot, A.J., McKerrow, 1998. Gondwanan palaeogeography and palaeoclimatology. *Journal of African Earth Sciences* 28, 99-114.
- Seward, D., Grujic, D., Schreurs, G., 1998. Exhumation history of the East Madagascar continental margin; inferences from apatite fission-track analysis. *Journal of African Earth Sciences* 27, 176-178.
- Seward, D., Grujic, D., Schreurs, G., 1999. Exhumation history of Southern Madagascar as revealed by Zircon and Apatite Fission-Track Thermochronology. *Gondwana Research* 2, 353-354.
- Seward, D., Grujic, D., Schreurs, G., 2000. Post Pan-African Events in Madagascar: Inferences from Apatite Fission-Track Analysis, 9th International Conference on Fission Track Dating and Thermochronology. Geological Society of Australia Abstract series, Lorne, Australia, 58, 289.
- Shackleton, R.M., 1996. Final collision zone between East and West Gondwana: where is it? *Journal of African Earth Sciences* 23, 271-287.
- Sherlock, S.C., Hetzel, R., 2001. A laser-probe  $^{40}\text{Ar}/^{39}\text{Ar}$  study of pseudotachylite from the Tambach Fault Zone, Kenya: direct isotopic dating of brittle faults. *Journal of Structural Geology*, 23, 33-44.
- Stern, R.J., 1994. Arc assembly and continental collision in the Neoproterozoic East African orogen: implications for the consolidation of Gondwanaland. *Ann. Rev. Earth Planet. Sci.* 22, 319-351.
- Stollhofen, H., 1999. Karoo Synrift-Sedimentation und ihre tektonische Kontrolle am entstehenden Kontinentalrand Namibias. *Z. dt. Geol. Ges.* 149, 519-632.
- Storey, M., Mahoney, J.J., Saunders, A.D., Duncan, R.A., Kelley, S.P., Coffin, M.F., 1995. Timing of hot spot-related volcanism and the breakup of Madagascar and India. *Science* 267, 852-855.

- Subrahmanyam, V., Gopala Rao, D., Ramana, M.V., Krishna, K.S., Murty, G.P.S., Gangadhara Rao, M., 1995. Structure and tectonics of the southwestern continental margin of India. *Tectonophysics* 249, 267-282.
- Summerfield, M.A., 1985. Plate tectonics and landscape development on the African continent. In: M. Morisawa and J.T. Hack (eds) *Tectonic Geomorphology*. Allen and Uwin, Boston and London, 27-51.
- Tucker, R.D., Ashwal, L.D., Handke, M.J., Hamilton, M.A., Le Grange, M., Rambeloson, R.A., 1999. U-Pb geochronology and isotope geochemistry of the Archean and Proterozoic rocks of north-central Madagascar. *Journal of Geology* 107, 135-153.
- van Wijk, J.W., Cloetingh, S.A.P.L., 2002. Basin migration caused by slow lithospheric extension. *Earth and Planetary Science Letters* 198, 275-288.
- Veevers, J.J., Powell, C.M., 1994. Permian-Triassic Pangean basins and foldbelts along the Panthalassan margin of Gondwanaland. *Geological Society of America; Memoir* 184, 368 pp.
- Visser, J.N.J., Praekelt, H.E., 1996. Subduction, mega-shear systems and late Palaeozoic basin development in the African segment of Gondwana. *Geologische Rundschau* 85, 632-646.
- Wagner, G.A., van den Haute, P., 1992. *Fission-Track Dating*. Ferdinand Enke Verlag, Stuttgart, 285 pp.
- Wescott, W., Diggens, J.N., 1997. Depositional history and stratigraphical evolution of the Sakoa Group (Lower Karoo Supergroup) in the southern Morondava Basin, Madagascar. *Journal of African Earth Sciences* 24, 581-601.
- Wescott, W., Diggens, J.N., 1998. Depositional history and stratigraphical evolution of the Sakamena Group (Middle Karoo Supergroup) in the southern Morondava Basin, Madagascar. *Journal of African Earth Sciences* 27, 467-479.
- Windley, B.F., Razafiniparany, A., Razakamanana, T., Ackermann, D., 1994. Tectonic framework of the Precambrian of Madagascar and its Gondwana connections; a review and reappraisal. *Geologische Rundschau* 83, 642-659.
- Ziegler, P.A., 1992. Plate tectonics, plate moving mechanisms and rifting. *Tectonophysics* 215, 9-34.

## Chapter 4

### **Titanite and apatite fission track analyses on basement rocks of central-southern Madagascar: constraints on exhumation and denudation rates along the eastern rift shoulder of the Morondava basin**

B. Emmel <sup>a</sup>, J. Jacobs <sup>a</sup> & T. Razakamanana <sup>b</sup>

*Journal of African Earth Sciences, accepted*

<sup>a</sup> Fachbereich Geowissenschaften, Universität Bremen, Postfach 330440, 28334 Bremen, Germany

<sup>b</sup> Département des Sciences de la Terre, Université de Toliara, Madagascar

## Abstract

Titanite and apatite fission track (FT) thermochronology from basement rocks in central-southern Madagascar reveals a protracted post Late Neoproterozoic/Early Cambrian history of extensional tectonism, denudation and sedimentation. Titanite FT ages range between  $379\pm 38$  Ma and  $276\pm 17$  Ma and apatite FT ages vary between  $379\pm 19$  Ma and  $150\pm 8$  Ma. Combined titanite and apatite FT data from the western palaeo margin of Madagascar suggest denudation rates of  $\sim 200\text{-}100$   $\text{mMa}^{-1}$  during Carboniferous times. The Late Neoproterozoic/Early Cambrian Ejeda shear zone was probably reactivated during this time. In contrast, for the same period denudation rates inland are  $\sim 110\text{-}25$   $\text{mMa}^{-1}$ . During Permo-Triassic rifting, areas that previously underwent fast denudation were buried by sedimentary cover up to  $\sim 4.5$  km. At this time, a graben developed along the transcontinental Bongolava-Ranotsara shear zone (BRSZ). Graben faults are exposed at the northeastern graben shoulder. Identical titanite and apatite FT ages close to the BRSZ indicate rapid cooling associated with fluid circulation during Early Permian times.

The initial Gondwana break-up during Middle Jurassic times and the drift of Madagascar along the Davie transform fault did not significantly influence the FT-data and had only minor geomorphic impact in the study area. Only the far southwestern part of the island is characterised by a higher degree of denudation (max.  $\sim 3.5$  km) during Early Jurassic times. Early Cretaceous and Cenozoic volcanic activity affected the apatite FT data from southern Madagascar. Modelled time-temperature (T-t) paths argue for a reheating of samples from southern Madagascar to temperatures of  $\sim 60\text{-}80$  °C during the times of magmatism, before final cooling to surface temperatures.

**Keywords:** Madagascar, fission-track thermochronology, Gondwana break-up, denudation, shear zone reactivation

## 1. Introduction

After the final amalgamation of Gondwana during Late Neoproterozoic/Early Cambrian times Madagascar had a central position in Gondwana adjacent to Tanzania and Kenya (Fig. 4.1), along the eastern front of the East African Orogen (e.g. Stern, 1994; Shackleton, 1996; Collins and Windley, 2002; Reeves et al., 2002). During the Late Neoproterozoic (610-605 Ma; de Wit et al., 2001) and/or the Cambrian (530-500 Ma; Martelat et al., 2000) a network of shear zones developed in southern Madagascar. Such pre-existing structures are sensitive to tectonic reactivation (e.g. Pili et al., 1997; Raab et al., 2002), but it is often difficult to constrain this reactivation temporally and spatially. In Madagascar, it is believed that Late Neoproterozoic/Cambrian shear zones were reactivated and controlled the opening of the Late Palaeozoic basins and the later drift evolution of Madagascar (Montenat et al., 1996; Piqué et al., 1999 a). Likewise, a present day extensional regime is inferred from Recent reactivation of these former zones of weaknesses (Bertil and Regnault, 1998; Piqué et al., 1999 b). Up to now, a limited number of low temperature geochronological data exists from southern Madagascar (e.g. Seward et al., 1998, 1999, 2000). Without these data these tectonic inferences are poorly dated and the magnitudes of exhumation completely unknown.

Phanerozoic crustal extension between East Africa and Madagascar initiated large Permian to Quaternary sedimentary basins that stretch along the western coast of Madagascar (Figs. 4.2 and 4.3). New tectono-sedimentary models from the Morondava basin (Clark and Ramanampisoa, 2002) suggest that the oldest sequences and the drift evolution (since Callovian times) are temporally and spatially separated.

Combined titanite and apatite FT thermochronology is a powerful tool to constrain the low temperature history of rocks (~300-60 °C). The range in closure temperatures between titanite FT (~300 °C) and apatite FT (~110-60 °C) allows estimates of exhumation rates. Furthermore, combined data are useful to record effects of advective heating along fault zones and other zones of crustal weakness. Apatite FT analysis is sensitive enough to delineate block-tectonics with differential vertical movements of more than ~2 km and heating affects due to sedimentary overload >2 km.

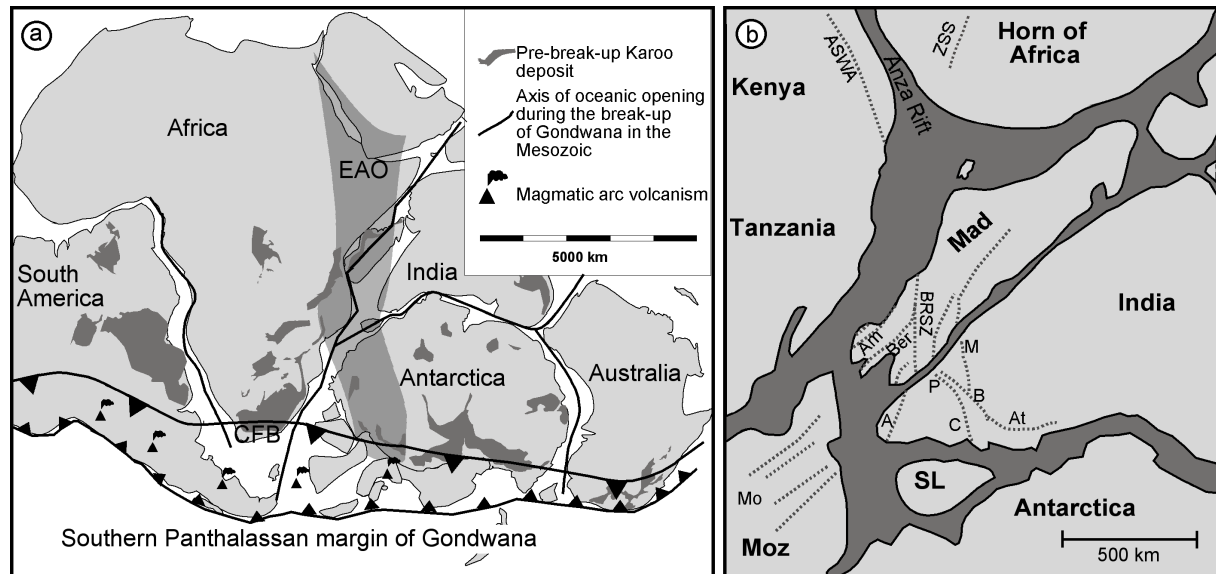


**Fig. 4.1:** a) Location of the study area in a pre-drift reconstruction of Gondwana from Palaeozoic to Mesozoic times (after Stollhofen (1999) compiled from de Wit et al. (1988) and de Wit and Ransome (1992)). b) Reconstruction of central Gondwana at ~200 Ma (from Reeves et al., 2002). Grey: Precambrian crustal fragments; dark grey: originally continental rocks lost by rifting; dotted lines: distribution of major shear zones (from Bonavia and Chorowicz (1992), Shackleton (1996), Martelat et al. (2000), de Wit et al. (2001) and Meißner et al. (2002)). A: Achankovil shear zone; Am: Ampanihy shear zone; ASWA: Aswa shear zone; At: Attur high strain zone; B: Bhavani high strain zone; Ber: Beraketa shear zone; BRSZ: Bongolava-Ranotsara shear zone; C: Cauvery shear zone; CFB: Cape Fold Belt; EAO: East-African Orogen; P: Phalгат high strain zone; M: Moyar high strain zone; Mad: Madagascar; Mo: Morille shear belt; Moz: Mozambique; SL: Sri Lanka; SSZ: Surma shear zone.

## 2. Geological framework of Madagascar

The eastern two thirds of Madagascar are mainly composed of Archean to Late Proterozoic basement rocks (Windley et al., 1994; Tucker et al., 1999; Collins and Windley, 2002). Along the western coast of Madagascar three north-south stretching sedimentary basins overlie the basement. From north to south, these are the Diego, the Majunga and the Morondava basins (Fig. 4.2).

According to Windley et al. (1994), the Precambrian of Madagascar is divided into two major blocks by the northwest-southeast trending BRSZ. On the basis of lithotectonic and isotopic evidences the northern part of the island is subdivided into five tectonic units (Collins et al., 2000; Fig. 4.2). In the northeastern part of the island the Antongil block (after Hottin, 1976) consists of amphibolite- and greenschist-facies metapelites that "rim" a meta-granite terrain. The Antananarivo block is the dominant unit north of the BRSZ. It mainly consists of late Archean granitoids, interlayered with Late Proterozoic granites, syenites and gabbros (Tucker et al., 1999; Kröner et al., 2000). The unit was thrust east across the Antongil block during the Late Proterozoic (Collins et al., 2003).

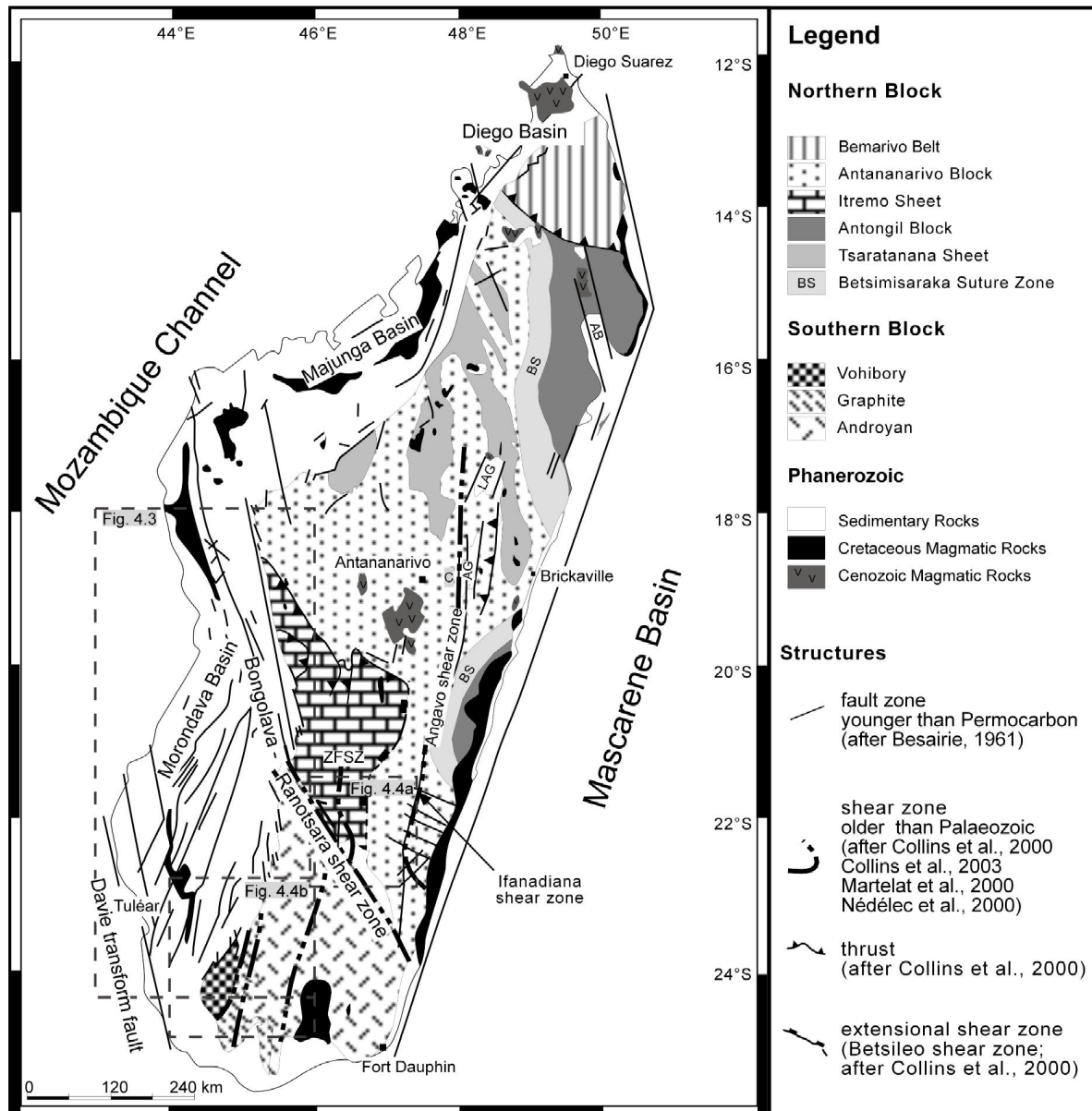


**Fig. 4.2:** Generalised geological and structural map of Madagascar (modified after Besairie (1961, 1973), Collins et al. (2000, 2003), Martelat et al. (2000) and Nédélec et al. (2000)). AB: Anongil bay, AG: Ankay graben; BS: Betsimisaraka suture zone; C: Carion Granite; LAG: Lac Alaotra graben.

To the west of the Antongil block lies the Tsaratanana unit. It contains of three north-south striking greenstone belts composed of mafic and pelitic gneisses interlayered with chromites and intruded by gabbros and granites. In the far north of Madagascar, the Bemarivo orogenic belt truncates the other units. The belt is composed of metasediments, granites, and gneisses and was thrust across central Madagascar during the Late Neoproterozoic (Buchwaldt and Tucker, 2001; Collins et al., 2001).

The Itremo sheet (Collins et al., 2000) consists of predominant metasedimentary rocks of the Itremo Group (Cox et al., 1995, 1998), deposited between 1700-800 Ma (Cox et al., 2000). The Itremo Group structurally overlays the Antananarivo block. According to Collins et al. (2000) it is bound by extensional faults with the Antananarivo block.

The Precambrian rocks south of the transcontinental BRSZ is divided into lithostratigraphic sequences by Besairie (1953, 1964, 1967, 1973) and de Wit et al. (2001). From the west to the east these are the Vohibory, Graphite and Androyan sequences (Fig. 4.2). They consist mainly of granulite to upper amphibolite facies paragneisses and granites. Windley et al. (1994) subdivided the southern block into six tectonic belts. From west to east these are the Vohibory, Ampanihy, Bekily, Betroka, Tranomaro and Fort Dauphin/Anosyan belts. Ductile shear zones mark the boundaries between these tectonic belts (Rolin, 1991; Windley et al., 1994; Martelat et al., 2000; de Wit et al., 2001).

Four large shear zones have been identified in southern Madagascar (Fig. 4.4a, b). Three shear zones trend approximately north-south (Ejeda, Ampanihy and Beraketa shear zones, Martelat et al., 2000; the Beraketa SZ is also called the Vorokafotra SZ by Rolin, 1991) fourth, the BRSZ stretches northwest-southeast. The extension of the Ejeda shear zone in southwestern Madagascar is unknown because Phanerozoic sedimentary rocks largely cover the shear zone. The Ampanihy and Beraketa shear zones are 10 to 20 km wide and can be traced for ~300 km along strike. A set of en-echelon faults forms part of the northwest-southeast striking BRSZ with a combined strike length of >400 km (de Wit et al., 2001). At Ihosy, the BRSZ has a width of ~20-25 km. North of the BRSZ the Zazafotsy shear zone (ZFSZ; Martelat et al., 2000) strikes nearly north-south. The S-shaped ZFSZ has a width of ~20-30 km and an observed length of ~100 km but the northern continuation is not clear (Fig. 4.4a). Approximately 20 km east of the ZFSZ Collins et al. (2000) described a west-dipping extensional shear zone that was traced north over 200 km, the Betsileo shear zone.

According to Ashwal et al. (1999) and de Wit et al. (2001), collision in southern Madagascar occurred between ~650-610 Ma. After the collision-related metamorphism an extended period of static annealing at mid crustal level occurred. Finally, the orogen collapsed between ~600-500 Ma (de Wit et al., 2001) or ~550 Ma (Collins et al., 2000; Kröner et al., 2000). In contrast to this, Martelat et al. (2000) reported two deformation events (D1 and D2) in southern Madagascar. Chronological constraints argue for a D1 event (590-530 Ma) that is attributed to crustal thickening and a D2 event (530-500 Ma) that is related to the formation of an anastomosing network of ductile shear zones (Fig. 4) related to transpressional tectonics. The following cooling history of central Madagascar has been described by Meert et al. (2001). They yielded a U-Pb zircon age of  $532 \pm 5$  Ma from the post tectonic Carion granite in central Madagascar (Fig. 4.2). Cooling to below 500 °C is constrained by a hornblende

$^{40}\text{Ar}/^{39}\text{Ar}$  age of  $513\pm 3$  Ma. Biotite ( $479\pm 1$  Ma) and modelled K-feldspar ages show cooling from  $350^\circ\text{C}$  at 465 Ma to  $100^\circ\text{C}$  by 410 Ma.

The thickness of the Madagascan continental crust is  $\sim 35\text{-}40$  km determined from seismic and gravity data (Rechenmann, 1982; Fournu, 1987; Fournu and Roussel, 1994; Pili et al., 1997), with the crust-mantle boundary suggested to be uplifted by  $\sim 10$  km beneath major ductile shear zones (Pili et al., 1997).

The shear zones of Madagascar are important for Gondwana reconstruction (Fig. 4.1b). Early interpretations suggested an extension of the BRSZ into the major Surma shear zone in East Africa (Bonavia and Chorowicz, 1992) or parallel to the Aswa shear zone (Chorowicz et al., 1987). The eastern continuation of the BRSZ into India could be the Palghat-Cauvery shear zone of South India (Harris et al., 1996), the Achankovil shear zone (Windley et al., 1994) or the poorly known KKPT (Karur, Kambam, Painavu and Trichur) shear zone (Ghosh et al., 1998). Recent reconstructions from de Wit et al. (2001) correlate the north-south striking shear zones of Madagascar with the Morille shear belts of northern Mozambique.

Following Late Neoproterozoic ductile deformation, Madagascar underwent a long period of extensional tectonism, associated with basin formation, major faulting, exhumation and transform margin formation. Neoproterozoic/Early Cambrian shear zones were reactivated and controlled the opening of the large Madagascan basins, the Majunga and Morondava basins, and the later opening of the Somali basin and the Mozambique channel (e.g. Pili et al., 1997; Piqué et al., 1999 a). The intracratonic rift basin evolution is recorded in the sedimentary rocks of the Madagascan Karoo Supergroup (Upper Carboniferous-Middle Jurassic), which is divided into the Sakoa, Sakamena and the Isalo groups (Besairie, 1972).

Prior to the deposition of the oldest Karoo Supergroup sediments (Late Carboniferous), the Precambrian basement underlying the Morondava basin underwent uplift and erosion. Sediments initially accumulated on an irregular basement surface with several small pull-apart basins formed due to east-west extension and left-lateral strike slip movements along reactivation zones (Wescott and Diggins, 1997). The early extensional basin evolution was possibly related to north-south directed compression in the south African Cape Fold Belt (de Wit and Ransome, 1992). The Upper Carboniferous to Lower Permian north-south trending Sakoa Group (tillites overlain by coal bearing horizons) represents the oldest sedimentary rocks in the Morondava basin. The Lower Sakoa (tillites) unconformably overlies the basement and pre-dates the rifting. The Middle and Upper Sakoa deposits represent the evolution of the syn-rift phase. Many small rift initiation faults became inactive and extension focussed on a few large faults (Wescott and Diggins, 1997).

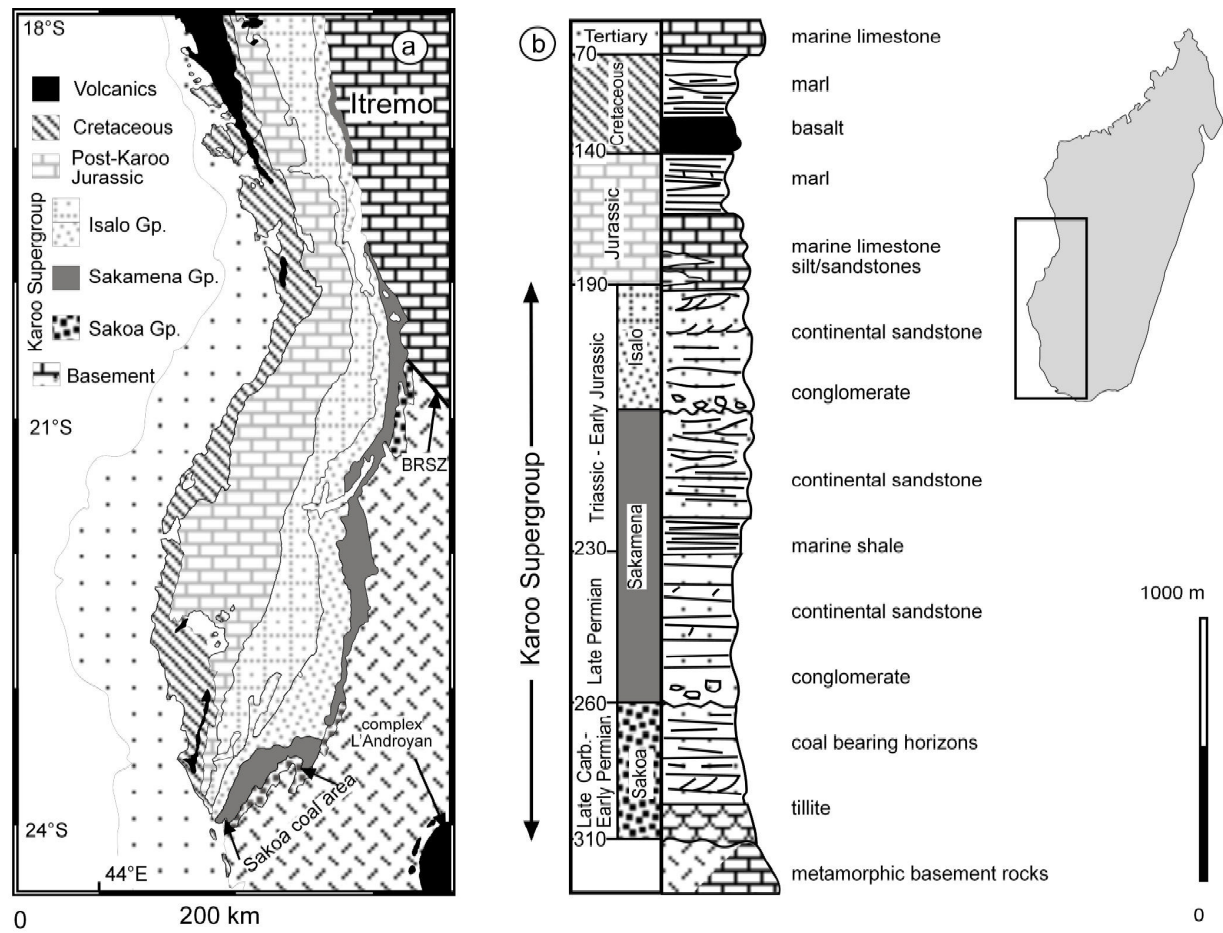


**Fig. 4.3:** a) Simplified geological map of the Morondava basin (modified after Besairie, 1972). b) Synthetic lithostratigraphical column of the Morondava basin with normalised sedimentary thickness (modified after Piqué, 1999).

The Sakamena Group, which unconformably overlies the Sakoa Group, comprises Late Permian continental sandstones and conglomerates overlain by Early Triassic marine shales and sandstones. The sandstones formed in response to a renewed episode of uplift (Wescott and Diggins, 1998). The Middle Triassic to Early Jurassic Isalo Group is situated unconformably over the Sakamena Group. The Isalo Group is entirely composed of continental sandstones and conglomerates (Piqué, 1999) and the Early to Middle Jurassic Isalo II is assumed to represent the maximum extension of the Karoo basin.

Between Middle and Late Jurassic times a transform margin formed off the northern Majunga basin, as seafloor spreading began in the Somali basin. The sedimentary environment along the western margin of Madagascar changed from almost continental to predominantly marine (Coffin and Rabinowitz, 1992). The Davie ridge southwest of Madagascar is a fossil transcurrent fault that guided the translation (Ségoufin and Patriat, 1981; Coffin and Rabinowitz, 1987). The strike slip motions along the Davie transform fault stopped in Early Cretaceous times as India rifted off Madagascar but restarted in the Miocene (Malod et al., 1991).

Late Cretaceous mafic igneous rocks are known from the eastern and western coasts of Madagascar, from the volcanic complex L'Androyan in the southern part of the island, from numerous dykes that truncate the basement and from the outlier plateaux basalts in the centre of the island (Fig. 4.3a; Storey et al., 1995; Rasamimanana et al., 1998). The basalts are thought to be related to the Marion hot spot (Storey et al., 1995) and magmatic activities during the Upper Cretaceous break-up of Madagascar and Seychelles-India. According to Storey et al. (1995) the thick lava accumulation at volcano de L'Androy in the south of Madagascar (Fig. 4.3a) marks the focal point of the Marion hot spot and they suggested that the whole island might have been buried under basalt in Cretaceous times.  $^{40}\text{Ar}/^{39}\text{Ar}$  analysis and an U/Pb zircon age imply that the volcanic rocks were emplaced at ~91-84 Ma (Storey et al., 1995; Torsvik et al., 1998).

Crustal extension restarted in Oligocene-Miocene times and continued during the Pliocene and the Quaternary (Malod et al., 1991). During the Pliocene, the formation of ~north-south striking grabens and increasing volcanic activity indicate a major extensional period in central Madagascar (Bertil and Regnault, 1998). These zones of reactivation are aligned along pre-existing basement structures (Bertil and Regnault, 1998; Piqué et al., 1999 b). During an Oligocene-Pliocene phase (~28-3 Ma) of enhanced magmatism, the volcanic centres of the Ankaratra and the Itasy area were emplaced in the middle of the island (Piqué, 1999). Indicators for present day magmatic activities are geysers, active seismicity, solfatares and hot springs (Mottet, 1981).

### 3. Previous fission track analyses in Madagascar

The first FT data from southern Madagascar were reported from Grujic (1995). He yielded two zircon ages of  $320\pm 25$  Ma and 265 Ma and two apatite FT ages of  $180\pm 23$  Ma. The zircon FT ages were interpreted as a result of Karoo rift initiation and possible reactivation of the Ampanihy shear zone.

Seward et al. (1998, 1999, 2000) report zircon and apatite FT ages from central and south Madagascar. Two zircon FT analyses were only carried out on samples from southwestern Madagascar; south of the BRSZ. These ages are  $384\pm 71$  Ma and  $238\pm 56$  Ma. Apatite FT data were obtained by Seward et al. (1998, 2000) from both north of the BRSZ (the Andingitra region, Fig. 4 a), and south of the BRSZ. Those north of the BRSZ yielded ages between  $397\pm 36$  Ma and  $201\pm 21$  Ma, whereas those south of the BRSZ yielded ages between  $181\pm 17$  Ma and  $166\pm 14$  Ma. The younger ages south of the BRSZ were interpreted to indicate reactivation of the BRSZ after the Neoproterozoic/Cambrian orogenesis, and a younger uplift of the southern block (Seward et al., 1998, 2000). Apatite FT ages from

southernmost Madagascar vary between  $221\pm 51$  Ma and  $68\pm 8$  Ma of which the youngest ages were attributed to total annealing during the passage of Madagascar over the Marion hot spot (Seward et al., 1999, 2000).

#### 4. Method

Titanite FT analysis documents the cooling of a sample to below 310-265 °C (Coyle and Wagner, 1998) and as such preserves chronological information for temperatures intermediate between  $^{40}\text{Ar}$ - $^{39}\text{Ar}$  biotite (~300 °C) and zircon FT data (310-210 °C; e.g. Yamada et al., 1995). Apatite FT analysis is an established technique to identify vertical movements of crustal units in the very low temperature range between ~110 and 60 °C.

Titanite and apatite samples were separated and processed by conventional techniques (crushing, Wilfley table, magnetic separation and heavy liquids). Titanite and apatite FT ages were measured using the external detector method (Gleadow, 1981). Apatites were etched for 50 sec. in 5%  $\text{HNO}_3$  (23 °C). Titanites were etched individually for 17-22 min in a mixture of HF,  $\text{HNO}_3$ , HCl and  $\text{H}_2\text{O}$  (1:2:3:6) to reveal spontaneous tracks (e.g. Wagner and Van den Haute, 1992). Samples were irradiated in channel 7 and 8 of the Thetis reactor at the Institute for Nuclear Sciences at Gent (Belgium), using a total thermal neutron flux of  $1\times 10^{16}$   $\text{ncm}^{-2}$  (Apatite FT analysis) and  $0.6\times 10^{16}$   $\text{ncm}^{-2}$  (Titanite FT analysis). Detectors were etched for 15 min in 40% HF (23°C) to reveal induced tracks. Ages were calculated using the Zeta calibration method (Hurford and Green, 1983). All reported ages are pooled ages (median ages) except for those samples that failed the  $\chi^2$ -test. The  $\chi^2$ -test compares measured track densities with those expected from a poissonian distribution. Samples with  $\chi^2$  values < 5 % are characterised by a considerable scatter in the single grain ages. In this case the population geometric mean age (central age) is given (Galbraith, 1981; Green, 1981).

Apatite FT data, including single grain apatite FT ages, track length and standard deviation, were used to model specific hypothetical temperature-time (T-t) paths with an inverse modelling procedure, applying the program "MONTE TRAX" (Gallagher, 1995). No chemical composition data for the analysed apatites were available. The Laslett annealing model for Durango apatite was adopted (Laslett et al., 1987). In most cases three large T-t boxes were pre-set to allow a modelling of an unconstrained cooling path and the possibility for reheating. The modelling was carried out using a "genetic algorithm" (Gallagher and Sambridge, 1994), in which the best fitting model of the recent modelled generation is used as a basis for the next modelling step. Twenty generations were modelled with 100 individual T-t histories being tested per generation.

## 5. Results

Thirty-nine samples were collected and studied along a northeast-southwest traverse over the BRSZ, from a vertical profile at Tsaranoro (~800 m) and from other parts in southwest Madagascar (Fig. 4.4a, b). Samples from different basement units were collected at elevations between 1870 m and 240 m (Tab. 1).

The ages of five titanite FT samples range from  $359\pm 20$  Ma to  $276\pm 17$  Ma (Tab. 4.1). Thirty-seven apatite FT ages and the corresponding mean track length (MTL) vary from  $379\pm 19$  Ma to  $150\pm 8$  Ma and from  $13.69\pm 0.16$   $\mu\text{m}$  to  $11.69\pm 0.27$   $\mu\text{m}$ , respectively. Below, samples are presented according to their geographic position from north to south.

### 5.1. Samples northeast of the Bongolava-Ranotsara and Zazafotsy shear zones

Most of the twenty apatite and three titanite samples in this region belong to a vertical profile at Tsaranoro, with elevations ranging between 1870 m and 860 m (Tab. 4.1; Fig. 4.4a). The titanite FT ages northeast of the BRSZ/ZFSZ are  $379\pm 38$  Ma,  $336\pm 20$  Ma and  $276\pm 17$  Ma. Apatite FT ages range between  $305\pm 16$  Ma and  $186\pm 14$  Ma with MTL's varying between  $13.69\pm 0.16$   $\mu\text{m}$  and  $11.98\pm 0.22$   $\mu\text{m}$  and respective standard deviations ranging from  $1.76$   $\mu\text{m}$  to  $0.96$   $\mu\text{m}$ . Nine samples failed the  $\chi^2$ -test, which indicates that the data represent a complex age population. The apatite FT age of sample BE 058 ( $263\pm 11$  Ma) is only 13 Ma younger than its respective titanite FT age ( $276\pm 17$  Ma) and together with the relatively long apatite MTL of  $13.69\pm 0.16$   $\mu\text{m}$ , indicate rapid cooling at this time.

### 5.2. Samples from/around the Bongolava-Ranotsara and Zazafotsy shear zones

Six samples from the BRSZ and ZFSZ were collected at altitudes around 800 m (Fig. 4.4a and Tab. 4.1). Five apatite FT ages range between  $379\pm 19$  Ma and  $296\pm 26$  Ma, only sample BE 064 has a younger apatite FT age of  $242\pm 9$  Ma. The MTL's of the older samples vary between  $13.57\pm 0.45$   $\mu\text{m}$  and  $13.14\pm 0.14$   $\mu\text{m}$ , with standard deviations ranging between  $1.55$   $\mu\text{m}$  and  $1.15$   $\mu\text{m}$ . Sample BE 064 has a MTL of  $12.20\pm 0.12$   $\mu\text{m}$  and a corresponding standard deviation of  $0.84$   $\mu\text{m}$ . The  $\chi^2$ -values range between 97 % and 0 %, whereby five samples passed the  $\chi^2$ -test indicating a single apatite population.

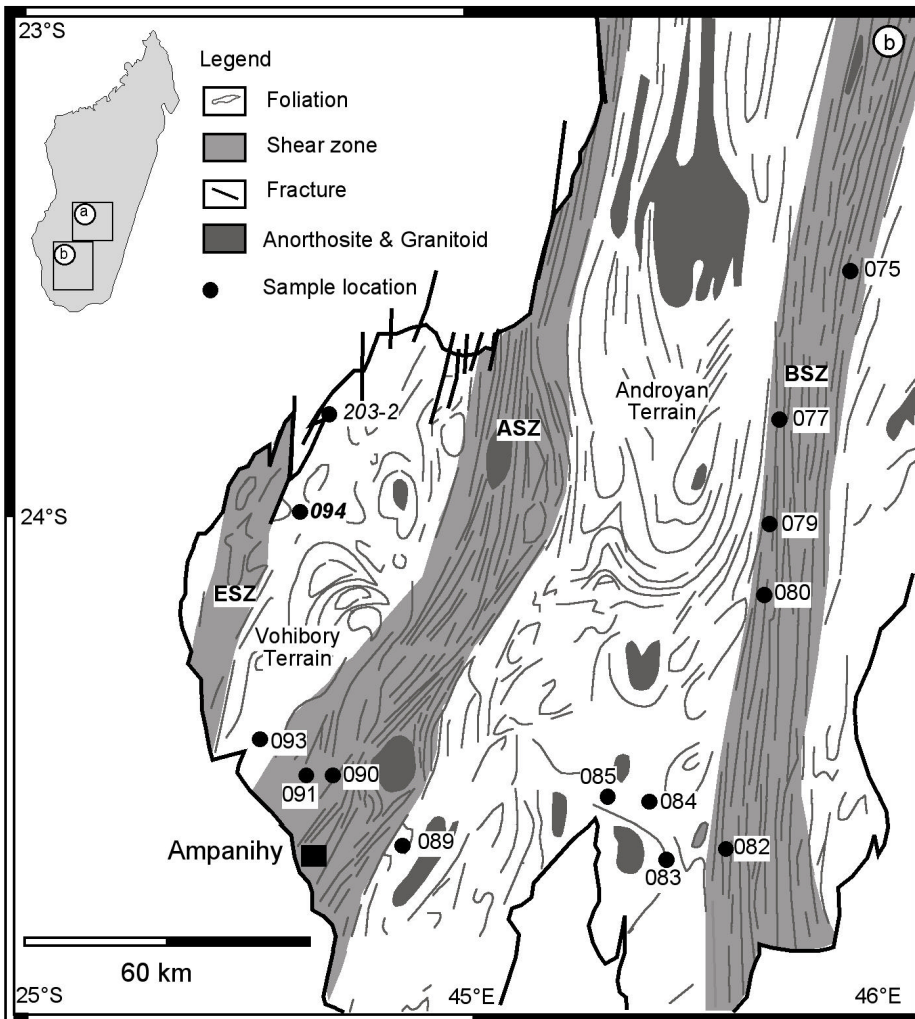
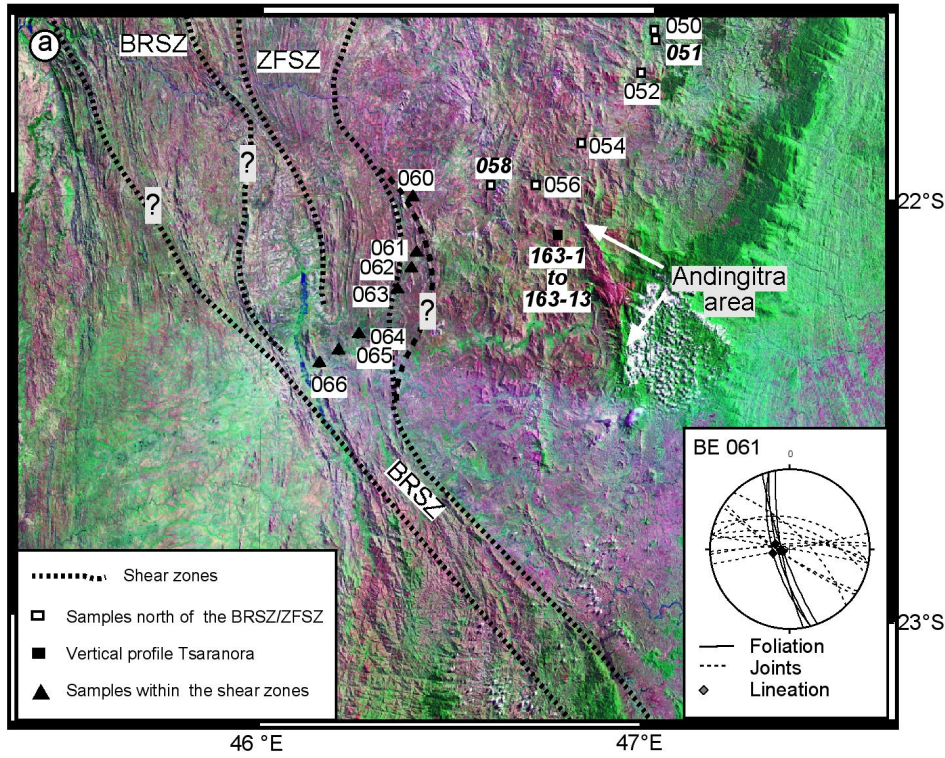


**Fig. 4.4:** a) Landsat 5 satellite image of the area around Ihoay with sample locations. Dashed lines mark the extension of the shear zones. Note that the interpreted eastern extension of the ZFSZ varies from the interpretation of Martelat et al. (2000). BRSZ: Bongolava-Ranoitsara shear zone; ZFSZ: Zazafoitsy shear zone (after Martelat et al., 2000). b) Simplified structural map of southwest Madagascar (from Martelat et al., 2000) with sample locations. Light lines indicate the foliation plane directions. Shaded areas outline the directions of the shear zones. ESZ: Ejeda shear zone; ASZ: Ampanihy shear zone; BSZ: Beraketa shear zone. Bold, italic **sample numbers**: samples with titanite and apatite FT ages; italic **sample numbers**: samples with titanite FT ages; normal sample numbers: samples with apatite FT ages.

Sample Nr. Rock Type	E-Longitude S-Latitude	Elev. [m]	Grains Mineral	(Ns) $\rho_s$ [ $\times 10^5 \text{cm}^{-2}$ ]	(Ni) $\rho_i$ [ $\times 10^5 \text{cm}^{-2}$ ]	(Nd) $\rho_d$ [ $\times 10^5 \text{cm}^{-2}$ ]	P( $\chi^2$ ) [%]	FT Age $\pm$ 1 $\sigma$ [Ma]	U-content [ppm]	MTL $\pm$ 1 $\sigma$ [ $\mu\text{m}$ ] Nr. Lengths	Standard deviation [ $\mu\text{m}$ ]
BE 050 granitic gneiss	47°00.17' 21°36.38'	1150	20 apatite	1728 36.13	1854 38.76	7318 15.2	3	232 $\pm$ 12	36	12.31 $\pm$ 0.19 (49)	1.33
BE 051 dioritic migmatite	46°59.86' 21°36.90'	1175	20 apatite	651 11.53	847 15.0	7569 15.93	87	201 $\pm$ 12	14	12.68 $\pm$ 0.32 (17)	1.33
BE 052 granitic migmatite	46°58.17' 21°42.45'	1200	20 apatite	1915 17.82	2432 22.63	7569 15.88	8	205 $\pm$ 9	22	12.80 $\pm$ 0.17 (50)	1.19
BE 054 Kfsp-granite	46°48.61' 21°51.78'	1075	20 apatite	2344 19.97	2636 22.46	7569 15.8	2	231 $\pm$ 11	20	12.87 $\pm$ 0.14 (45)	0.96
BE 056 granod. gneiss	46°42.09' 21°57.86'	800	20 apatite	2638 31.87	3138 37.91	7400 15.18	1	209 $\pm$ 10	35	12.78 $\pm$ 0.18 (36)	1.1
BE 058 granod. gneiss	46°35.02' 21°57.78'	800	20 apatite	2036 17.36	1991 16.98	7569 15.78	7	263 $\pm$ 11	15	13.69 $\pm$ 0.16 (40)	1.03
<b>vertical profile Tsaranora</b>											
BE 163-1 granite	46°46.47' 22°04.79'	1385	19 apatite	2508 27.72	2981 32.95	7400 16.13	34	222 $\pm$ 9	29	12.66 $\pm$ 0.18 (50)	1.28
BE 163-2 augen gneiss	46°46.47' 22°04.79'	1330	20 apatite	921 11.24	1072 13.09	7400 16.1	0	235 $\pm$ 17	12	12.00 $\pm$ 0.27 (21)	1.23
BE 163-3 granitic gneiss	46°46.47' 22°04.79'	1130	20 apatite	1407 23.67	1949 32.79	7400 16.07	98	190 $\pm$ 9	29	12.18 $\pm$ 0.18 (74)	1.59
BE 163-4 granite	46°46.47' 22°04.79'	1870	20 apatite	1906 37.95	1628 32.41	7400 16.05	3	305 $\pm$ 16	29	11.98 $\pm$ 0.22 (46)	1.49
BE 163-5 granite	46°46.47' 22°04.79'	1840	20 apatite	1890 32.75	1800 31.19	7400 16.02	0	280 $\pm$ 16	27	12.24 $\pm$ 0.22 (42)	1.42
BE 163-6 granite	46°46.47' 22°04.79'	1730	20 apatite	2025 27.96	2127 29.37	7400 15.99	13	249 $\pm$ 11	25	12.27 $\pm$ 0.17 (69)	1.38
BE 163-7 granite	46°46.47' 22°04.79'	1680	20 apatite	1980 35.92	1804 32.72	7400 15.96	1	286 $\pm$ 16	30	12.19 $\pm$ 0.25 (26)	1.26
BE 163-8 granite	46°46.47' 22°04.79'	1510	14 apatite	1311 27.356	1304 27.21	7400 15.93	0	267 $\pm$ 21	24	12.64 $\pm$ 0.49 (13)	1.76
BE 163-9 granite	46°46.47' 22°04.79'	1460	20 apatite	2137 24.29	2662 30.26	7400 15.9	40	209 $\pm$ 9	27	12.21 $\pm$ 0.10 (45)	1.22
BE 163-10 granite	46°46.47' 22°04.79'	1300	11 apatite	1095 20.04	1541 28.20	7400 15.87	0	186 $\pm$ 14	27	12.58 $\pm$ 0.21 (31)	1.17
BE 163-11 augen gneiss	46°46.47' 22°04.79'	1200	20 apatite	1202 19.84	1485 24.50	7400 15.84	62	210 $\pm$ 10	22	12.35 $\pm$ 0.23 (37)	1.4
BE 163-12 augen gneiss	46°46.47' 22°04.79'	1130	19 apatite	1575 31.12	2065 40.80	7400 15.81	15	198 $\pm$ 9	36	12.03 $\pm$ 0.25 (28)	1.31
BE 163-13 augen gneiss	46°46.47' 22°04.79'	860	20 apatite	2211 47.76	2515 54.33	7400 15.79	11	227 $\pm$ 9	49	12.78 $\pm$ 0.14 (83)	1.31
BE 060 granitic gneiss	46°23.37' 22°00.45'	870	20 apatite	1611 25.61	1041 16.55	7400 15.15	97	379 $\pm$ 19	15	13.14 $\pm$ 0.14 (67)	1.15
BE 062 granitic gneiss	46°22.83' 22°09.88'	830	20 apatite	2388 26.31	1975 21.76	7400 15.12	32	297 $\pm$ 13	20	13.39 $\pm$ 0.17 (50)	1.22
BE 063 granitic gneiss	46°21.33' 22°13.35'	760	15 apatite	1017 25.39	757 18.90	7569 15.47	21	337 $\pm$ 19	17	13.57 $\pm$ 0.45 (12)	1.55
BE 064 migmatic gneiss	46°14.53' 22°19.62'	700	20 apatite	3364 43.19	3326 42.70	7318 14.64	49	242 $\pm$ 9	39	12.20 $\pm$ 0.12 (50)	0.84
BE 065 granitic gneiss	46°11.67' 22°21.75'	700	18 apatite	1019 18.947	840 15.62	7318 14.55	0	296 $\pm$ 26	15	13.52 $\pm$ 0.19 (54)	1.39
BE 066 migmatic gneiss	46°08.87' 22°24.35'	770	18 apatite	1778 25.09	1224 17.27	7569 15.62	8	367 $\pm$ 17	16	13.26 $\pm$ 0.23 (39)	1.44
BE 075 migmatic gneiss	45°54.09' 23°33.32'	700	16 apatite	1086 41.269	767 29.147	7617 16.25	70	372 $\pm$ 21	25	13.74 $\pm$ 0.21 (63)	1.65
BE 077 migmatic gneiss	45°42.32' 23°49.90'	680	16 apatite	1511 84.59	2391 134	7569 15.6	6	162 $\pm$ 7	118	-	-
BE 079 charnockit	45°37.21' 24°03.56'	585	20 apatite	401 3.64	436 3.96	7400 15.09	59	227 $\pm$ 17	4	-	-
BE 080 migmatic gneiss	45°39.21' 24°09.19'	545	19 apatite	602 6.87	857 9.78	7400 15.06	14	174 $\pm$ 11	10	-	-
BE 082 leuco granite	45°35.31' 24°39.87'	420	20 apatite	3811 34.81	4896 44.72	7318 14.68	0	187 $\pm$ 9	44	13.37 $\pm$ 0.12 (100)	1.19
BE 083 gneiss	45°27.27' 24°38.81'	325	20 apatite	1831 21.14	2519 29.08	7400 15.04	31	179 $\pm$ 8	27	13.02 $\pm$ 0.21 (49)	1.45
BE 084 diorite	45°26.07' 24°36.38'	345	20 apatite	585 12.21	778 16.23	7400 15.01	7	185 $\pm$ 12	15	13.15 $\pm$ 0.12 (52)	1.43
BE 085 metadiorite	45°17.80' 24°35.93'	330	20 apatite	120 1.586	120 1.59	7400 14.98	65	245 $\pm$ 32	1	-	-

Sample Nr. Rock Type	E-Longitude S-Latitude	Elev. [m]	Grains Mineral	(Ns) $\rho_s^s$ [ $\times 10^6 \text{cm}^{-2}$ ]	(Ni) $\rho_i^i$ [ $\times 10^6 \text{cm}^{-2}$ ]	(Nd) $\rho_d^d$ [ $\times 10^6 \text{cm}^{-2}$ ]	P( $\chi^2$ ) [%]	FT Age $\pm$ 1 $\sigma$ [Ma]	U- content [ppm]	MTL $\pm$ 1 $\sigma$ [ $\mu\text{m}$ ] Nr. Lengths	Standard deviation [ $\mu\text{m}$ ]
BE 089 amphibolite	44°52.89' 24°41.27'	240	20 apatite	2698 35.92	2967 39.51	7400 14.95	15	223 $\pm$ 9	38	13.08 $\pm$ 0.13 (100)	1.30
BE 090 amphibolite	44°39.04' 24°32.54'	250	20 apatite	4396 38.53	6059 53.11	7400 14.92	46	178 $\pm$ 6	49	13.06 $\pm$ 0.12 (86)	1.09
BE 091B amphibolite	44°37.39' 24°31.23'	240	20 apatite	2807 50.31	3545 63.53	7569 15.57	32	202 $\pm$ 8	56	13.25 $\pm$ 0.12 (78)	1.03
BE 093 granitic gneiss	44°30.88' 24°21.18'	260	20 apatite	2481 21.07	3002 25.50	7400 14.89	0	200 $\pm$ 12	24	12.61 $\pm$ 0.18 (60)	1.38
BE 094 amphibolite	44°38.34' 23°59.47'	445	20 apatite	831 8.25	1353 13.43	7400 14.86	64	150 $\pm$ 8	14	12.53 $\pm$ 0.22 (40)	1.42
BE 051 dioritic migmatite	46°59.86' 21°36.90'	1175	19 titanite	1290 47.30	523 19.18	15914 22.56	5	336 $\pm$ 20	31		
BE 058 granod. gneiss	46°35.02' 21°57.78'	800	14 titanite	961 67.16	477 33.33	15914 22.53	60	276 $\pm$ 17	57		
BE 163-2 augen gneiss	46°46.47' 22°04.79'	1330	3 titanite	405 136.03	142 47.70	15914 22.08	17	379 $\pm$ 38	80		
BE 203-2 dioritic gneiss	44°45.05' 23°50.12'	365	11 titanite	1594 156.58	587 57.66	15914 21.91	23	359 $\pm$ 20	97		
BE 094 amphibolite	44°38.34' 23°59.47'	445	16 titanite	1616 97.26	665 40.02	15914 22.5	89	330 $\pm$ 18	67		

**Tab. 4.1:** FT results from basement rocks of central-southern Madagascar. Ages calculated using dosimeter glasses: IRMM-540 (apatite) with  $\xi_{\text{RMM-540}}=333\pm 9$ ; CN2 (titanite) with  $\xi_{\text{CN2}}=124\pm 3.25$ . FT ages are reported as pooled ages if  $\chi^2 > 5\%$ , otherwise the central age is given. Elev.: Elevation,  $\rho_s$ ,  $\rho_i$ ,  $\rho_d$ ,  $N_s$ ,  $N_i$ ,  $N_d$ : density and number of counted spontaneous, induced and dosimeter glass tracks, U-content = Uranium content;  $P(\chi^2)$ : Chi-square probability.

### 5.3. Samples south of the Bongolava-Ranotsara shear zone

Samples south of the BRSZ belong to four different tectonostratigraphic terrains and were collected at elevations ranging between 680 m and 240 m. Nine samples were collected from the Beraketa and Ampanihy shear zones, two from the Androyan terrain and two from the Vohibory terrain (Fig. 4.4b). Two titanite FT ages from the Vohibory terrain yield ages of  $359\pm 20$  Ma (BE 203-2) and  $330\pm 18$  Ma (BE 094). Fourteen apatite FT ages range between  $372\pm 21$  Ma and  $150\pm 8$  Ma. MTL range between  $13.74\pm 0.21$   $\mu\text{m}$  and  $11.69\pm 0.27$   $\mu\text{m}$ , with standard deviations varying between 1.65  $\mu\text{m}$  and 1.03  $\mu\text{m}$ . Eleven samples passed the  $\chi^2$ -test with values ranging between 70 % and 6 %.

## 6. Interpretation of titanite and apatite FT data

The titanite and apatite FT data presented in this study give new thermochronological information about the post Neoproterozoic/Cambrian cooling and exhumation history of the basement prior to earliest basin formation. For all samples, titanite and apatite FT ages are

younger than their assumed metamorphic and/or emplacement ages, indicating that substantial thermal events affected the samples since the rocks formed. Titanite FT ages indicate cooling of central-southern Madagascar to below  $\sim 300$  °C during Carboniferous-Early Permian times with fast cooling at the basement/sedimentary cover contact (BE 203-2) and advective heating at the eastern margin of the ZFSZ (BE 058).

Sample BE 203-2 is in direct contact with the oldest sedimentary rocks of the Sakoa Group. The titanite FT age from this sample provides that the rock cooled from  $\sim 300$  °C to surface temperatures between  $359 \pm 20$  Ma and Late Carboniferous times ( $\sim 300$  Ma), prior to the deposition of the oldest Sakoa sediments. Further details of the cooling history are obtained from vitrinite reflectance data from the Sakoa coal area (Fig. 4.3a). Reflectance indices from this area range between 0.88 and 0.79 (Ramanampisoa et al., 1990; Radke et al., 2000) and indicate a second heating to temperatures of  $\sim 140$ - $120$  °C (calculated after Burnham and Sweeney, 1989) after deposition of the Late Carboniferous/Early Permian Sakoa Group.

The titanite FT age of sample BE 094, located  $\sim 20$  km southwest of sample BE 203-2, is  $330 \pm 18$  Ma and has a corresponding apatite FT age of  $150 \pm 8$  Ma. The sample is interpreted to have had a similar Late Carboniferous cooling history as sample BE 203-2 with cooling to surface temperatures during Late Carboniferous/Early Permian times with a potential post-Permian phase of burial heating.

Sample BE 058 points at a phase of rapid cooling from  $\sim 300$  °C at  $276 \pm 17$  Ma to below  $\sim 110$  °C by  $263 \pm 11$  Ma. The relatively long apatite MTL ( $13.69 \pm 0.16$   $\mu\text{m}$ ) is indicative for rapid cooling through the apatite partial annealing zone (PAZ:  $\sim 110$ - $60$  °C). The data may reflect structural reactivation or locally elevated temperatures possibly due to hydrothermal fluid flow caused by reactivation of zones of basement weakness at the margin of the ZFSZ or the Betsileo shear zone.

Apatite FT results are presented in a number of diagrams (Fig. 4.5a-d), all of which clearly express the unique thermochronological evolution of the BRSZ/ZFSZ. From west to east apatite FT ages generally increase towards the BRSZ/ZFSZ from  $\sim 190$  Ma to  $\sim 300$  Ma. East of the BRSZ/ZFSZ the ages decrease to  $\sim 250$  Ma. In the same direction MTL increase from  $\sim 12.8$   $\mu\text{m}$  to  $\sim 13.3$   $\mu\text{m}$  within the shear zones and decrease to values of  $\sim 12.5$   $\mu\text{m}$  east of the shear zones (Fig. 4.5a). Much of which can be explained by a change in elevation from west to east with the elevation vs. apatite FT age diagram showing a decrease of ages from  $\sim 300$  Ma to  $\sim 160$  Ma with decreasing elevation (Fig. 4.5b). The samples from the vertical profile (filled boxes Fig. 4.5b) show a linear correlation. The samples south of the BRSZ give no linear correlation with elevation, probably because of the broad spatial distribution of the samples. In general, the relationship of elevation and MTL shows increasing MTL from  $\sim 12.2$

$\mu\text{m}$  to  $\sim 13.2 \mu\text{m}$  with decreasing altitudes (Fig. 4.5c). The samples from the BRSZ/ZFSZ, however do not follow these trends (Fig. 4.5a-c).

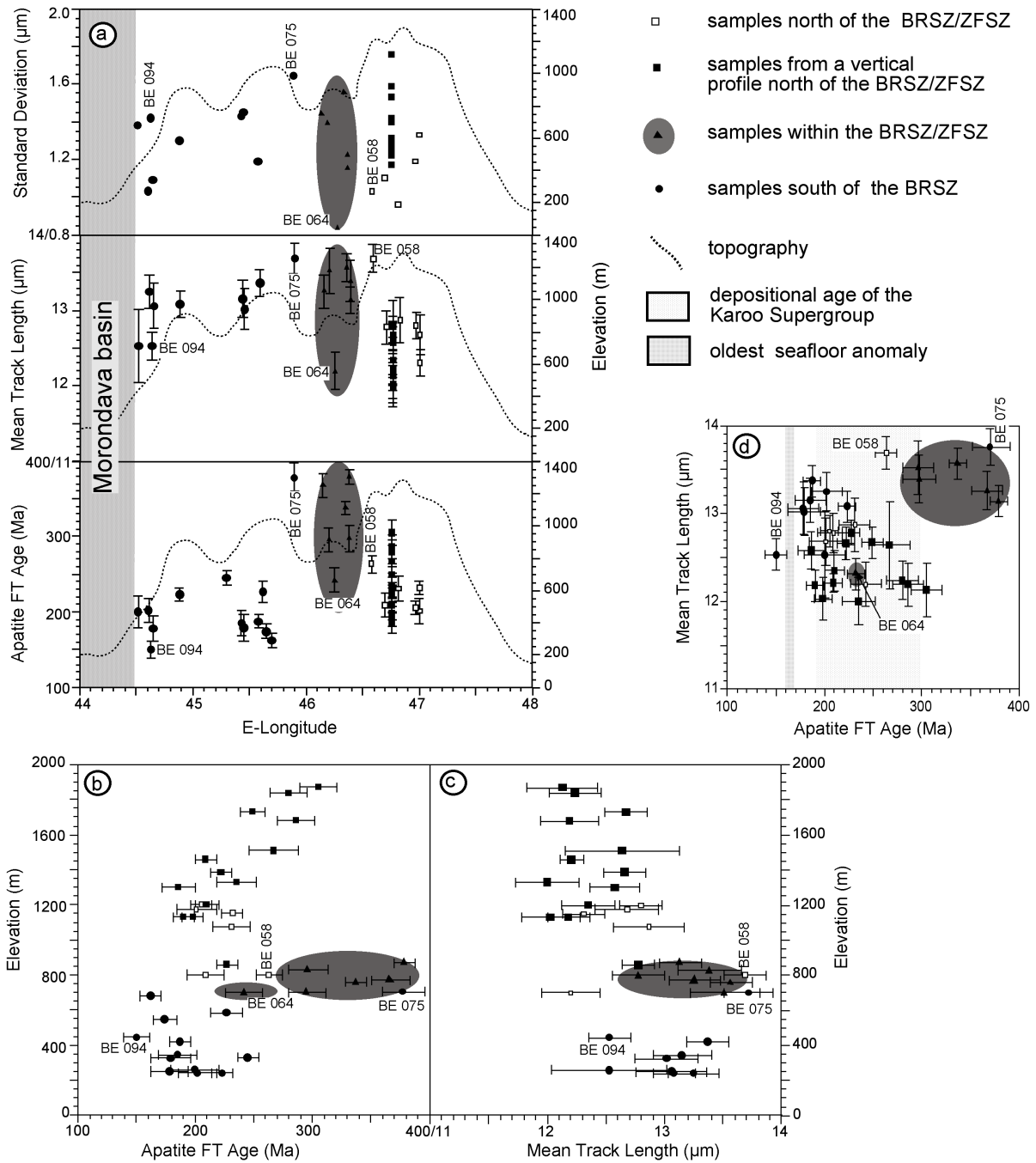


**Fig. 4.5:** a) Apatite FT age, mean track length and standard deviation plotted against the E-Longitude from the Morondava basin towards the Indian Ocean. A present day topographic section from  $24.5^{\circ}\text{S}/44^{\circ}\text{E}$  to  $20.5^{\circ}\text{S}/48^{\circ}\text{E}$  is given by the dotted line. b) Relationship between the sample elevation and the apatite FT ages. c) Relationship between sample elevation and mean track length. d) Relationship between apatite FT age and mean track length. In all diagrams error bars are plotted as  $1\sigma$ .

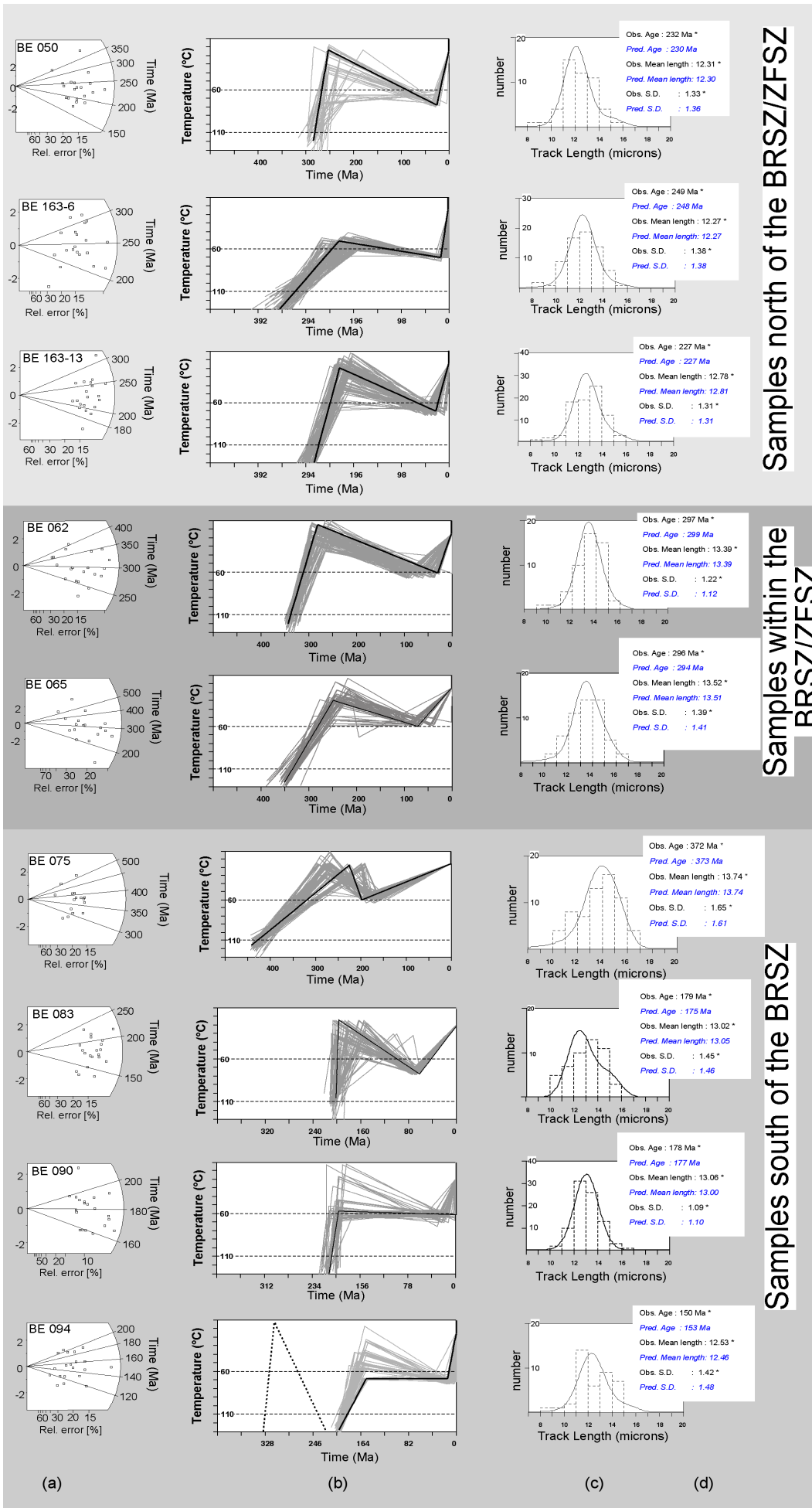


**Fig. 4.6:** Modelled representative apatite FT samples from samples located north, within, and south of the BRSZ/FSZ. a) Radial plots: Sample number is given on the left side of the plot. Note the variations in the apatite FT age between individual grains. b) T-t path: the cooling histories were modelled using the program MONTE TRAX (Gallagher, 1995). The black line represents the thermal history that fits best the observed data; grey lines represent other possible cooling histories. Dashed line in model sample BE 094 represents a possible cooling path obtained from titanite FT data and depositional age of the western adjacent sedimentary rocks of the Sakoa Group c) Length histogram: The measured mean confined track lengths are shown as histograms. The curve displays the modelled track length distribution for the "best fit". d) Fitting parameters: Obs.: Observed, Pred.: predicted, SD: standard deviation.

Nearly all samples outside the BRSZ/ZFSZ have typical characteristics of mixed ages (broad single grain age distribution, short mean track length), indicating complex cooling paths. They all give evidence of a period of rapid cooling during Carboniferous-Triassic times and are influenced by later tectonic and/or magmatic events.

Modelled thermal histories for the samples north of the BRSZ/ZFSZ (Fig. 4.6) indicate that these samples quickly passed through the apatite PAZ in Carboniferous to Permian times and were partially annealed thereafter. As expected (because tectonically unaffected), the topographic highest (~1800 m) samples from the vertical profile passed earlier through the apatite PAZ (~300 Ma) than the samples from lower altitudes (~1200 m, ~250-300 Ma).

Nearly all samples (except: BE 064) from the BRSZ and ZFSZ have apatite FT ages of ~380-300 Ma and relatively long MTL ranging from 13.14-13.52  $\mu\text{m}$ . A few apatite FT ages are older than the titanite FT ages from the areas north and south of the BRSZ. The modelled apatite FT data indicate that the area inside the shear zones cooled to below ~110 °C approximately during Late Devonian to Early Carboniferous times and stayed in a nearly stable position until the Recent. The samples could have been buried several times to a max. of ~2 km, but a reheating to temperatures >65 °C can be excluded.

Most modelled T-t histories of the samples south of the BRSZ point at a Late Triassic phase of enhanced cooling. Sample BE 075 is located ~130 km southwest of the BRSZ and it is the oldest apatite FT sample from the southern block. The modelled T-t history (Fig. 4.6) is similar like those from the modelled BRSZ/ZFSZ samples with cooling during Devonian times. Only sample BE 094 shows cooling being delayed until the Early Jurassic (Fig. 4.6). Sample BE 094 has an apatite FT age of  $150 \pm 8$  Ma and is approximately 30 Ma younger than the samples located further east. The MTL of  $12.53 \pm 0.22$   $\mu\text{m}$  is shorter than the MTL seen in eastern samples. A standard deviation of 1.42  $\mu\text{m}$  in sample BE 094 is also higher than the eastern samples, indicating a significantly different cooling history. The modelled cooling path of sample BE 094 shows that it rapidly cooled through the PAZ at ~190 Ma. Like many other samples, the modelled T-t history of sample BE 094 suggests reheating to temperatures of ~70°C during Cenozoic times (Fig. 4.6).

The modelled Late Cretaceous (~90-80 Ma) - Neogene phases of reheating probably originated from magmatic activities, as indicated by several volcanic provinces (Figs. 4.2 and 4.3). The single grain ages and the modelled T-t paths of the samples near to the volcanic area L'Androyan (BE 082, BE 083 and BE 084) give evidence of a thermal overprint during Early-Late Cretaceous times (Figs. 4.6 and 4.7).

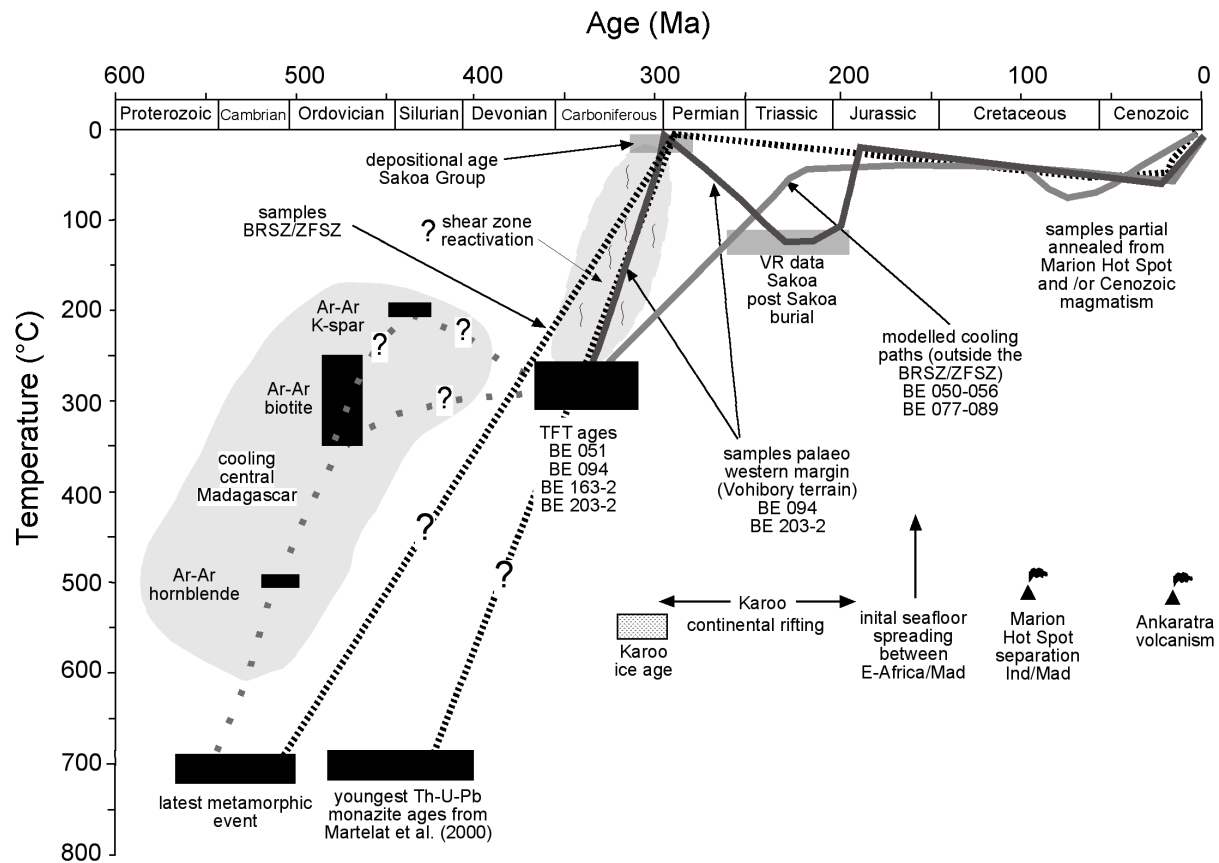


**Fig. 4.7:** Summary of the complete post Cambrian T-t histories from central-southern Madagascar.  $^{40}\text{Ar}/^{39}\text{Ar}$  ages are from the Carion granite ~400 km northwest of the working area (Meert et al., 2001). This figure emphasises the different cooling histories of samples from the western margin of Madagascar (BE 203-2 and BE 094), from inside the BRSZ/ZFSZ and outside the shear zones. For the detailed high temperature history (700-300 °C) of southern Madagascar see de Wit et al. (2001).

## 7. Discussion

The Neoproterozoic/Cambrian high temperature history of southern Madagascar is documented in a number of publications (e.g. Paquette et al., 1994; Kröner et al., 1996; Ashwal et al., 1998, 1999; Meert et al., 2001). Although these geochronological data do not show a consistent evolution of the entire island, the Neoproterozoic/Cambrian cooling to below ~700-500 °C seems to range from ~600 Ma to ~500 Ma in most areas.

The mid-Carboniferous was a time of mountain building along much of the Palaeo-Pacific margin (Veevers and Powell, 1994). At this time Madagascar had a central position within Gondwana and was far away from any potential subduction zones (Fig. 4.1a). A number of authors have suggested that most of the Gondwana supercontinent (including large parts of Australia and India) was characterised by large-scale uplift that may have affected or caused the Late Carboniferous-Early Permian glaciation (Veever and Powell, 1994; Visser and

Praekelt, 1996; Wescott and Diggins, 1997). This uplift has been interpreted to be related to subduction along the Palaeo-Pacific Ocean and a change in stress regime during the development of the Permo-Triassic Cape Fold Belt in South Africa (Fig. 4.1a). Up to now there was no evidence for uplift in Madagascar at this time. However, our titanite FT ages and the oldest apatite FT ages from central-southern Madagascar reflect a phase of enhanced cooling during Carboniferous-Triassic times that would be consistent with increased uplift driven exhumation at this time.

Denudation rates were calculated for samples for which combined titanite FT and apatite FT data are available and for samples with a clear relationship to the overlying sedimentary successions (Fig. 4.8). Generally, denudation rates and burial amounts were calculated with an assumed geothermal gradient of  $30\text{ }^{\circ}\text{Ckm}^{-1}$ . This rate is supported by Recent rifting examples (e.g. Red Sea) where although high heat flow is recorded towards the centre of the rift, the geothermal gradients quickly revert to normal values at the margin of the continents (Makris et al., 1991).

Titanite FT and apatite FT data argue that during Carboniferous times (~350-300 Ma) denudation of ~10-5 km of crustal section at the evolving basement/sedimentary cover contact and ~5.5-1.3 km in the hinterland occurred. Consequently, for the period between 350 and 300 Ma denudation rates of ~200-100  $\text{mMa}^{-1}$  for the present basement/basin contact are estimated. In contrast, denudation rates in the hinterland are ~110-25  $\text{mMa}^{-1}$ . These calculated rates differ significantly from those reported by Seward et al. (1999) for the Andingitra area (north of the BRSZ and ZFSZ). Solely based on apatite FT data they calculated a very low exhumation rate of 8  $\text{mMa}^{-1}$  for the 400-200 Ma episode.

Vitrinite reflectance data suggest that the area around the sample BE 203-2 (western margin) was subsequently buried to depths of ~4.5-4 km after the Early Permian, but the denudation in the hinterland continued at least until Early Triassic times.

The topography of the intracontinental Karoo basin margin changed significantly during the early evolution of the Morondava basin. The data argue for highest denudation rates at the margin of the Morondava basin. This argues for a high relief and thus we interpret the eastern Morondava rift shoulder as a former escarpment (Fig. 4.8). Between ~350-300 Ma, the FT data suggest that either this escarpment retreated towards the east or that rapid in-place excavation occurred. As a result of the high relief, denudation occurred most rapidly at the Late Carboniferous scarp front. As the escarpment evolved and stepped back sediments buried these quickly exhumed areas (Fig. 4.8).

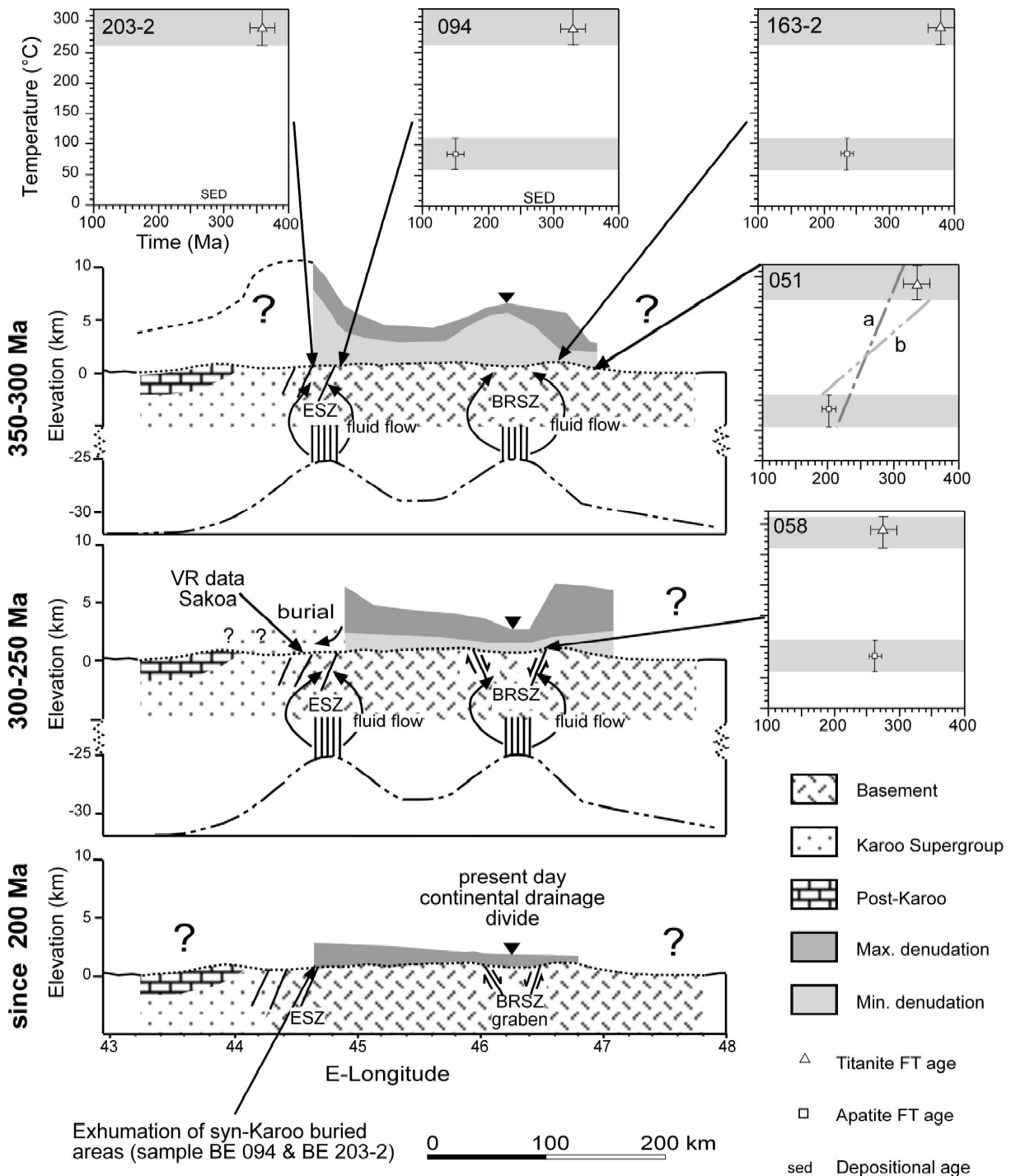


**Fig. 4.8:** Sketch of the western Madagascan margin during the 350-200 Ma interval. The calculated denudation rates argue for two different margin models during the subsequent rift-drift evolution. During the 350-300 Ma episode maximum denudation occurred at the future basement/basin contact. Sample BE 058 dates reactivation of faults along the BRSZ and the associated graben evolution. Since 200 Ma, only minor denudation occurred along the continental margin. Position of sample BE 094 was projected ~30 km west of sample BE 203-2 on the basis of the west-east distance from the sample location to the Sakoa area. Denudation rates were calculated by the following equation: Denudation rate = Cooling rate/Geothermal gradient. Maximum denudation rates were calculated using slope (Cooling rate) a (min. with slope b) and a geothermal gradient of  $30\text{ }^{\circ}\text{Ckm}^{-1}$ . Denudation inside the BRSZ was calculated under consideration of the latest metamorphic event around the BRSZ (500 Ma/700 °C) and the average value of the "old" apatite FT ages from the BRSZ (335 Ma/60-120 °C). Position of the mantle-crust boundary from Pili et al. (1997).

From Late Carboniferous times until Early Permian times large parts of Gondwana (two thirds of Africa, India, Antarctica and Australia) were covered with an ice sheet (e.g. Scotese et al., 1999). During deglaciation these areas could have undergone rapid denudation due to chemical and mechanical weathering. To what extent these processes affected the FT data in the working area remains speculative. An evidence for a minor impact of deglaciation driven high denudation is given by the totally different denudation rates calculated for samples at the rift shoulder (high) and in the hinterland (low). Thus, we suggest that reactivation and uplift along the Morondava rift shoulder affected the denudation pattern to a higher degree. Martelat et al. (2000) report their youngest Th-U-Pb monazite ages (~480-375 Ma) from within the shear zones (including the BRSZ). They interpreted these ages as the result of Pb loss by circulating fluids in the shear zones after Cambrian transpressional deformation of the metamorphic basement in southern Madagascar. Furthermore, other geochronological data argue for latest post orogenic thermal activity to be found inside the BRSZ (de Wit et al., 2001, see Tab. 4.2). The oldest apatite FT ages were dated in the area around Ihosy, within the BRSZ and ZFSZ.

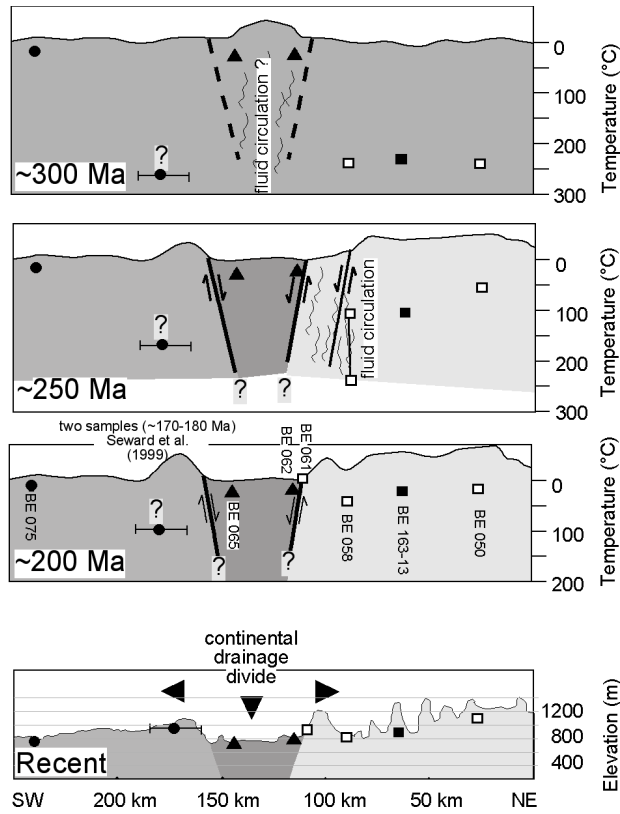
Author	Locality	Event	Technique	Age (Ma)
Meert et al. (2001)	central Madagascar	emplacement of Carion granite cooling from 350°C to 100°C	SHRIMP U-Pb Ar/Ar hornblende, biotite and K-feldspar	532 466-410
Fernandez et al. (2001)	Itremo (central Madagascar)	latest thermal overprint	Ar/Ar biotite	490
Kröner et al. (1996)	Ihosy	high grade metamorphism and anatexis	Pb/Pb zircon	560-530
Martelat et al. (2000)	southern Madagascar	two deformation events between 590-500 Ma	Th-U-Pb electron microprobe dating of monazite	outside the SZ 590-515 Beraketa SZ 500-490 BRSZ 480-375
De Wit et al. (2001)	southern Madagascar	collision in southern Madagascar four deformation events D1-D3 compressional deformation D4 exhumation caused from 520-490 extensional tectonics	U/Pb zircon and monazite titanite and rutile	D1: 647-630 D2: 628-627 D3: 614-609 D4: 550-520 (BRSZ)
Paquette et al. (1995)	southern Madagascar	high grade metamorphic event between 590-565 Ma	U/Pb zircon Sm-Nd mineral/whole rock	580-525 590-490
Ashwal et al. (1998)	SW Madagascar	metamorphism	Sm-Nd whole rock/mineral	560±50
Ashwal et al. (1999)	SW Madagascar	granulite/amphibolite grade metamorphic event	U/Pb zircon	630-550

**Tab. 4.2:** Summary of geochronological data from central and southern Madagascar. Geochronological data from central Madagascar are from the Itremo Group ~250 km north of the BRSZ (Fernandez et al., 2001) and from the Carion granite ~400 km north of the working area (Meert et al., 2001).

The modelled apatite FT data from the BRSZ indicate a cooling through the PAZ of apatite (~110-60 °C) in Late Devonian-Carboniferous times. The apatite FT data most likely represent simple cooling ages from the 530-500 Ma D2 event (Martelat et al., 2000) or from the phase of fluid circulation (Fig. 4.9a). Thereafter, the BRSZ was not affected by temperatures >65 °C again (Fig. 4.7). In contrast, samples from northeast and southwest of the BRSZ/ZFSZ show evidence of exhumation and cooling during Late Permian-Triassic times. The fact that the samples from the BRSZ/ZFSZ show the oldest apatite FT ages at lower elevations could indicate that the BRSZ represents an early break-up graben as rocks either side of it have been exhumed relative to the shear zones (Fig. 4.9a). The present day topography and drainage system mirrors this graben structure (Fig. 4.9a, c). In central and northern Madagascar the continental drainage divide occurs within the central highland, west of the eastern escarpment (Fig. 4.9b).

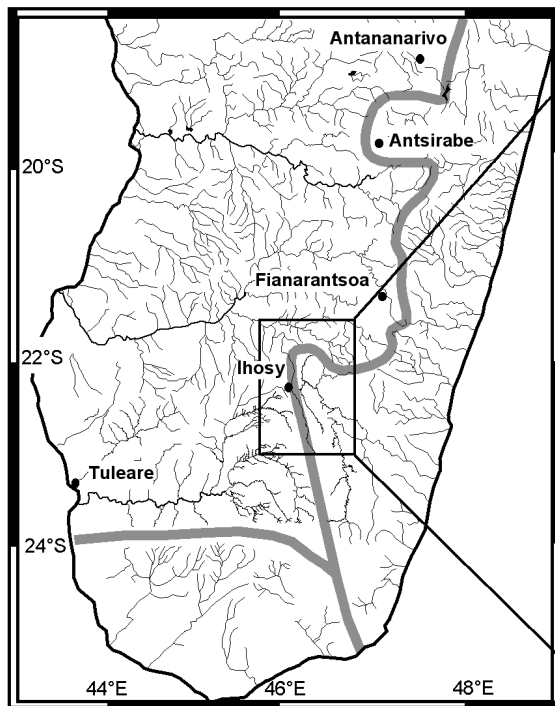
Only southwest of Fianarantsoa is the divide deflected westward by the topographic break across the BRSZ (Johnson, 2002). Furthermore, graben parallel faults with down dip slickensides were identified at the northern rim of the BRSZ/ZFSZ (Fig. 4.4a). Although undated, they could represent the tectonism associated with graben formation. Permian titanite FT and apatite FT ages from sample BE 058, at the margin of the ZFSZ could give a minimum age for the graben formation. Mesozoic graben-fill is not recorded, but may lie undetected under Tertiary sediments or has been eroded during the later graben evolution. An early Gondwana break-up graben would fit into recent tight Gondwana reconstruction (Reeves et al., 2002) in which the Bongolava-Ranotsara graben would find its continuation in the Anza rift of East Africa. Like the Bongolava-Ranotsara graben, the Anza rift is suggested to have had a Permo-Carboniferous rift phase (Bosworth and Morley, 1994; Yardimcilar and Reeves, 1998).

The transform margin evolution started with the beginning of drift between Madagascar and East Africa along the Davie transform fault as oceanic crust formed in the Somali basin to the north (Coffin and Rabinowitz, 1987). In contrast to the Carboniferous-Triassic evolution of the eastern Morondava rift shoulder, the post Jurassic western transform margin evolution of Madagascar is characterised by low denudation rates. They probably indicate minor relief during this time (Fig. 4.8). A number of apatite FT ages from southern Madagascar are Jurassic but single grain age distribution and modelled thermal histories show that these are mixed ages (Fig. 4.6). Only one sample from far southwest Madagascar (BE 094) points at an Early Jurassic cooling that could correlate with the beginning of the translation along the Davie transform fault. The modelled cooling path implies a denudation of ~3.5-1.5 km during Early Jurassic times (Fig. 4.6).

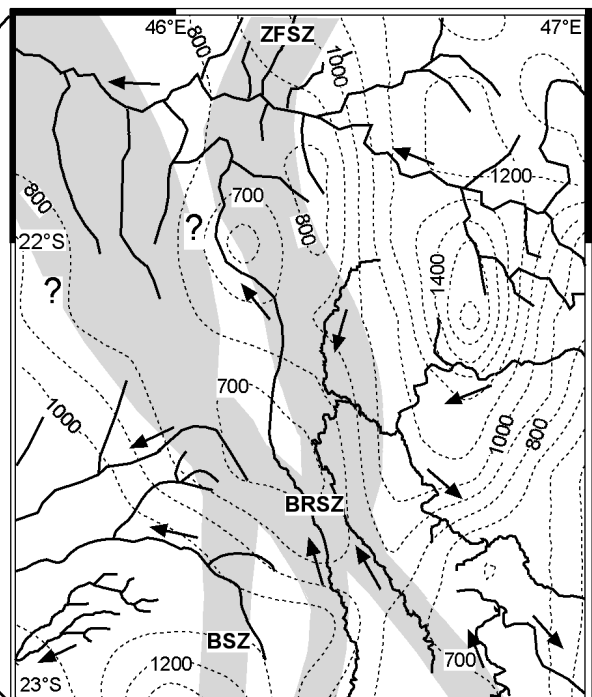


(a)

**Fig. 4.9:** a) Sketch of the BRSZ graben development. The estimated temperatures for different time spans were obtained from titanite FT data, from modelled T-t histories (Fig. 4.6) and two apatite FT ages from Seward et al. (1999). The FT data from Seward et al. (1999) are without single grain ages, length information, modelled cooling paths and exact sample location. We estimated the temperatures due to the titanite FT ages of the adjacent samples and the samples own apatite FT ages. The present day topography is based on the GTOPO30 data set. b) The drainage system of southern Madagascar shows a marked deviation in the continental drainage divide at the BRSZ. The continental drainage divide is given as a grey line. c) Topographic map (based on ETOPO5 data set) and drainage system from the area around Ihosy. The BRSZ is situated in a valley, the graben flanks are characterised by elevated areas. Arrows indicate the direction of the drainage.



(b)



(c)

Predictions of rift-related denudation across continental transform margins vary significantly between ~350 and ~3500 m, depending on the model used. Simple heat conduction models suggest transient uplift of >2000 m across a transform margin (e.g., Todd and Keen, 1989). The total accumulated denudation, comprising surficial erosion and local isostatic rebound in response to the erosion, would be up to ~3500 m (Lorenzo and Vera, 1992). Gadd and Scrutton (1997) used a 2D numerical thermal model to calculate uplift and subsidence profiles across a transform margin. For a margin with a length of 900 km and a spreading rate of  $1 \text{ cm yr}^{-1}$ , they calculated thermal uplift between 335–470 m (assuming regional isostasy) and 1300–1400 m (local isostasy), with maximum uplift occurring along the continent-ocean boundary.

In southern Madagascar, it is difficult to calculate denudation rates for the Jurassic using apatite FT data because in most areas only small amounts (up to ~2 km) were eroded. Furthermore, Cretaceous and Tertiary magmatic events affected the apatite FT data and different geothermal gradients for sedimentary rocks and basement rocks must be assumed.

These two temporally separated tectonic/denudation patterns (Fig. 4.8) would explain the changes in the sedimentary trend from deposits of the Karoo Supergroup to the Jurassic-Quaternary sedimentary rocks and the different brittle structures observed. New tectono-sedimentary models (Clark and Ramanampisoa, 2002) clarify that the Karoo sequence and the drift evolution are temporally and spatially separated. The Karoo represents a failed rift (Clark and Ramanampisoa, 2002) caused by orthogonal northwest-southeast rifting (Malod et al., 1991; Montenat et al., 1996). In contrast, the Middle Jurassic - Quaternary sedimentary record displays the transform margin evolution along the western coast caused by the southward drift of Madagascar along the Davie fracture zone (Ségoufin and Patriat, 1981). The change in the tectonic regime caused different apatite FT patterns and led to different dynamic margin behaviour with possibly interfering effects.

All modelled T-t paths show a reheating into the upper temperature zone (~60-80 °C) of the PAZ that is temporally not well constrained. At this stage it is not clear whether this is a real thermal event or an artefact of the model parameters. In general, a modelled Late Cretaceous reheating for the samples near the Cretaceous L'Androyan volcanic complex is possible. The modelled T-t paths of the other samples from southern Madagascar favour Neogene reheating (Figs. 4.6 and 4.7). Both options would imply a rise of the isotherm possibly caused by magmatism. The break-up of the Australia-India-Madagascar block and the opening of the Indian ocean during the Cretaceous was caused by active rifting and was associated with Marion hot spot related volcanism (Storey et al., 1995). This hot spot may have affected samples (reheating to max. 80 °C) adjacent (~30 km) to the volcanic complex L'Androyan (BE 077 - BE 082) but it did not reset the apatite FT age of any studied samples.

## 8. Conclusions

With combined titanite and apatite FT analyses of basement rocks from southwest Madagascar it was possible to reconstruct the thermal evolution of the eastern Morondava rift shoulder. The FT data argue for fluid activity in shear zones along the western margin and along the BRSZ/ZFSZ in Carboniferous-Permian times. Along the western margin high degrees of denudation predate the Karoo rifting. During this time the structural framework for the later Karoo basin developed. A graben formed along the BRSZ/ZFSZ in Permo-Triassic times that may have influenced the early rift kinematics. Since the Triassic a merely uniform thermal evolution with denudation of crustal material of ~2 km occurred in most areas of southern Madagascar. The Middle Jurassic southerly drift of Madagascar and the final separation between Madagascar and East Africa had only minor effects on the western margin. In contrast to the Carboniferous-Permian thermal evolution, structural reactivation or increased denudation did not accompany the transform margin evolution. This new model for the southwestern Madagascan continental margin correlates with recent sedimentary models for the Morondava basin (Clark and Ramanampisoa, 2002). Cretaceous and later volcanic activity affected the apatite FT data from southern and central Madagascar.

## Acknowledgements

This project was supported in part by Deutsche Forschungsgemeinschaft grant Ja 617/17. The quality of the paper benefited from the reviews by A. Collins and M. de Wit. We thank G. Schreurs for logistic informations.

## References

- Ashwal, L., Hamilton, M.A., Morel, V.P.I., Rabeloson, R., 1998. Geology, petrology and isotope geochemistry of massif-type anorthosites from southwest Madagascar. *Contributions to Mineralogy and Petrology* 133, 389-401.
- Ashwal, L.D., Tucker, R.D., Zinner, E.K., 1999. Slow cooling of deep crustal granulites and Pb-loss in zircon. *Geochimica et Cosmochimica Acta* 63, 2839-2851.
- Bertil, D., Regnault, J.M., 1998. Seismotectonics of Madagascar. *Tectonophysics* 294, 57-74.
- Besairie, H., 1953. 1:100.000 geological map series of Madagascar, *Sévice Géologique de Madagascar*, Antananarivo.

- Besairie, H., 1961. Carte Tectonique de Madagascar 1:3000000. Service Géologique de Madagascar, Antananarivo.
- Besairie, H., 1964. Madagascar carte géologique, 1:1.000.000. Service Géologique de Madagascar, Antananarivo.
- Besairie, H., 1967. The Precambrian of Madagascar. The Precambrian vol. 3, London, 1967, 133-142.
- Besairie, H., 1972. Géologie de Madagascar I: Les terrains sédimentaires. Annales Géologique Madagascar, 35, 463pp.
- Besairie, H., 1973. La géologie globale et ses applications a l'Océan Indien et a Madagascar. Doc. Bur. Geol., 186: 30 pp. Antananarivo, Madagascar.
- Besairie, H., 1973. Carte géologique à 1:2000000 de Madagascar. Service Géologique de Madagascar, Antananarivo.
- Bonavia, F.F., Chorowicz, J., 1992. Northward exhumation of the Pan-African of northeast Africa guided by a re-entrant zone of the Tanzania craton. *Geology* 20, 1023-1026.
- Bosworth, W., Morley C.K., 1994. Structural and stratigraphic evolution of the Anza rift, Kenya. *Tectonophysics* 236, 93-115.
- Buchwaldt, R., Tucker, R.D., 2001. P-T-Time constraints on the metamorphic rocks of north Madagascar and their relevance on the assembly of Gondwanaland. *Geological Society of America Abstracts with Programs* 33, A436.
- Burnham, A.K., Sweeney, J.J., 1989. A chemical model of vitrinite maturation and reflectance. *Geochimica et Cosmochimica Acta* 53, 2649-2657.
- Chorowicz, J., Le Fournier, J., Vidal, G., 1987. A model for rift development in eastern Africa. *Geological Journal* 22, 495-513.
- Clark, D.N., Ramanampisoa, L., 2002. Hydrocarbon Potential of Madagascar. PESGB-HGS: First Annual International Symposium-Abstracts and Program, Kingston University 1, 26-27.
- Coffin, M.F., Rabinowitz, P.D., 1987. Reconstruction of Madagascar and Africa; evidence from the Davie fracture zone and western Somali Basin. *Journal of Geophysical Research, B, Solid Earth and Planets* 92, 9385-9406.
- Coffin, M.F., Rabinowitz, P.D., 1992. The Mesozoic East African and Madagascan conjugate continental margins; stratigraphy and tectonics. In: Watkins, Joel, S ; Feng, Zhiqiang ; McMillen and Kenneth (Editors), *Geology and geophysics of continental margins*. American Association of Petroleum Geologists, 207-240.
- Collins, A.S., Razakamanana, T., Windley, B.F., 2000. Neoproterozoic extensional detachment in central Madagascar; implications for the collapse of the East African Orogen. *Geological Magazine* 137, 39-51.

- Collins, A., Windley, B., Kröner, A., Fitzsimons, I., 2001. The Tectonic Architecture of Central Madagascar: Implications on the Evolution of the East African Orogeny. *Gondwana Research* 4, 152-153.
- Collins, A.S., Windley, B.F., 2002. The Tectonic Evolution of Central and Northern Madagascar and its Place in the Final Assembly of Gondwana. *Journal of Geology* 110, 325-339.
- Collins, A.S., Fitzsimons, I.C.W. Hulscher, B., Razakamanana, T., 2003. Structure of the eastern margin of the East African Orogen in central Madagascar. *Precambrian Research* 123, 111-133.
- Cox, R., Armstrong, R.A., Ashwal, L.D., de Wit, M.J., 1995. Sedimentology, tectonics and geochronology of Proterozoic shelf sediments of the Itremo Group, central Madagascar; implications for the assembly of East Gondwana. In: Anonymous (Editor), Geological Society of America, 1995 annual meeting. Abstracts with Programs - Geological Society of America. Geological Society of America (GSA), Boulder, CO, United States, pp. 161.
- Cox, R., Armstrong, R.A., Ashwal L.D., 1998. Sedimentology, geochronology and provenance of the Proterozoic Itremo Group, central Madagascar, and implications for the pre-Gondwana palaeogeography. *Journal of the Geological Society* 155, 1009-1024.
- Cox, R., Coleman, D.S., Wooden, J.L., Chokel, C.B., 2000. SHRIMP data from detrital zircons with metamorphic overgrowth reveal tectonic history of the Proterozoic Itremo Group, central Madagascar. *GSA Abstract with Programs* 37, A248.
- Coyle, D.A., Wagner, G.A., 1998. Positioning the titanite fission-track partial annealing zone. *Chemical Geology* 149, 117-125.
- de Wit, M.J., Jeffery, M., Bergh, H., Nicolaysen, L., 1988. Geological map of sectors of Gondwana reconstructed to their positions 150 Ma, scale 1:10.000.000. American Association Petroleum Geologists.
- de Wit, M.J., Ransome, I.G.D., 1992. Regional inversion tectonics along the southern margin of Gondwana. Inversion tectonics of the Cape Fold Belt, Karoo and Cretaceous basins of southern Africa. de Wit, M.J., Ransome, I.G.D, (Editors) Rotterdam (Balkema), 15-21.
- de Wit, M.J., Bowring, S.A., Ashwal, L.D., Randrianasolo, L.G., Morel, V.P.I., Rambeloson, R.A., 2001. Age and tectonic evolution of Neoproterozoic ductile shear zones in southwestern Madagascar, with implications for Gondwana studies. *Tectonics* 20, 1-45.

- Fernandez, A., Huber, S., Schreurs, G., Villa, I., Rakotondrazafy, M., 2001. Tectonic Evolution of the Itremo Region (Central Madagascar) and Implications for Gondwana Assembly. *Gondwana Research* 4, 165-168.
- Fournou, J.P., 1987. Contribution à L'étude de la discontinuité de Mohorovicic d'après les ondes sismiques observées à Madagascar. *Annales Geophysicae* 5B, 175-186.
- Fournou, J.P., Roussel, J., 1994. Imaging of the Moho depth in Madagascar through the inversion of gravity data; geodynamic implications. *Terra Nova* 6, 512-519.
- Gadd, S.A., Scrutton R.A., 1997. An integrated thermomechanical model for transform continental margin evolution. *Geo-Marine Letters* 7, 21-30.
- Galbraith, R.F., 1981. On statistical models for fission track counts. *Mathematical Geology* 13, 471-478.
- Gallagher, K., Sambridge, M., 1994. Genetic algorithms: a powerful method for large scale non-linear optimisation problems. *Comput. Geosci.* 20, 1229-1236.
- Gallagher, K., 1995. Evolving temperature histories from apatite fission-track data. *Earth and Planetary Science Letters* 136, 421-435.
- Gleadow, A.J.W., 1981. Fission-track dating methods: what are the real alternatives? *Nuclear Tracks* 5, 3-14.
- Ghosh, J.G., Zartman, R.E., de Wit, M.J., 1998. Re-evaluation of tectonic framework of southernmost India: new U-Pb geochronological and structural data, and their implication for Gondwana reconstruction. *Journal of African Earth Earth Sciences* 27, 85-86.
- Green, P.F., 1981. A new look at statistics in fission-track dating. *Nuclear Tracks* 5, 77-86.
- Grujic, D., 1995. Thermotectonic evolution of East Gondwana: granulites of southern Madagascar. *Journal of South American Earth Sciences* 8, 7-8.
- Harris, N., Bartlett, J., Santosh, M., 1996. Neodymium isotope constraints on the tectonic evolution of East Gondwana. *Journal of Southeast Asian Earth Sciences* 14, 119-125.
- Hottin, G., 1976. Presentation et essai d'interprétation du de Madagascar. *Bull. Bur. Rech. Geol. Min.* 4, 117-153.
- Hurford, A.J., Green, P.F., 1983. The zeta age calibration of fission-track dating. *Isotope Geoscience* 1, 285-317.
- Johnson, B.K., 2002. Soil characterisation and reconnaissance survey of the Ranomafana national park area, southeastern Madagascar. PhD thesis. North Carolina State University.
- Kröner, A., Braun, I., Jaeckel, P., 1996. Zircon geochronology of anatectic melts and residues from a high grade pelitic assemblage at Ihosy, southern Madagascar: evidence for Pan-African granulite metamorphism. *Geological Magazine* 133, 311-323.

- Kröner, A., Hegner, E., Collins, A.S., Windley, B.F., Brewer, T.S., Razakamanana, T., Pidgeon, R.T., 2000. Age and magmatic history of the Antananarivo Block, central Madagascar, as derived from zircon geochronology and Nd isotopic systematics. *American Journal of Science* 300, 251-288.
- Laslett, G.M., Green, P.F., Duddy, I.R., Gleadow, A.J.W., 1987. Thermal annealing of fission tracks in apatite 2. A Quantitative Analysis. *Chemical Geology (Isotope Geoscience Section)* 65, 1-13.
- Lorenzo, J.M., Vera, E.E., 1992. Thermal uplift and erosion across the continent-ocean transform boundary of the southern East African Rift Plateau. *Earth and Planetary Science Letters* 108, 79-92.
- Makris, J., Tsironidis, J., Richter, H., 1991. Heat flow density distribution in the Red Sea. *Tectonophysics* 198, 383-393.
- Malod, J.-A., Mougénot, D., Raillard, S., Maillard, A., 1991. Nouvelles contraintes sur la cinématique de Madagascar: les structures de la chaîne Davie. *Comptes rendus de l'Académie des Sciences de Paris, Séries II* 312, 1639-1646.
- Martelat, J.E., Lardeaux, J.M., Nicollet, C., Rakotondrazafy, R., 2000. Strain pattern and late Precambrian deformation history in southern Madagascar. *Precambrian Research* 102, 1-20.
- Meert, J.G., Hall, C., Nédélec, A., Razanatseheno, M.O.M., 2001. Cooling of a Late-Syn Orogenic Pluton: Evidence from Laser Raman Modelling of the Carion Granite, Madagascar. *Gondwana Research* 4, 541-550.
- Meißner, B., Deters, P., Srikantappa, C., Köhler, H., 2002. Geochronological evolution of the Moyar, Bhavani and Palghat shear zones of southern India: implications for east Gondwana correlations. *Precambrian Research* 114, 149-175.
- Montenat, C., Ramahavory, L., Croisile, M., 1996. Tectonic and sedimentary evolution of the western Madagascan margin during the Jurassic in the Morondava Basin, Madagascar. *Bull. Centres Rech. Explor.-Prod. Elf Aquitaine* 20, 323-340.
- Mottet, G., 1981. *L'Ankaratra et ses bordures (Madagascar)*, Thèse, Université de Lyon, France.
- Nédélec, A., Ralison, B., Bouchez, J.L., Grégoire, V., 2000. Structure and metamorphism of the granitic basement around Antananarivo: A key to the Pan-African history of central Madagascar and its Gondwana connections. *Tectonics* 19, 997-1020.
- Paquette, J.L., Nédélec, A., Moine, B., Rakotondrazafy, M., 1994. U-Pb single zircon Pb-evaporation and Sm-Nd isotopic study of a granulite domain in SE Madagascar. *Journal of Geology* 102, 523-538.
- Pili, E., Ricard, Y., Lardeaux, J.-M., Sheppard, S.M.F., 1997. Lithospheric shear zones and mantle-crust connections. *Tectonophysics* 280, 15-29.

- Piqué, A., 1999. The geological evolution of Madagascar: An introduction. *Journal of African Earth Sciences* 28, 919-930.
- Piqué, A., Laville, E., Bignot, G., Rabarimanana, M., Thouin, C., 1999 a. The initiation and development of the Morondava Basin [Madagascar] from the Late Carboniferous to the middle Jurassic: Sedimentary, palaeontological and structural data. *Journal of African Earth Sciences* 28, 931-948.
- Piqué, A., Laville, E., Chotin, P., Chorowicz, J., Rakotondraompiana, S., Thouin, C. 1999 b. Neogene and present extension in Madagascar: Structural and geophysical data. *Journal of African Earth Sciences* 28, 975-983.
- Raab, M.J., Brown, R.W., Gallagher, K., Carter, A., Weber, K., 2002. Late Cretaceous reactivation of major crustal shear zones in northern Namibia: constraints from apatite fission track analysis. *Tectonophysics* 349, 75-92.
- Radke, M., Vriend, S.P., Ramanampisoa, L.R., 2000. Alkyldibenzofurans in terrestrial rocks: Influence of organic facies and Maturation. *Geochimica et Cosmochimica Acta* 64, 275-286.
- Ramanampisoa, L.R., Radke, M., Schaefer, R.G., Littke, R., Rulkötter, J., Horsfield, B., 1990. Organic-geochemical characterisation of sediments from the Sakoa coalfield, Madagascar. *Organic Geochemistry* 16 (Advances in Organic Geochemistry), 235-246.
- Rasamimanana, G., Bardintzeff, J.M., Rasendrasoa, J., Bellon, H., Thouin, C., Gioan, P., Piqué, A., 1998. Les épisodes magmatiques du Sued-Ouest de Madagascar (bassin de Morondava), marqueurs des phénomènes de rifting crétaé et néogène. *Comptes Rendus de l'Académie des Sciences, Paris, Sciences de la Terre et des Planètes*, 326, 685-691.
- Rechenmann, J., 1982. Gravimétrie de Madagascar. Interprétation et relation avec la géologie. *OSTROM, Geophys.* 18, 3-128.
- Reeves, C.V., Sahu, B.K., de Wit, M.J., 2002. A re-examination of the paleo-position of Africa's eastern neighbours in Gondwana. *Journal of African Earth Sciences* 34, 101-108.
- Rolin, P., 1991. Présence de décrochements précambriens dans le boucliers méridional de Madagascar: Implications structurales et géodynamiques. *C. R. Acad. Sci., Sér. 2*, 625-629.
- Scotese, C.R., Boucot, A.J., Mckerrow, W.S., 1999. Gondwanan palaeogeography and palaeoclimatology. *Journal of African Earth Sciences* 28, 99-114.
- Ségoufin, J., Patriat, P., 1981. Reconstruction de l'océan Indien occidental pour les époques des anomalies M21, M2 et 34. Paléoposition de Madagascar. *Bull. Soc. Géologique France* 7(23), 603-607.

- Seward, D., Grujic, D., Schreurs, G., 1998. Exhumation history of the East Madagascar continental margin; inferences from apatite fission-track analysis. *Journal of African Earth Sciences* 27, 176-178.
- Seward, D., Grujic, D., Schreurs, G., 1999. Exhumation history of Southern Madagascar as revealed by Zircon and Apatite Fission-Track Thermochronology. *Gondwana Research* 2, 353-354.
- Seward, D., Grujic, D., Schreurs, G., 2000. Post Pan-African Events in Madagascar: Inferences from Apatite Fission-Track Analysis, 9th International Conference on Fission Track Dating and Thermochronology. Geological Society of Australia Abstract series, Lorne, Australia, 58, 289.
- Shackleton, R.M., 1996. Final collision zone between East and West Gondwana: where is it? *Journal of African Earth Sciences* 23, 271-287.
- Stern, R.J., 1994. Arc assembly and continental collision in the Neoproterozoic East African orogen: implications for the consolidation of Gondwanaland. *Ann. Rev. Earth Planet. Sci.* 22, 319-351.
- Stollhofen, H., 1999. Karoo Synrift-Sedimentation und ihre tektonische Kontrolle am entstehenden Kontinentalrand Namibias. *Z. dt. Geol. Ges.* 149, 519-632.
- Storey, M., Mahoney, J.J., Saunders, A.D., Duncan, R.A., Kelley, S.P., Coffin, M.F. 1995. Timing of hot spot-related volcanism and the breakup of Madagascar and India. *Science* 267, 852-855.
- Todd, B.J., Keen, C.E., 1989. Temperature effects and their geological consequences at transform margins. *Canadian Journal of Earth Sciences* 26, 2591-2603.
- Torsvik, T.H., Tucker, R.D., Ashwal, L.D., Eide, E.A., Rakotosolofo, N.A., de Wit, M.J., 1998. Late Cretaceous magmatism in Madagascar: palaeomagnetic evidence for a stationary Marion hotspot. *Earth and Planetary Science Letters* 164, 221-232.
- Tucker, R.D., Ashwal, L.D., Handke, M.J., Hamilton, M.A., Le Grange, M., Rabeloson, R.A., 1999. U-Pb geochronology and isotope geochemistry of the Archean and Proterozoic rocks of north-central Madagascar. *Journal of Geology* 107, 135-153.
- Veevers, J.J., Powell, C.M., 1994. Permian-Triassic Pangean basins and foldbelts along the Panthalassan margin of Gondwanaland. *Geological Society of America; Memoir*, 184, 368 pp.
- Visser, J.N.J., Praekelt, H.E., 1996. Subduction, mega-shear systems and late Palaeozoic basin development in the African segment of Gondwana. *Geologische Rundschau* 85, 632-646.
- Wagner, G.A., van den Haute, P., 1992. *Fission-Track Dating*. Ferdinand Enke Verlag, Stuttgart, 285 pp.

- Wescott, W., Diggins, J.N., 1997. Depositional history and stratigraphical evolution of the Sakoa Group (Lower Karoo Supergroup) in the southern Morondava Basin, Madagascar. *Journal of African Earth Sciences* 24, 581-601.
- Wescott, W., Diggins, J.N., 1998. Depositional history and stratigraphical evolution of the Sakamena Group (Middle Karoo Supergroup) in the southern Morondava Basin, Madagascar. *Journal of African Earth Sciences* 27, 467-479.
- Windley, B.F., Razafiniparany, A., Razakamanana, T., Ackermann, D., 1994. Tectonic framework of the Precambrian of Madagascar and its Gondwana connections; a review and reappraisal. *Geologische Rundschau* 83, 642-659.
- Yamada, R., Tagami, S., Nishimura, S., Ito, H. 1995. Annealing kinetics of fission track in zircon: An experimental study. *Chemical Geology* 122, 249-258.
- Yardimcilar, C., Reeves, C.V. 1998. Evidence from aeromagnetic anomalies for the pre-drift fit of Madagascar against East Africa. *Journal of African Earth Sciences* 27, 215-216.



## Chapter 5

### **Thermal history of the southern Morondava basin (south-west Madagascar) and a Late Permian - Jurassic provenance record: constraints from detrital fission track and palaeo-current data**

Emmel, B.; Geiger, M. and Jacobs, J.

*Basin Research, submitted*

Department of Geowissenschaften, University of Bremen, P.O. Box 330440, 28334  
Bremen, Germany

## Abstract

Apatite fission track (FT) analyses were carried out on sedimentary rocks from the Morondava basin (south-west Madagascar) belonging to the Sakoa Group, the Sakamena Group, and Jurassic strata. Detrital apatite FT ages range from  $462\pm 28$  Ma to  $192\pm 9$  Ma and provide detailed information about the thermal history and potential source rock regions of the southern Morondava basin.

The Sakoa coal area located in south-west Madagascar was subjected to fast cooling prior to the Late Carboniferous initial rifting between East Africa and Madagascar. The area reached the surface just before the Late Carboniferous to Early Permian deposition of the Sakao Group. During the Late Permian to Late Triassic Karoo rift phase the region was subsequently covered by ~2-4 km of sedimentary rocks. From the Late Triassic to the Early Jurassic the area was exhumed, and the denuded rocks represent one main source for parts of the studied Jurassic detrital samples.

Detrital apatite FT and palaeo-current data from the Late Permian to Early Triassic Sakamena Group and from Jurassic strata were used to constrain the provenance. Single grain age FT distribution of samples belonging to the Sakamena Group and modelled time-temperature (T-t) paths suggest a provenance in the central part of the island at this time. Reworked sedimentary rocks, which cooled during Late Proterozoic/Early Cambrian times can be considered as a subordinate additional source.

The Jurassic strata contain two sources with different apatite FT ages. The basin-fill, however, can originate from the same region. Reworked sedimentary rocks with high number of Cambrian single grain ages are the main source for successions from the Upper Bajocian and Callovian with detrital apatite ages of  $>380$  Ma. Samples with FT ages of  $<300$  Ma are derived from sources with mainly Early Permian single grain ages. The single grain age distributions of all studied Jurassic samples show an influence of both sources. Using basement FT and palaeo-current data the provenance was most likely the south-western basement margin of Madagascar, which was affected by denudation during the Middle Jurassic transform margin formation.

**Keywords:** fission track, thermochronology, Madagascar, Gondwana, provenance analysis

## 1. Introduction

Heavy minerals are widespread accessories in siliciclastic sedimentary rocks. Their single grain petrography, geochemical signatures and morphology are common provenance indicators. However, physical abrasion and chemical weathering of heavy minerals limit the efficiency of these methods. Since the 1980s, dating of detrital minerals using a variety of modern geochronological techniques has become a useful tool to discriminate source rock regions. In particular, dating of individual grains has been proven to be a sensitive provenance indicator. Especially if source regions have similar rock types but different apparent ages, the age distribution of detrital heavy minerals can be used to constrain multiple sources. Comparing detrital single grain ages with geochronological data from potential sources can illuminate locations of proto-sources.

Titanite, zircon and apatite FT analyses are sensitive geo- and thermochronological techniques to reconstruct low-temperature (310-60 °C) thermal histories of rifted continental margins (e.g. Brown *et al.*, 1990; Forster & Gleadow, 1992a; Gallagher *et al.*, 1994) and sedimentary basins (e.g. Gleadow *et al.*, 1983; Green *et al.*, 1989). Further, combined basement and basin FT patterns can be a useful tools for the discrimination of the sedimentary provenance (e.g. Carter, 1999). Because in most cases only a limited geochronological data set is available, it is essential to consider other possible source indicators. Multiple proxies can simplify and specify the determination of potential source rock regions. In the provenance record of the Morondava basin we have therefore taken into account palaeo-current data and complement them with our own field observations and basement geochronological data.

In addition to the provenance study, apatite FT ages, which were reset, e.g. due to a thick sedimentary cover, can be used to model the thermal history of sedimentary basins. In this study, we also combine published vitrinite reflectance data (Ramanampisoa *et al.*, 1990; Radke *et al.* 2000) with titanite (Emmel *et al.*, in press) and apatite FT data from samples collected from the Sakoa Group to constrain the thermal history of the Sakoa coal area (representing the thermal evolution of the south-western Morondava basin).

## 2. Geology and tectonic evolution of south-west Madagascar

Following Late Neoproterozoic/Early Cambrian ductile deformation during the amalgamation of Gondwana (e.g. Kröner *et al.*, 2000; Collins *et al.*, 2001; Meert *et al.*, 2002), Madagascar underwent a long period of extensional tectonism, with associated rifting, major faulting, and basin formation, exhumation, denudation and deposition along the evolving continental margins. Late Neoproterozoic to Early Cambrian high strain zones were repeatedly

reactivated since Carboniferous times, and guided the opening of the Morondava and Majunga basins (e.g. Pili *et al.*, 1997; Piqué *et al.*, 1999; Emmel *et al.*, in press). The Morondava basin is characterised by a set of half grabens, conjugate to the East African basins, and local horst and graben structures which can be traced into the metamorphic basement. The oldest (Late Carboniferous to Early Permian) sedimentary rocks are exposed in the southern and central part of the basin (Figs. 5.1a, b; 5.2a). The thickness of the sediments increases from north towards the south. This indicates a progression of rifting from south to north (de Wit, 2003).

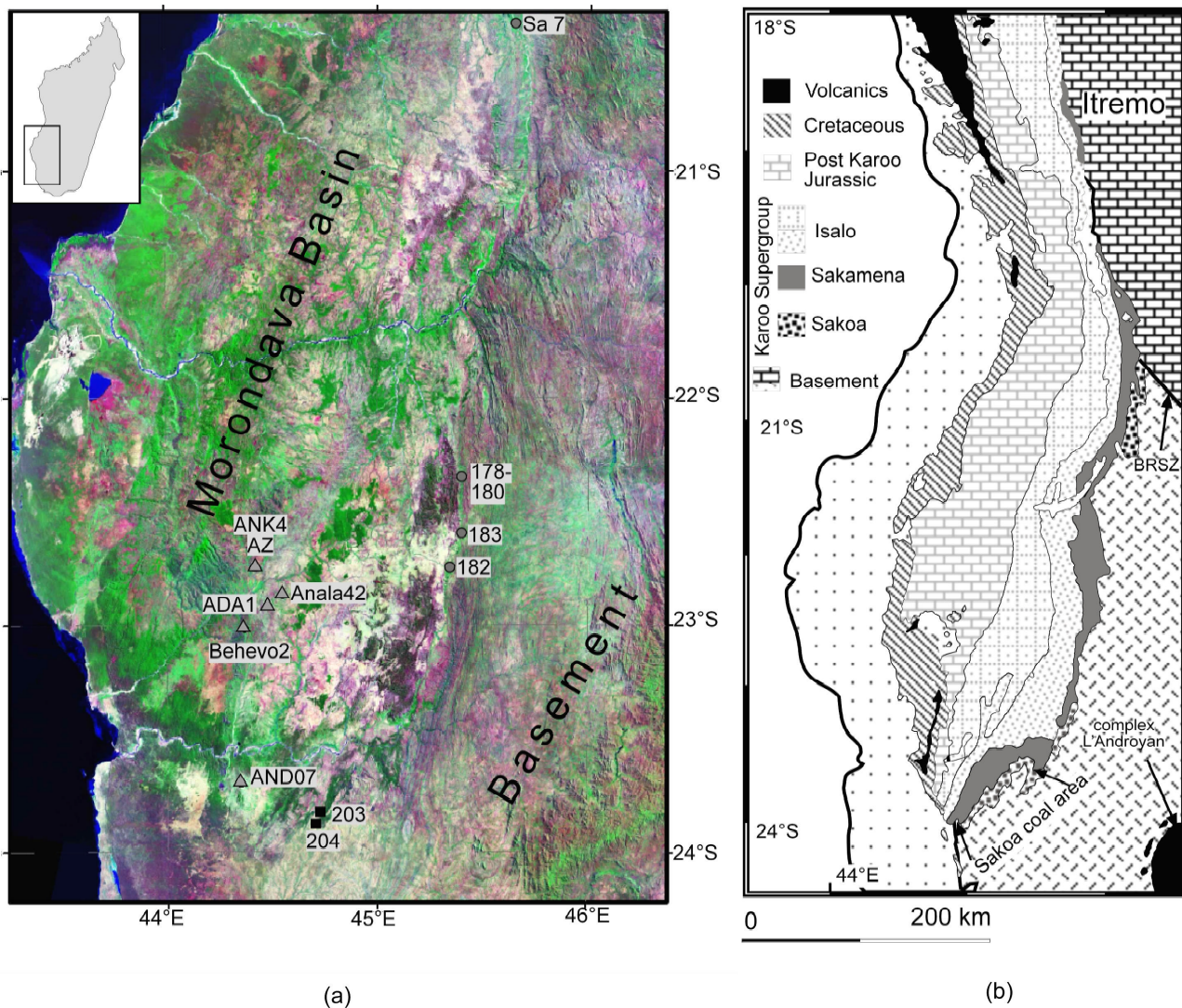


**Fig. 5.1:** a) Landsat 7 TM satellite image of the Morondava basin and the adjacent eastern basement units with sample locations. Note the NS trending faults parallel to the basement foliation along the eastern margin of the Morondava basin b) Simplified geological map of the Morondava basin (modified after Besairie, 1972).

## 2.1 Karoo Supergroup

During the Permo-Carboniferous, Gondwana was covered with an extensive ice sheet (e.g. Scotese *et al.*, 1998). Accompanied by the retreat of the ice caps, sedimentation commenced. The oldest sedimentary rocks recorded in southern Madagascar belong to the Sakoa Group, the basal deposits of the Karoo Supergroup (Figs. 5.1a, b; 5.2a). The Sakoa succession is restricted to several local pull-apart basins, which evolved along N-S trending strike-slip faults. The development of these pull-apart basins is thought to result from compressive tectonics (Schandelmeier *et al.*, in press). Glacial and glaciomarine sediments occur at the base of the Sakoa Group. A coal bearing sequence (Fig. 5.2a) overlies diamictites, sandstones, and conglomerates. A marine transgression near the end of the Early Permian led to the deposition of the Vohitolia limestone which terminates the Sakoa depositional cycle (Besairie, 1972). The Sakoa Group reaches a thickness of ~2000 m (Wescott & Diggins, 1997).

Locally, the Late Permian to Early Triassic Sakamena Group unconformably overlies the Sakoa Group. In most parts of the Morondava basin the Sakamena Group rests directly on metamorphic basement (Fig. 5.1a, b). The ~2000-4000 m thick succession comprises fluvial continental conglomerates, sandstones, and red bed units (Boast & Nairn, 1982). In contrast to the Sakoa Group, the Sakamena Group records the maturation of rifting and basin formation between Madagascar and East-Africa, which led to a peneplanation of the palaeo-landscape (Nichols & Daly, 1989).

The Middle and Upper Triassic Isalo Group terminates the Karoo Supergroup megasequence (Fig. 5.2a). Usually, this unit lies unconformably on the Sakamena Group, but locally rests directly upon basement (Fig. 5.1a, b). It reaches a maximum thickness of ~6000 m, and consists of medium to coarse sandstones with evidence of a minor marine inversions at the top (Besairie, 1972). The sandstones are thought to have been deposited mainly in braided river channels, while in some areas there is evidence for the development of alluvial fans. It has been suggested that during the deposition of the Isalo Group the Karoo rifting and extension reached its maximum stage (Wescott & Diggins, 1997).

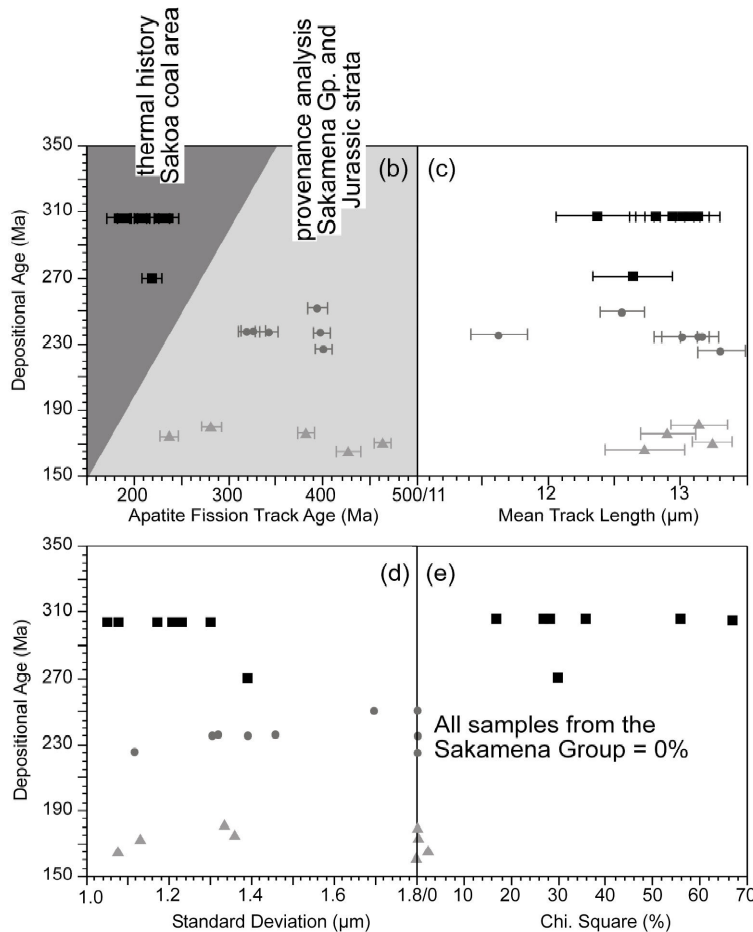
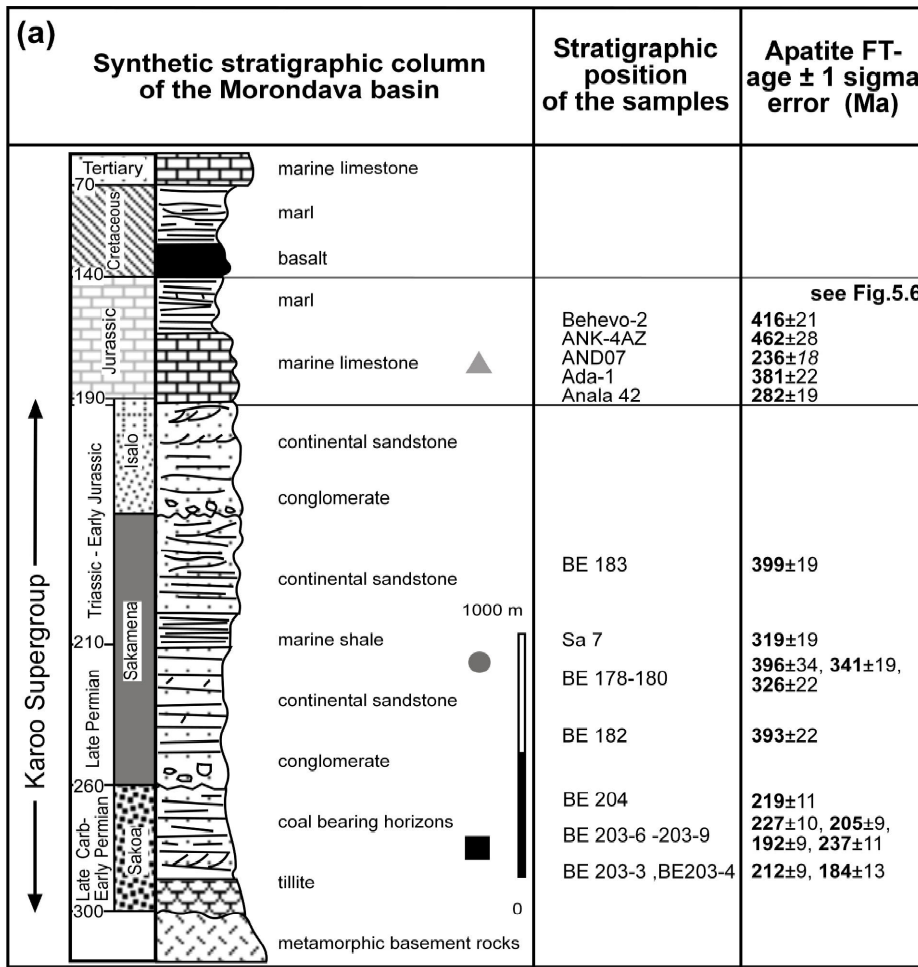


**Fig. 5.2:**  
 a) Synthetic stratigraphic column of the Morondava basin (modified after Piqué, 1999) with sample number and related apatite FT ages.  
 b-e) Relationships between the different apatite FT parameters and the approximate stratigraphic ages.

## 2.2 Jurassic

From the Bajocian (Middle Jurassic) a passive margin formed along the north-western coast of Madagascar, whereas a transform margin evolved along the south-western coast. The Davie Ridge south-west of Madagascar is a fossil transform fault that governed the translation between East Africa and Madagascar (Coffin & Rabinowitz, 1987). During the translation the sedimentary environment in the adjacent Morondava basin changed from mostly continental to predominantly marine (Coffin & Rabinowitz, 1992).

With the end of the predominantly terrestrial sedimentation of the Late Triassic Isalo Group, deposition of the first marine strata occurred in the Morondava basin. This is documented in the subsurface, e.g. well NAM.1 (Montenat *et al.*, 1996; Ramahavory *et al.*, 1996) and MG.1 (Uhmann, 1996), and a few outcrops in the central Morondava and Majunga basins (Geiger *et al.*, in press). The unit consists of marls, limestones and sandstones, and is considered to be of Toarcian age (Geiger *et al.*, in press). Widespread marine deposition prevailed from the Bajocian after the sea transgressed landwards. A carbonate environment became established throughout the basin during the Bajocian to Lower Bathonian, while in the north of the basin a carbonate platform (Bemaraha plateau, name-giving for the Bemaraha Formation) is exposed. In the south a mudflat environment representing a coastal facies variation (Sakaraha Formation) crops out. During the Middle Bathonian a major siliciclastic pulse terminated the carbonate platform by a widespread progradation of a fluvial/deltaic environment (Ankazoabo and Sakanavaka Formation), in contrast to the central basin, where terrigenous sedimentation continued through the Upper Callovian (Besairie, 1972). In the southern part of the basin marine strata with mainly marls and limestones reappeared already from the Lower Callovian. The base of the Oxfordian strata continues the Callovian like marls and shales with local laterally constrained sandstone bodies through the Upper Jurassic. These coarser siliciclastic units show the proximity of land. In the south a dominant sandstone unit appears in the Lower Oxfordian, succeeded by thin marl units ranging up to the Kimmeridgian. A Cretaceous (Aptian) transgression cuts off the Jurassic sediment record.

In the southern central part of the basin a thick sandstone unit which ranges from the Middle Oxfordian to the Tithonian occurs, whereas to the north marls and shales are more dominant in outcrops during the entire Upper Jurassic (Besairie, 1972). Rare subsurface data from the basin (Montenat *et al.*, 1996; Uhmann, 1996; du Toit *et al.*, 1997) indicates a locally asynchronous deposition of coarser siliciclastic units from the Callovian to the Tithonian, probably caused by localized tectonism.

## 2.3 Post Jurassic

The Early Cretaceous deposits of the southern Morondava basin are predominantly marine, while from the Albian (113-97 Ma) terrigenous sediments were deposited (Luger *et al.*, 1994). From Turonian time widespread basaltic volcanism affected especially the northern Morondava basin (Mailaka) but locally also the south. These basalts are thought to be related to the Marion hot spot, which was involved in the break-up of Madagascar and India (Storey *et al.*, 1995). Eocene marine deposits occur along the south-western margin of the island around the north-north-west to south-south-east trending Tulear fault.

## 3. Material and Methods

Apatite FT dating is a sensitive low temperature (110-60 °C) thermochronological technique that can provide important data to characterise and date cycles of tectonism, denudation and burial (e.g. Carter, 1999). Detrital apatite FT data can provide two independent variables about the evolution of a sedimentary basin.

- Apatite FT data is suitable for provenance analysis if the single grain ages are unaffected by thermal overprinting.
- The technique is useful to constrain the low temperature thermal history of a sedimentary basin if apatites were partially or totally annealed after deposition due to sediment overload. Supplemented by geochronological techniques with higher closure temperatures - e.g. titanite, zircon FT analysis and  $^{39}\text{Ar}/^{40}\text{Ar}$  dating - in most cases it is possible to reconstruct a complete thermal history for a specific part of a basin.

Apatite grains were separated by conventional techniques (crushing, Wilfley table, magnetic separation and heavy liquids). Single grain apatite FT analyses were carried out using the external detector method (Gleadow, 1981) for a good estimate of age components within a mixture of single grain ages. This technique permits the recognition of different age populations in one sample.

Apatites were etched for 50 sec. in 5 %  $\text{HNO}_3$  (23 °C) to reveal spontaneous tracks (e.g. Wagner & van den Haute, 1992). Samples were irradiated in channel 8 of the Thetis reactor at the Institute for Nuclear Sciences at Gent (Belgium), using a total thermal neutron flux of  $1 \times 10^{16} \text{ ncm}^{-2}$ . Mica detectors were etched for 15 min in 40 % HF (23 °C) to reveal induced tracks. Ages were calculated using the Zeta calibration method (Hurford & Green, 1983). All ages are reported as central ages with 1 sigma errors. Samples with  $\chi^2$ -probabilities <5 %

are characterised by a considerable scatter in the single grain ages and possibly represent the cooling histories of diverse source rocks.

In the case where detrital FT data shows the characteristics useful for provenance analysis (FT age > depositional age, low  $\chi^2$ -probabilities, broad single grain age distribution) the program "POPSHARE" (Dunkl, 2002) was used to examine principal age components. This program uses the individual grain ages and their 1  $\sigma$ -errors for which the SIMPLEX algorithm (references in Dunkl, 2002) calculates a statistical best fit for pre-selected age components (minimum two components).

The level of annealing of tracks in apatite can be recorded by measuring horizontal confined track length distribution. Apatite FT data, including single grain ages, track lengths and standard deviations, were used to model specific hypothetical time-temperature (T-t) paths with an inverse modelling procedure, applying the program "MONTE TRAX" (Gallagher, 1995). No chemical composition data for the analysed apatites were available. The Laslett annealing model for Durango apatite was adopted (Laslett *et al.*, 1987). In most cases three or four T-t boxes (pre-sedimentation, stratigraphic age and post depositional thermal evolution) were pre-set to allow modelling of an unconstrained cooling path and the possibility for heating after deposition. The modelling was carried out using a "genetic algorithm" (Gallagher & Sambridge, 1994b), in which the best fitting models of the recent modelled generation are used as a basis for the next modelling iteration. The "new generation" is reviewed to identify better models. Twenty generations were modelled with 100 individual T-t histories being tested per generation.

In figure 5.3 and in this chapter section 4.4 we present distribution maps for different basement FT patterns from central and southern Madagascar. We constructed the maps using the "Natural Neighbour" gridding method to minimise errors in interpretation. Data points closer to the grid node were given more weight. Thus, directions of higher or lower continuity between specific data points can be separated. The "Natural Neighbour" gridding method is well suited for natural phenomena created by physical processes. However, the distribution maps requires critical evaluation because compositional differences between the single titanite/apatite grains, partial annealing of some samples and low frequency of samples could have a misleading effect on the maps.

## 4. Geochronological data from potential Gondwana sources

To constrain possible Morondava basin detrital source rock regions it is essential to review geochronological data from regions, which were close prior to the break-up of Gondwana. An excellent summary of high temperature geochronological data from Gondwana is given by Meert *et al.* (2003). The database documents in detail the Pan-African high temperature history of Gondwana. Also a number of publications containing apatite FT ages/data are available. Unfortunately, only sparse information about the temperature range between 300-110 °C is present from most parts of Gondwana.

In the following, geochronological data are reported from Gondwana fragments, which were once adjacent to Madagascar.

### 4.1 East Africa

The high-temperature history of East Africa is characterised by the thermal effects associated with the Pan-African orogeny. Therefore the main age components of the high temperature geochronological techniques are between 600-500 Ma. Only FT data provide detailed information about the post Pan-African cooling history.

#### 4.1.1 Kenya

Key *et al.* (1989) report Rb-Sr and K-Ar ages from north central Kenya. The data argue for four thermal events between ~620 Ma and ~530 Ma belonging to the Pan-African orogeny. Titanite and zircon FT ages range between ~540 Ma and ~480 Ma (Gleadow, 1980) and indicate cooling of the basement to below ~300-200 °C shortly after the Pan-African period. Apatite FT data reported by Wagner *et al.* (1992) vary between  $319 \pm 15$  Ma and  $27 \pm 2$  Ma, whereby the oldest ages (~320-290 Ma) occur in south-west Kenya. Another apatite FT study (Forster & Gleadow, 1992b) in central Kenya obtained ages ranging between  $207 \pm 17$  Ma and  $55 \pm 4$  Ma. The data argue for episodes of rapid cooling and denudation, in Early Cretaceous (130-110 Ma), Late Cretaceous-Palaeocene (70-60 Ma), and possibly Miocene (~10 Ma) times.

#### 4.1.2 Tanzania, Malawi and Mozambique

Möller *et al.* (2000) report U-Pb monazite and zircon ages (closure temperature: 800-600 °C) from Tanzania ranging from 655 Ma to 610 Ma. The youngest high-temperature

geochronological data known from Tanzania are  $^{40}\text{Ar}$ - $^{39}\text{Ar}$  on muscovite (closure temperature: 400-350 °C) ranging between 495±2 Ma and 487±2 Ma (Maboko *et al.*, 1989). Apatite FT analysis from the Malawi and Rukwa rifts in Malawi and south-west Tanzania yield ages varying from 296±10 Ma to 30±15 Ma (van der Beek *et al.*, 1998). Reconstructed thermal histories give evidence for three phases of accelerated cooling at 250-200 Ma, ~150 Ma and <50-40 Ma (van der Beek *et al.*, 1998). Nobel *et al.* (1997) reported apatite FT ages from basement rocks of east Tanzania ranging between 221±11 Ma to 48±3 Ma. This data set argues for three periods of accelerated cooling during Early Cretaceous (140-120 Ma), Late Cretaceous-Early Palaeogene (80-60 Ma) and Late Eocene- Early Oligocene (40-30 Ma) times. A denudation of 9 km since the Late Carboniferous was calculated.

Conventional  $^{207}\text{Pb}/^{206}\text{Pb}$  and SHRIMP zircon ages of ~615 Ma from the Lurio belt in Mozambique date the Pan-African peak of high-grade metamorphism (e.g. Kröner *et al.*, 1997). At present, no FT data from Mozambique are available.

#### 4.2 South-west India and Sri Lanka

$^{40}\text{Ar}$ - $^{39}\text{Ar}$  ages ranging between ~550 and ~500 Ma date the latest Pan-African activities in western India (Rathore *et al.*, 1999). The next younger ages are apatite FT ages reported from the Dharwa craton region of south-west India (Gunnell, 2000) range between ~300 Ma and ~50 Ma. The ages increase in a general way from the coastline inland. Kalaswad *et al.* (1993) report twelve apatite FT ages from south-west India ranging between 226±19 Ma and 165±21 Ma. Modelled data suggest an Early Triassic and a Paleocene phase of rapid cooling.

The youngest high temperature geochronological data from Sri Lanka are Rb-Sr whole rock/mineral ages from post tectonic granites ranging between 533±6 Ma and 464±28 Ma (Fernando *et al.*, 1999) suggesting a relatively young high-temperature cooling history compared to other parts of Gondwana. At present, no FT data from Sri Lanka are published.

#### 4.3 East Antarctica

We specifically report geochronological data from central Dronning Maud Land because from this part of East Antarctica a large geochronological data-set is available and it was relatively close to Madagascar before Gondwana break-up. U-Pb SHRIMP zircon data from Jacobs *et al.* (1998) document the latest Pan-African metamorphic activities at 530-515 Ma in Central Dronning Maud Land. K-Ar and Rb-Sr biotite ages on charnockites indicate the cooling of the basement to below 300 °C at ~450 Ma (Heinjes-Kunst & Markl, 1998).

Meier (1999) reported titanite and zircon FT ages from Dronning Maud Land ranging between  $531\pm 51$  Ma to  $293\pm 28$  Ma and  $364\pm 47$  to  $237\pm 31$  Ma, respectively. The titanite FT ages are interpreted to represent post orogenic differential cooling. The zircon FT ages represent a Late Carboniferous to Early Triassic phase of cooling associated with denudation of  $\approx 6$  km crustal section. It is suggested that Central Dronning Maud Land served as a source during Permo-Triassic times. The apatite FT ages vary between  $315\pm 18$  and  $83\pm 3$  Ma. During the Early Jurassic a major cooling step affected the basement, probably related to mantle plume activities (Meier, 1999).

#### 4.4 Madagascar

Seward *et al.* (1998, 1999, 2000) reported basement zircon and apatite FT ages from central and south Madagascar. Two zircon FT ages from south-western Madagascar are  $384\pm 71$  Ma and  $238\pm 56$  Ma and apatite FT ages from central and southern Madagascar range between  $397\pm 36$  and  $68\pm 8$  Ma. Emmel *et al.* (in press, submitted) reported basement titanite and apatite FT ages from central and southern Madagascar ranging between  $483\pm 33$  Ma and  $266\pm 13$  Ma and  $403\pm 33$  Ma to  $79\pm 5$  Ma, respectively.

Using titanite FT data of 26 samples (Emmel *et al.*, in press, submitted) an age distribution map for central and southern Madagascar was compiled (Fig. 5.3a). The map shows a restricted area of old titanite FT ages ( $>400$  Ma) east of Fianarantsoa. This area differs significantly from the other regions with titanite FT ages  $<400$  Ma.

With a set of 126 samples (Seward *et al.*, 1998, Emmel *et al.*, in press, submitted; Emmel, unpublished data) an apatite FT distribution map for the basement of central and southern Madagascar was constructed (Fig. 5.3b). In general, the apatite FT ages decrease from the present basin/basement contact towards the eastern coast. The oldest samples come from the centre of the island. "Younger" domains are located especially along the eastern coast ( $\sim 90$ - $80$  Ma), along the south-western margin ( $\sim 200$  Ma) and subordinate in the north-west ( $\sim 100$ - $80$  Ma). The apatite FT age distribution seems to be influenced by Pan-African ductile structures like e.g. the Bongolava-Ranotsara shear zone (BRSZ) or the Angavo shear zone. The modelled cooling histories of 38 samples were used to construct a distribution map, which shows the timing of rapid cooling phases for the basement of central and southern Madagascar (Fig. 5.3c). Additionally, to get a better resolution, titanite FT results and the depositional age for location BE 203 (Emmel *et al.*, in press), as well as apatite FT ages of six samples along the eastern coast (Seward *et al.*, 1998; Emmel *et al.*, in press, submitted) were used. The map suggests that areas of rapid cooling retreated towards the east during Late Palaeozoic to Mesozoic times. This main trend is disturbed by a north-west to south-east trending pattern, which corresponds to the orientation of an early break-up graben along

the BRSZ (Emmel *et al.*, in press). The apatite FT data from the easternmost parts are significantly influenced by Late Cretaceous magmatism associated with the Madagascar-India break-up. The Cretaceous apatite FT ages were affected by rapid denudation during Cretaceous times and/or magmatic activities. Thus, the pre-Cretaceous thermal history is not recorded in the apatites.

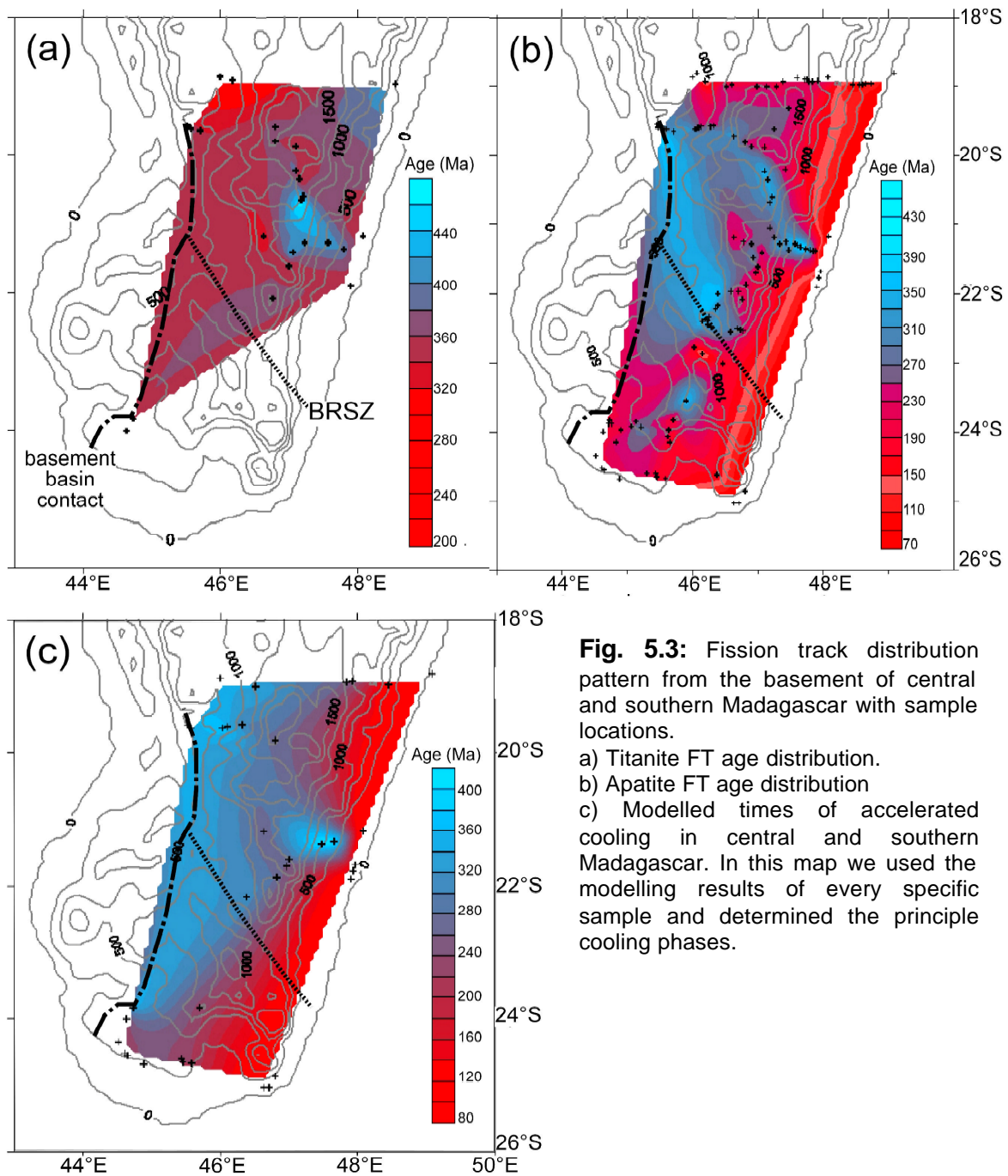


**Fig. 5.3:** Fission track distribution pattern from the basement of central and southern Madagascar with sample locations.

a) Titanite FT age distribution.  
 b) Apatite FT age distribution  
 c) Modelled times of accelerated cooling in central and southern Madagascar. In this map we used the modelling results of every specific sample and determined the principle cooling phases.

## 5. Tracking the provenance

FT data of sedimentary rocks store information about the thermal history of their eroded corresponding provenance rock. Using different geo- and thermochronological techniques it is possible to reconstruct representative cooling histories for eroded basement material, which was deposited in the basin. For instance, apatite FT data permits to model T-t paths representing the cooling history between 110-60 °C. Using titanite and apatite FT data the cooling from 310-60 °C can additionally be constrained. It might be possible to record two temporally separate cooling events. Thus, using combined titanite and apatite FT ages one can hypothetically obtain a chronological calibration of a sedimentary stratum. Consequently, apatite FT data of a sedimentary rock reflects the age spectrum of an eroded unknown unit, which perhaps was previously overlying in situ units with appropriate apatite or more likely titanite FT patterns. This shows that it is useful to resolve the cooling history of potential source rock regions with combined geochronological techniques to constrain provenance in a satisfactory manner. Although geochronological dating of single grain ages is a very sensitive provenance tool, the data from Gondwana (see above) shows that it is very difficult to constrain a provenance only with age information. Without additional sedimentological information a potential provenance can hardly be constrained within an extensive area like Gondwana. Therefore, provenance analyses of the Morondava basin is additionally based on sedimentological observations, such as mineralogy and maturity of the detritus (Uhmann, 1996), palaeo-currents (Nichols & Daly, 1989; in here), reconstructed palaeo-slopes (see Nichols & Daly, 1989; Piqué *et al.*, 1999) and reconstructed palaeo-environments (Wescott & Diggens, 1997, 1998). The sedimentological data propose that the source of the sedimentary fill laid east of the present-day basement/basin contact. Thus, we compare basement FT data with detrital FT data and try to correlate similar patterns.

As a first approach, only basement rocks with ages younger than the detrital apatite FT ages in the basin sediments are considered as a possible source, because the formerly overlying and now eroded basement units must have supplied sediment deposited in the basin. Afterwards the single grain age distribution of the sedimentary rocks and the potential sources were compared (e.g. Fig. 5.4). Ideal additional information are provided by basement titanite single grain age distributions (e.g. see Fig. 5.4). Thereafter, we used modelled cooling paths of basement samples and compared these with depositional ages of the sedimentary units. We related basement areas with high cooling rates with the depositional age of one specific group/formation. This is based on the assumption that rapid cooling is related to erosion and subsequent sedimentation in the adjacent basin. But even areas with older cooling phases can supply material after a phase of retarded erosion, e.g. due to new climate conditions.

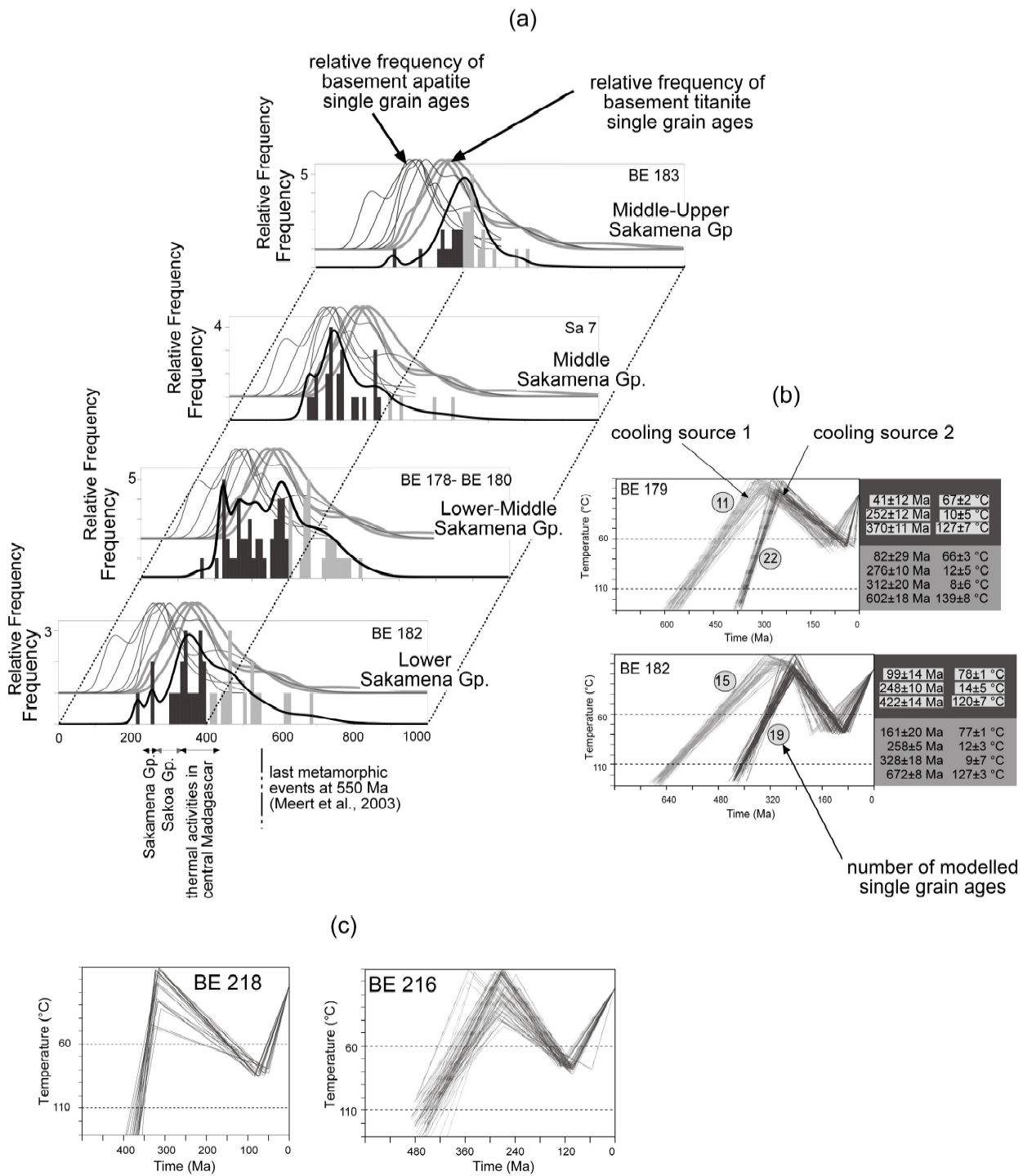


**Fig. 5.4:** a) Single grain age distribution of detrital apatite FT ages from the Sakamena Group and correlation with the relative frequency of basement FT single grain age distribution. b) Modelled Tt path of two representative samples from the Sakamena Group show the possible cooling paths of two sources. Modelling was carried out using single grain ages >400 Ma (a, grey bars) for the possible older source and for the possible younger source ages <400 Ma (a, black bars). For the specific sample we used the same length data in both models. c) Two representative cooling paths of samples within the AGSZ (Emmel et al., submitted) show a similar cooling pattern as source 2.

Sample Nr. Rock Type	E- Long. S- Lat.	Elev. [m] Strat.	Gr.	(N <sub>s</sub> ) r <sub>s</sub> [x10 <sup>5</sup> cm <sup>-2</sup> ]	(N <sub>i</sub> ) r <sub>i</sub> [x10 <sup>5</sup> cm <sup>-2</sup> ]	(N <sub>d</sub> ) r <sub>d</sub> [x10 <sup>5</sup> cm <sup>-2</sup> ]	P(χ <sup>2</sup> ) [%]	Apatite Fission Track Age ± 1σ [Ma]	U-cont. [ppm]	MTL ± 1 s? [μm] (Nr. of measured lengths)	SD [μm]
BE 203-3 tillite	44°45' 23°50'	365 Lower Sakoa	28	1890 16.791	2282 20.274	7617 15.621	28	212 ± 9	18	12.82 ± 0.21 (35)	1.21
BE 203-4 tillite	44°45' 23°50'	365 Lower Sakoa	19	445 10.206	619 14.197	7617 15.61	36	184 ± 13	14	12.36 ± 0.3 (12)	1.05
BE 203-6 mud and sandstone	44°45' 23°50'	315 Lower Sakoa	26	1812 18.335	2040 20.643	7617 15.57	17	227 ± 10	20	12.94 ± 0.21 (39)	1.3
BE 203-7 sandstone	44°45' 23°45'	315 Lower Sakoa	24	1673 24.027	2080 29.873	7617 15.556	56	205 ± 9	28	12.95 ± 0.15 (51)	1.08
BE 203-8 silt and sandstone	44°45' 23°50'	330 Lower Sakoa	27	1600 15.298	2121 20.28	7617 15.54	67	192 ± 9	22	13.13 ± 0.17 (51)	1.23
BE 203-9 sandstone	44°45' 23°50'	320 Lower Sakoa	26	1550 20.691	1656 22.106	7617 15.52	27	237 ± 11	20	13.03 ± 0.18 (42)	1.17
BE 204 sandstone	44°44' 23°53'	325 Upper Sakoa	20	1300 21.15	1548 25.185	7617 15.943	30	219 ± 11	24	12.64 ± 0.30 (22)	1.39
sa 7 sandstone	45°39' 20°21'	200 Middle Sakamena	26	1901 24.835	1522 19.884	7318 15.324	0	319 ± 19	18	11.6 ± 0.17 (65)	1.39
BE 178 sandstone	45°24' 22°21'	630 Low. - Mid. Sakamena	20	2311 24.479	1937 20.517	7400 15.497	0	326 ± 22	18	13.16 ± 0.18 (67)	1.46
BE 179 sandstone	45°24' 22°21'	630 Low. - Mid. Sakamena	33	3997 27.291	3132 21.385	7617 16.12	0	341 ± 19	19	13.01 ± 0.16 (70)	1.32
BE 180 sandstone	45°24' 22°21'	630 Low. - Mid. Sakamena	16	1988 30.219	1452 22.071	7617 16.104	0	396 ± 34	20	13.14 ± 0.25 (27)	1.31
BE 183 sandstone	45°23' 22°36'	910 Mid. - Up. Sakamena	30	3555 23.472	2279 15.047	7617 16.071	0	399 ± 19	14	13.30 ± 0.12 (93)	1.12
BE 182 mud and sandstone	45°21' 22°46'	685 Lower Sakamena	34	3369 27.731	2362 19.442	7617 16.086	0	393 ± 22	18	12.55 ± 0.17 (96)	1.7
Anala 42 fine sand	44°33' 22°52'	480 Lower ? Bajocian	33	4256 22.381	3822 20.099	7617 15.476	0	282 ± 19	21	13.14 ± 0.14 (92)	1.34
ADA-1 marl	44°29' 22°55'	410 Upper ? Bajocian	35	5035 28.774	3338 19.076	7617 15.508	0	381 ± 22	19	12.89 ± 0.18 (56)	1.36
AND 07 marl	44°21' 23°42'	420 Bathonian	23	1958 18.534	2049 19.395	7400 15.468	0	236 ± 18	19	13.24 ± 0.16 (52)	1.13
ANK 4 AZ marl	44°25' 22°45'	550 Lower Calloviaian	23	1011 26.786	544 14.413	7617 15.46	6	462 ± 28	14	- -	-
Behevo 2 marl	44°25' 23°01'	450 Calloviaian	26	1646 22.7	987 13.612	7617 15.492	7	416 ± 21	15	12.73 ± 0.17 (40)	1.08

**Tab. 5.1:** Apatite FT results from sedimentary rocks of the Morondava basin. Ages were calculated using dosimeter glasses: IRMM-540 (apatite) with  $\xi_{\text{IRMM-540}}=333\pm 9$ . Apatite FT ages are reported as pooled ages if  $\chi^2 > 5\%$ , otherwise the central age is given. Elev.: Elevation; Gr.: Grains,  $\rho_s$ ,  $\rho_i$ ,  $\rho_d$ ,  $N_s$ ,  $N_i$ ,  $N_d$ : density and number of counted spontaneous, induced and dosimeter glass tracks;  $P(\chi^2)$ : Chi-square probability; U-cont.: Uranium content; MTL: Mean track length; SD: standard deviation.

## 6. Results and interpretation

Apatite FT ages from 18 samples range between  $462\pm 28$  Ma and  $184\pm 13$  Ma. The apatite MTL vary between  $13.30\pm 0.12$   $\mu\text{m}$  and  $12.36\pm 0.3$   $\mu\text{m}$  with corresponding standard deviations between 1.70  $\mu\text{m}$  and 1.05  $\mu\text{m}$ . The  $\chi^2$ -probabilities range between 67 % and 0 % (Fig. 5.2; Tab. 5.1).

Specific FT ages of sediment samples were grouped into four age spectra according to time intervals and appropriate geological episodes: the Pan-African age group (>500 Ma), the Palaeozoic age group (~500-300 Ma), the Karoo age group (~300-220 Ma) and the break-up age group (<220 Ma)

In the following, the apatite FT results from the particular sedimentary units are described in ascending stratigraphic order.

### 6.1 Sakoa Group

Seven samples from the Sakoa Group were collected at two outcrops south of the Sahavazy River. Two samples are tillites collected from the base of the Sakoa Group (Fig. 5.1b, Tab. 5.1). Four samples are sand-, silt- and/or mudstones belonging to the overlaying units. All samples belong to the lower Sakoa Group except sample BE 204, which is a sandstone from the upper Sakoa Group collected ~6 km south-south-west of outcrop BE 203 (Fig. 5.1a, Tab. 5.1).

Apatite FT ages range between  $237\pm 11$  Ma and  $184\pm 13$  Ma. The single grain ages vary between  $367\pm 98$  Ma and  $115\pm 28$  Ma. The Karoo and break-up related single grain age components are dominant. The MTL vary between  $13.13\pm 0.17$   $\mu\text{m}$  and  $12.36\pm 0.3$   $\mu\text{m}$  with standard deviations ranging between 1.39  $\mu\text{m}$  and 1.05  $\mu\text{m}$ .  $\chi^2$ -values are between 67 % and 17 %.

The apatite FT data from the Sakoa samples reflect the thermal history of the southern Morondava basin. The samples from the Sakoa Group have all significantly younger FT ages than their stratigraphic ages (Fig. 5.2a, b). Regarding the 1-sigma error, most of the single grain ages are younger than the depositional ages. Furthermore, the  $\chi^2$ -values indicate a single population of ages.

Modelled T-t paths of two samples suggest that the samples reached a maximum palaeo-temperature at ~245-230 Ma (Fig. 5.5). Following, the samples cooled to below 60 °C during the ~200-180 Ma time interval. The models suggest a second phase of heating to temperatures between ~60 °C and ~70 °C during Late Tertiary times (Fig. 5.5).

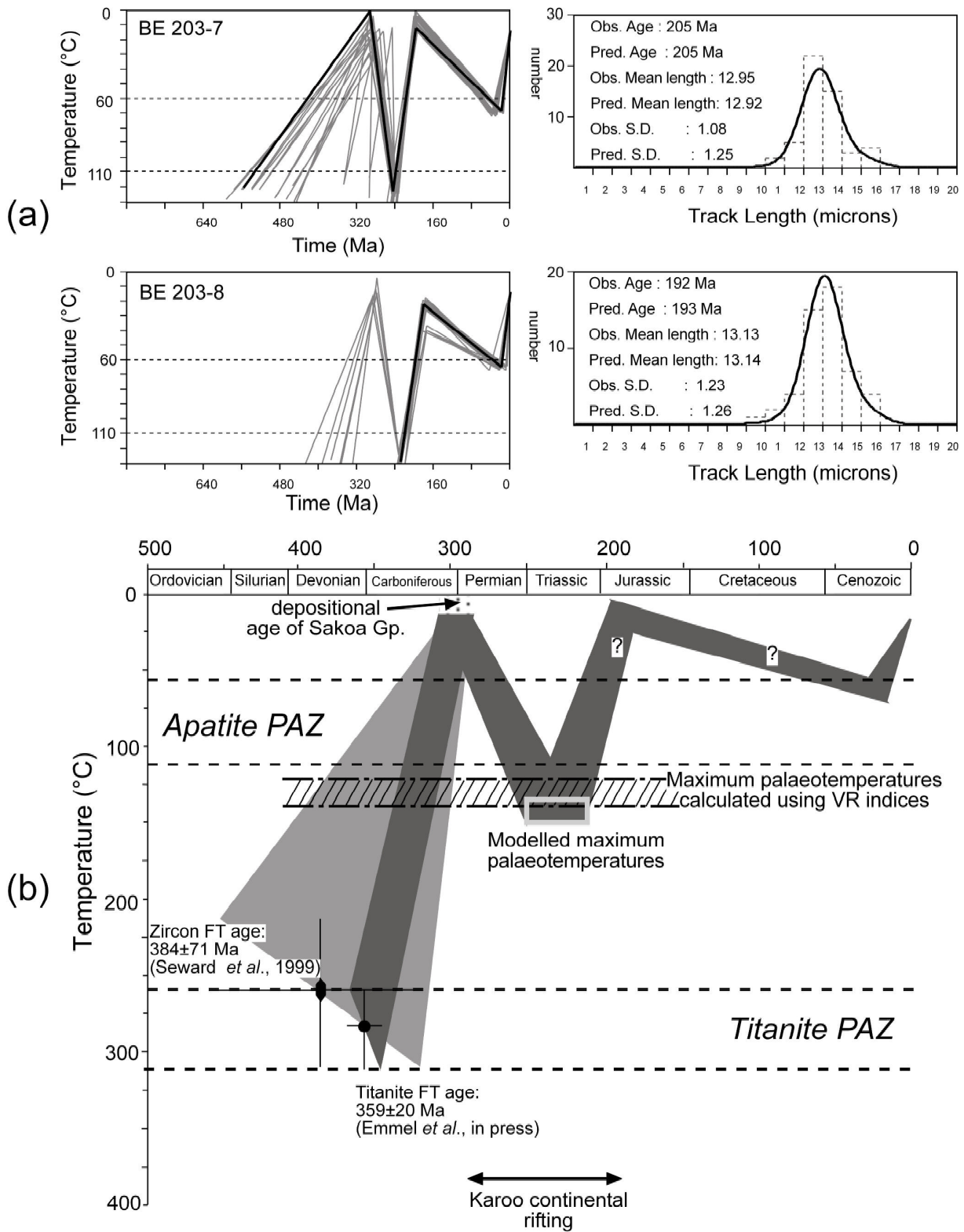


**Fig. 5.5:** a) Modelled time-temperature histories of two samples from the Sakoa Group with fitting parameters b) Thermal history of the Sakoa coal area based on titanite FT data (Emmel *et al.*, in press a), zircon FT data (Seward *et al.*, 1999), vitrinite reflectance indices (Ramanampisoa *et al.*, 1990; Radke *et al.*, 2000) and modelling results of detrital apatite FT parameters (this research). Note: The zircon FT age is from a samples located ~25 km south-west of outcrop BE 203.

Figure 5.2a shows a simplified stratigraphic column of the southern Morondava basin with apatite FT ages. Only the stratigraphically oldest samples from the Morondava basin were buried by a thick cover of sediments giving rise to temperatures  $>110\text{ }^{\circ}\text{C}$  and resetting of the apatite FT ages.

## 6.2 Sakamena Group

Six samples, five sandstones and one composite sample (mixed mud- and sandstones), belonging to the Sakamena Group were collected at four different outcrops (Fig. 5.1a, b). Five samples are from sections along the Menamaty and Benahy Rivers in the southern Morondava basin. Sample BE 182 belongs to the Lower Sakamena Formation, samples BE 178- BE 180 classify to the Lower-Middle Sakamena Formation, whereas sample BE 183 comes from the Middle to Upper Sakamena Formation. The north-south distance between the samples from the Sakamena Group is less than  $\sim 50\text{ km}$ , except sample SA 7 (sandstone, Middle Sakamena Formation), which was collected from a far northern area at the Sakeny River in the Morondava basin  $\sim 225\text{ km}$  north of the other sample locations (Fig. 5.1a).

The apatite FT ages range between  $399\pm 19\text{ Ma}$  and  $319\pm 19\text{ Ma}$  and are older than the stratigraphic ages and are therefore suitable for provenance analysis (Fig. 5.2a, b). The single grain ages scatter between  $680\pm 106\text{ Ma}$  and  $167\pm 44\text{ Ma}$  and belong mainly to the Pan-African, Palaeozoic and Karoo single grain age groups (Tab. 5.2). Only two single grain ages belong to the break-up related age group (Sample BE 179). The MTL vary between  $13.3\pm 0.12\text{ }\mu\text{m}$  and  $11.6\pm 0.17\text{ }\mu\text{m}$  with corresponding standard deviations between  $1.7\text{ }\mu\text{m}$  and  $1.12\text{ }\mu\text{m}$ . All samples from the Sakamena Group have  $\chi^2$ -probabilities of 0 % which is indicative for different populations of single grain ages with different cooling histories. Almost all apatite FT ages and single grain ages within the  $1\sigma$  error are older than the depositional ages, suggesting that the samples have experienced minor or no partial annealing since deposition.

The stratigraphically oldest sample BE 182 has the oldest and the highest proportion of single grain ages  $>400\text{ Ma}$ . Three samples (Sa7, BE 178 and BE 179) belonging to the Lower to Middle Sakamena show relatively uniform single grain age distributions indicating a similar potential source rock region. One sample from the Middle to Upper Sakamena Formation (BE 183) shows a relatively narrow single grain age distribution arguing for a local source. Modelled T-t histories of all samples from the Sakamena Group show two different sources. The older source possibly cooled during Late Proterozoic/Early Cambrian times through the partial annealing zone (PAZ:  $110\text{-}60\text{ }^{\circ}\text{C}$ ). The younger source cooled during Devonian/Early Permian times through the  $110\text{-}60\text{ }^{\circ}\text{C}$  temperature range. Thus, we suggest

cooled basement rocks as one source and reworked sedimentary rocks as another potential source, because no single grain age pattern of basement rocks fits the Late Proterozoic detrital single grain ages and modelled cooling of these samples. The highest rates of Late Proterozoic-Early Devonian single grain ages are present in sample BE 182 belonging to the Lower Sakamena Group suggests a main contingent of reworked sedimentary units during the Late Permian.

### 6.3 Jurassic strata

The Jurassic samples are from five different outcrops in the southern Morondava basin. The stratigraphic ages range from the Bajocian to the Callovian. All samples except AND07 are less than ~30 km apart. Sample AND07 is located 90 km south of the other Jurassic samples and ~40 km west-north-west from the Sakoa outcrop BE 203 (Fig. 5.1a).

The apatite FT ages range between  $462\pm 28$  Ma and  $236\pm 18$  Ma (Tab. 5.1). The single grain ages show a very broad age distribution from Proterozoic to Jurassic and cover all discussed age groups. Samples AND 07 and Anala 42 show affinities to the break-up related age group. The MTL of all samples vary between  $13.24\pm 0.16$   $\mu\text{m}$  and  $12.89\pm 0.18$   $\mu\text{m}$  with standard deviations ranging between  $1.36$   $\mu\text{m}$  and  $1.08$   $\mu\text{m}$ . The  $\chi^2$ -values are between 7 % and 0 %. All apatite FT and most of the single grain ages are older than the depositional ages of the particular samples (Fig. 5.2a, b).

The Jurassic samples can be distinguished into two groups. Samples AND07 and Anala 42 have significantly younger apatite FT ages (~235 Ma and ~280 Ma) than the Callovian samples (see Tab. 1). The MTL of the two samples are  $>13$   $\mu\text{m}$ , whereas the Callovian samples have MTL  $<13$   $\mu\text{m}$ . The principal age components vary for each sample (Tab. 5.2). Samples AND07 and Anala 42 have a remarkable high proportion (~50 %) of an Early Jurassic age component (Tab. 5.2). Modelled T-t paths of samples Anala 42 and AND07 argue for source rocks, which passed the PAZ during the Cambrian and Late Permian, whereby most single grain ages fit into the Late Permian cooling (Fig. 5.6). Samples ADA 01, ANK 4 AZ and Behevo 2 have apatite FT ages ranging between ~460 Ma and ~380 Ma. The modelled provenance cooling path of sample ADA-1 suggests similar cooling episodes as AND07 and Anala 42, only the single grain age proportion fitting the older cooling path is higher (Fig. 5.6).

Samples AND07, Anala 42 and ADA 01 were deposited in a coastal carbonate platform environment. The palaeo-current data obtained from channel axes, flute casts, ripple marks, foresets, and oriented wood infer predominantly north, north-west and south-west directed palaeo-currents. Sample Behevo 2 and ANK 4 AZ belong to an open shelf environment with south-west directed palaeo-currents (Fig. 5.7a).

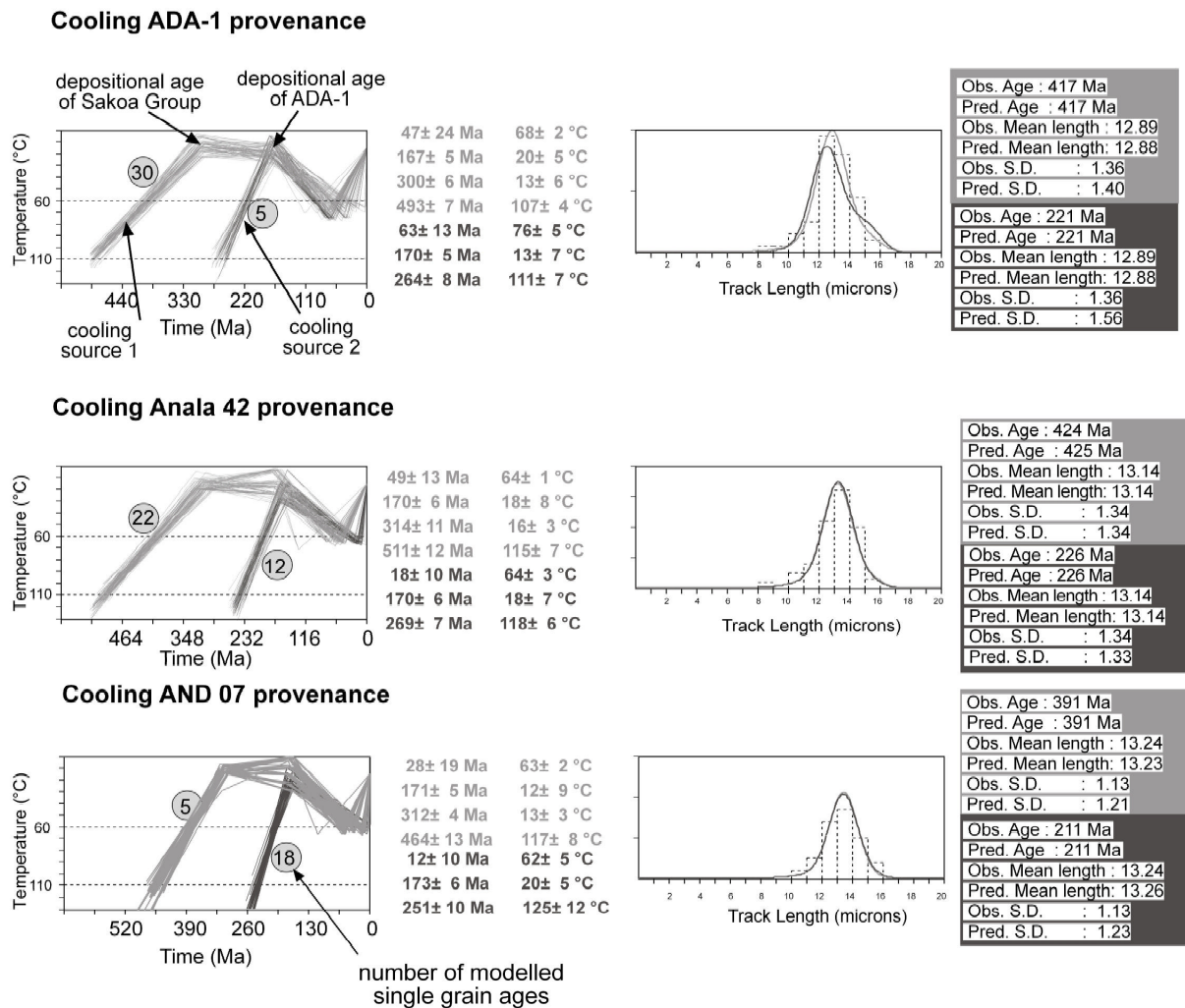


**Fig. 5.6:** Modelling results from the Jurassic strata. The modelling was carried out using the single grain ages >300 Ma and <300 Ma but the same length parameters for the specific samples. Two main sources could be distinguished. One source represents reworked sedimentary units and a second source is characterised by a mainly Triassic cooling episode.

## 7. Discussion

### 7.1 Sedimentological indications; basement development

From the Late Carboniferous, with the first evidence of tectonic instability between East- and West- Gondwana, three sedimentary basins were formed along the western continental margin of Madagascar. Sedimentary strata of the Morondava basin generally strike approximately north- south and dip to the west. The oldest units are in the east (Late Carboniferous- Early Permian) and stratigraphic ages become younger towards the west (Quaternary). Based on palaeo-current data, Nichols & Daly (1989) concluded that the Precambrian metamorphic basement east of the Morondava basin must be the source rock

region of the Karoo Supergroup. The mineralogical immaturity and textural sub-maturity of the Late Carboniferous to Early Permian Sakoa deposits suggest a short transport distance. In contrast, the Late Triassic to Early Jurassic Isalo Group deposits are mineralogically and texturally more mature than the Sakoa and Sakamena deposits, arguing for an increase in the distance from the source since Late Carboniferous times. Sedimentation followed a regional west to south-west palaeo-slope (Nichols & Daily, 1989). The palaeo-landscape changed from a steeper topography to a more or less flat, levelled landscape during Late Carboniferous/Early Permian times (Wescott & Diggens, 1997).

Basement apatite FT data (Emmel *et al.*, in press a, b) support the assumption of a steep topography prior to the opening of the Karoo basin and an increasing distance from the source since Late Carboniferous times. The western basement margin was influenced by rapid cooling before the initial opening of the Karoo rift system and was followed by an eastward migration of areas with highest denudation during the Karoo rift phase (Fig. 5.3b, c).

Modes of basin-filling changed significantly from the Middle Jurassic onwards. Oceanisation within the Somali basin led to an increase of the marine influence. The continental margin style along the present-day western and north-western coast of Madagascar changed from a rift shoulder to a passive margin type. Along the present-day south-western coast of Madagascar a transform margin developed.

Basement apatite FT data suggest a Jurassic phase of rapid cooling along the south-western continental margin of Madagascar, associated with an amount of denudation of up to 3.5 km crustal section. The denudation patterns of the central part of the island were unaffected by these tectonic changes (Emmel *et al.*, in press, submitted).

Sample AND 07 and ADA 01 are taken from a coastal carbonate platform facies. The depositional age of sample AND 01 is Bajocian, whereas the depositional age of ADA 01 is not well dated, it ranges from Upper Bajocian to Lower Bathonian. The Callovian samples record an open shelf environment with temporally terrestrial input. Palaeo-current data suggest a sedimentary input mainly from the east and the south and to a lesser extend from the north (Fig. 5.7). However, palaeo-current data from shelf regions probably with meandering rivers should be considered only with caution (Fig. 5.8). However, also during Jurassic times the present basement units of central and southern Madagascar are most probably the predominant source for Jurassic sediments. With the present geochronological data longer transport distances from far eastern (India, Sri Lanka) and far southern (East Antarctica) sources cannot be ruled out but this palaeo drainage is difficult to reconstruct. However, palaeo-current data exclude a provenance to the west (East African).

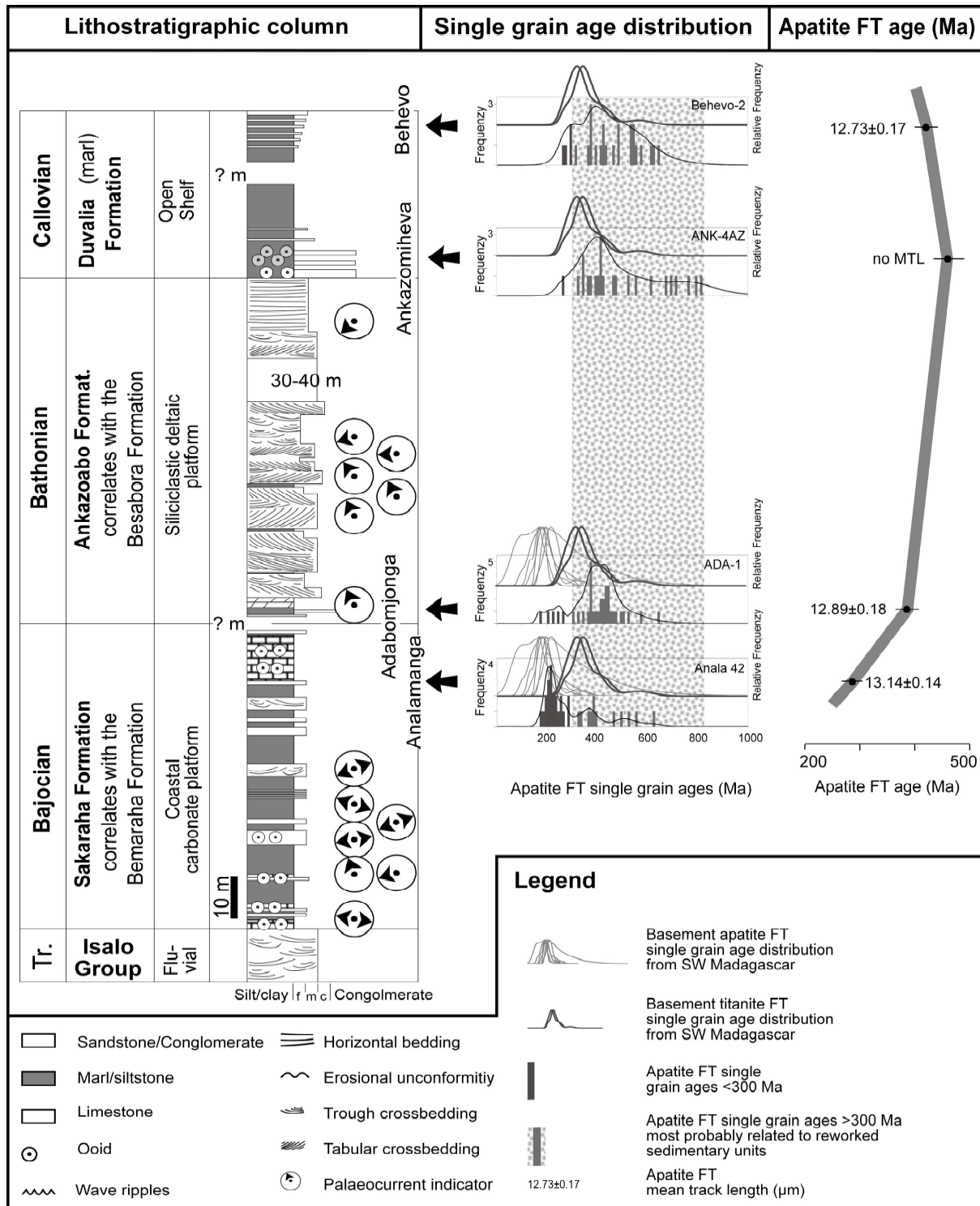


**Fig. 5.7:** Apatite FT pattern of the Jurassic samples a) Synthetic lithostratigraphic column for the Jurassic of the southern Morondava basin, compiled from four detailed profiles at Analamanga, Adabomjonga, Ankazomiheva and Behevo. b) Single grain age distribution of the Jurassic samples from the central southern Morondava basin c) Apatite FT age trend during the Jurassic.

## 7.2 Thermal history of the Sakoa Group, southern Morondava basin

The detrital apatite FT data from the Sakoa Group reflects the thermal history of the southern Morondava basin (Fig. 5.5). Basement titanite (Emmel *et al.*, in press), zircon FT data (Seward *et al.*, 1999), and depositional ages (Wescott & Diggins, 1997) imply fast cooling before the initial opening of the Karoo basins. The Sakoa coal area was at the surface during Late Carboniferous-Early Permian deposition of the Sakao sediments. Thereafter, sedimentation continued in the Sakoa coal area. Vitrinite reflectance indices from the southern Morondava basin range between 0.79 and 0.88 (Ramanampisoa *et al.*, 1990; Radke *et al.*, 2000). These data argue for a syn- to post- Sakoa burial to temperatures of ~120-140 °C (calculated after Burnham & Sweeney, 1989; Fig. 5.5). Modelled T-t paths indicate that the Sakoa Group reached their maximum palaeo-temperatures during the deposition of the Sakamena and Isalo Group, which correlates with maximum extension of the Karoo rift (Nichols & Daily, 1989). Well data give present geothermal gradients of the Morondava basin which range between 65 °C/km and 34 °C/km (e.g. Uhmman, 1996). These geothermal gradients and the suggested maximum palaeo-temperatures infer a burial depth between ~2 km to ~4 km during the deposition of the Isalo Group. Modelled T-t paths show that after sedimentation the samples were exhumed during Middle Triassic to Early Jurassic times (Fig. 5.5). This is contemporaneous with the initial break-up of the Gondwana supercontinent, which was preceded by the emplacement of a large continental flood basalt province, the Karoo magmatic province in South Africa. The denuded sedimentary cover must have been reworked and redeposited.

## 7.3 Provenance analysis applying FT data

### 7.3.1 Late Permian - Early Triassic provenance

All samples from the Sakamena Group were used for provenance analysis. The single grain age distribution patterns argue for three different sources.

Samples Sa7, BE 178, and BE 179 show a similar single grain age distribution as do combined titanite and apatite FT single grain ages from basement samples located east of Fianarantsoa between the Itremo region and the Angavo shear zone (Fig. 5.4). The modelled cooling paths of the three sedimentary samples show cooling of the source from 110 °C to below 60 °C between ~450 Ma and ~320 Ma, which correlates with an episode of basement cooling dated at 420-330 Ma (Emmel *et al.*, submitted). A common source for these rocks would imply a mainly east-west directed drainage system and possibly north-south flowing rivers along active faults at the palaeo eastern margin of the Morondava basin (Fig. 5.8,

similar to the present day drainage system). This assumption is supported by palaeo-current data, which mainly imply sediment transport into the central Morondava basin from the east and locally from the north (Fig. 5.9; Nichols & Daily, 1987).

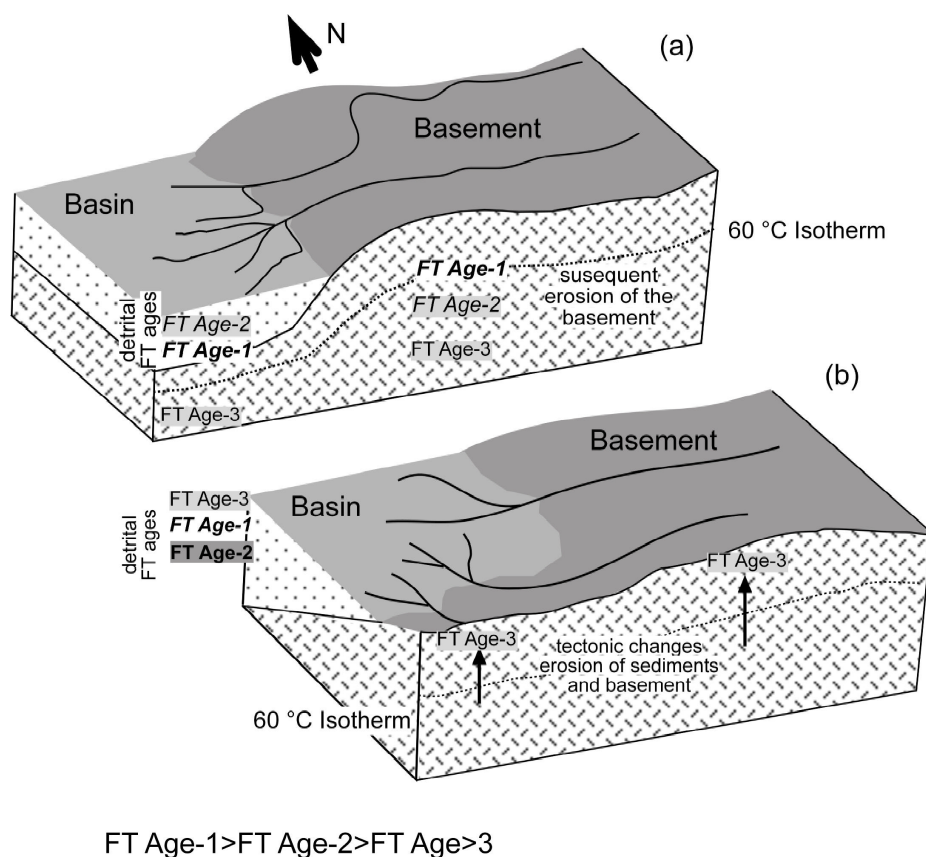


**Fig. 5.8:** Sketch of a basin-basement environment, which explains the apparent FT and drainage pattern from south-west Madagascar.

a) Model representative for the Sakamena Group with a mainly east-west directed drainage system but locally along faults apparent north-south trending palaeo-current pattern. b) Model for the Jurassic strata. During the transform margin evolution former sedimentary units were reworked and deposited in north-western areas. The palaeo-current data could be very inhomogeneous.

Sample BE 183 with an apatite FT age of ~400 Ma has a narrow single grain age distribution and relatively long MTL of  $13.30 \pm 0.12 \mu\text{m}$  arguing for a local source and a tectono-thermal event at ~400 Ma that formed the FT parameter. Possibly, the same source as for samples Sa 7, BE 178, and BE 179 can be assumed. Advective heating along ductile high strain zones occurred episodically from ~420-300 Ma east of Fianarantsoa (Emmel *et al.*, submitted). Alternatively, the detrital apatite FT ages are simple cooling ages after the latest thermal events at 500-430 Ma in central Madagascar (Fernandez *et al.*, 2003).

In contrast to the previously discussed samples, single grain ages of sample BE 180 and BE 182 have a representative Proterozoic (>500 Ma) age component suggesting an "older" provenance. Possibly reworked early Karoo deposits e.g. former Late Carboniferous to Early Permian Sakoa Group deposits could be one source. Alternatively, a region between Fianarantsoa and the Angavo shear zone could be another potential source. In this basement area the oldest titanite (~420-400 Ma) and apatite FT ages (~460-360 Ma) are dated and fit

the detrital single grain ages. The modelled T-t history of sample BE 182 shows that the potential source rock cooled at ~500 Ma to 110 °C (Fig. 5.4). The cooling path gives evidences for a reheating to temperatures of ~75 °C at ~260 Ma most probably due to a sedimentary cover. Thus, the original FT "fingerprint" of the reworked source is disturbed. Moreover a potential second source rock complicates the discrimination of the provenance.

### 7.3.2 Jurassic provenance

Apatite FT data obtained from the Jurassic strata is suitable for provenance analysis. From the Jurassic siliciclastic inputs, Uhmann (1996) analysed heavy minerals of Jurassic sedimentary rocks from the southern Morondava basin and discovered a conspicuous high heavy mineral fraction in the Callovian strata. The abundance of the opaque heavy mineral fraction increases since the Middle Jurassic. From the Bathonian, garnet steadily increases in size and becomes more rounded. After a maximum peak in the Callovian, the grain sizes successively decrease during the Upper Jurassic. Small, highly weathered garnets in Late Jurassic strata point to reworked material.

The oldest detrital apatite FT ages (~420-460 Ma) are observed in the Callovian strata (ANK-4AZ and Behevo-2), and correspond to the position of maximum garnet content. The broad single grain age spectrum from ~800 Ma to ~250 Ma with a very high percentage of single grain ages >500 Ma suggests one potential source with the same age as the older Sakamena source.

Detrital apatite FT ages of the Bajocian-Bathonian samples AND 07, ADA-1 and Anala 42 suggest a provenance with a totally different geochronological "fingerprint" (Fig. 5.7). The single grain age distribution (especially AND 07 and Anala 42) shows that the dominant fraction dates to the Early Jurassic. Nevertheless, a Proterozoic age component is always present. The modelled T-t paths (Fig. 5.6) indicate two different proto sources, which cooled rapidly during Cambrian and Late Permian times. Modelled T-t paths of potential source rock regions in the south-western part of the island (especially in the Sakoa area) indicate that during Late Triassic to Early Jurassic times extensive cooling occurred. Thus, we suggest that the potential source of the basin-fill derived from adjacent south-eastern basement units and eroded reworked Karoo sediments, which were exhumed during the Late Triassic to Early Jurassic (see section 7.2). Despite corresponding geochronological data, a provenance further south (e.g. Antarctica) is unlikely. Since the Early Jurassic a transform margin evolved along the south-western coast of the island and must have developed a morphological barrier. North-south oriented palaeo-current data from Bathonian strata at the southern margin of the Morondava basin support an east-west trending shoreline (Geiger *et al.*, in press.). Overall, the heavy mineral suits and the FT data show that reworked sediment

material gains an increasing importance towards the Callovian while the impact of eroded basement material decreased during the Jurassic.

### 7.3.3 Detrital fission track age clusters

Using the program "Pophare" (Dunkl, 2003) principal age components for samples from the Sakamena Group and the Jurassic strata were classified into four clusters. We compared the clusters with the previously supposed age groups and see a good match.

#### a) Pan-African cluster (>500 Ma)

In more than half of the samples this cluster covers more than 5 % of the single grain ages. These ages are associated with cooling after the latest metamorphic events in central Madagascar at ~550 Ma (Meert *et al.*, 2002). Single grain ages >500 Ma occur sporadically in apatites from basement samples especially from a region south-east of Fianarantsoa (Emmel *et al.*, submitted). Some detrital apatite FT single grain ages are older than basement titanite FT single grain ages and suggest a source rock older than based on the basement titanite FT ages. Most probably these single grain ages belong to far older reworked sedimentary units (e.g. Sakoa Group or even Itremo units).

#### b) Palaeozoic cluster (500-300 Ma)

This age cluster can be detected in all samples. The samples belonging to the Sakamena Group have 25-100 % minerals belonging to this cluster. Also the post-Karoo Jurassic samples with apatite FT ages >300 Ma are mainly composed of this cluster (>75 %) and the samples with apatite FT ages <300 Ma have still a fraction ~20-40 %.

The Palaeozoic tectono-thermal evolution of central Madagascar starts with the emplacement of a pegmatite field at 500-435 Ma associated with fluid circulation (Fernandez *et al.*, 2003). Basement titanite and apatite FT data from central and southern Madagascar argue for several phases of rapid cooling prior to the opening of the Karoo rift system especially during the 420-300 Ma episode in the central part of the island. The driving forces for vertical offsets are speculative, but they are probably due to convergent tectonics in relation with subduction along the palaeo-pacific margin (Schandelmeier *et al.*, in press; Emmel *et al.*, submitted).

The Palaeozoic proportion in Jurassic samples is most probably derived from reworked sedimentary rocks which formerly overlay the Sakoa deposits and the present day exposed basement units in the south-eastern Morondava basin.

c) Karoo cluster (300-220 Ma)

This cluster is common (>30 %) for the samples belonging to the Lower-Middle Sakamena Group and subordinately for AND07. The Karoo rift evolution reached its maximum stage during Middle to Late Triassic times affecting the margin topography significantly (Wescott and Diggins, 1997, 1998; Emmel *et al.*, in press). Remarkably, relatively low amounts of single grain ages belong to this age cluster. This suggests little exhumation during this rift episode compared to higher exhumation rates prior and during the initial Karoo rift phase.

Sample <i>stratigraphy</i>	AFT- Age (Ma)	Method	Age 1 ± SD	Age 1	Age 2 ± SD	Age 2	Age 3 ±	Age 3	RMS	W2
			(Ma) <i>Pan-African</i>	(%)	(Ma) <i>Palaeozoic</i>	(%)	SD (Ma)	(%)		
<b>BE 178</b> Low. - Mid. Sakamena	326±22	RMS Gaussian	517±5	16	382±4	27	271±38	57	0.006 0.012	0.013 0.8
<b>BE 179</b> Low. - Mid. Sakamena	341 ± 19	RMS Gaussian			396±68	65	258±78	35	0.023 0.021	0.022 0.68
<b>BE 180</b> Low. - Mid. Sakamena	396±34	RMS Gaussian	540±22	25	451±9	38	276±58	37	0.004 0.014	0.015 0.808
<b>composite 178-180</b> Middle Sakamena	-	RMS Gaussian			472 ± 65 379 ± 17	39 20	267 ± 46	41	0.016 0.012	0.012 0.798
<b>BE 183</b> Mid. - Up. Sakamena	399±19	RMS Gaussian	550±6	6	414±11 384±55	30 64			0.014 0.017	0.018 0.718
<b>BE 182</b> Lower Sakamena	393±22	RMS Gaussian			424±116 351±26	77 23			0.015 0.017	0.019 0.815
<b>Sa 7</b> Middle Sakamena	319±19	RMS Gaussian			343±103	71	279±16	29	0.017 0.022	0.02 0.7
<b>Anala 42</b> Lower Bajocian	282±19	RMS Gaussian	529±37	11	339±67	37	213±22	52	0.009 0.011	0.013 0.823
<b>AND-0.7</b> Bathonian	236±18	RMS Gaussian			378±6	20	267±12 181±26	23 57	0.008 0.014	0.014 0.764
<b>Ada-1</b> Upper Bajocian	381±22	RMS Gaussian			419±57	86	212±41	14	0.022 0.019	0.02 0.757
<b>Behevo 2</b> Callovian	416±21	RMS Gaussian	554±39	22	386±95	78			0.021 0.022	0.023 0.646
<b>ANK 4 AZ</b> Lower Callovian	462±28	RMS Gaussian	725±57	19	484±178 394±43	38 43			0.011 0.017	0.018 0.772
<b>composite "old" Jurassic</b>	-	RMS Gaussian	667 ± 82	17	404 ± 80	83			0.043 0.02	0.019 0.634

**Tab. 5.2:** Results of the age cluster determination using the program POPSHARE (Dunkl, 2003). The age clusters with percentage and statistical fitting are given. AFT: apatite fission track, SD: standard deviation. Goodness of fitting: RMS (root mean square), W1 (weighted with grain error), W2 (weighted by the local tangent), K-S (Kolmogorov-Smirnov test).

d) *Break-up cluster (220-180 Ma)*

This youngest age cluster is only present in (~10-60 %) the Bathonian - Bajocian samples. The cluster reflects Middle Jurassic denudation along the south-western continental transform margin immediately adjacent to the Bathonian - Bajocian samples.

#### 7.4 Sedimentary and tectonic model for the Late Carboniferous to the Late Jurassic

In southern Madagascar the initial evolution of the Karoo rift was succeeded by local fractures and the development of small pull-apart basins (Schandelmeier *et al.*, in press) along N-S trending ductile high strain zones. Heavy mineral and textural data suggest a nearby source rock region for the Sakoa deposits (Nichols & Daly, 1989; Uhmman, 1996). This assumption is supported by basement FT data, which argue for denudation along the present basement/basin contact prior and during deposition of the Sakoa Group resulting from the erosion of a high relief during this time (Emmel *et al.*, in press).

Based on textural data Nichols & Daily (1989) suggest two main sources for the Lower-Middle Sakamena detritus. Most of the material seems to originate from eastern adjacent basement units and reworked conglomeratic sediments. Limestone fragments in the Lower Sakamena deposits argue for reworked sedimentary units derived from the Middle Permian Vohitola limestone belonging to the Upper Sakoa Group (Wescott & Diggins, 1997).

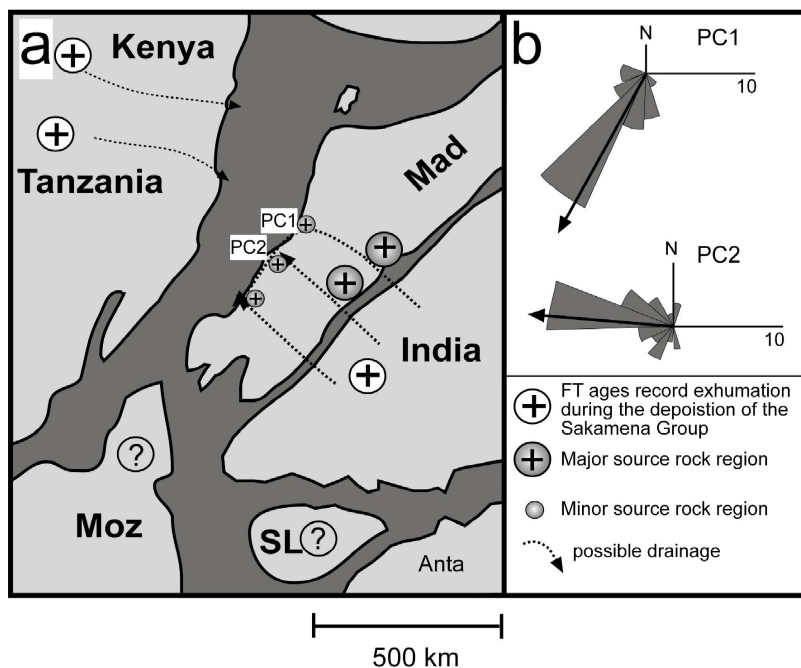


**Fig. 5.9:** a) Reconstruction of central Gondwana (from Reeves *et al.*, 2002). Grey: Precambrian crustal fragments; dark grey: crust extended in the Phanerozoic. Arrows mark the possible drainage directions during Permo-Triassic times  
b) Palaeo-current data (PC1 and PC 2) from the Middle Sakamena (from Nichols & Daily, 1989).  
Abbreviations:  
Anta: Antarctica  
Mad: Madagascar  
Moz: Mozambique  
SL: Sri Lanka

Rounding of quartz and increasing sediment maturity indicate an increase in the distance between the source rock and the basin from Late Permian to Early Jurassic times. This

assumption is supported by the correspondence of basement FT data with those of the Sakamena and Isalo Groups, for which a far inland basement region is determined as the source (Figs. 5.3 and 5.4). The shift in the provenance areas from Late Carboniferous to Early Jurassic times was most probably caused by rift migration as indicated by basement FT data (Fig. 5.3, Emmel *et al.*, in press, submitted). The increasing source rock distance could have led to a smoother topography.

The Karoo-related part of the Morondava basin is characterised by a migration of the depocenter from east to west (Piqué *et al.*, 1999) while the exhumed basement migrated from west to east (Emmel *et al.*, in press, submitted). Van Wijk & Cloetingh (2002) describe modelled basin migration caused by slow lithospheric extension. If extension is characterised by low velocities ( $<8 \text{ mmyr}^{-1}$ ) over a period  $>100 \text{ Ma}$  no break-up occurs, i.e. no oceanic crust is developed, but the lithosphere anomalies migrate away from the rift locus. The model suggests that new basins form outside the initial rift locus. In the case of Madagascar, this could have led to the westward shift of the depocenter which is observed within the Morondava basin (e.g. Piqué, 1999). Moreover, this may be connected with the postulated eastward migration of the exposed basement with highest denudation rates due to isostatic response over slightly stretched lithosphere.

During Jurassic times, Gondwana was particularly influenced by mantle plume activities, which especially affected South Africa and Antarctica (e.g. Brewer *et al.*, 1992; Encarnacion *et al.*, 1996). It is still discussed controversially if the Bouvet-Karoo mantle plume led to the break-up of Gondwana (e.g. Cox, 1988, Courtillot *et al.*, 1999, Hawkesworth *et al.*, 1999). Basement FT data from Dronning Maud Land record fast cooling at  $\sim 180 \text{ Ma}$ , possibly associated with updoming above the plume head (Meier, 1999). Only  $\sim 15 \text{ Ma}$  later the Somali basin between Madagascar and East Africa was opened. The opening the Somali basin and the evolution of the transform continental margin in south-western Madagascar changed the tectonic features and the sediment supply in Madagascar significantly. Pre-dating this event, the south-western part of the metamorphic basement was affected by denudation of  $\sim 3.5 \text{ km}$  vertical section during Early Jurassic times, synchronous with the emplacement of the Bouvet-Karoo mantle plume in South Africa and Antarctica. However, the eroded units were deposited north-west of the source area as terrestrial more siliciclastic episodes into a carbonate environment during the Middle Jurassic. This argues for uplift along the south-western margin during the transform movements along the Davie fracture zone and a change in the palaeo-slopes and drainage directions. Palaeo-current measurements from Bathonian strata at the southern Morondava basin margin suggest an east-north-east to west-south-west trending shoreline.

## 8. Conclusion

This study shows the advantages of combined FT analysis to describe the thermal history of sedimentary basins and together with known basement FT distribution and palaeo-current data to discriminate a possible provenance. The margin evolution from an initial rift to a transform margin and the associated basement denudation pattern in south-western Madagascar are reflected by changes in provenance through time. The Karoo deposits display the shift from near to a distal source area. This is confirmed by basement FT data. The two main Late Permian to Early Triassic provenance of the Sakamena Group were basement units in the centre of the island and reworked sedimentary rocks along the north-south stretching palaeo basin margin. The evolution of a transform margin along the south-western part of Madagascar during Early Jurassic times led to intensified exhumation and reworking of former sedimentary units. FT and palaeo-current data argue for a Jurassic sedimentary and basement provenance in the south-western part of the island. Enhanced denudation of basement along the evolving transform margin provided material for the basin-fill. Also, sedimentary units were reworked and redeposited in the Jurassic strata. The present day Morondava basin shape in south-west Madagascar is a relict of these events. Parts of the present Vohibory basement outcrop region were most probably covered by sedimentary units up to 4 km from Early Permian to Early Jurassic times.

## References

- BESAIRIE, H. (1972) Géologique de Madagascar.I: Les terrains sédimentaires. *Annales Géologique Madagascar*, 35: 463p.
- BOAST, J. & NAIRN, A. E. M. (1982) An outline of the geology of Madagascar. In: *The ocean basins and margins, Vol. 6, The Indian Ocean* (Ed. by J. Boast and A.E.M. Nairn), pp. 649-696. Plenum Press, New York, London.
- BREWER, T.S., HERGT, J.M., HAWKESWORTH, C.J., REX, D. & STOREY, B.C. (1992) Coats Land dolerites and the generation of Antarctic continental flood basalts. In: *Magmatism and the Causes of Continental Break-up* (Ed. by B.C. Storey, T. Alabaster and R.J. Pankhurst) pp. 185-208. *Geological Society Special Publication*, **68**.
- BROWN, R.W., RUST, D.J., SUMMERFIELD, M.A., GLEADOW, A.J.W. & DE WIT, M.J.D. (1990) An early Cretaceous phase of accelerated erosion on the southwestern margin of Africa: Evidence from apatite fission track analysis and the offshore sedimentary record. *Nuclear Tracks and Radiation Measurements*, **17**, 339-351.

- BURNHAM, A.K. & SWEENEY, J.J. (1989) A chemical model of vitrinite Maturation and reflectance. *Geochimica et Cosmochimica Acta*, **53**, 2649-2657.
- CARTER, A. (1999) Present status and future avenues of source region discrimination and characterization using fission track analysis. *Sedimentary Geology*, **124**, 31-45.
- COFFIN, M.F. & RABINOWITZ, P.D. (1987) Reconstruction of Madagascar and Africa; evidence from the Davie fracture zone and western Somali Basin. *Journal of Geophysical Research, B, Solid Earth and Planets*, **92**, 9385-9406.
- COFFIN, M.F. & RABINOWITZ, P.D. (1992) The Mesozoic East African and Madagascan conjugate continental margins; stratigraphy and tectonics. In: *Geology and geophysics of continental margins* (Ed. by Watkins, Feng, Zhiqiang, McMillen and Kenneth), AAPG Memoir. American Association of Petroleum Geologists, pp. 207-240.
- COLLINS, A., WINDLEY, B., KRÖNER, A. & FITZSIMONS, I. (2001) The Tectonic Architecture of Central Madagascar: Implications on the Evolution of the East African Orogeny. *Gondwana Research*, **4**, 152-153.
- COURTILLOT, V., JAUPART, C., MANIGHETTI, P., TAPPONNIER, P. & BESSE, J. (1999) On causal links between flood basalts and continental breakup. *Earth and Planetary Science Letters*, **166**, 177-195.
- COX, K.G. (1992) Karoo igneous activity, and early stages of the break-up of Gondwanaland. In: *Magmatism and the Causes of Continental Break-up* (Ed. by B.C. Storey, T. Alabaster and R.J. Pankhurst) pp. 185-208. *Geological Society Special Publication*, **68**.
- DE WIT, M.J. (2003) Madagascar: Heads It's a Continent, Tails It's an Island. *Annu. Rev. Earth Planet. Sci.*, **31**, 213-248.
- DUNCAN, R.A., HOOPER, P.R., REHACEK, J., MARSH, J.S. & DUNCAN, A.R. (1997) The timing and duration of the Karoo igneous event, southern Gondwana. *Journal of Geophysical Research*, **102**, 18127-18138.
- DUNKL, I. (2003) <http://homepages.uni-tuebingen.de/istvan.dubkl/>Popshare 1.R (2003)
- DU TOIT, S.R. KIDSTON, A.G. & SLIND, O.L. (1997) The hydrocarbon Potential of the East African Continental Margin. Alconsult International Ltd., on behalf of the Canadian International Development Agency (DIDA), Calgary, 132 pp
- EMMEL, B., JACOBS, J. & RAZAKAMANANA, T. Titanite and apatite fission track analyses on basement rocks of central-southern Madagascar: constraints on exhumation and denudation rates along the eastern rift shoulder of the Morondava Basin. *Journal of African Earth Sciences*, in press.
- EMMEL, B., JACOBS, J., GRASER, G., KASTOWSKI, M. & RAZAKAMANANA, T. Post collisional (<500 Ma) tectono-thermal evolution of Central Madagascar: a combined structural and fission track study. *Tectonophysics*, submitted.

- ENCARNACION, J., FLEMING, T.H., ELLIOT, H.V. & EALES, H.V. (1996) Synchronous emplacement of Ferrar and Karoo dolerites and the early breakup of Gondwana. *Geology*, **24**, 535-538.
- FERNANDEZ, A., SCHREURS, G., VILLA, I.M., HUBER, S. & RAKOTONDRAZAFY, M. (2003) Age Constraints on the tectonic of the Itremo region in Central Madagascar. *Precambrian Research*, **123**, 87-110.
- FERNANDO, W.I.S., IIZUMI, S. & KITAGAWA, R. (1999) Post tectonic granites in Sri Lanka. *Gondwana Research*, **2**, 290-291.
- FOSTER, D.A. & GLEADOW, A.J.W. (1992a) Reactivated tectonic boundaries and implications for the reconstruction of southeastern and northern Victoria Land, Antarctica, *Geology*, **20**, 267-270.
- FOSTER, D.A. & GLEADOW, A.J.W. (1992b) The morphotectonic evolution of rift-margin mountains in central Kenya: constraints from apatite fission-track thermochronology. *Earth and Planetary Science Letters*, **113**, 157-171.
- GALBRAITH, R.F. (1981) On statistical models for fission track counts. *Mathematical Geology*, **13**, 471-478.
- GALLAGHER, K., HAWKESWORTH, C.J. & MANTOVANI, M.S.M. (1994a) The denudational history of the onshore continental margin of SE Brazil from fission track data. *Journal of Geophysical Research*, **99**, 18117-18145.
- GALLAGHER, K. & SAMBRIDGE, M (1994b) Genetic algorithms: a powerful method for large scale non-linear optimisation problems. *Comput. Geosci.*, **20**, 1229-1236.
- GALLAGHER, K. (1995) Evolving temperature histories from apatite fission-track data. *Earth and Planetary Science Letters*, **136**, 421-435.
- GEIGER, M., CLARK, D.N. & METTE, W. (2003) Sedimentological and seismic data from the Middle Jurassic strata in the Morondava Basin (SW Madagascar) and implications to the Gondwana Breakup. *Journal of African Earth Sciences*, in press.
- GLEADOW, A.J.W. (1980) Fission track age of the KBS Tuff and associated hominid remains in northern Kenya. *Nature*, **284**, 225-230.
- GLEADOW, A.J.W. (1981) Fission-track dating methods: what are the real alternatives? *Nuclear Tracks*, **5**, 3-14.
- GLEADOW, A.J.W., DUDDY, I.R. & LOVERING, J.F. (1983) Fission track analysis: a new tool for the evaluation of thermal histories and hydrocarbon potential. *Journal Australian Petrology Engineering Association*, **23**, 93-102.
- GREEN, P.F. (1981) A new look at statistics in fission-track dating. *Nuclear Tracks*, **5**, 77-86.

- GREEN, P.F., DUDDY, I.R., GLEADOW, A.J.W. & LOVERING, J.F. (1989) Apatite Fission-Track Analysis as a Palaeotemperature Indicator for Hydrocarbon Exploration. In: *Thermal History of Sedimentary Basins-Methods and Case Histories* (Ed. by N.D. Naeser), pp. 181-195. Springer, New York.
- GUNELL, Y. (2000) Apatite fission track thermochronology: an overview of its potential and limitations in geomorphology. *Basin Research*, **12**, 115-132.
- HAWKESWORTH, C., KELLEY, S., TURNER, S., LE ROEX, A. & STOREY, B. (1999) Mantle process during Gondwana break-up and dispersal. *Journal of African Earth Sciences*, **28**, 239-261.
- HENJES-KUNST, F. & MARKL, G. (1998) Charnokitic intrusive rocks and related lamprophyres in central Dronning Maud Land, East Antarctica: evidence for long-lasting igneous activities in Late Pan-African times. *Journal of African Earth Sciences*, **21**, 110.
- HURFORD, A.J. & GREEN, P.F. (1983) The zeta age calibration of fission-track dating. *Isotope Geoscience*, **1**, 285-317.
- JACOBS, J., FANNING, C. M., HENJES-KUNST, F., OLESCH, M & PAECH, H.J. (1998) Continuation of the Mozambique Belt into East Antarctica: Grenville-age metamorphism and polyphase Pan-African high grade events in Central Dronning Maud Land. *Journal of Geology*, **106**, 385-406.
- KALASWAD, S., RODEN, M.K., MILLER, D.S. & MORISAWA, M (1993) Evolution of the continental margin of western India: new evidence from apatite fission-track dating. *Journal of Geology*, **101**, 667-673.
- KEY, R.M., CHARLSEY T. J., HACKMAN, B. D. & WILKINSON, A. F. (1989) Superimposed Upper Proterzoic collision-controlled orogenies in the Mozambique Belt of Kenya. *Precambrian Research*, **44**, 197-225.
- KRÖNER, A., SACCI, R., JAECKEL, P. & COSTA, M (1997) Kibaran magmatism and Pan-African granulite metamorphism in northern Mozambique: single zircon ages and regional implications. *Journal of African Earth Sciences*, **25**, 467-484.
- KRÖNER, A., HEGNER, E., COLLINS, A. S., WINDLEY, B. F., BREWER, T. S., RAZAKAMANANA, T. & PIDGEON, R. T. (2000) Age and magmatic history of the Antananarivo Block, central Madagascar, as derived from zircon geochronology and Nd isotopic systematics. *American Journal of Science*, **300**, 251-288.
- LASLETT, G.M., GREEN, P.F., DUDDY, I.R. & GLEADOW, A.J.W. (1987) Thermal annealing of fission tracks in apatite 2. A Quantitative Analysis. *Chemical Geology (Isotope Geoscience Section)*, **65**, 1-13.

- LUGER, P., GROESCHKE, M., BUSSMANN, M., DINA, A., METTE, W., UHMANN, A. & KALLENBACH, H. (1994) Comparison of the Jurassic and Cretaceous sedimentary cycles of Somalia and Madagascar; implications for the Gondwana breakup. *Geologische Rundschau*, **83**, 711-727.
- MABOKO, M.A.H., MCDOUGALL, I. & ZEITLER, P.K. (1989) Dating late Pan-African cooling in the Uluguru granulite complex of eastern Tanzania using the  $^{40}\text{Ar}/^{39}\text{Ar}$  technique. *Journal of African Earth Sciences*, **9**, 159-167.
- MEERT, J. (2003) A synopsis of Events Related to the Assembly of Eastern Gondwana. *Tectonophysics*, **262**, 1-40.
- MEERT, J.G., NÉDÉLEC, A. & HALL, C. (2002) The stratoid granites of central Madagascar: palaeomagnetism and further age constraints on neoproterozoic deformation. *Precambrian Research*, **120**, 101-129.
- MEIER, S. (1999) Paleozoic and Mesozoic tectono-thermal history of central Dronning Maud Land, East Antarctica - evidence from fission track thermochronology. *Berichte zur Polarforschung*, **337**, p. 192.
- MÖLLER, A., MEZGER, K. & SCHENK, V. (2000) UPb dating of metamorphic minerals: prolonged slow-cooling of high pressure granulites in Tanzania, East Africa. *Precambrian Research*, **104**, 123-146.
- MONTENAT, C., RAMAHAVORY, L. & CROISILE, M. (1996) Tectonic and sedimentary evolution of the western Madagascan margin during the Jurassic in the Morondava Basin, Madagascar. *Bulletin-Centres-de-Recherches-Exploration-Production-Elf-Aquitaine*, **20**, 323-340.
- NICHOLS, G.J. & DAILY, M.C. (1989) Sedimentation in an intracratonic extensional basin: the Karoo of the Central Morondava Basin, Madagascar. *Geological Magazine*, **126**, 339-354.
- NOBLE, W.D., FOSTER, D.A. & GLEADOW, A.J.W. (1997) The post-Pan-African thermal and extensional history of crystalline basement rocks in eastern Tanzania. *Tectonophysics*, **275**, 331-350.
- PILI, E., RICARD, Y., LARDEAUX, J.-M. & SHEPPARD, S.M.F. (1997) Lithospheric shear zones and mantle-crust connections. *Tectonophysics*, **280**, 15-29.
- PIQUÉ, A. (1999) The geological evolution of Madagascar: An introduction. *Journal of African Earth Sciences*, **28**, 919-930.
- PIQUÉ, A., LAVILLE, E., BIGNOT, G., RABARIMANANA, M. & THOUIN, C. (1999) The initiation and development of the Morondava Basin [Madagascar] from the Late Carboniferous to the middle Jurassic: Sedimentary, palaeontological and structural data. *Journal of African Earth Sciences*, **28**, 931-948.

- RADKE, M., VRIEND, S.P. & RAMANAMPISOA, L.R. (2000) Alkyldibenzofurans in terrestrial rocks: Influence of organic facies and Maturation. *Geochimica et Cosmochimica Acta*, **64**, 275-286.
- RAMANAMPISOA, L. R., RADKE, M., SCHAEFER, R. G., LITTKE, R., RULKÖTTER, J. & HORSFIELD, B. (1990) Organic-geochemical characterisation of sediments from the Sakoa coalfield, Madagascar. *Organic Geochemistry*, **16**(Advances in Organic Geochemistry), 235-246.
- RATHORE, S.S., VENKATESAN, T. R. & SRIVASTAVA, R. K. (1999) Rb-Sr isotope dating of Neoproterozoic (Malani Group) magmatism from southwest Rajasthan, India: Evidence of younger Pan-African thermal event by  $^{40}\text{Ar}/^{39}\text{Ar}$  studies. *Gondwana Research*, **2**, 271-281.
- SCHANDELMEIER, H., BREMER, F. & HOLL, H. Kinematic of the Morondava rift basin, SW Madagascar - from shearzone controlled wrench tectonic to normal extension. *Journal of African earth sciences*, in press.
- SCOTESE, C.R., BOUCOT, A.J. & MCKERROW, W.S. (1998) Gondwanan palaeogeography and palaeoclimatology. *Journal of African Earth Sciences*, **28**, 99-114.
- SEWARD, D., GRUJIC, D. & SCHREURS, G. (1998) Exhumation history of the East Madagascar continental margin; inferences from apatite fission-track analysis. In: *Gondwana 10; event stratigraphy of Gondwana* (Ed. by Almond *et al.*), *Journal of African Earth Sciences*. pp. 176-178.
- SEWARD, D., GRUJIC, D. & SCHREURS, G. (1999) Exhumation history of Southern Madagascar as revealed by Zircon and Apatite Fission-Track Thermochronology. *Gondwana Research*, **2**, 353-354.
- SEWARD, D., GRUJIC, D. & SCHREURS, G. (2000) Post Pan-African Events in Madagascar: Inferences from Apatite Fission-Track Analysis. In: *9th International Conference on Fission Track Dating and Thermochronology* (Ed. by W.P. Noble, P.B. O'Sullivan and R.W. Brown). *Geological Society of Australia Abstract series*, **58**, 289.
- STOREY, M., MAHONEY, J. J., SAUNDERS, A. D., DUNCAN, R. A., KELLEY, S. P. & COFFIN, M. F. (1995) Timing of hot spot-related volcanism and the breakup of Madagascar and India. *Science*, **267**, 852-855.
- UHMANN, A. (1996). Sedimentologische und fazielle Entwicklung in Jura und Kreide im Morondava Becken (Südwest- Madagaskar), PhD Thesis University Berlin, Berlin, pp.
- VAN DER BEEK, P., MBEDE, E., ANDRIESSEN, P. & DELVAUX, D. (1998) Denudation history of the Malawi and Rukwa Rift flanks (East African Rift System) from apatite fission track thermochronology. *Journal of African Earth Sciences*, **26**, 363-385.
- VAN WIJK, J.W. & CLOETINGH, S.A.P.L (2002) Basin migration caused by slow lithospheric extension. *Earth and Planetary Science Letters*, **198**, 275-288.

WAGNER, G.A. & VAN DEN HAUTE, P. (1992) Fission-Track Dating. Ferdinand Enke Verlag, Stuttgart, 285 pp.

WAGNER, M., ALTHERR, R. & VAN DEN HAUTE, P. (1992) Apatite fission-track analysis of Kenyan basement rocks: constraints on the thermotectonic evolution of the Kenya dome. A reconnaissance study. *Tectonophysics*, **204**, 93-110.

WESCOTT, W. & DIGGENS, J.N. (1997) Depositional history and stratigraphical evolution of the Sakoa Group (Lower Karoo Supergroup) in the southern Morondava Basin, Madagascar. *Journal of African Earth Sciences*, **24**, 581-601.

WESCOTT, W. & DIGGENS, J.N. (1998) Depositional history and stratigraphical evolution of the Sakamena Group (Middle Karoo Supergroup) in the southern Morondava Basin, Madagascar. *Journal of African Earth Sciences*, **27**, 467-479.



## **Chapter 6**

### **Post collisional tectono-thermal evolution of Madagascar in a global tectonic setting**

## 1. Introduction

As outlined in chapter two, the far field stress regime caused by global plate kinematics mainly controls the subsequent evolution of an intracontinental rift system. During Late Palaeozoic to Early Mesozoic times, a global plate boundary reorganisation governed the onset of the Pangea break-up (Fig. 6.1). This break-up was probably accompanied by a reorganisation of the deep mantle convection system beneath Pangea, whereby the supercontinent possibly had an insulating effect (Ziegler, 1993; Nikishin et al., 2002).

The continental separation of Madagascar evolved over a period of ~200 Ma and is characterised by three main tectonic events:

- The Karoo rift is documented in the Late Carboniferous to Early Jurassic sedimentary rocks of the Morondava basin.
- The break-up between Madagascar and East Africa was guided by the Davie transform fault. A transform margin evolved along the southwest coast of the island and the Somali and Mozambique basins were opened (~165 Ma).
- The break-up between Madagascar and India occurred during Late Cretaceous times when the Mascarene basin was opened.

The interpreted thermochronological data from Madagascar give new information about thermo-tectonic processes related to the initial phase of the continental separation between Madagascar and East Africa, and about the basement exhumation dynamics during the time of the Karoo rift phase.

Combined titanite and apatite FT data from central and southern Madagascar give evidence that thermal activities occurred in the centre of the island up to ~100 Ma before the onset of the Karoo rifting. These data also indicate during Carboniferous times enhanced denudation along the north-south trending palaeo western margin, whereby denudation amounts in southern Madagascar ( $200\text{-}100\text{ mMa}^{-1}$ ) are higher than in central Madagascar ( $\sim 80\text{ mMa}^{-1}$ ). The spatial variations in the denudation dynamics are reflected by the thickness of the Morondava basin sediments, which decreases from south to north. Both observations support the assumption of a gradual rift progression from south to north (de Wit, 2003). Apatite FT data of most samples from the study area were influenced by the Late Carboniferous to Early Jurassic Karoo rift phase. Modelled T-t histories suggest during the Late Palaeozoic to Early Mesozoic rift phase a migration of highest denudation from west to east. Only samples from a narrow strip along the eastern coast are characterised by

Cretaceous apatite FT ages, which are related to enhanced denudation during and after the Madagascar-India break-up.

Following, a model for the subsequent continental separation of the island in a global kinematic scenario, based on FT and structural data from Madagascar, will be proposed.

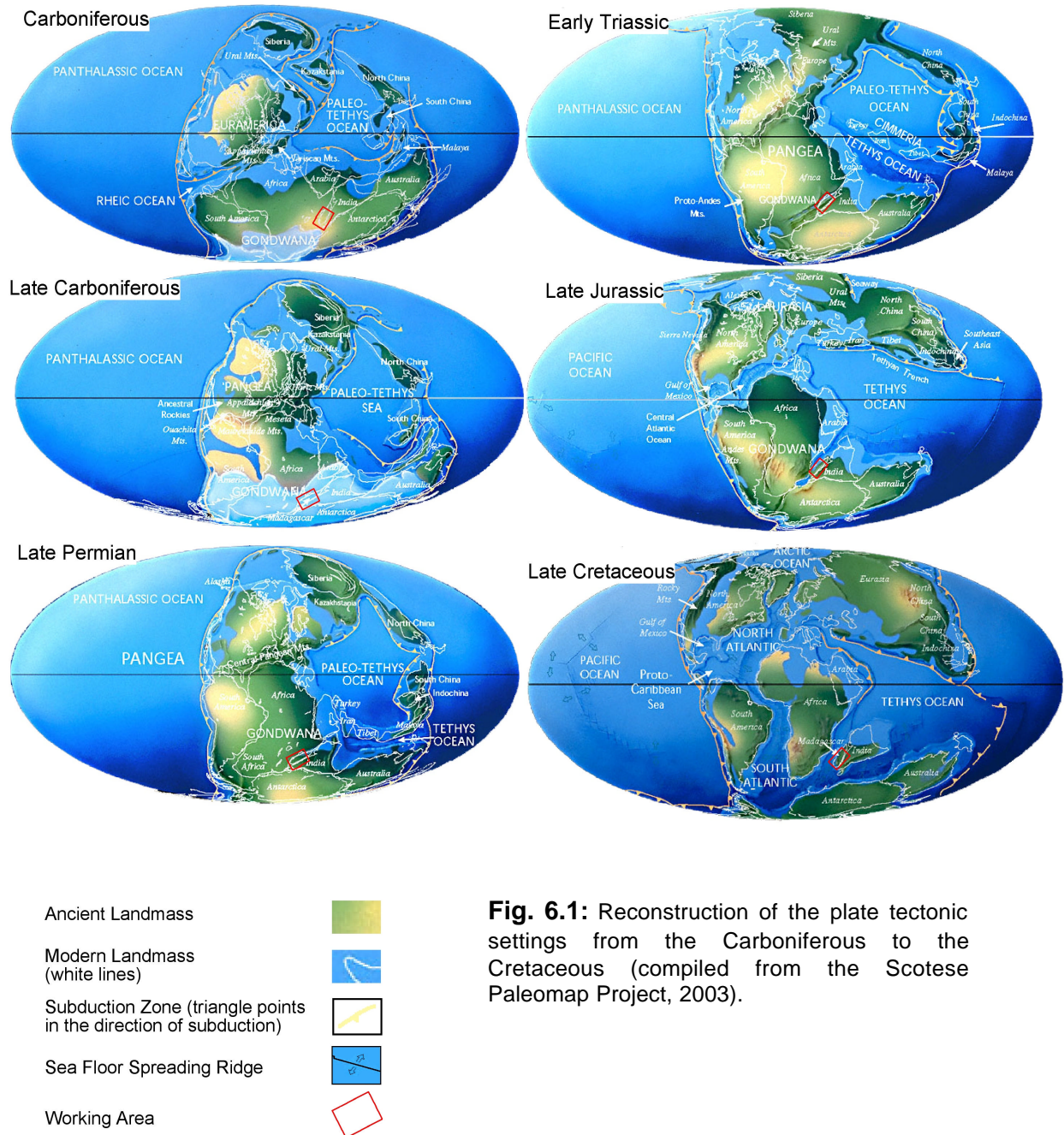


**Fig. 6.1:** Reconstruction of the plate tectonic settings from the Carboniferous to the Cretaceous (compiled from the Scotese Paleomap Project, 2003).

## 2. Thermal stage

During Late Devonian to earliest Carboniferous times the collision of Gondwana and Laurussia occurred, and the Variscan mountains consolidated during the Hercynian orogenic cycle. Subduction zones fringed most parts of Gondwana. Madagascar had a central position within the Gondwana sector of the Pangea supercontinent (Ziegler, 1992).

Combined titanite and apatite basement FT data from Madagascar suggest a phase of increased cooling in central Madagascar between ~420 Ma and ~360 Ma. Furthermore, during the Carboniferous several Late Neoproterozoic/Early Cambrian ductile high strain zones were reactivated, associated with thermal activities and/or accelerated exhumation (BetSZ, BRSZ, AGSZ, EDSZ).

What kind of process/processes could have caused the observed thermal activities and/or the enhanced exhumation?

In central Madagascar structural and petrographic evidences along the BetSZ (Collins et al., 2000) and the widespread occurrences of “stratoid granites” indicate a post Pan-African phase of extension (~630-550 Ma; Paquette and Nédélec, 1998; Collins et al., 2000). It is believed that the “stratoid granites” are related to a delamination of the lithospheric mantle at ~630 Ma (Paquette and Nédélec, 1998). The decoupling of lithosphere and the ascending hotter asthenospheric material can cause a strong crustal warming and rapid isostatic uplift. The estimated removal duration after lithospheric thickening vary between 10 Ma (Marotta et al., 1998) and a few hundreds of Ma (Buck and Töksi, 1983). Therefore, it could be possible that the observed thermal activities and the initial basin development are related to the suggested post-collisional delamination. But, further age constraints ( $^{40}\text{Ar}/^{39}\text{Ar}$  on biotite) of the “stratoid granites” revealed a post-extensional phase of reheating and rapid cooling during the 550-520 Ma interval (Meert et al., 2002). Furthermore, in southern Madagascar geochronological constraints indicate transpressional tectonics during the 530-500 Ma episode (Martelat et al., 2000). Meert et al. (2002) suggest that these thermal events are related to renewed collisional tectonism during the final stages of the Gondwana assembly.

The present crustal thickness of Madagascar is inhomogeneous and ranges between ~35 km and 40 km (Rechenmann, 1982; Fournon and Roussel, 1994). Figure 6.2 shows a gravity map of Madagascar (Pili et al., 1997). Madagascar is characterised by an average Bouguer gravity value of -30 mGal. In southwest Madagascar positive anomalies occur along the western margin of the basement (EDSZ and ASZ: 50 mGal) and negative anomalies are associated with the eastern margin of the Morondava basin (-60 mGal). Pili et al. (1997) suggest that the positive anomalies are related to an upwelling mantle beneath shear zones during Jurassic and Cretaceous times, although the timing of the upwelling was not dated.

Carboniferous and Triassic apatite FT ages from samples located within the BRSZ and the ASZ do not support the assumed timing of the mantle upwelling.

Another question arises about the cause of the negative anomalies along the eastern margin of the Morondava basin? In general, negative gravity anomalies are related to mass deficits of a sedimentary basin, an upwelling asthenosphere or a thickened crust. The thickness of the sedimentary cover increases from the eastern margin towards the centre of the Morondava basin. Consequently, it would be expected that the gravity values decrease in the same direction, but the gravity data from the Morondava basin show a reverse trend. Negative anomalies occur along the eastern margin, while towards the centre of the basin the gravity values increase (see white box Fig. 6.2). Additionally, along the eastern margin of the island negative anomalies are observed along areas without sedimentary cover.

Published gravity data from East Africa (Tesha et al., 1997) suggest a by up to 25 km thickened crust in the region around Precambrian sutures. The thickening of the crust is related to the Pan-African development of the Mozambique belt. Correlation of gravity data and the location of the Tanzania rift system reflect that the Cenozoic rift structures most probably developed within zones of thickened crust (Tesha et al., 1997; Nyblade and Pollack, 1992).

In the Madagascar rift model an initial thickened crust (up to a few kilometres) was adopted as indicated by the bouguer gravity data from Madagascar, the observations along the Tanzania rift system and the lack of Palaeozoic volcanic rocks. In response to isostatic compensation, a thickened crust will have a deeper and hence a hot root of continental crust. The model suggests heat transfer along pre-existing ductile high strain zones. This predicted process has been documented in this study using FT analyses from samples of shear zones (Chapter three and four). As a consequence, softening of the continental crust along defined directions occurred, predetermined by the former zones of weakness.

This process, which probably initiated the Karoo rifting was suggested but not documented by Wopfner (2002). It was termed as, self-induced Pangea heat anomaly with a peak phase at ~320 Ma, coinciding with the Hercynian orogeny (Wopfner, 2002). FT data indicate that multiple processes of heat loss started at ~420 Ma, approximately 100 Ma after the last stage of the Pan-African orogen, and occurred temporally until the early Karoo rift phase at ~260 Ma. If these thermal activities are associated with uplift of several tectonic blocks remains unresolved, but the lack of Early Carboniferous sedimentary record in the interior of Gondwana suggests uplift and erosion during this time (Visser and Praekelt, 1996). Additionally, oldest reworked detrital FT ages from the Late Permian and Jurassic strata document an erosion of the crustal section, which passed the 100 °C isotherm between ~460 Ma and ~400 Ma (Chapter five).

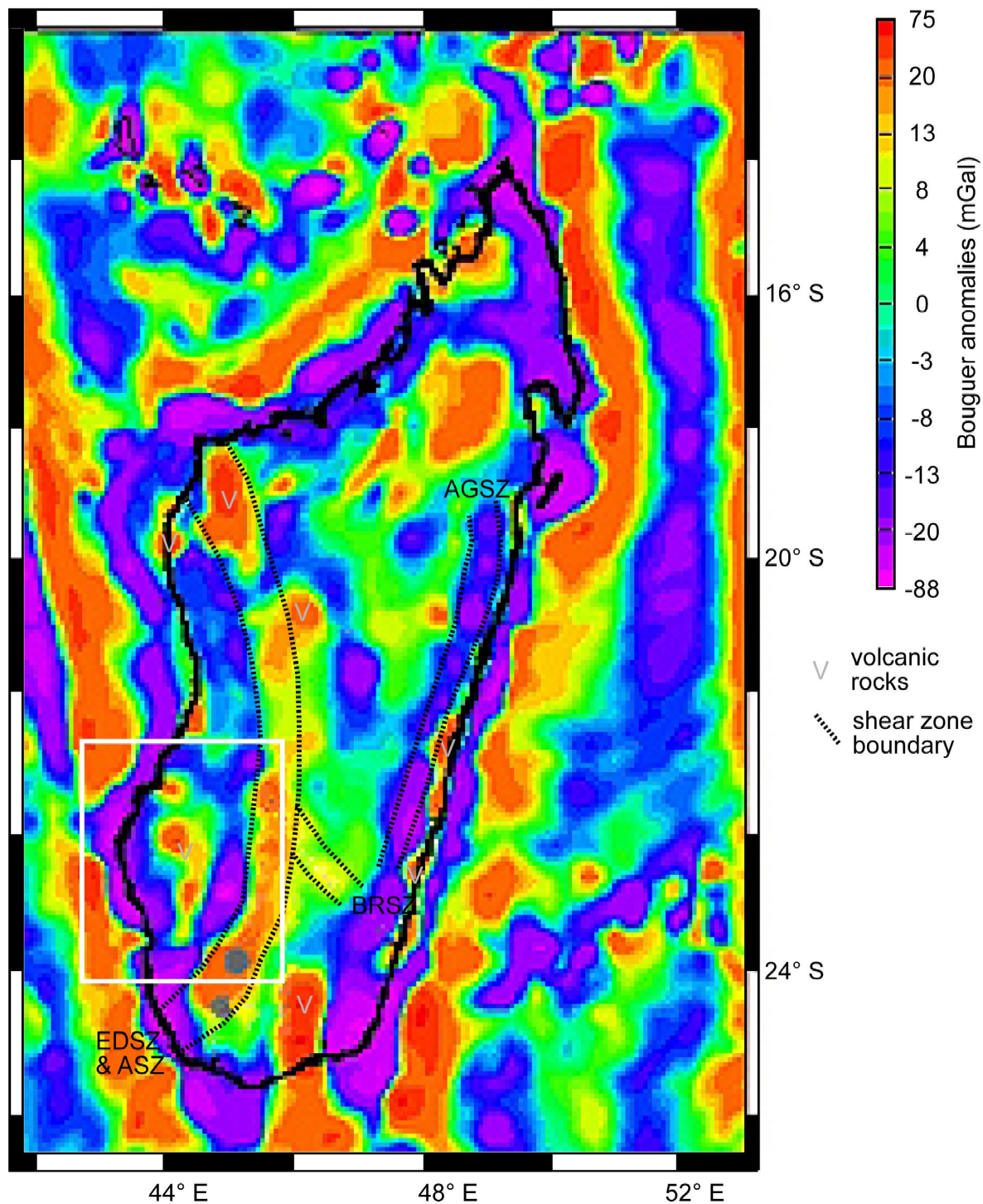


**Fig. 6.2:** Gravity map of Madagascar (Pili et al., 1997). The gravity anomalies follow the trend of Late Neoproterozoic/Early Cambrian ductile high strain zones like the EDSZ and ASZ, AGSZ and the BRSZ.

The Bouguer anomalies suggest a continuation of the EDSZ and ASZ underneath the sedimentary cover in the northern Morondava basin. Note the negative anomalies along the eastern margin of the Morondava basin, and along the AGSZ. The linear anomaly along the south-western margin of the island corresponds to the Davie fracture zone. The white box indicates the area within and around the southern Morondava basin.

### 3. Wrench stage

From the Carboniferous to Early Permian times a plate boundary reorganisation controlled the onset of Pangea break-up. The Variscan and Appalachian consolidations between Gondwana and Laurussia came to an end. Pangea was still fringed by subduction zones along the Panthalassan and Palaeotethys margins (Fig. 6.1) but it showed signs of instabilities (Ziegler, 1990, Nikishin et al., 2002). Gondwana itself was subdivided into large blocks along mega-shear systems, which experienced rotational motions at different angular speeds. In the interior of the supercontinent, fault-controlled rifts were opened along shear zones. According to Visser and Praekelt (1998) the Permo-Carboniferous of Gondwana is characterised by the development of coastal and inboard basin systems that are caused by lateral crustal movements, as well as by crustal sagging related to heat loss. In contrast to these suggestions, FT data from southern and central Madagascar indicate bulging along the palaeo western basement margin following previous thermal activities. This could have been caused by density loss of a crustal block that was exposed to thermal penetration. Delayed isostatic compensation could have caused an uplift of this crustal section.

The vertical separation of the different basement blocks in Madagascar was triggered by the far field compressional stress, which also led to the subsequent opening of pull apart basins between the active strike slip faults (Fig. 6.3) during the Late Carboniferous to the latest Permian (Schandelmeier et al., in press). The EDSZ and ASZ bound the pull apart basins of southern Madagascar. FT data from several shear zones in Madagascar indicate thermal activities pre-dating the opening of the Morondava basin at the end of Carboniferous. Probably, an initial thermal weakening of the ductile high strain zones amplified the sensitivity for mechanical load. Thus, the shear zones predetermined the location for the initial opening of the Morondava basin.

Within the pull apart basins the oldest Karoo sedimentary rocks (Sakoa Group) were deposited. Mineralogy and maturity of the Sakoa detritus suggest a relative near source (Uhmann, 1996). This argues for a local narrow area of bulging along the north-south trending pull apart basins.

This local model for the rift initiation corresponds with the assumed inversion tectonics along the southern Trans-African Shear System (de Wit et al., 1995) which caused basin formation within uplifted mid-Carboniferous belts (Visser and Praekelt, 1996).

#### 4. Rift stage

During the Late Permian to Middle Triassic (Fig. 6.1) a reorganisation of plate boundaries governed the break-up of Gondwana. Active orogenic belts encircled Pangea with the exception of the north-eastern margin of Gondwana. Here divergent stress led to the separation of a number of terrain's (central and eastern Iranian and the Tibet blocks; Ziegler, 1992). From the Late Permian to Early Jurassic increased compressional stress within the supercontinent caused crustal uplift (Visser and Praekelt, 1998). Despite the far field compressional stress, coevally rifting comes to the maximum stage. During this time a new stress tensor must have governed the proceeding rift development. This is indicated by a relative northward movement of Madagascar (de Wit et al., 1995) and a break in sedimentation especially along north-west trending Mesozoic East African rift basins (Visser and Praekelt, 1996, Delvaux, 2001). Moreover, structural data from southern Madagascar indicate that during the Early to Middle Triassic the rift-style changed from a strike-slip controlled process to a normal extension accompanied by the formation of half grabens (Schandelmeier et al., in press). Modelled basement FT data indicate that cooling at this time was not restricted to the areas within/around the shear zones, in contrast to the initial stages. It rather affected the whole basement of southern and central Madagascar. The FT data imply a more or less gradual eastward migration of highest denudation and an associated migration of the source area from the rift shoulder towards the east (Fig. 6.3).

#### 5. Passive margin stage

Subduction along the northern Tethys margin still lasted during the Jurassic (Fig. 6.1). Mantle plume activities penetrated Gondwana during Middle Jurassic times. In South Africa the Bouvet-Karoo mantle plume led to the extrusion of flood basalts at ~180 Ma (i.e. Duncan et al., 1997). This possibly marks a change in the mantle convection system, as mentioned by Visser and Praekelt (1998). Noticeable, approximately 20 Ma after the plume activity oceanic seafloor spreading resulted in the opening of the Somali and Mozambique basins (Fig. 6.4) and caused the development of oceanic crust between Madagascar and East Africa. Basement FT data show that only the south-western part of the continental margin close to the Davie fracture zone was influenced by higher denudation of up to ~4 km crustal section. Furthermore, detrital FT data from south-west Madagascar indicate that Karoo rift related sedimentary units were reworked and redeposited within the post Karoo Jurassic strata north-west of the source during the transform margin evolution.

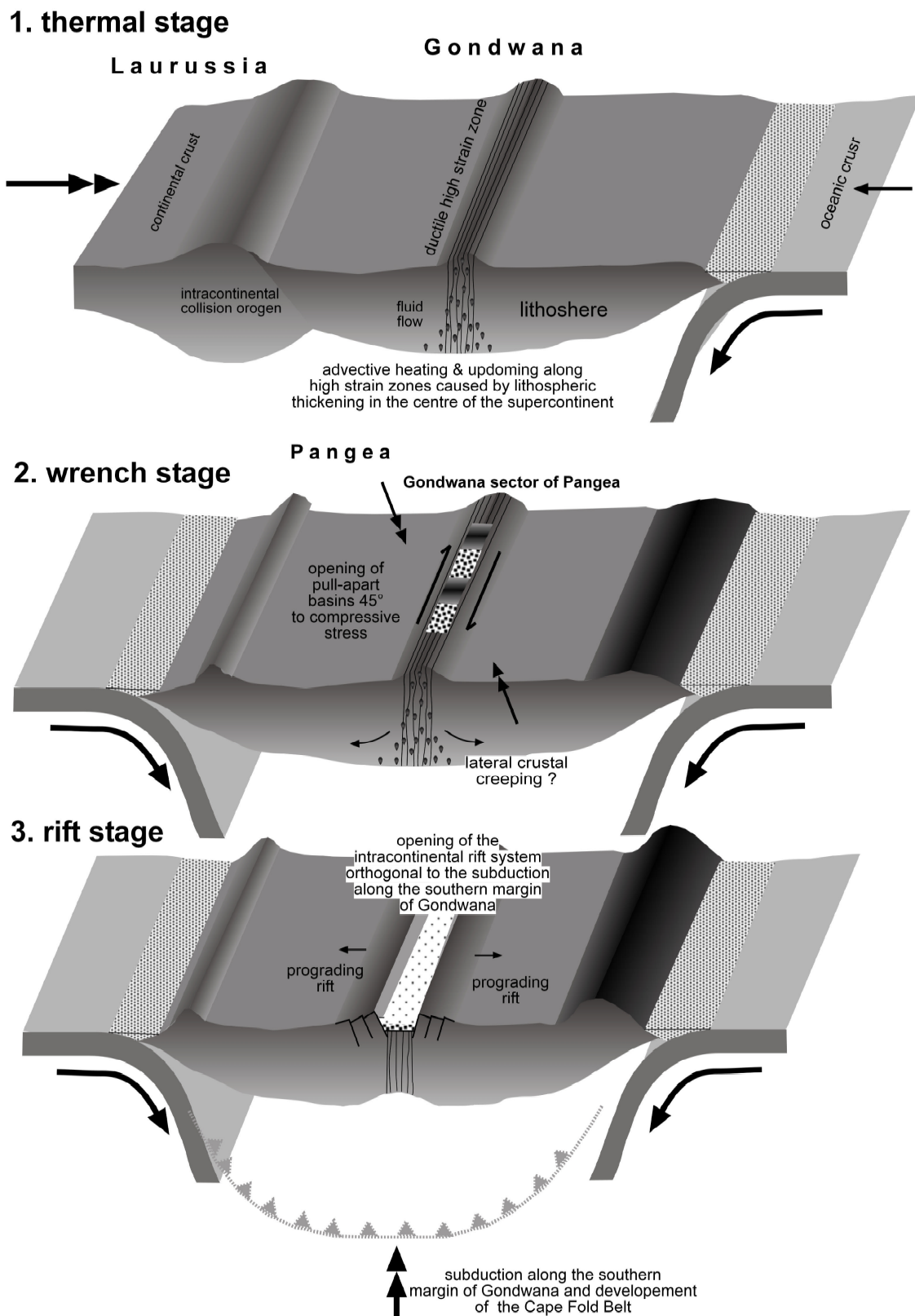


**Fig. 6.3:** Simplified schematic model of the Karoo rift initiation in Madagascar related to an initial thickened crust (not to scale).

During the **thermal stage** hot fluids penetrated ductile high strain zones. Probably elongated areas along these zones were bulged. Related to a NW-SE compressional far field stress regime along these weakened parts pull apart basins were opened (**wrench stage**). A plate boundary reorganisation and a new far field stress tensor led to main rift evolution during Late Permian to Late Jurassic times (**rift stage**).

During the Late Cretaceous, subduction along the northern Tethys margin provided the stress for the Madagascar-India separation. Strike slip motion along ductile high strain zones at the eastern margin of Madagascar, accompanied with Marion hot spot activities led to the rapid northward motion of India and to the development of the eastern continental margin of Madagascar. Basement titanite FT and structural data from the eastern coast indicate a minor tectono-thermal influence of the Marion hot spot during the Madagascar-India separation. Furthermore, the shape of the eastern margin points to a mainly strike slip related opening of the Mascarene basin. Apatite FT data indicate that the development of the north-south trending Ankay graben (Chapter 3, Fig. 3.4) at the western margin of the AGSZ was most probably coupled with the Madagascar-India break-up.

## **6. Comparison with the Mesozoic East African rift system**

The Mesozoic East African rift system is the western analogue of the Madagascar rift (Fig. 6.4). The Gondwana rift system developed in the foreland of the Gondwana orogen during Late Carboniferous to Early Triassic times. The progression of the Mesozoic East African rift system can be related to compressional intraplate stresses emanating from the South African-Antarctic segment of the proto-Cordillera-Gondwana orogen and from the northern Neo-Tethys margin of the Gondwana supercontinent (cf. Storey et al., 1992; Delvaux, 2001; Nikishin et al., 2002). Examples for repeatedly reactivated structures are known from East Africa along the Ubende Shear Belt at the eastern margin of the Tanzanian craton (Delvaux, 2001). Two sets of basins developed in East Africa, in response to the compressional and transpressional deformations, during the Late Carboniferous to the Middle Triassic. These are mainly northwest-southeast trending basins, like the Tanaganyika-Rukwa-Malavi zone (Fig. 6.4). North-east trending basins are e.g. the Luangwa basin in Zambia (Nyambe and Utting, 1997), the Selous basins in East Tanzania (Wopfner and Kaaya, 1992), and the Tanga basin in East Kenya (Fig. 6.4). Sedimentation in the northwest-southeast trending basins ended during the Late Permian due to north-south compression, and to regional uplift along the future zone of crustal failure between West- and East-Gondwana. In contrast, the northeast-southwest trending basins contain a more complete stratigraphic succession ranging from Late Carboniferous up to Early Jurassic strata (Delvaux, 2001). In Madagascar, the Morondava basin correlates with the northeast-southwest trending East African basins, whereas the Bongolava-Ranotsara graben corresponds with the northwest-southeast trending basins. The sedimentary record in the Morondava basins ranges from Late Carboniferous to recent successions, whereas along the Bongolava-Ranotsara graben undated sedimentary units were deposited. Apatite FT data indicate a Permian age of active faults along the graben.

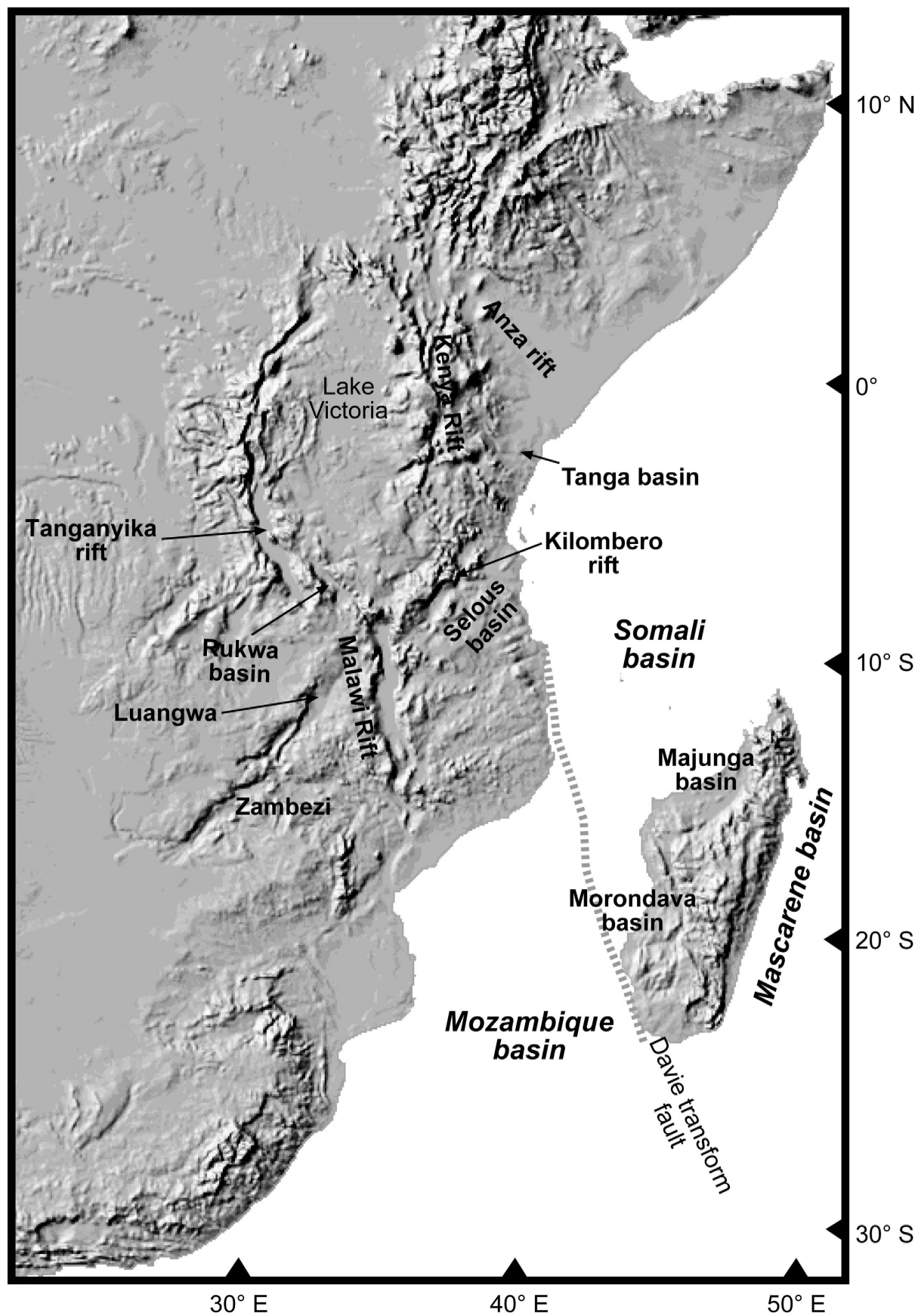


**Fig. 6.4:** Topographic map of the East African Rift system (from <http://edcaac.usgs.gov/gtopo30>) with some major basins and rifts.

## 6.1 Related geochronological data from East Africa

The FT data from Madagascar provide a unique insight in the earliest rift evolution. Most apatite FT data from East Africa are affected by temperatures  $>110^{\circ}\text{C}$  related to the Cretaceous, Tertiary and Cenozoic rift evolution. Therefore, the Mesozoic rift development is not recorded by low-temperature thermochronological data. However, some geochronological data sensitive to higher closure temperatures give evidence for the earliest rift evolution in East Africa. Laser  $^{40}\text{Ar}/^{39}\text{Ar}$  data of pseudotachylites from the Kenyan part of the Late Proterozoic/Early Palaeozoic Mozambique Belt (Tambach Fault Zone) gave a formation age of  $\sim 400$  Ma. Sherlock and Hetzel (2001) related these ages to the earliest formation of the Kenya rift. Hagen et al. (2001) detected a post-metamorphic cooling event at  $\sim 420$  Ma indicated by  $^{40}\text{Ar}/^{39}\text{Ar}$  ages derived from detrital K-feldspar of the Kilombero rift in Tanzania. Bojar et al. (2002) report titanite and zircon FT ages ranging between  $\sim 410$  Ma to  $\sim 315$  Ma from the Arabian Nubian Shield. They suggest that these data represent an intraplate thermo-tectonic episode during Late Devonian to Early Carboniferous times, which is related to the Gondwana Laurussia collision. These ages are comparable with the observed Devonian to Early Carboniferous thermochronological ages in Madagascar and suggest a wide-ranging thermal event during this epoch. Moreover, some apatite FT data support this assumption. The oldest apatite FT data from East Africa were dated in south-west Kenya and range between  $\sim 320$  Ma and  $\sim 290$  Ma. Relatively long MTL vary between  $14.00\ \mu\text{m}$  and  $12.75\ \mu\text{m}$ , and argue for a cooling to below  $60^{\circ}\text{C}$  at around 310 Ma (Wagner et al., 1992). However, most apatite FT data from Kenya are related to later rift episodes monitoring rapid cooling and denudation, in Early Cretaceous (130-110 Ma), Late Cretaceous-Paleocene (70-60 Ma), and possibly Miocene ( $\sim 10$  Ma) times (Forster and Gleadow, 1992).

Using apatite FT data a Triassic and a Late Jurassic cooling phase were detected along the Malawi and Rukwa rifts by van der Beek et al. (1998). Further to the east (east of the Selous and Mikumi basin) apatite FT ages reported by Noble et al. (1997) indicate cooling events during Early Cretaceous and Late Cretaceous-Early Palaeogene and Late Eocene-Early Oligocene times. Here, apatite FT data give no evidences about the initial opening of the Karoo related basins.

The FT data from the East African rift system provide only sparse information about cooling or denudation that are related to the initial stage of the Late Palaeozoic-Mesozoic rifting event (for detailed FT data see chapter 5.4.1). In contrast to Madagascar, the apatite FT fingerprint of the initial East African rift phase was erased from later tectonic activities. The onset of the Gondwana fragmentation is only spatially preserved by a few low-temperature

geochronological data of localities far west of the present East African continental margin, and away from younger rifts.

### References:

- Bojar, A.-V., Fritz, H., Kargl, S., Unzog, W., 2002. Phanerozoic tectonothermal history of the Arabian-Nubian shield in the Eastern Desert of Egypt: evidence from fission track and paleostress data. *Journal of African Earth Sciences*, 34: 191-202.
- Buck, W., Tosöz, M., 1983. Thermal effects of continental collisions: thickening a variable viscosity lithosphere. *Tectonophysics*, 100, 53-69.
- Collins, A.S., Razakamanana, T., Windley, B.F., 2000. Neoproterozoic extensional detachment in central Madagascar; implications for the collapse of the East African Orogen. *Geological Magazine* 137, 39-51.
- Delvaux, D., 2001. Tectonic and palaeostress evolution of the Tanganyika-Rukwa-Malawi rift segment, East Africa Rift System. In: P.A. Ziegler, A.H.F. Robertson, S. Crasquin-Soleau (eds) *Peri-Tethys Memoir 6: Peri-Tethyan Rift/Wrench Basins and Passive Margins*. *Mém. Mus. natn. Hist. nat.*, 186, 545-566.
- De Wit, M.J. 2003. Madagascar: Heads It's a Continent, Tails It's an Island. *Annu. Rev. Earth Planet. Sci.*, 31, 213-248.
- Duncan, R.A., Hooper, P.R., Rehacek, J., Marsh, J.S., Duncan, A.R., 1997. The timing and duration of the Karoo igneous event, southern Gondwana. *Journal of Geophysical Research*, 102, 18127-18138.
- Foster, D.A., Gleadow, A.J.W., 1992. The morphotectonic evolution of rift-margin mountains in central Kenya: constraints from apatite fission-track thermochronology. *Earth and Planetary Science Letters*, 113(1-2): 157-171.
- Fournon, J.P., Roussel, J., 1994. Imaging of the Moho depth in Madagascar through the inversion of gravity data; geodynamic implications. *Terra Nova* 6, 512-519.
- Hagen, E., Kelley, S.P., Dypvik, H., Nilsen, O., Kjølhamar, B., 2001. Direct dating of authigenic K-feldspar overgrowths from the Kilombero Rift of Tanzania. *Journal of Geological Society, London*, 158, 801-807.
- Marotta, A., Fernández, M., Sabadini, R., 1998. Mantle unrooting in collisional settings. *Tectonophysics*, 296, 31-46.
- Martelat, J.E., Lardeaux, J.M., Nicollet, C., Rakotondrazafy, R., 2000. Strain pattern and late Precambrian deformation history in southern Madagascar. *Precambrian Research* 102, 1-20.

- Meert, J.G., Nédélec, A., Hall, C., 2002. The stratoid granites of central Madagascar: paleomagnetism and further age constraints on neoproterozoic deformation. *Precambrian Research* 120, 101-129.
- Nikishin, A.M., Ziegler, P.A., Abbott, D., Brunet, M.-F., Cloetingh, S., 2002. Permo-Triassic magmatism and rifting in Eurasia: implications for mantle plumes and mantle dynamics. *Tectonophysics*, 351, 3-39.
- Noble, W.D., Foster, D.A., Gleadow, A.J.W., 1997. The post-Pan-African thermal and extensional history of crystalline basement rocks in eastern Tanzania. *Tectonophysics*, 275, 331-350.
- Nyambe, I.A., Utting, J., 1997. Stratigraphy and palynostratigraphy, Karoo Supergroup (Permian and Triassic), mid-Zambezi Valley, southern Zambia. *Journal of African Earth Sciences*, 24, 563-584.
- Paquette, J.L.; Nédélec, A., 1998. A new insight into Pan-African tectonics in the east-west Gondwana collision zone by U-Pb zircon dating of granites from central Madagascar. *Earth Planet. Sci. Lett.*, 155, 45-56.
- Rechenmann, J., 1982. Gravimetrie de Madagascar. Interpretation et relation avec la geologie. *OSTROM, Geophys.* 18, 3-128.
- Schandelmeier, H., Bremer, F., Holl, H.-G., in press. Kinematic evolution of the Morondava rift basin of SW Madagascar - from shear zone controlled wrench tectonics to normal extension. *Journal of African Earth Sciences*.
- Scotese, C.R., 2003 Paleomap Project. <http://www.scotese.com>.
- Sherlock, S.C., Hetzel, R., 2001. A laser-probe  $^{40}\text{Ar}/^{39}\text{Ar}$  study of pseudotachylite from the Tambach Fault Zone, Kenya: direct isotopic dating of brittle faults. *Journal of Structural Geology*, 23, 33-44.
- Tesha, A.L., Nyblade, A.A., Keller, G.R., Doser, D.I., 1997. Rift localization in suture-thickened crust: evidence from Bouguer gravity anomalies in northeastern Tanzania, East Africa. *Tectonophysics*, 278, 315-328.
- Uhmann, A., 1996. Sedimentologische und fazielle Entwicklung in Jura und Kreide im Morondava Becken (Südwest- Madagaskar), PhD Thesis Berlin.
- Van der Beek, P., Mbede, E., Andriessen, P., Delvaux, D., 1998. Denudation history of the Malawi and Rukwa Rift flanks (East African Rift System) from apatite fission track thermochronology. *Journal of African Earth Sciences*, 26, 363-385.
- Visser, J.N.J., Praekelt, H.E., 1996. Subduction, mega-shear systems and late Palaeozoic basin development in the African segment of Gondwana. *Geologische Rundschau*, 85, 632-646.
- Visser, J.N.J., Praekelt, H.E., 1998. Late Palaeozoic crustal block rotations within the Gondwana sector of Pangea. *Tectonophysics*, 287, 201-212.

- Wagner, M., Altherr, R., Van den haute, P., 1992. Apatite fission-track analysis of Kenyan basement rocks: constraints on the thermotectonic evolution of the Kenya dome. A reconnaissance study. *Tectonophysics*, 204, 93-110.
- Wopfner, H., Kaaya, C.Z., 1991. Stratigraphy and morhotectonics of Karoo deposits of the northern Selous Basin, Tanzania. *Geological Magazine*, 128, 319-334.
- Wopfner, H., 2002. Tectonic and climatic events controlling deposition in Tanzanian Karoo basins. *Journal of African Earth Sciences*, 34, 167-177.
- Ziegler, P.A., 1993. Plate-moving mechanism: their relative importance. *Journal of the Geological Society, London*, 150, 927-940.
- Ziegler, P.A., Cloethingh, S., van Wees, J.-D., 1995. Dynamics of intra-plate compressional deformation: the Alpine foreland and other examples. *Tectonophysics*, 252, 7-59.



## **Appendix**

### **Equations, parameters and statistics**

## A1 Sampling and preparation

Samples were collected in central and southern Madagascar. The sample location was determined using a global positioning system (GPS), and geological and topographic maps with different scales (1:2.000.000 to 1:500.000). The elevations were measured using GPS, and a barometric altimeter with an estimated error of  $\pm 50$  m. Samples were prepared following conventional techniques with different equipment and chemicals (see Fig. A.1a). The prepared mounts, age standards and standard glasses were packed for irradiation in a defined order to monitor the neutron fluence of the reactor and to allow an exact determination of  $r_d$  for every mount/sample (Fig. A.1b).

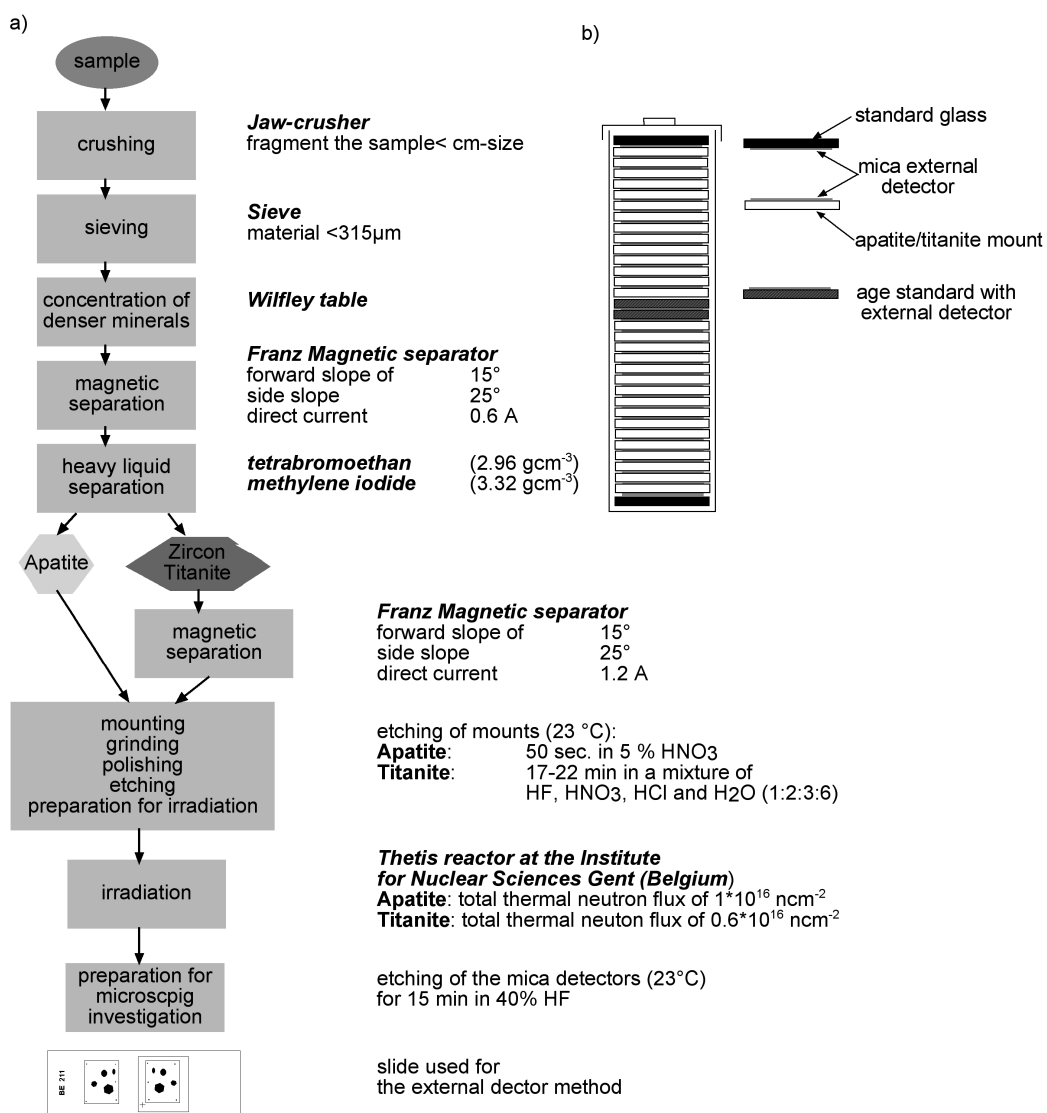


**Fig. A.1:** a) Flow chart of titanite and apatite separation and preparation. b) Package of samples in a polyethylene can. One IRMM-540 standard glass was packed at the top and one at the bottom of the pile to monitor the thermal fluence of the reactor. The standard glass external detectors were counted to determine the  $N_d$  and  $\rho_d$  values. Flux gradients were assumed to be linear and  $\rho_d$  values were calculated for every mount.

## A 2 Technical equipment, software, track counting and measurement

- ZEISS Axioplan microscope connected with an Apple Macintosh LC II™ computer
- CalComp Drawing Board II™ with a 16-button cursor
- Automated Kinetek™ scanning stage
- Drawing tube
- “FT-stage” software (Dumitru, 1993)
- TRACKKEY software (Dunkl, 2002)
- MONTE TRAX software (Gallagher, 1995)
- POPSHARE software (Dunkl, 2003)

The counting of fission tracks was carried out in transmitted light with a total magnification of 1250x. All samples were dated by the external detector method, using a Zeta calibration factor (Hurford and Green, 1983) and all tracks were counted under the same conditions. If possible, twenty or more grains were dated, by counting identical areas on the mount and its print. The dosimeter glass detectors were counted under the same conditions to determine  $r_d$ .

Confined tracks were measured parallel to the C-axis by digitising the track ends using the drawing tube. All track lengths were measured in transmitted and reflected light with a total magnification of 2000x.

## A 3 Zeta calibration

The personal Zeta calibration factor was established by counting age standards of known isotopic ages. To calibrate the apatite Zeta three different age standards of three different irradiation's (HB 025-027) were used. In total, the weighted mean Zeta of  $333 \pm 9$  was calculated by six single Zeta factors (see Tab. A.1). Hereby, two of the qualitative best standards from every age standard and irradiation were used. The neutron fluence of the reactor was monitored by the IRMM-540 (Institute for Reference Materials and Measurements) dosimeter glass with a uranium content of  $13.9 \pm 0.5$  ppm.

For the titanite Zeta calibration only the Mount Dromedary age standard was available. The neutron fluence was monitored by CN2 (Corning Glass Inc.) glass with a uranium concentration of ~38 ppm.

<b>Age standard (isotopic age)</b>	<b>Irradiation</b>	<b>(N<sub>s</sub>)</b>	<b>(N<sub>i</sub>)</b>	<b>(N<sub>d</sub>)</b>	<b>Zeta</b>
<b>Mineral</b>	<b>Monitor</b>	<b>r<sub>s</sub>[x10<sup>5</sup>cm<sup>-2</sup>]</b>	<b>r<sub>i</sub>[x10<sup>5</sup>cm<sup>-2</sup>]</b>	<b>r<sub>d</sub>[x10<sup>5</sup>cm<sup>-2</sup>]</b>	
Durango (31.4±0.6 Ma <sup>*</sup> ) <i>Apatite</i>	HB-025 IRMM-540	192 1.173	1764 10.779	7318 15.97	362±28
Fish Canyon (27.8±0.2 Ma <sup>**</sup> ) <i>Apatite</i>	HB-025 IRMM-540	146 1.799	1430 17.621	7318 14.94	349±30
Durango <i>Apatite</i>	HB-026 IRMM-540	147 1.273	1174 10.17	7569 15.65	336±24
Mount Dromedary (98.8±0.6 Ma <sup>***</sup> ) <i>Apatite</i>	HB-026 IRMM-540	357 9.808	900 24.76	7569 15.65	321±14
Fish Canyon <i>Apatite</i>	HB-027 IRMM-540	129 1.603	1244 15.457	7400 15.38	351±33
Mount Dromedary <i>Apatite</i>	HB-027 IRMM-540	357 9.808	900 24.726	7400 15.41	326±21
Mount Dromedary <i>Titanite</i>	HB-030 CN-2	2937 44.775	4075 62.123	15914 22.25	<b>124±3</b>

**Tab. A.1:** Age standards employed for the Zeta calibration. The used apatite Zeta calibration factor of 333±9 is the weighted mean of six single Zeta calibration factors.

\* K-Ar McDowell and Keizer, 1977

\*\* <sup>40</sup>Ar/<sup>39</sup>Ar biotite Hurford and Hammerschidt, 1985

\*\*\* Rb-Sr, biotite Williams et al., 1982

The single Zeta calibration factors were calculated using equation one.

$$z = \frac{1}{I_t} [\exp(t_{std} I_t) - 1] \times \left( \frac{r_i}{g r_s} \right) \times \left( \frac{1}{r_d} \right) \quad [1]$$

#### A4 Fission track age calculation and statistics

The fission track method is based on the decay of a naturally radioactive parent to stable daughter atom. The parent/daughter isotopic concentration is measured by counting the area densities ( $r_{d,i,s}$ ) of chemical enlarged induced ( $N_i$ , related to the induced decay of <sup>235</sup>U) and spontaneous ( $N_s$ , related to the decay of <sup>238</sup>U) fission tracks. Based on a constant <sup>235</sup>U/<sup>238</sup>U ratio and nuclear fission rate an apparent fission track age of a mineral of interest (usually titanite, zircon and apatite) can be calculated from the related ratio of induced to spontaneous track densities.

Fission track ages were calculated using equation two:

$$t = \frac{1}{I_t} \ln [1 + I_t \times z \times r_{RATIO} \times g \times r_d] \quad [2]$$

The *pooled age* ( $t_p$ ) was calculated using the ratio ( $r_{RATIO}$ ):

$$r_{RATIO} = \frac{\sum N_s}{\sum N_i}$$

The *central age* ( $t_c$ ) is the weighted mean of the log normal distribution of single grain ages.

The ratio for the *central age* is determined after 20 iterations (Galbraight and Laslett, 1993):

weighted age (I)

$$r_{RATIO} = \frac{\sum w_j r_{sj}}{\sum w_j r_{ij}}$$

weighted age (II) ....

$$r_{RATIO} = \frac{\sum w_j \left( \frac{r_s}{r_i} \right)}{\sum w_j}$$

where:

$$w_j = \frac{1}{\sqrt{\left( \frac{1}{N_s} \right)_j + \left( \frac{1}{N_i} \right)_j}}$$

The *standard errors* were calculated applying the equations three to five:

one sigma error Zeta:

$$s(z) = z \times \sqrt{\left\{ \frac{1}{N_s} + \frac{1}{N_i} + \frac{1}{N_d} + \left[ \frac{se(t_{std})}{t_{std}} \right]^2 \right\}} \quad [3]$$

one sigma error pooled age:

$$s(t_p) = t_p \times \sqrt{\left\{ \frac{1}{N_s} + \frac{1}{N_i} + \frac{1}{N_d} + \left[ \frac{se(z)}{z} \right]^2 \right\}} \quad [4]$$

one sigma error central age:

$$s(t_c) = t_c \times \sqrt{\left\{ \frac{1}{h^2 (1-h)^2 \sum_{j=1}^n w_j} + \frac{1}{N_d} + \left[ \frac{se(z)}{z} \right]^2 \right\}} \quad [5]$$

whereby:

$$\frac{h}{(1-h)} = \frac{r_s}{r_i} \text{ after 20 iterations}$$

The distribution of single grain ages is numerically evaluated using the *chi-square* ( $c^2$ ) test.

The  $c^2$ -test is failed (because the range of the single grain ages will be greater than expected for a Poissonian distribution) if the  $c^2$ -probability is less than 5%. In the case of a failed  $c^2$  - test the grains belong to multiple age populations and the central age is given.

$$c^2 = \sum_{j=1}^n \frac{(N_{sj} - \bar{N}_{sj})^2}{\bar{N}_{sj}} + \sum_{j=1}^n \frac{(N_{ij} - \bar{N}_{ij})^2}{\bar{N}_{ij}} \quad [6]$$

where:

$$\bar{N}_{sj} = \frac{N_s}{N_s + N_i} (N_{sj} + N_{ij})$$

$$\bar{N}_{ij} = \frac{i_s}{N_s + N_i} (N_{sj} + N_{ij})$$

The *standard deviation* of the single measurements were calculated following equation seven:

$$SD = \sqrt{\frac{1}{n-1} \sum_{i=1}^n (x_i - \langle x \rangle)^2} \quad [7] \text{ with the arithmetic mean } \langle x \rangle = \frac{1}{n} \sum_{i=1}^n x_i$$

The most probable value of a measured quantity is the *weighted mean* of the observation.

$$\bar{x}_w = \frac{\sum_{j=1}^j x_j / SD_j^2}{\sum_{j=1}^j 1 / SD_j^2} \quad [8]$$

In chapter 5 statistic results obtained from the program POPSHARE were presented. The software is based on the SIMPLEX algorithm, which is one of the best known optimisation algorithm to solve the linear programming problem (*cf.* Cserepes, 1989). The program gives four statistical fits for the age populations, whereby two are related to the weighted single grain ages (see equation 8):

*Root mean square (RMS):*

$$RMS(x) = \sqrt{\langle x^2 \rangle} \quad [9]$$

The *Kolmogorov-Smirnov test* (Press et al., 1996) is used to decide if a sample comes from a population with a specific distribution. The K-S test is defined for two samples by their empirical cumulative distributions  $S_{N1}(x)$  and  $S_{N2}(x)$ :

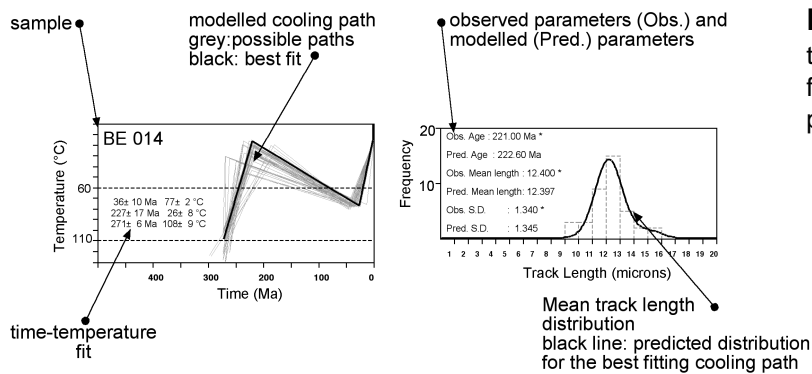
$$D_{K-S} = \max_{-\infty < x < +\infty} |S_{N1}(x) - S_{N2}(x)| \quad [10]$$

### A 5 Analytical data of samples used to construct age distribution maps (Chapter five, Fig. 5.3b)

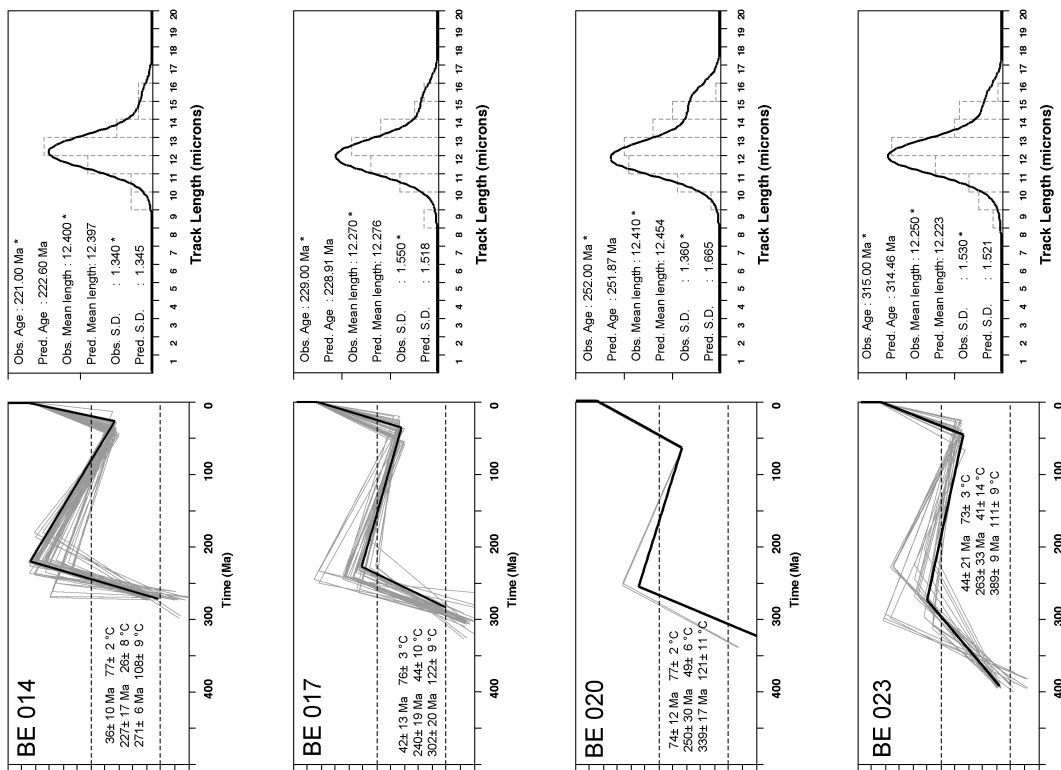
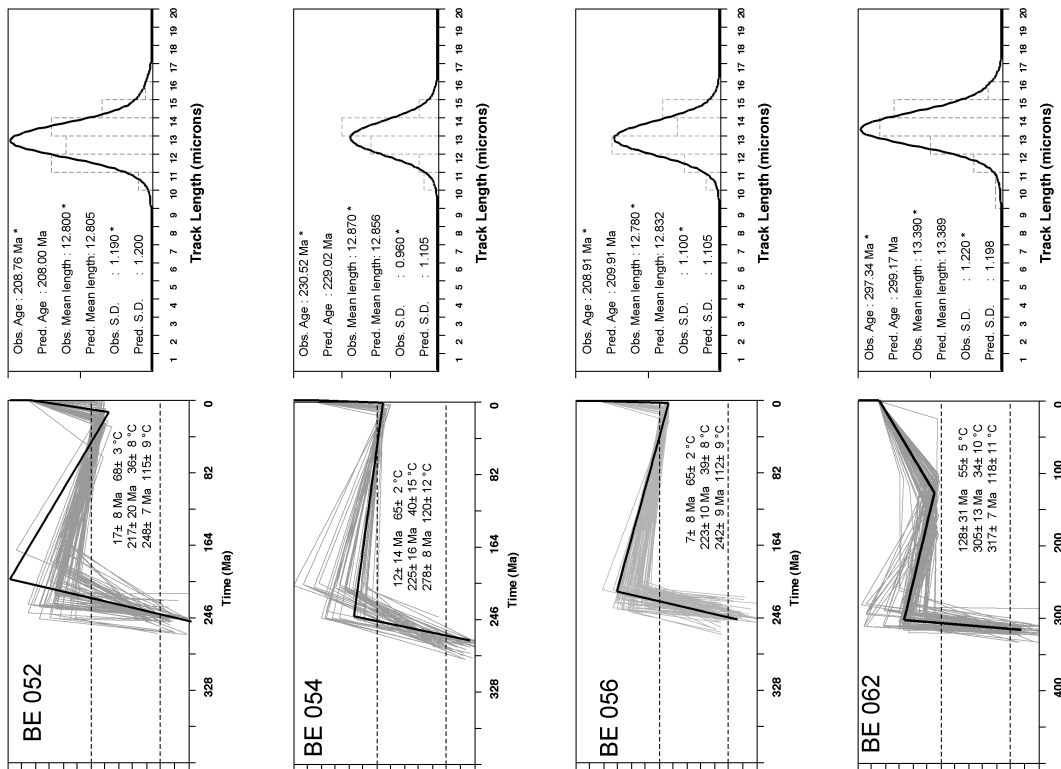
Sample Nr.	E-Longitude	Altitude	Grains	(N <sub>s</sub> )	(N <sub>i</sub> )	(N <sub>a</sub> )	P(c <sup>2</sup> )	Fission Track Age ± 1 s	U-content	Mean Track Length ± 1s SD [μm]
Rock Type	S-Latitude	[m]	Mineral	r <sub>s</sub> [x10 <sup>5</sup> cm <sup>-2</sup> ]	r <sub>i</sub> [x10 <sup>5</sup> cm <sup>-2</sup> ]	r <sub>a</sub> [x10 <sup>5</sup> cm <sup>-2</sup> ]	[%]	[Ma]	[ppm]	Nr. of ms. tracks
BE 164 migmatite	46°14.03' 22°26.86'	710	23 apatite	2049 11.859	1732 10.025	7617 16.216	94	312 ± 14	10	12.68 ± 0.39 1.87 (23)
BE 165 meta granite	46°17.55' 22°29.50'	690	20 apatite	2563 30.816	1996 23.999	7617 16.2	6	337 ± 14	22	12.66 ± 0.28 1.91 (48)
BE 173 granitic gneiss	46°41.31' 22°29.99'	845	20 apatite	766 8.952	724 8.461	7617 16.168	6	279 ± 17	8	-
BE 176 granitic gneiss	46°46.06' 22°31.94'	645	13 apatite	613 13.466	675 14.828	7617 16.152	66	240 ± 15	13	11.70 ± 0.59 1.85 (10)
BE 177 granitic gneiss	46°43.60' 22°30.68'	910	20 apatite	1973 35.359	1445 25.896	7617 16.136	6	357 ± 16	23	12.43 ± 0.22 1.81 (67)
BE 184 granodiorite	44°39.33' 24°23.86'	270	20 apatite	2961 42.821	3634 52.553	7617 16.055	52	214 ± 8	46	12.26 ± 0.19 1.65 (73)
BE 185 migmatic gneiss	44°50.84' 24°09.12'	450	20 apatite	3819 22.491	4176 24.594	7617 16.04	10	240 ± 9	22	12.78 ± 0.26 1.58 (38)
BE 189 charnokite	45°12.76' 23°56.05'	530	22 apatite	434 6.115	377 5.312	7617 16.023	57	300 ± 23	5	-
BE 190 anorthosite	45°08.75' 23°50.83'	475	20 apatite	2180 21.414	2303 22.622	7617 16.007	78	248 ± 10	20	12.89 ± 0.26 1.31 (26)
BE 193 paragneiss	45°04.26' 23°55.12'	540	20 apatite	2742 40.043	3009 43.942	7617 15.991	43	238 ± 9	38	12.14 ± 0.25 1.68 (47)
BE 196 granitic gneiss	44°54.88' 23°57.59'	540	20 apatite	2095 16.639	2882 22.89	7617 15.975	89	191 ± 8	23	12.50 ± 0.25 1.59 (39)
BE 201 migmatic gneiss	44°46.72' 23°53.00'	450	20 apatite	382 4.079	460 4.912	7617 15.959	19	217 ± 16	5	-
BE 203-1 amphibolite	44°44.89' 23°50.01'	340	20 apatite	1090 22.21	1375 28.018	7617 15.653	95	203 ± 10	25	12.87 ± 0.19 1.54 (63)
BE 203-2 gneiss	44°45.05' 23°50.12'	365	27 apatite	1564 17.2	1672 18.306	7617 15.64	0	207 ± 21	18	12.86 ± 0.16 1.07 (43)

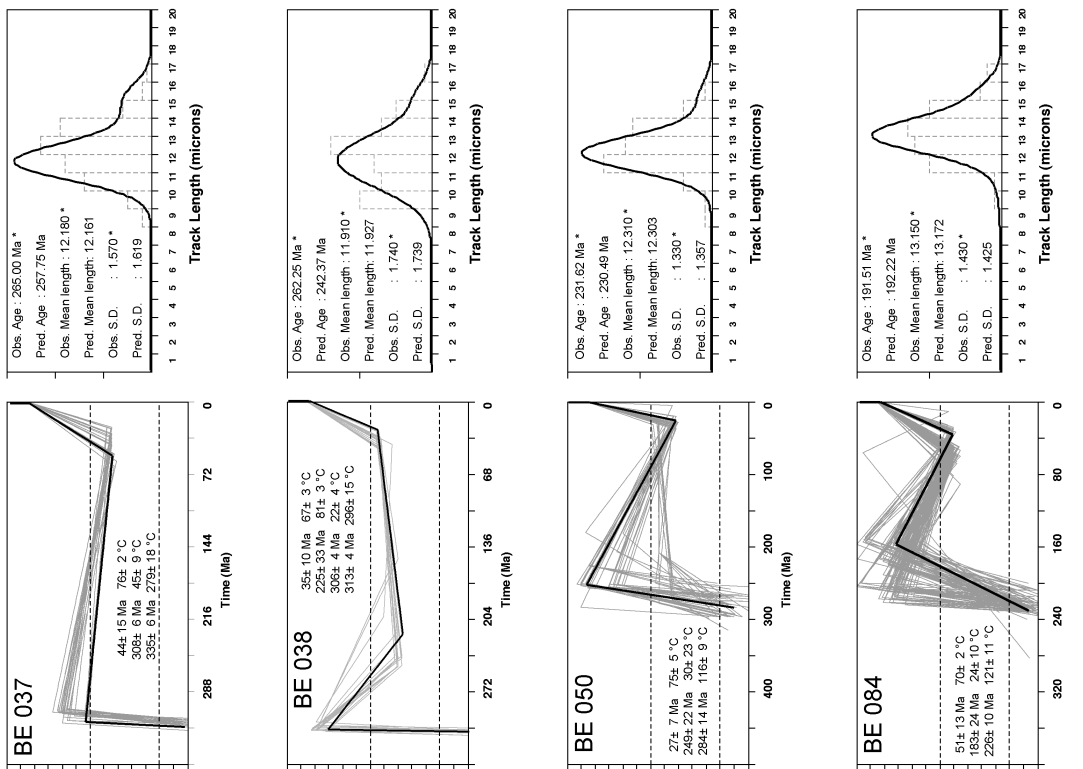
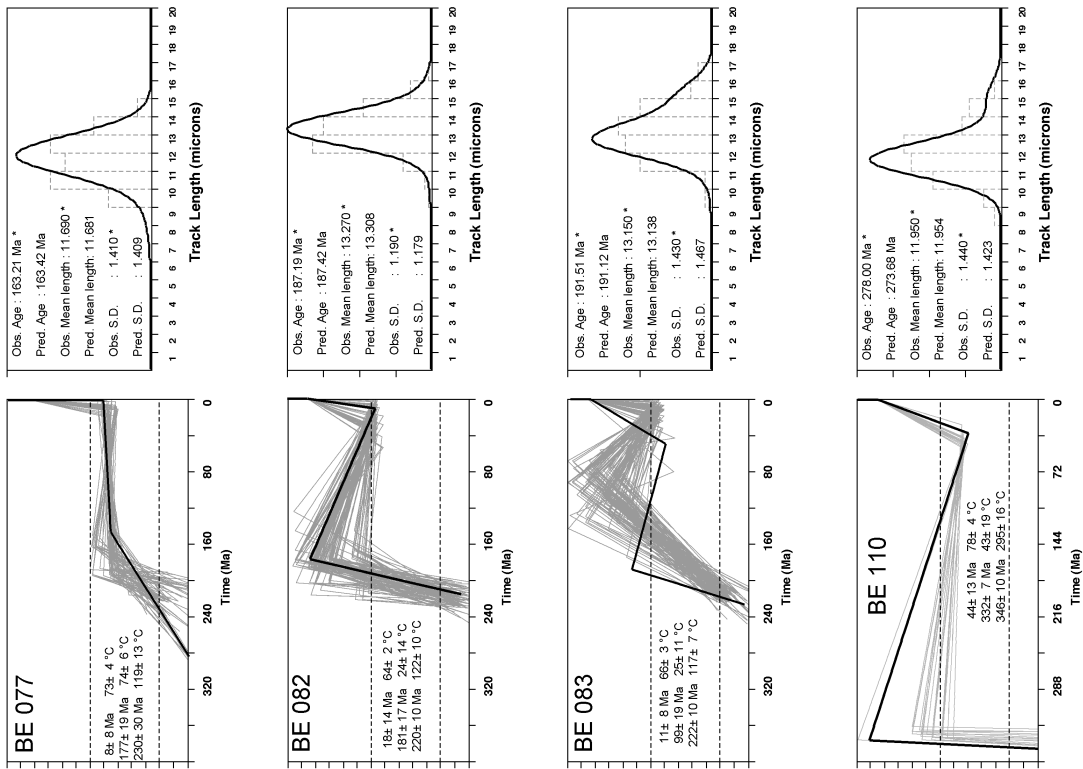
**Tab. A.2:** Analytic data of samples used for the construction of the age distribution map. Abbreviations see chapter five Tab.2

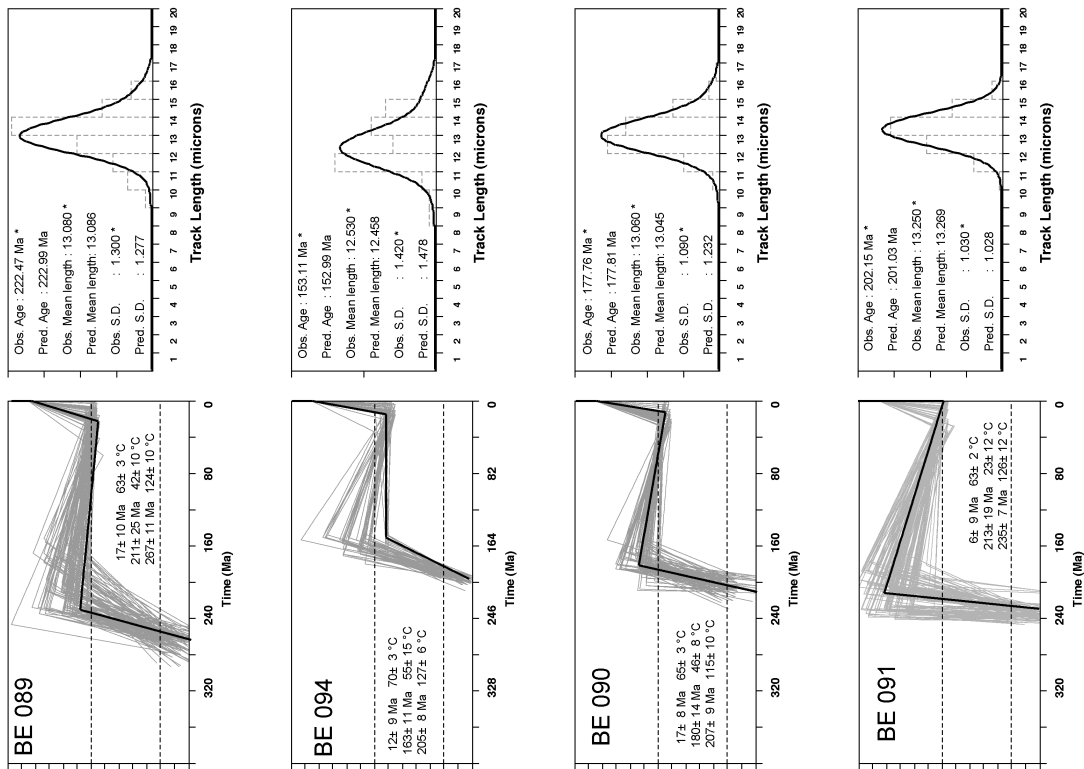
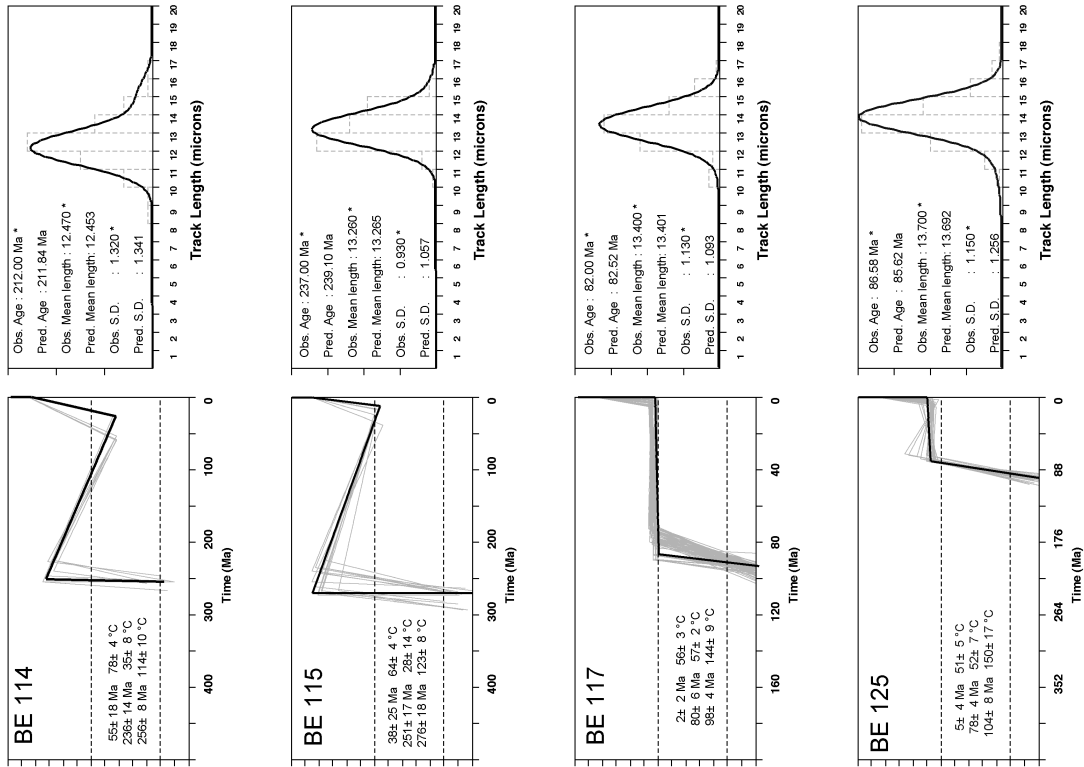
### A 6 Modelled cooling paths of samples used to construct a map, which shows the times of rapid cooling (Chapter five, Fig. 5.3c)

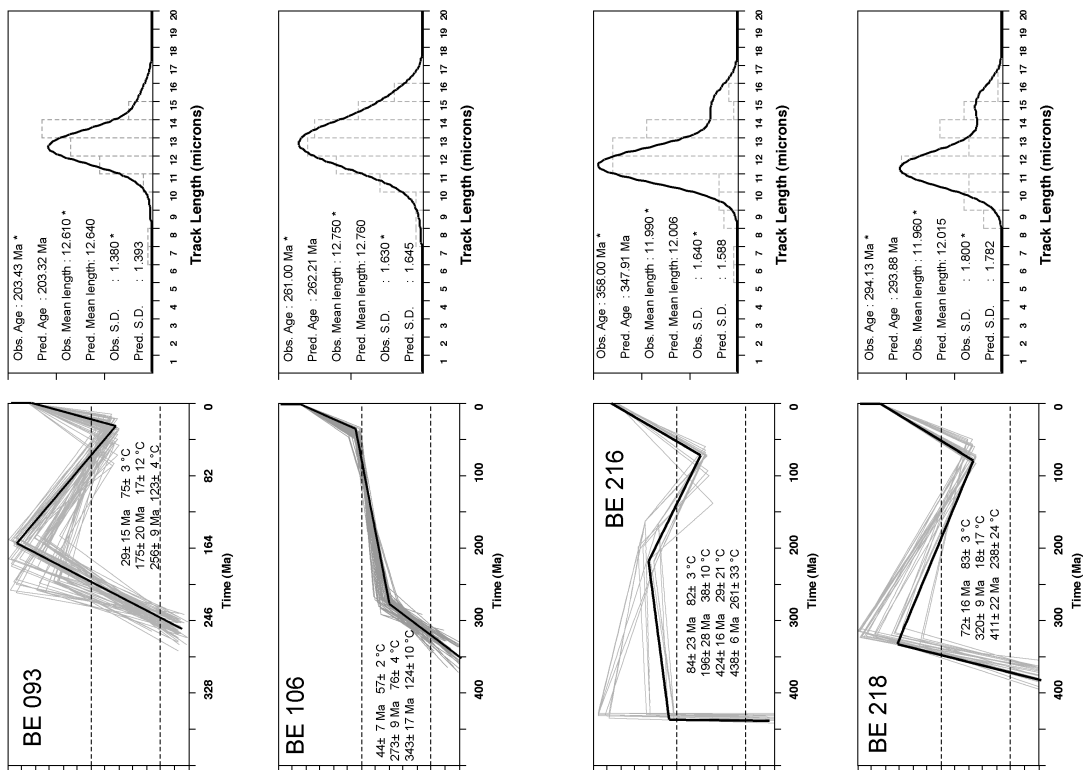


**Fig. A.2:** Explanation of the parameters obtained from the modelled cooling paths









## A 7 General abbreviations:

- $g$  = geometry factor of 0.5 for the external detector method
- $\lambda_t$  = the total decay constant of  $^{238}\text{U}$  ( $1.551 \cdot 10^{-10} \text{ a}^{-1}$ )
- $N_s$  = number of counted spontaneous tracks (in the mount)
- $N_i$  = number of counted induced tracks (in the external detector)
- $N_d$  = number of tracks counted in glass monitor (in the external detector)
- $\rho_s$  = the measured spontaneous fission track density ( $\text{tracks} \times \text{cm}^{-2}$ )
- $\rho_d$  = track density recorded in the detector ( $\text{tracks} \times \text{cm}^{-2}$ )
- $\rho_i$  = the measured induced fission track density ( $\text{tracks} \times \text{cm}^{-2}$ )
- $s(t, \zeta)$  = one sigma error of the FT age, Zeta
- $SD$  = standard deviation of the single measurements
- $t_{\text{std}}$  = standard sample of known age
- $t$  = time (fission track age)
- $\zeta$  = Zeta calibration factor

**References:**

- Cserepes, L., 1989. Numerical mathematics – for geophysics students, Tankönyvkiadó, Budapest, 358 pp.
- Dumitru, T.A., 1993. A new computer-automated microscope stage system for fission-track analysis. *Nucl. Tracks Radiat Meas.*, 21, 575-580.
- Dunkl, I., 2002. TRACKKEY: a Windows program for calculation and graphical presentation of fission track data. *Computers and Geosciences*, 28, 3-12.
- Dunkl, I., 2003. <http://homepages.uni-tuebingen.de/istvan.dunkl/seiten/popshare.html>
- Galbraight, R.F., Laslett, G.M., 1993. Statistical models for mixed fission track ages. *Nucl. Tracks Radiat.Meas.*, 5, 459-470.
- Gallagher, K., 1995. Evolving temperature histories from apatite fission-track data. *Earth and Planetary Science Letters* 136, 421-435.
- Hurford, A.J., Green, P.F., 1983. The zeta age calibration of fission-track dating. *Isotope Geoscience*, 1, 285-317.
- Hurford, A.J., Hammerschidt, K., 1985.  $^{40}\text{Ar}/^{39}\text{Ar}$  and K/AR dating of the Bishop and Fish Canyon Tuffs: Calibration ages for fission-track dating standards. *Chemical Geology (Isotope Geoscience Section)*, 58, 23-32.
- McDowell, F.W., Keizer, R.P., 1977. Timing of mid-Tertiary volcanism in the Sierra Madre Occidental between Durango City and Mazatlan, Mexico. *Geological Society of America Bulletin*, 88, 1479-1487.
- Press, W.H., Flannery, B.P., Teukolsky, S.A., Vetterling, W.T., 1996. Numerical recipes in Pascal. Cambridge University Press, Cambridge, 759 pp.
- Williams, I.S., Tetley, N.W., Compston, W., McDougall, I., 1982. A comparison of K-Ar and Rb-Sr ages of rapidly cooled igneous rocks: two points in the Paleozoic time scale re-evaluated. *Journal of the Geological Society of London*, 139, 557-568.

## **Acknowledgements**

First of all I would like to thank PD Dr. J. Jacobs for giving me the opportunity to carry out this thesis, supervising the project, and his constant support. I also thank Prof. Dr. J. Kuss, who initiated this DFG project, and for taking on the second expert report.

Thanks to the partners of the DFG “Bündelprojekt”, especially my colleges Dipl. Geol. M. Geiger and Dipl. Geol. F. Bremer for numerous discussions and helpful suggestions which improved this thesis. Furthermore, I would like to thank our collaborators from Madagascar, especially Prof. Dr. T. Razakamanana for the help and support during the two field trips. Prof. M. Olesch for providing the fission track laboratory and the workplace.

V. Kolb, B. Schröder and P. Witte are to be thanked for technical and administrative support. Thanks to Mr. Schulz for sawing some samples and the preparation of thin sections.

Many thanks to my current and former colleges of the working group “Geologie der Polargebiete” Dr. F. Lisker, Dr. B. Ventura, Dr. B. Kleinfeld, Dr. M. Gorke, Dipl. Geol. M. Daßinnies, Dipl. Geol. G. Graser, Dipl. Geol. M. Kastowski for corrections, helpful comments, data acquisition, and the pleasant time at the University of Bremen.

Above all I want to say thanks to my parents, my son and my friends who supported me during the last three and a half years.

The work was partly funded by the German Research Foundation (DFG) grant Ja617/17. Further financial support came from the University of Bremen (FNK).

Name: *Benjamin Emmel*

Datum: 09.07.2004

Anschrift: *Mittelstraße 4*  
*28203 Bremen*

## **Erklärung**

Hiermit versichere ich, dass ich

- die Arbeit ohne fremde Hilfe angefertigt habe
- keine anderen als die von mir angegebenen Quellen und Hilfsmittel benutzt habe
- die den benutzten Quellen wörtlich oder inhaltlich entnommenen Stellen als solche kenntlich gemacht habe

(Ort und Datum)

(Unterschrift)